UNIVERSITY OF CALIFORNIA
RIVERSIDE

Light-Induced Fourier Transform Infrared Difference Spectroscopy Study of the Molecular Mechanism of Photosynthetic Oxygen Evolution

A Dissertation submitted in partial satisfaction
of the requirements for the degree of

Doctor of Philosophy

in

Chemistry

by

Christopher John Kim

December 2020

Dissertation Committee:
Dr. Richard J. Debus, Chairperson
Dr. Ryan Julian
Dr. Chia-en Chang

The Dissertation of Christopher John Kim is approved:

_____

_____

_____

Committee Chairperson

University of California, Riverside

ACKNOWLEDGEMENTS

Dr. Richard J. Debus. Thank you for giving me the opportunity to learn and work under your supervision and for your mentorship, patience, and support during my time at UCR. I am amazed by your passion and dedication to teaching and research and have benefitted immensely from the countless conversations and discussions. Thank you for encouraging me to explore different ideas and for constantly making time to address my many, many questions. I often boast that I have had a uniquely positive experience as a graduate student.

Anh P. Nguyen. Thank you all your support in the lab. The body of work in this dissertation was only made possible by your laboratory expertise, management of cell cultures, and countless "prep" days.

Mom, Dad, Grandma, Grandpa. My accomplishments are the product of generations of prayers and sacrifices. I am constantly bolstered by your prayers for me and your pride in my studies.

Grace. This Ph.D. was only made possible through your countless sacrifices and steadfast support. I am truly a lucky guy. We started dating shortly before I started my PhD. Five years, two knee surgeries, thousands of miles travelled, one wedding, one pandemic, and one daughter later, we are finally closing this chapter of our lives – it's been a wild ride. I look forward to seeing what the next chapter of our lives has in store for us.

Charis. Maybe one day, you will find this document, and maybe one day, you will understand it in its entirety. Your smiles and laughter are the highlight of my day.

This research was made possible by the work and expertise shared by our many collaborators and through the funding of the Department of Energy, Office of Basic Energy Sciences, Division of Chemical Sciences (Grant DE- SC0005291).

The text of this dissertation, in full or in part, is a reprint of the material as it appears in:

(1) Kim, C. J., and Debus, R. J. (2017) Evidence from FTIR Difference Spectroscopy That a Substrate H_2O Molecule for O_2 Formation in Photosystem II Is Provided by the Ca Ion of the Catalytic Mn4CaO5 Cluster. *Biochemistry 56*, 2558–2570.

(2) Kim, C. J., Bao, H., Burnap, R. L., and Debus, R. J. (2018) Impact of D1-V185 on the Water Molecules That Facilitate O_2 Formation by the Catalytic Mn_4CaO_5 Cluster in Photosystem II. *Biochemistry 57*, 4299–4311.

(3) Kim, C. J., and Debus, R. J. (2019) One of the Substrate Waters for O2 Formation in Photosystem II Is Provided by the Water-Splitting Mn_4CaO_5 Cluster's Ca^{2+} Ion. *Biochemistry 58*, 3185–3192.

(4) Kim, C. J., and Debus, R. J. (2020) Roles of D1-Glu189 and D1-Glu329 in O_2 Formation by the Water-Splitting Mn4Ca Cluster in Photosystem II. *Biochemistry 59*, 3902–3917.

The co-author, Richard J. Debus, directed and supervised the research which forms the basis for this dissertation. The other co-authors provided methodological and technical expertise.

In addition to the papers listed above, I am co-author on the following manuscripts that were published (or are in preparation) as part of my thesis work but are not covered in individual chapters. The results and conclusions from these papers are highly relevant to the chapters of this dissertation:

(1) Banerjee, G., Ghosh, I., Kim, C. J., Debus, R. J., and Brudvig, G. W. (2018) Substitution of the D1-Asn87 site in photosystem II of cyanobacteria mimics the chloride-binding characteristics of spinach photosystem II. *J. Biol. Chem. 293*, 2487–2497.

(2) Ghosh, I., Banerjee, G., Kim, C. J., Reiss, K., Batista, V. S., Debus, R. J., and Brudvig, G. W. (2019) D1-S169A Substitution of Photosystem II Perturbs Water Oxidation. *Biochemistry 58*, 1379–1387.

(3) Banerjee, G., Ghosh, I., Kim, C. J., Debus, R. J., and Brudvig, G. W. (2019) Bicarbonate rescues damaged proton-transfer pathway in photosystem II. *Biochim. Biophys. Acta - Bioenerg. 1860*, 611–617.

(4) Ghosh, I., Banerjee, G., Reiss, K., Kim, C. J., Debus, R. J., Batista, V. S., and Brudvig, G. W. (2020) D1-S169A substitution of photosystem II reveals a novel S2-state structure. *Biochim. Biophys. Acta - Bioenerg. 1861*, 148301.

(5) de Lichtenberg, C., Pham, L. V., Walter, K., Liang, F., Kim, C. J., Magnusson, A., Ho, F., Debus, R. J., Lindblad, P., Messinger, J. Is exchange rate of the fast substrate water in the S2 state of photosystem II limited by diffusion through the water channels? Lessons from mutations in the O1 channel. *Manuscript in preparation*.

(6) de Lichtenberg, C., Kim, C. J., Debus, R. J., Messinger, J., Effects of the D61A and E189Q mutations on the exchange of substrate water in photosystem II. *Manuscript in preparation.*

ABSTRACT OF THE DISSERTATION

Light-Induced Fourier Transform Infrared Difference Spectroscopy Study of the Molecular Mechanism of Photosynthetic Oxygen Evolution

by

Christopher John Kim

Doctor of Philosophy, Graduate Program in Chemistry
University of California, Riverside, December 2020
Dr. Richard J. Debus, Chairperson

Oxygenic photosynthesis produces nearly all the O_2 on Earth and sustains nearly all of its biomass. This process is catalyzed by Photosystem II (PSII), a large, transmembrane protein embedded in the thylakoid membranes of plants, algae, and cyanobacteria. PSII is catalyzed by a Mn_4CaO_5 cluster. As light energy is absorbed by the reaction centers of PSII, the Mn_4CaO_5 cluster accumulates oxidizing equivalents through a discreet and precisely choreographed light-induced electron transfer. The light induced oxidations cause the catalytic cluster to cycle through five oxidation states, S_n (n=0-4) where 'n' refers to the number of oxidizing equivalents. After formation of the S_4 state, the cluster oxidizes two water molecules, releases O_2 and returns to the S_0 state, the lowest oxidation state of its catalytic cycle. The oxidation of water is a thermodynamically and kinetically demanding reaction. This is managed by PSII through the careful choreography of proton and electron transfers to the Mn_4CaO_5 cluster throughout the catalytic cycle. The

Mn_4CaO_5's reactivity in each catalytic step is carefully controlled by its protein environment. Identifying key amino acid residues, determining their responsibility in the reaction, and characterizing the proton egress pathways during the individual S state transitions are paramount in understanding the oxygen evolution mechanism.

This study interrogates and identifies the amino acid residues responsible for controlling the Mn_4CaO_5 cluster's reactivity and determines the role of each residue through Fourier transform infrared (FTIR) difference spectroscopy. FTIR difference spectroscopy is capable of characterizing the dynamic structural rearrangements during PSII's catalytic cycle. A combination of site-directed mutagenesis (D1-V185N, D1-S169A, D1-E189G, D1-E189S, D1-E329A), isotopic substitutions, and the substitution of Sr^{2+} for Ca^{2+} in PSII's catalytic center were used to further delineate the dominant water access and proton egress pathways that link the catalytic cluster with the thylakoid lumen, characterize the influence of specific protein residues on substrate water molecules and on the network of hydrogen bonds in these pathways, and elucidate the potential substrates and mechanisms of the S_2 to S_3 transition.

Table of Contents

List of Figures

Chapter 1

Introduction and Literature Review

1.1 BACKGROUND/SIGNIFICANCE

Global consumption of energy has steadily increased year over year from approximately 5 GJ per person per annum in the late-Paleolithic era to over 20 GJ per person per annum today. In absolute terms, the total global energy consumption has increased approximately 600,000 PJ *(1–3)*. This growth in energy consumption is heralded by the 150 years of fossil-fueled industrial development and is coupled to massive increase in productivity *(4, 5)*. However, the reliance on the combustion of oil, natural gas, and coal to fill energy demand is the primary driver to the changes in the composition of the atmosphere, the oceans, and climate change, which, in turn, underpin the endangering of ecosystems and the negative externalities that primarily impact the socioeconomically disadvantaged *(3, 6)*.

Of the many sustainable alternatives to fossil fuels, one option provides rich, high energy density and is freely and abundantly available: the sun. Although a mixture of sustainable alternatives (such as hydropower, biomass/biofuels, geothermal and ocean thermal energy conversion, wind and tidal power) will be important components of man's environmentally sustainable future, the solar resource dwarfs all renewable, nuclear, and fossil fuel capacities by orders of magnitude. More solar energy strikes the Earth in an hour than is consumed by mankind in one year. The primary challenge lies in harnessing solar energy and storing it – nature has mastered this quandary: plants rely solely on sunlight, water, and CO_2 to meet all their energy needs. There are many lessons to learn from natural

photosynthesis to construct useful and economically viable artificial systems to meet mankind's energy needs *(7–10)*.

1.2 INTRODUCTION TO PHOTOSYNTHESIS

Approximately 3 Billion years ago, nature developed a highly efficient light-driven nanomachine to capture and convert solar energy and store it in energetically rich chemical bonds. This process, called photosynthesis is carried out by both prokaryotic and eukaryotic domains and is classified based on its released byproducts: anoxygenic (non-oxygen evolving) and oxygenic (oxygen evolving). The complex reactions that consist of oxygenic photosynthesis occurs within the specialized organelles known as chloroplasts and can be simplified as the following reaction:

$$6CO_2 + 6H_2O \xrightarrow{h\nu} 6(CH_2O) + 6O_2 \quad (1)$$

Within less than a second of light absorption, O_2 is released. The process of oxygenic photosynthesis is comprised of two distinct reactions: light dependent and light independent reactions, also known as the Calvin cycle or dark reactions. The light independent reactions occur within the stroma, the fluid-filled space of the chloroplast. At its core, the light independent reactions consist of carbon fixation (the conversion of carbon dioxide and water into sugar) and the generation of one molecular equivalent of nicotinamide adenine dinucleotide phosphate ($NADP^+$) and two molecular equivalents of adenine diphosphate (ADP) for the light dependent reactions.

The light dependent reactions are performed by a chain of four large integral membrane protein super-complexes located in the thylakoid membrane: Photosystem II (PSII), Cytochrome b_6f (Cty b_6f), Photosystem I (PSI), and ATP Synthase. The light

reaction is initiated with the absorption of photon by light-harvesting antenna protein complexes. The absorbed energy is subsequently transferred from antenna pigment to antenna pigment until it reaches the reaction center by photoactive chlorophyll (chl) molecules located in PSI and PSII, which in turn loses an electron to the electron transport chain (ETC). The donated electron is replaced through the oxidation of water, in which O_2 is created as a byproduct. As first proposed by Hill and Bendall and further characterized by Duysens, the electron proceeds from PSII to Cty b_6f to PSI and ultimately leads to the reduction of $NADP^+$ to NADPH *(11, 12)*. Through a process called photophosphorylation, Cty b_6f utilizes energy of the electrons as they transverse through the ETC to pump protons from the stroma to the lumen. This transmembrane protein gradient generates the proton motive force used by ATP Synthase to generate adenine triphosphate (ATP) *(13)*.

1.3 PHOTOSYSTEM II

Virtually all the O_2 on Earth is created though oxygenic photosynthesis by PSII. A combination of computational modeling and crystallography has provided a three-dimensional picture of PSII's intricate features. Structures have been solved to 1.85 – 2.44 Å *(14–20)* in cyanobacteria, 2.7 – 3.8 Å in algae *(21–25)* and 2.7 - 5.3 Å *(26–28)* in plants. PSII is a water:plastoquinone oxido-reductase integral to the thylakoid membrane that consists of over 20 protein subunits, 60 organic and inorganic cofactors, and a Mn_4CaO_5 cluster: the oxygen evolving complex (OEC). It is an approximately 700 kDa dimer in vivo. Each monomeric complex consists of four, large, membrane-spanning proteins (D1 (PsbA), D2 (PsbD), CP43, CP47) twelve small membrane spanning proteins (PsbE, PsbF, PsbH, PsbI, PsbJ, PsbK, PsbL, PsbM, PsbTc, PsbW, PsbX, PsbZ), and four extensive

protein units (PsbO, PsbP, PsbQ, PsbTn). Structurally, D1 and CP43 subunits are the closest proximity to the OEC. The D1 and D2 are homologous and form a heterodimer at the core of each monomeric complex. The extensive units, PsbO, PsbP, and PsbQ, flank the OEC on the lumen side. The CP43 and CP47 polypeptides are surrounded by the D1-D2 dimer and serve as the light-harvesting antenna proteins of PSII, transferring excited energy to the photochemically active chl a (P_{680}) (Figure 1.1) *(29–34)*.

Through a series of highly concerted light-induced electron transfers, PSII accumulates four oxidizing equivalents to split water into H^+ and O_2. The catalytic cycle, therefore, consists of four sequential charge separation events coupled with four oxidation events. The charge separation events occur in PSII upon the transference of light energy from the antenna complexes and the excitation of P_{680} to P_{680}•. Within 3 picoseconds, P_{680}• reduces a pheophytin (Pheo) resulting in the formation of the radical pair, $P_{680}^{\bullet+}Pheo^{\bullet-}$. The charge separation is rapidly stabilized (within 300 ps *(35, 36)*) by the oxidation of $Pheo^{\bullet-}$ by the primary plastoquinone electron acceptor, Q_A. $Q_A^{\bullet-}$ is then oxidized by the loosely-bound, secondary plastoquinone electron acceptor Q_B via a non-heme iron center. The once reduced $Q_B^{\bullet-}$ accepts another electron. The doubly reduced Q_B is stabilized by stroma-side protons to form plastoquinol (PQH_2). PQH_2 leaves the binding site, upon which the empty Q_B binding site is filled with a plastoquinone from the PQ pool in the thylakoid membrane. Over the course of the entire catalytic cycle, two plastoquinols are produced *(37)*. The oxidation events begin with the reduction of $P_{680}^{\bullet+}$ by redox-active Tyrosine 161 (Y_z). $Y_z^{\bullet}$ subsequently oxidizes the Mn_4CaO_5 cluster (Figure 1.2). This process or extracting four protons and electrons from two water molecules is thermodynamically and kinetically

difficult. Proton and electron extraction must be coupled together to prevent charge accumulation on the OEC and the creation of an additional energetic barrier to oxidation.

1.4 THE WATER OXIDIZING COMPLEX

The Mn_4CaO_5 cluster serves as the interface between the single-electron photochemistry and the oxidation of water. As first discovered by Kok and Joliot, the Mn_4CaO_5 cluster cycles through five oxidation states with a period of four light-induced events *(38, 39)*. The light-induced oxidations cause the OEC to progress through five oxidation states, S_n (n=0-4) where n refers to the number of oxidizing equivalents. After four, separate, light-induced oxidations, the transient S_4 triggers the formation of the O-O bond, release of O_2, and the immediate relaxation to the S_0 state, where it subsequently rebinds to one substrate water molecule. Further oxidation returns the OEC from the S_0 state to the S_1 state: the S_1 state predominates as the dark-stable resting state. This cycle of S-states involves a precise sequence of electron and proton transfers in order to prevent the inhibition of the oxidation of the OEC by $Y_z^{\bullet}$ by its increasing redox potential. Proton transfers precede the oxidation of the Mn_4CaO_5 cluster during the S_2 to S_3 and the S_3 to S_4 transitions *(40, 41)*.

As mentioned above, the resulting proton gradient formed from oxidation of water (on the lumen side) and the formation of the plastoquinol (on the stroma side) provides the motive force for the synthesis of ATP. One catalytic cycle of PSII can be summarized in the following equation:

$$2H_2O + 2PQ + 4\,H^+_{stroma} \xrightarrow{h\nu} O_2 + 2PQH_2 + 4\,H^+_{lumen} \qquad (2)$$

Rapid advancements and progress in structural studies (including the development XFEL-based serial femtosecond X-ray crystallography, puled EPR spectroscopy, membrane inlet mass spectrometry, and computational studies) of PSII has advanced our understanding of the Mn_4CaO_5 cluster as its conformation changes throughout the course of the catalytic cycle [for recent reviews see *(42–48)*].

High resolution structures of the Mn_4CaO_5 cluster for all the S-states (except for the transient S_4) have been reported *(14, 15, 19, 49)*. The Mn_4CaO_5 cluster is arranged as a distorted chair-like structure where Mn1, Mn2, Mn3, Ca, O1, O2, O3, and O5 form a distorted cuboidal structure linked to the fourth "dangling" manganese ion (Mn4) by two μ-oxo O4 and O5. Four of these waters are bound to the Mn_4CaO_5 cluster: W1 and W2 are bound to Mn4, and W3 and W4 are bound to the calcium ion (Figure 1.3) *(50)*. The cluster is bound to PSII by six carboxylate groups and one histidine residue supplied by the D1 and CP43 proteins. There are numerous, immobilized water molecules localized around the Mn_4CaO_5 cluster that are involved in the hydrogen-bond networks, which efficiently transport protons away from the catalytic cluster and facilitate the access of the substrate water molecules. There are at least three pathways connecting the lumen of the thylakoid to the OEC: one including Mn4 and D1-D61, another including the Ca^2 ion and Tyrosine 161 (Y_z), and the third including the Cl^- ion located near D2-K317 *(42, 51–53)*. The network of hydrogen bonded water molecules beginning at D1-D61 has been identified as the proton egress pathway during the transition from the S_3 state to the S_4 state *(42, 51–56)*.

The S_0, S_1, and S_2 states have similar structures with the exception that the Mn3-Mn4 bond distances in the S_0 state is longer indicating that the O5 bridge is protonated

(57). In the dark-stable S_1 state, the O5 is shifted closer to Mn4; the Mn1-O5 distance is too long to be considered a bond *(15)*. The S_2 consists of one bipyramidal five-coordinate Mn(III) ion and three octahedral six-coordinate Mn(IV) ions *(58–60)* and the S_3 states consisting of four octahedral six-coordinate Mn(IV) ions *(61–63)*.

Computational calculations and experimental evidence have shown that, in the S_2 state, the Mn_4CaO_5 cluster can adopt two different conformations. The two conformations are isoenergetic and have a barrier of 6-7 kcal/mol, as calculated by QM/MM and EPR measurements *(64–68)*. The two different S_2 state structures have similar Mn-Mn distances but differ in their Mn-O distances and in their distribution of the manganese oxidation states. In the open cubane conformation, Mn4 is coordinated with O5. In the closed cubane conformation, Mn1 is coordinated with O5. The structural variance allows for the cofactor for the S_2 state to access different ground spin states. In the low spin structure, the Mn ions are predominantly antiferromagnetic, resulting in a multiline EPR signal at approximately g=2 (g-factor a dimensionless quantity used to characterize the angular momentum and magnetic moment of an item). This conformation is referred to as "open cubane." In the high spin structure, the Mn ions are predominantly ferromagnetic resulting in a broad EPR signal at $g > 4.1$. This conformation is referred to as "closed cubane" *(69–73)*.

Recent time-resolved serial femtosecond crystallography has shown the insertion of an oxygen (referred to as O6 or O_x) near O5 during the S_2 to S_3 transition *(19, 74)*. This, coupled with O5's unusually long distances to nearby Mn ions, suggests that O5 and a water molecule (or a water-derived ligand) are the substrates for O_2 formation *(57, 75–77)*. This unknown water's origin is debated; several different models have been suggested to

explain the origin of this water and mechanism for the formation of the O=O bond. The structural flexibility of the Mn_4CaO_5 cluster in the S_2 state is a key aspect in the proposed mechanisms. One set of models (referred to as the "carousel" or "pivot" model) argues that during the S_2 to transition, waters are rotated around Mn4 such that W2 would become O5 and the displaced O5 would shift over and become O6/O_x *(78–81)*. Another set of models suggest that O6/O_x originates from the calcium-bound W3 *(20, 82–84)*. In this model, W3 would either be inserted onto Mn1 and either become O6/O_x or force O5 to shift to become O6/O_x. Because the substrate waters are chemically identical to the bulk solvent, directly interrogating the origin of the unknown water is challenging.

1.5 LIGHT-INDUCED FOURIER TRANSFORM INFRARED DIFFERENCE SPECTROSCOPY

Reaction-induced Fourier transform infrared (FTIR) difference spectroscopy is a rapid, sensitive method that has since been demonstrated to be adept at characterizing changes in protein conformations, protonation states of amino acids, and the network of hydrogen bonded water molecules *(85, 86)*. Since the first publication of the S_2-minus-S_1 FTIR difference spectra by Noguchi et al. in 1992 *(87)* and subsequent S_3-minus-S_2 spectra by Chu et al. in 2000 *(88)*, the spectra of the entire catalytic cycle of PSII has been characterized *(89, 90)*.

Initial band assignments for PSII's IR spectra were assigned through the infrared characteristic group frequencies: vibrational frequencies of specific groups correspond to their specific chemical bonds *(91)*. These band group frequencies have been verified experimentally through a combination of site-directed mutagenesis and isotopic

substitutions. Bands in the mid-frequency (1800 – 1200 cm^{-1}) region include: the asymmetric and symmetric stretches at 1600 – 1500 cm^{-1} and 1450 – 1300 cm^{-1} respectively for deprotonated carboxylate (COO^-) groups, the carbonyl (C=O) stretches at 1600 – 1800 cm^{-1}, the amide I (C=O stretch) bands at 1700 – 1600 cm^{-1}, and the amide II (CN stretch and NH bend) bands at 1600 – 1500 cm^{-1} respectively for polypeptide amide groups *(92–98)*. Bands in the low-frequency region between 650-350 cm^{-1} have been attributed to vibrations involving Mn_4CaO_5 cluster *(94, 99–104)*. Assignments of O-H stretching and bending modes were identified by the frequency shifts caused by $H_2{}^{18}O$ substitutions and confirmed by its similarities to the O-D stretching and bending modes. These features have been monitored around 3200 – 2500 cm^{-1} for the highly polarized network of strong hydrogen bonds *(105)* near the Mn_4CaO_5 cluster *(55, 97, 106–111)* and around 3700 – 3500 cm^{-1} is for the O-H stretching vibrations for weakly hydrogen bonded water molecules *(55, 97, 115, 116, 103, 108–114)*. Weak H-O-H bending modes appear near 1640 cm^{-1} and have been monitored through D-O-D bending around 1250 – 1150 cm^{-1} *(55, 110, 117)*.

The combination of site-directed mutagenesis of amino acid ligands, isotope labeling, and spectroscopic characterizations of PSII core complexes can help identify the key amino acid residues responsible for the complex choreography involved in water oxidation and elucidate the proton egress pathways during the S-state cycle. (For reviews, see *(118, 119)*).

1.6 References

(1) Smil, V. (2017) Energy and civilization: A history. *Energy Civiliz. A Hist.* MIT Press.

(2) International Energy Agency (IEA). (2019) World Energy Outlook 2019 – Analysis - IEA. *World Energy Outlook 2019*.

(3) Valérie Masson-Delmotte,Panmao Zhai,Hans-Otto Pörtner,Debra Roberts, J. S. and P. R. S. (2018) Global warming of 1.5°C. *Ipcc - Sr15*.

(4) Brockway, P. E., Saunders, H., Heun, M. K., Foxon, T. J., Steinberger, J. K., Barrett, J. R., and Sorrell, S. (2017) Energy rebound as a potential threat to a low-carbon future: Findings from a new exergy-based national-level rebound approach. *Energies 10*, 51.

(5) Sakai, M., Brockway, P. E., Barrett, J. R., and Taylor, P. G. (2019) Thermodynamic efficiency gains and their role as a key "engine of economic growth." *Energies 12*, 110.

(6) Haberl, H., Fischer-Kowalski, M., Krausmann, F., Martinez-Alier, J., and Winiwarter, V. (2011) A socio-metabolic transition towards sustainability? Challenges for another Great Transformation. *Sustain. Dev. 19*, 1–14.

(7) United States. Dept. of Energy. Office of Science. (2004) Basic Research Needs for the Hydrogen Economy. Report of the Basic Energy Sciences Workshop on Hydrogen Production, Storage and Use, May 13-15, 2003. *Basic Res. Needs Hydrog. Econ.*

(8) Lewis, N. S., Crabtree, G., Nozik, A. J., Wasielewski, M. R., Alivisatos, P., Kung, H., Tsao, J., Chandler, E., Walukiewicz, W., Spitler, M., Ellingson, R., Overend, R., Mazer, J., Gress, M., Horwitz, J., Ashton, C., Herndon, B., Shapard, L., and Nault, R. M. (2005) Basic Research Needs for Solar Energy Utilization. Report of the Basic Energy Sciences Workshop on Solar Energy Utilization, April 18-21, 2005. *Basic Energy Sci. Work. Sol. Energy Util.* 276.

(9) Barber, J. (2009) Photosynthetic energy conversion: Natural and artificial. *Chem. Soc. Rev. 38*, 185–196.

(10) Scholes, G. D., Fleming, G. R., Olaya-Castro, A., and Van Grondelle, R. (2011, October) Lessons from nature about solar light harvesting. *Nat. Chem.* Nat Chem.

(11) Hill, R., and Bendall, F. (1960) Function of the two cytochrome components in chloroplasts: A working hypothesis. *Nature 186*, 136–137.

(12) Duysens, L. N. M., Amesz, J., and Kamp, B. M. (1961) Two photochemical systems in photosynthesis. *Nature 190*, 510–511.

(13) Shevela, D., Björn, L. O., and Govindjee. (2013) Oxygenic Photosynthesis, in *Natural and Artificial Photosynthesis*, pp 13–63. John Wiley & Sons Inc., Hoboken, NJ, USA.

(14) Umena, Y., Kawakami, K., Shen, J. R., and Kamiya, N. (2011) Crystal structure of oxygen-evolving photosystem II at a resolution of 1.9Å. *Nature 473*, 55–60.

(15) Suga, M., Akita, F., Hirata, K., Ueno, G., Murakami, H., Nakajima, Y., Shimizu, T., Yamashita, K., Yamamoto, M., Ago, H., and Shen, J. R. (2015) Native structure of photosystem II at 1.95 Å resolution viewed by femtosecond X-ray pulses. *Nature 517*, 99–103.

(16) Tanaka, A., Fukushima, Y., and Kamiya, N. (2017) Two different structures of the oxygen-evolving complex in the same polypeptide frameworks of photosystem II. *J. Am. Chem. Soc. 139*, 1718–1721.

(17) Hellmich, J., Bommer, M., Burkhardt, A., Ibrahim, M., Kern, J., Meents, A., Müh, F., Dobbek, H., and Zouni, A. (2014) Native-like Photosystem II Superstructure at 2.44 Å Resolution through Detergent Extraction from the Protein Crystal. *Structure 22*, 1607–1615.

(18) Young, I. D., Ibrahim, M., Chatterjee, R., Gul, S., Fuller, F. D., Koroidov, S., Brewster, A. S., Tran, R., Alonso-Mori, R., Kroll, T., Michels-Clark, T., Laksmono, H., Sierra, R. G., Stan, C. A., Hussein, R., Zhang, M., Douthit, L., Kubin, M., De Lichtenberg, C., Vo Pham, L., Nilsson, H., Cheah, M. H., Shevela, D., Saracini, C., Bean, M. A., Seuffert, I., Sokaras, D., Weng, T. C., Pastor, E., Weninger, C., Fransson, T., Lassalle, L., Bräuer, P., Aller, P., Docker, P. T., Andi, B., Orville, A. M., Glownia, J. M., Nelson, S., Sikorski, M., Zhu, D., Hunter, M. S., Lane, T. J., Aquila, A., Koglin, J. E., Robinson, J., Liang, M., Boutet, S., Lyubimov, A. Y., Uervirojnangkoorn, M., Moriarty, N.

W., Liebschner, D., Afonine, P. V., Waterman, D. G., Evans, G., Wernet, P., Dobbek, H., Weis, W. I., Brunger, A. T., Zwart, P. H., Adams, P. D., Zouni, A., Messinger, J., Bergmann, U., Sauter, N. K., Kern, J., Yachandra, V. K., and Yano, J. (2016) Structure of photosystem II and substrate binding at room temperature. *Nature 540*, 453–457.

(19) Kern, J., Chatterjee, R., Young, I. D., Fuller, F. D., Lassalle, L., Ibrahim, M., Gul, S., Fransson, T., Brewster, A. S., Alonso-Mori, R., Hussein, R., Zhang, M., Douthit, L., de Lichtenberg, C., Cheah, M. H., Shevela, D., Wersig, J., Seuffert, I., Sokaras, D., Pastor, E., Weninger, C., Kroll, T., Sierra, R. G., Aller, P., Butryn, A., Orville, A. M., Liang, M., Batyuk, A., Koglin, J. E., Carbajo, S., Boutet, S., Moriarty, N. W., Holton, J. M., Dobbek, H., Adams, P. D., Bergmann, U., Sauter, N. K., Zouni, A., Messinger, J., Yano, J., and Yachandra, V. K. (2018) Structures of the intermediates of Kok's photosynthetic water oxidation clock. *Nature 563*, 421–425.

(20) Ibrahim, M., Fransson, T., Chatterjee, R., Cheah, M. H., Hussein, R., Lassalle, L., Sutherlin, K. D., Young, I. D., Fuller, F. D., Gul, S., Kim, I. S., Simon, P. S., de Lichtenberg, C., Chernev, P., Bogacz, I., Pham, C. C., Orville, A. M., Saichek, N., Northen, T., Batyuk, A., Carbajo, S., Alonso-Mori, R., Tono, K., Owada, S., Bhowmick, A., Bolotovsky, R., Mendez, D., Moriarty, N. W., Holton, J. M., Dobbek, H., Brewster, A. S., Adams, P. D., Sauter, N. K., Bergmann, U., Zouni, A., Messinger, J., Kern, J., Yachandra, V. K., and Yano, J. (2020) Untangling the sequence of events during the $S_2 \rightarrow S_3$ transition in photosystem II and implications for the water oxidation mechanism. *Proc. Natl. Acad. Sci. U. S. A. 117*, 12624–12635.

(21) Ago, H., Adachi, H., Umena, Y., Tashiro, T., Kawakami, K., Tian, N. K. L., Han, G., Kuang, T., Liu, Z., Wang, F., Zou, H., Enami, I., Miyano, M., and Shen, J. R. (2016) Novel features of eukaryotic photosystem II revealed by its crystal structure analysis from a red alga. *J. Biol. Chem. 291*, 5676–5687.

(22) Sheng, X., Watanabe, A., Li, A., Kim, E., Song, C., Murata, K., Song, D., Minagawa, J., and Liu, Z. (2019) Structural insight into light harvesting for photosystem II in green algae. *Nat. Plants 5*, 1320–1330.

(23) Shen, L., Huang, Z., Chang, S., Wang, W., Wang, J., Kuang, T., Han, G., Shen, J. R., and Zhang, X. (2019) Structure of a $C_2S_2M_2N_2$-type PSII–LHCII supercomplex from the green alga Chlamydomonas reinhardtii. *Proc. Natl. Acad. Sci. U. S. A. 116*, 21246–21255.

(24) Nagao, R., Kato, K., Suzuki, T., Ifuku, K., Uchiyama, I., Kashino, Y., Dohmae, N., Akimoto, S., Shen, J. R., Miyazaki, N., and Akita, F. (2019) Structural basis for energy harvesting and dissipation in a diatom PSII–FCPII supercomplex. *Nat. Plants 5*, 890–901.

(25) Pi, X., Zhao, S., Wang, W., Liu, D., Xu, C., Han, G., Kuang, T., Sui, S. F., and Shen, J. R. (2019) The pigment-protein network of a diatom photosystem II–light-harvesting antenna supercomplex. *Science 365*, eaax4406.

(26) Wei, X., Su, X., Cao, P., Liu, X., Chang, W., Li, M., Zhang, X., and Liu, Z. (2016) Structure of spinach photosystem II-LHCII supercomplex at 3.2 Å resolution. *Nature 534*, 69–74.

(27) Van Bezouwen, L. S., Caffarri, S., Kale, R., Kouřil, R., Thunnissen, A. M. W. H., Oostergetel, G. T., and Boekema, E. J. (2017) Subunit and chlorophyll organization of the plant photosystem II supercomplex. *Nat. Plants 3*, 1–11.

(28) Su, X., Ma, J., Wei, X., Cao, P., Zhu, D., Chang, W., Liu, Z., Zhang, X., and Li, M. (2017) Structure and assembly mechanism of plant $C_2S_2M_2$-type PSII-LHCII supercomplex. *Science 357*, 815–820.

(29) 9) Cox, N., Pantazis, D. A., and Lubitz, W. (2020) Current Understanding of the Mechanism of Water Oxidation in Photosystem II and Its Relation to XFEL Data. *Annu. Rev. Biochem. 89*, 795–820.

(30) Huang, K., Zhang, J. Y., Liu, F., and Dai, S. (2018) Synthesis of Porous Polymeric Catalysts for the Conversion of Carbon Dioxide. *ACS Catal. 8*, 9079–9102.

(31) Chrysina, M., Heyno, E., Kutin, Y., Reus, M., Nilsson, H., Nowaczyk, M. M., DeBeer, S., Neese, F., Messinger, J., Lubitz, W., and Cox, N. (2019) Five-coordinate MnIV intermediate in the activation of nature's water splitting cofactor. *Proc. Natl. Acad. Sci. U. S. A. 116*, 16841–16846.

(32) Junge, W. (2019) Oxygenic photosynthesis: History, status and perspective. *Q. Rev. Biophys. 52*.

(33) Pantazis, D. A. (2018) Missing Pieces in the Puzzle of Biological Water Oxidation. *ACS Catal. 8*, 9477–9507.

(34) Vinyard, D. J., and Brudvig, G. W. (2017) Progress Toward a Molecular Mechanism of Water Oxidation in Photosystem II. *Annu. Rev. Phys. Chem. 68*, 101–116.

(35) Schatz, G. H., Brock, H., and Holzwarth, A. R. (1988) Kinetic and Energetic Model for the Primary Processes in Photosystem II. *Biophys. J. 54*, 397–405.

(36) Schatz, G. H., Brock, H., and Holzwarth, A. R. (1987) Picosecond kinetics of fluorescence and absorbance changes in photosystem II particles excited at low photon density. *Proc. Natl. Acad. Sci. 84*, 8414–8418.

(37) Vinyard, D. J., Ananyev, G. M., and Charles Dismukes, G. (2013, June) Photosystem II: The reaction center of oxygenic photosynthesis. *Annu. Rev. Biochem.* Annu Rev Biochem.

(38) Kok, B., Forbush, B., and McGloin, M. (1970) Cooperation of Charges in Photosynthetic O_2 Evolution–I. A Linear Four Step Mechanism. *Photochem. Photobiol. 11*, 457–475.

(39) Joliot, P., Barbieri, G., and Chabaud, R. (1969) Un Nouveau Modele Des Centres Photochimiques Du Systeme II. *Photochem. Photobiol. 10*, 309–329.

(40) Klauss, A., Haumann, M., and Dau, H. (2015) Seven steps of alternating electron and proton transfer in photosystem ii water oxidation traced by time-resolved photothermal beam deflection at improved sensitivity. *J. Phys. Chem. B 119*, 2677–2689.

(41) Dau, H., Limberg, C., Reier, T., Risch, M., Roggan, S., and Strasser, P. (2010) The Mechanism of Water Oxidation: From Electrolysis via Homogeneous to Biological Catalysis. *ChemCatChem*. John Wiley & Sons, Ltd.

(42) Vogt, L., Vinyard, D. J., Khan, S., and Brudvig, G. W. (2015) Oxygen-evolving complex of Photosystem II: An analysis of second-shell residues and hydrogen-bonding networks. *Curr. Opin. Chem. Biol.* Elsevier Ltd.

(43) Pérez-Navarro, M., Neese, F., Lubitz, W., Pantazis, D. A., and Cox, N. (2016) Recent developments in biological water oxidation. *Curr. Opin. Chem. Biol.* Elsevier Ltd.

(44) Askerka, M., Brudvig, G. W., and Batista, V. S. (2017) The O_2-Evolving complex of photosystem II: Recent insights from quantum

mechanics/molecular mechanics (QM/MM), extended X-ray absorption fine structure (EXAFS), and femtosecond X-ray crystallography data. *Acc. Chem. Res. 50*, 41–48.

(45) Cox, N., Pantazis, D. A., Neese, F., and Lubitz, W. (2013) Biological water oxidation. *Acc. Chem. Res. 46*, 1588–1596.

(46) Siegbahn, P. E. M. (2013) Water oxidation mechanism in photosystem II, including oxidations, proton release pathways, O-O bond formation and O_2 release. *Biochim. Biophys. Acta - Bioenerg. 1827*, 1003–1019.

(47) Cox, N., and Messinger, J. (2013) Reflections on substrate water and dioxygen formation. *Biochim. Biophys. Acta - Bioenerg. 1827*, 1020–1030.

(48) Cox, N., Pantazis, D. A., Neese, F., and Lubitz, W. (2015) Artificial photosynthesis: Understanding water splitting in nature. *Interface Focus*. Royal Society of London.

(49) Suga, M., Akita, F., Yamashita, K., Nakajima, Y., Ueno, G., Li, H., Yamane, T., Hirata, K., Umena, Y., Yonekura, S., Yu, L. J., Murakami, H., Nomura, T., Kimura, T., Kubo, M., Baba, S., Kumasaka, T., Tono, K., Yabashi, M., Isobe, H., Yamaguchi, K., Yamamoto, M., Ago, H., and Shen, J. R. (2019) An oxyl/oxo mechanism for oxygen-oxygen coupling in PSII revealed by an x-ray free-electron laser. *Science (80-.). 366*, 334–338.

(50) Vogt, L., Ertem, M. Z., Pal, R., Brudvig, G. W., and Batista, V. S. (2015) Computational insights on crystal structures of the oxygen-evolving complex of photosystem II with either Ca^{2+} or Ca^{2+} substituted by Sr^{2+}. *Biochemistry 54*, 820–825.

(51) Bondar, A. N., and Dau, H. (2012) Extended protein/water H-bond networks in photosynthetic water oxidation, in *Biochimica et Biophysica Acta - Bioenergetics*, pp 1177–1190.

(52) Linke, K., and Ho, F. M. (2014) Water in Photosystem II: Structural functional and mechanistic considerations. *Biochim. Biophys. Acta - Bioenerg.*

(53) Vassiliev, S., Zaraiskaya, T., and Bruce, D. (2012) Exploring the energetics of water permeation in photosystem II by multiple steered molecular dynamics simulations. *Biochim. Biophys. Acta - Bioenerg. 1817*, 1671–1678.

(54) Service, R. J., Hillier, W., and Debus, R. J. (2010) Evidence from FTIR difference spectroscopy of an extensive network of hydrogen bonds near the oxygen-evolving Mn4Ca cluster of photosystem II Involving D1-Glu65, D2-Glu312, and D1-Glu329. *Biochemistry 49*, 6655–6669.

(55) Debus, R. J. (2014) Evidence from FTIR difference spectroscopy that D1-Asp61 influences the water reactions of the oxygen-evolving Mn_4CaO_5 cluster of photosystem II. *Biochemistry 53*, 2941–2955.

(56) Dilbeck, P. L., Hwang, H. J., Zaharieva, I., Gerencser, L., Dau, H., and Burnap, R. L. (2012) The D1-D61N mutation in Synechocystis sp. PCC 6803 allows the observation of pH-sensitive intermediates in the formation and release of O_2 from photosystem II. *Biochemistry 51*, 1079–1091.

(57) Lohmiller, T., Krewald, V., Sedoud, A., Rutherford, A. W., Neese, F., Lubitz, W., Pantazis, D. A., and Cox, N. (2017) The First State in the Catalytic Cycle of the Water-Oxidizing Enzyme: Identification of a Water-Derived μ-Hydroxo Bridge. *J. Am. Chem. Soc. 139*, 14412–14424.

(58) Kulik, L. V., Epel, B., Lubitz, W., and Messinger, J. (2007) Electronic structure of the Mn_4O_xCa cluster in the S_0 and S_2 states of the oxygen-evolving complex of photosystem II based on pulse ^{55}Mn-ENDOR and EPR spectroscopy. *J. Am. Chem. Soc. 129*, 13421–13435.

(59) Kulik, L. V., Epel, B., Lubitz, W., and Messinger, J. (2005) ^{55}Mn pulse ENDOR at 34 GHz of the S_0 and S_2 states of the oxygen-evolving complex in photosystem II. *J. Am. Chem. Soc. 127*, 2392–2393.

(60) Haumann, M., Müller, C., Liebisch, P., Iuzzolino, L., Dittmer, J., Grabolle, M., Neisius, T., Meyer-Klaucke, W., and Dau, H. (2005) Structural and oxidation state changes of the photosystem II manganese complex in four transitions of the water oxidation cycle ($S_0 \rightarrow S_1$, $S_1 \rightarrow S_2$, $S_2 \rightarrow S_3$, and $S_{3,4} \rightarrow S_0$) characterized by X-ray absorption spectroscopy at 20 K and room temperature. *Biochemistry 44*, 1894–1908.

(61) Cox, N., Retegan, M., Neese, F., Pantazis, D. A., Boussac, A., and Lubitz, W. (2014) Electronic structure of the oxygen-evolving complex in photosystem II prior to O-O bond formation. *Science (80-.). 345*, 804–808.

(62) Zaharieva, I., Chernev, P., Berggren, G., Anderlund, M., Styring, S., Dau, H., and Haumann, M. (2016) Room-Temperature Energy-Sampling Kβ X-ray

Emission Spectroscopy of the Mn_4Ca Complex of Photosynthesis Reveals Three Manganese-Centered Oxidation Steps and Suggests a Coordination Change Prior to O_2 Formation. *Biochemistry 55*, 4197–4211.

(63) Schuth, N., Zaharieva, I., Chernev, P., Berggren, G., Anderlund, M., Styring, S., Dau, H., and Haumann, M. (2018) Kα X-ray Emission Spectroscopy on the Photosynthetic Oxygen-Evolving Complex Supports Manganese Oxidation and Water Binding in the S3 State. *Inorg. Chem. 57*, 10424–10430.

(64) Pantazis, D. A., Ames, W., Cox, N., Lubitz, W., and Neese, F. (2012) Two interconvertible structures that explain the spectroscopic properties of the oxygen-evolving complex of photosystem II in the S 2 state. *Angew. Chemie - Int. Ed. 51*, 9935–9940.

(65) Yamanaka, S., Isobe, H., Kanda, K., Saito, T., Umena, Y., Kawakami, K., Shen, J. R., Kamiya, N., Okumura, M., Nakamura, H., and Yamaguchi, K. (2011) Possible mechanisms for the O-O bond formation in oxygen evolution reaction at the $CaMn_4O_5(H_2O)_4$ cluster of PSII refined to 1.9 Å X-ray resolution. *Chem. Phys. Lett. 511*, 138–145.

(66) Bovi, D., Narzi, D., and Guidoni, L. (2013) The S_2 State of the oxygen-evolving complex of photosystem-ii explored by QM/MM Dynamics: Spin surfaces and metastable states suggest a reaction path towards the S_3 state. *Angew. Chemie - Int. Ed. 52*, 11744–11749.

(67) Isobe, H., Shoji, M., Yamanaka, S., Umena, Y., Kawakami, K., Kamiya, N., Shen, J. R., and Yamaguchi, K. (2012) Theoretical illumination of water-inserted structures of the $CaMn_4O_5$ cluster in the S_2 and S_3 states of oxygen-evolving complex of photosystem II: Full geometry optimizations by B3LYP hybrid density functional. *Dalt. Trans. 41*, 13727–13740.

(68) Vinyard, D. J., Khan, S., Askerka, M., Batista, V. S., and Brudvig, G. W. (2017) Energetics of the S_2 State Spin Isomers of the Oxygen-Evolving Complex of Photosystem II. *J. Phys. Chem. B 121*, 1020–1025.

(69) Boussac, A., and Rutherford, A. W. (2000) Comparative study of the g=4.1 EPR signals in the S_2 state of photosystem II. *Biochim. Biophys. Acta - Bioenerg. 1457*, 145–156.

(70) Haddy, A. (2007) EPR spectroscopy of the manganese cluster of photosystem II. *Photosynth. Res. 92*, 357–368.

(71) Boussac, A., Rutherford, A. W., and Sugiura, M. (2015) Electron transfer pathways from the S_2-states to the S_3-states either after a Ca^{2+}/Sr^{2+} or a Cl^-/I^- exchange in Photosystem II from Thermosynechococcus elongatus. *Biochim. Biophys. Acta - Bioenerg. 1847*, 576–586.

(72) Boussac, A., Ugur, I., Marion, A., Sugiura, M., Kaila, V. R. I., and Rutherford, A. W. (2018) The low spin - high spin equilibrium in the S_2-state of the water oxidizing enzyme. *Biochim. Biophys. Acta - Bioenerg. 1859*, 342–356.

(73) Boussac, A. (2019) Temperature dependence of the high-spin S_2 to S_3 transition in Photosystem II: Mechanistic consequences. *Biochim. Biophys. Acta - Bioenerg. 1860*, 508–518.

(74) Suga, M., Akita, F., Sugahara, M., Kubo, M., Nakajima, Y., Nakane, T., Yamashita, K., Umena, Y., Nakabayashi, M., Yamane, T., Nakano, T., Suzuki, M., Masuda, T., Inoue, S., Kimura, T., Nomura, T., Yonekura, S., Yu, L. J., Sakamoto, T., Motomura, T., Chen, J. H., Kato, Y., Noguchi, T., Tono, K., Joti, Y., Kameshima, T., Hatsui, T., Nango, E., Tanaka, R., Naitow, H., Matsuura, Y., Yamashita, A., Yamamoto, M., Nureki, O., Yabashi, M., Ishikawa, T., Iwata, S., and Shen, J. R. (2017) Light-induced structural changes and the site of O=O bond formation in PSII caught by XFEL. *Nature 543*, 131–135.

(75) Rapatskiy, L., Cox, N., Savitsky, A., Ames, W. M., Sander, J., Nowaczyk, M. M., Rögner, M., Boussac, A., Neese, F., Messinger, J., and Lubitz, W. (2012) Detection of the water-binding sites of the oxygen-evolving complex of photosystem II using W-band ^{17}O electron-electron double resonance-detected NMR spectroscopy. *J. Am. Chem. Soc. 134*, 16619–16634.

(76) Navarro, M. P., Ames, W. M., Nilsson, H., Lohmiller, T., Pantazis, D. A., Rapatskiy, L., Nowaczyk, M. M., Neese, F., Boussac, A., Messinger, J., Lubitz, W., and Cox, N. (2013) Ammonia binding to the oxygen-evolving complex of photosystem II identifies the solvent-exchangeable oxygen bridge (μ-oxo) of the manganese tetramer. *Proc. Natl. Acad. Sci. U. S. A. 110*, 15561–15566.

(77) Lohmiller, T., Krewald, V., Navarro, M. P., Retegan, M., Rapatskiy, L., Nowaczyk, M. M., Boussac, A., Neese, F., Lubitz, W., Pantazis, D. A., and Cox, N. (2014) Structure, ligands and substrate coordination of the oxygen-evolving complex of photosystem II in the S_2 state: A combined EPR and DFT study. *Phys. Chem. Chem. Phys. 16*, 11877–11892.

(78) Retegan, M., Krewald, V., Mamedov, F., Neese, F., Lubitz, W., Cox, N., and Pantazis, D. A. (2016) A five-coordinate Mn(IV) intermediate in biological

water oxidation: Spectroscopic signature and a pIVot mechanism for water binding. *Chem. Sci. 7*, 72–84.

(79) Askerka, M., Wang, J., Vinyard, D. J., Brudvig, G. W., and Batista, V. S. (2016) S_3 State of the O_2-Evolving Complex of Photosystem II: Insights from QM/MM, EXAFS, and Femtosecond X-ray Diffraction. *Biochemistry 55*, 981–984.

(80) Askerka, M., Vinyard, D. J., Brudvig, G. W., and Batista, V. S. (2015) NH_3 Binding to the S_2 State of the O_2-Evolving Complex of Photosystem II: Analogue to H_2O Binding during the $S_2 \rightarrow S_3$ Transition. *Biochemistry 54*, 5783–5786.

(81) Retegan, M., and Pantazis, D. A. (2016) Interaction of methanol with the oxygen-evolving complex: Atomistic models, channel identification, species dependence, and mechanistic implications. *Chem. Sci.*, pp 6463–6476. Royal Society of Chemistry.

(82) Isobe, H., Shoji, M., Shen, J. R., and Yamaguchi, K. (2015) Strong Coupling between the Hydrogen Bonding Environment and Redox Chemistry during the S_2 to S_3 Transition in the Oxygen-Evolving Complex of Photosystem II. *J. Phys. Chem. B 119*, 13922–13933.

(83) Ugur, I., Rutherford, A. W., and Kaila, V. R. I. (2016) Redox-coupled substrate water reorganization in the active site of Photosystem II - The role of calcium in substrate water delivery. *Biochim. Biophys. Acta - Bioenerg. 1857*, 740–748.

(84) Shoji, M., Isobe, H., and Yamaguchi, K. (2015) QM/MM study of the S_2 to S_3 transition reaction in the oxygen-evolving complex of photosystem II. *Chem. Phys. Lett. 636*, 172–179.

(85) Zscherp, C., and Barth, A. (2001) Reaction-induced infrared difference spectroscopy for the study of protein reaction mechanisms. *Biochemistry 40*, 1875–1883.

(86) Barth, A., and Zscherp, C. (2002, November) What vibrations tell us about proteins. *Q. Rev. Biophys.* Q Rev Biophys.

(87) Noguchi, T., Ono, T. aki, and Inoue, Y. (1992) Detection of Structural Changes upon S_1-to-S_2 Transition in the Oxygen-Evolving Manganese Cluster in

Photosystem II by Light-Induced Fourier Transform Infrared Difference Spectroscopy. *Biochemistry 31*, 5953–5956.

(88) Chu, H. A., Hillier, W., Law, N. A., Sackett, H., Haymond, S., and Babcock, G. T. (2000) Light-induced FTIR difference spectroscopy of the S_2-to-S_3 state transition of the oxygen-evolving complex in Photosystem II. *Biochim. Biophys. Acta - Bioenerg. 1459*, 528–532.

(89) Hillier, W., and Babcock, G. T. (2001) S-state dependent fourier transform infrared difference spectra for the photosystem II oxygen evolving complex. *Biochemistry 40*, 1503–1509.

(90) Noguchi, T., and Sugiura, M. (2001) Flash-induced fourier transform infrared detection of the structural changes during the S-state cycle of the oxygen-evolving complex in photosystem II. *Biochemistry 40*, 1497–1502.

(91) Tammer, M. (2004) G. Sokrates: Infrared and Raman characteristic group frequencies: tables and charts. *Colloid Polym. Sci.* John Wiley & Sons.

(92) Noguchi, T., Ono, T. aki, and Inoue, Y. (1995) Direct detection of a carboxylate bridge between Mn and Ca^{2+} in the photosynthetic oxygen-evolving center by means of Fourier transform infrared spectroscopy. *BBA - Bioenerg. 1228*, 189–200.

(93) Noguchi, T., and Sugiura, M. (2003) Analysis of flash-induced FTIR difference spectra of the S-state cycle in the photosynthetic water-oxidizing complex by uniform ^{15}N and ^{13}C isotope labeling. *Biochemistry 42*, 6035–6042.

(94) Kimura, Y., Mizusawa, N., Ishii, A., Yamanari, T., and Ono, T. A. (2003) Changes of Low-Frequency Vibrational Modes Induced by Universal ^{15}N- and ^{13}C-Isotope Labeling in S_2/S_1 FTIR Difference Spectrum of Oxygen-Evolving Complex. *Biochemistry 42*, 13170–13177.

(95) Yamanari, T., Kimura, Y., Mizusawa, N., Ishii, A., and Ono, T. A. (2004) Mid- to low-frequency fourier transform infrared spectra of S-state cycle for photosynthetic water oxidation in Synechocystis sp. PCC 6803. *Biochemistry 43*, 7479–7490.

(96) Noguchi, T., Ono, T. aki, and Inoue, Y. (1995) A carboxylate ligand interacting with water in the oxygen-evolving center of photosystem II as revealed by Fourier transform infrared spectroscopy. *BBA - Bioenerg. 1232*, 59–66.

(97) Noguchi, T., and Sugiura, M. (2002) FTIR detection of water reactions during the flash-induced S-state cycle of the photosynthetic water-oxidizing complex. *Biochemistry 41*, 15706–15712.

(98) Noguchi, T., Sugiura, M., Inoue, Y., Itoh, K., and Tasumi, M. (1999) FTIR studies on the amino-acid ligands of the photosynthetic oxygen-evolving Mn-cluster, in *Fourier Transform Spectroscopy: Twelfth International Conference*, pp 459–460. Waseda University Press Tokyo.

(99) Chu, H. A., Gardner, M. T., O'Brien, J. P., and Babcock, G. T. (1999) Low-frequency fourier transform infrared spectroscopy of the oxygen- evolving and quinone acceptor complexes in photosystem II. *Biochemistry 38*, 4533–4541.

(100) Chu, H. A., Sackett, H., and Babcock, G. T. (2000) Identification of a Mn-O-Mn cluster vibrational mode of the oxygen-evolving complex in photosystem II by low-frequency FTIR spectroscopy. *Biochemistry 39*, 14371–14376.

(101) Chu, H. A., Hillier, W., Law, N. A., and Babcock, G. T. (2001) Vibrational spectroscopy of the oxygen-evolving complex and of manganese model compounds. *Biochim. Biophys. Acta - Bioenerg. 1503*, 69–82.

(102) Kimura, Y., Ishii, A., Yamanari, T., and Ono, T. A. (2005) Water-sensitive low-frequency vibrations of reaction intermediates during S-state cycling in photosynthetic water oxidation. *Biochemistry 44*, 7613–7622.

(103) Chu, H. A., Debus, R. J., and Babcock, G. T. (2001) D1-Asp170 Is structurally coupled to the oxygen evolving complex in photosystem II as revealed by light-induced fourier transform infrared difference spectroscopy. *Biochemistry 40*, 2312–2316.

(104) Chu, H. A., Gardner, M. T., Hillier, W., and Babcock, G. T. (2000) Low-frequency fourier transform infrared spectroscopy of the oxygen-evolving complex in Photosystem II. *Photosynth. Res. 66*, 57–63.

(105) Zundel, G. (2007) Hydrogen Bonds with Large Proton Polarizability and Proton Transfer Processes in Electrochemistry and Biology, pp 1–217. John Wiley & Sons, Ltd.

(106) Noguchi, T., Suzuki, H., Tsuno, M., Sugiura, M., and Kato, C. (2012) Time-resolved infrared detection of the proton and protein dynamics during photosynthetic oxygen evolution. *Biochemistry 51*, 3205–3214.

(107) Pokhrel, R., Service, R. J., Debus, R. J., and Brudvig, G. W. (2013) Mutation of lysine 317 in the D2 subunit of photosystem II alters chloride binding and proton transport. *Biochemistry 52*, 4758–4773.

(108) Banerjee, G., Ghosh, I., Kim, C. J., Debus, R. J., and Brudvig, G. W. (2018) Substitution of the D1-Asn87 site in photosystem II of cyanobacteria mimics the chloride-binding characteristics of spinach photosystem II. *J. Biol. Chem. 293*, 2487–2497.

(109) Nakamura, S., Ota, K., Shibuya, Y., and Noguchi, T. (2016) Role of a Water Network around the Mn_4CaO_5 Cluster in Photosynthetic Water Oxidation: A Fourier Transform Infrared Spectroscopy and Quantum Mechanics/Molecular Mechanics Calculation Study. *Biochemistry 55*, 597–607.

(110) Kim, C. J., and Debus, R. J. (2017) Evidence from FTIR Difference Spectroscopy That a Substrate H_2O Molecule for O_2 Formation in Photosystem II Is Provided by the Ca Ion of the Catalytic Mn_4CaO_5 Cluster. *Biochemistry 56*, 2558–2570.

(111) Nagao, R., Ueoka-Nakanishi, H., and Noguchi, T. (2017) D1-Asn-298 in photosystem II is involved in a hydrogen-bond network near the redox-active tyrosine Y_Z for proton exit during water oxidation. *J. Biol. Chem. 292*, 20046–20057.

(112) Noguchi, T. (2008) FTIR detection of water reactions in the oxygen-evolving centre of photosystem II. *Philos. Trans. R. Soc. B Biol. Sci. 363*, 1189–1194.

(113) Pokhrel, R., Debus, R. J., and Brudvig, G. W. (2015) Probing the effect of mutations of asparagine 181 in the D1 subunit of photosystem II. *Biochemistry 54*, 1663–1672.

(114) Noguchi, T., and Sugiura, M. (2000) Structure of an active water molecule in the water-oxidizing complex of photosystem II as studied by FTIR spectroscopy. *Biochemistry 39*, 10943–10949.

(115) Shimada, Y., Suzuki, H., Tsuchiya, T., Tomo, T., Noguchi, T., and Mimuro, M. (2009) Effect of a single-amino acid substitution of the 43 kDa chlorophyll protein on the oxygen-evolving reaction of the cyanobacterium Synechocystis sp. PCC 6803: Analysis of the Glu354Gln mutation. *Biochemistry 48*, 6095–6103.

(116) Service, R. J., Yano, J., Dilbeck, P. L., Burnap, R. L., Hillier, W., and Debus, R. J. (2013) Participation of glutamate-333 of the D1 polypeptide in the ligation of the Mn_4CaO_5 cluster in photosystem II. *Biochemistry 52*, 8452–8464.

(117) Suzuki, H., Sugiura, M., and Noguchi, T. (2008) Monitoring water reactions during the S-state cycle of the photosynthetic water-oxidizing center: detection of the DOD bending vibrations by means of Fourier transform infrared spectroscopy. *Biochemistry 47*, 11024–11030.

(118) Debus, R. J. (2015) FTIR studies of metal ligands, networks of hydrogen bonds, and water molecules near the active site Mn_4CaO_5 cluster in Photosystem II. *Biochim. Biophys. Acta - Bioenerg. 1847*, 19–34.

(119) Noguchi, T. (2015) Fourier transform infrared difference and time-resolved infrared detection of the electron and proton transfer dynamics in photosynthetic water oxidation. *Biochim. Biophys. Acta - Bioenerg. 1847*, 35–45.

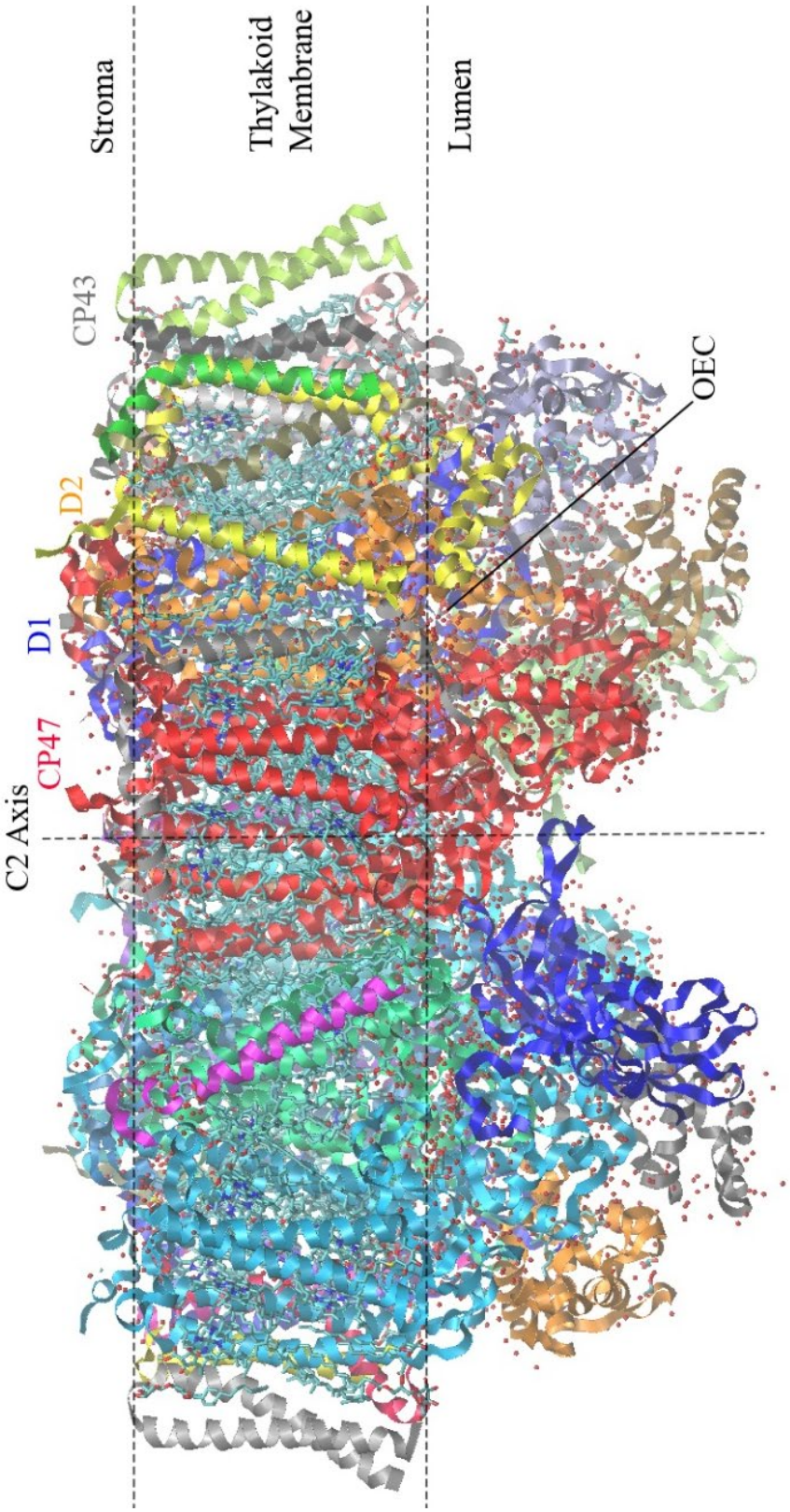
Stroma
Thylakoid Membrane
Lumen
CP43
D2
D1
CP47
C2 Axis
OEC

FIGURE 1.1 View along the membrane plane of PSII. Alpha helices are depicted as ribbons, beta strands as arrows. On the right half, the D1 subunit is depicted in blue, the D2 subunit in orange, the CP43 subunit in gray, the CP47 subunit in red, and water molecules as burgundy dots. Figure was created from the 4UB6 structure *(14)*.

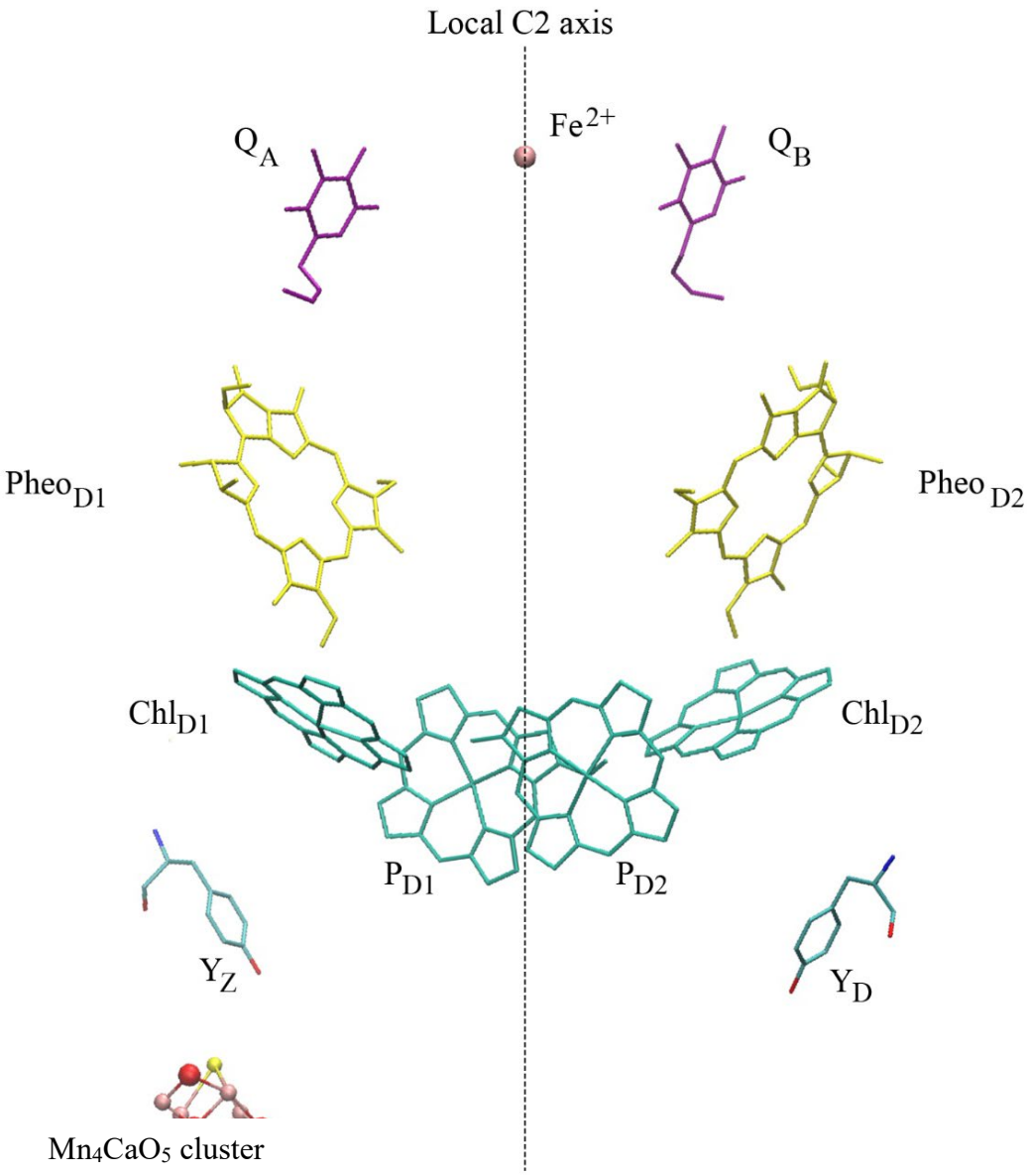

FIGURE 1.2 Key cofactors in the electron transport chain. The hydrophobic tails of chlorophylls, pheophytins, and plastoquinones have been omitted for clarity. Figure was created from the 4UB6 structure *(14)*.

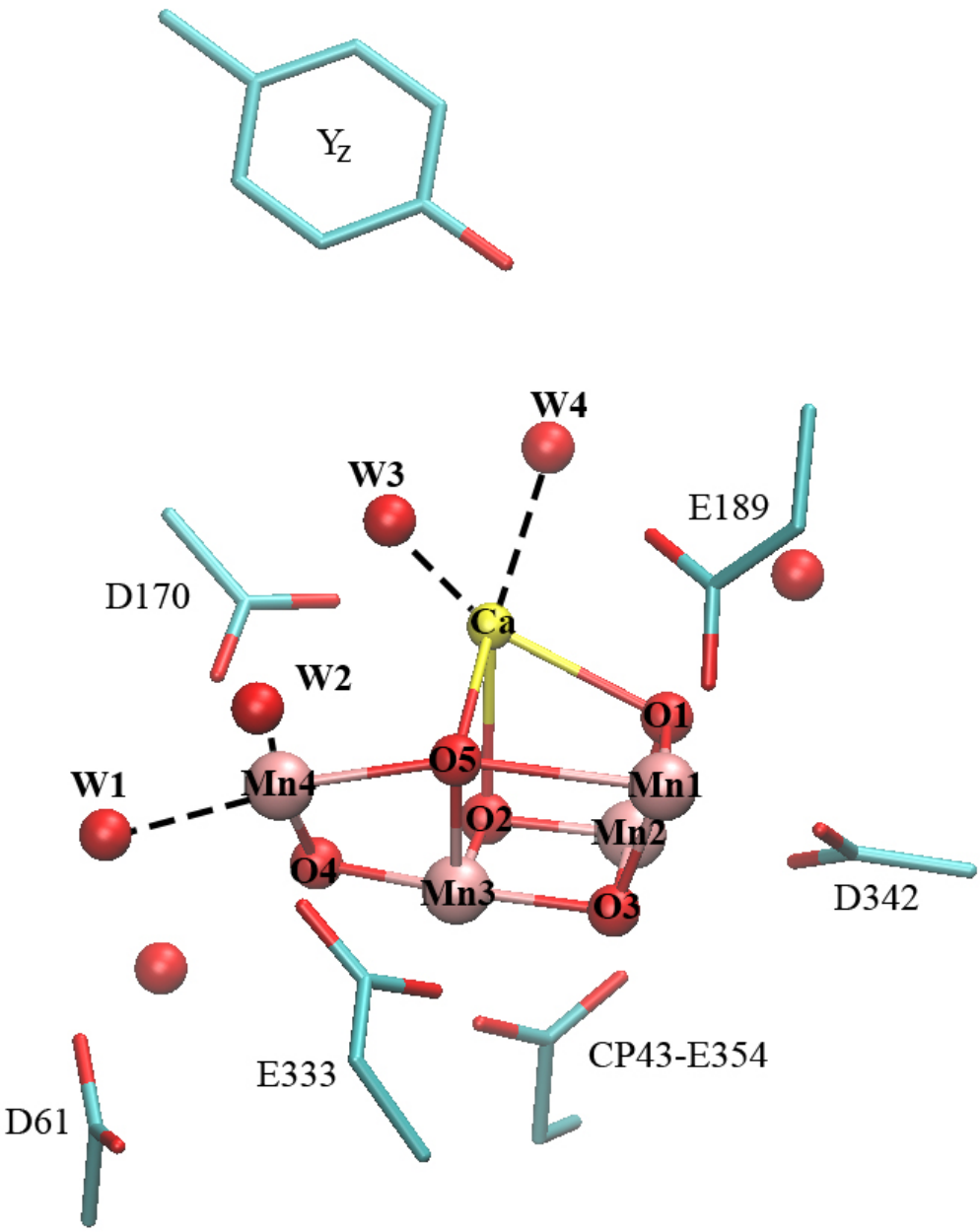

FIGURE 1.3 The Mn_4CaO_5 cluster and its environment. Only selected residues are illustrated. All residues are from the D1-subunit unless otherwise specified. Pink spheres, manganese; yellow sphere, calcium; red spheres, oxygen atoms. Water molecules, W3 and W4, are coordinated to Ca^{2+} and water molecules, W1 and W2, are coordinated to Mn4. Figure was created from the 4UB6 structure *(14)*.

Chapter 2

Evidence from FTIR Difference Spectroscopy that a Substrate H_2O Molecule for O_2 Formation in Photosystem II is Provided by the Ca ion of the Catalytic Mn_4CaO_5 Cluster

2.1 ABSTRACT

The O_2-producing Mn_4CaO_5 catalyst in Photosystem II oxidizes two water molecules (substrate) to produce one O_2 molecule. Considerable evidence supports identifying one of the two substrate waters as the Mn_4CaO_5 cluster's oxo bridge known as O_5. The identity of the second substrate water molecule is less clear. In one set of models, the second substrate is the Mn-bound water molecule known as W2. In another set of models, the second substrate is the Ca^{2+}-bound water molecule known as W3. In all of these models, a deprotonated form of the second substrate moves to a position next to O5 during the catalytic step immediately prior to O-O bond formation. In this study, FTIR difference spectroscopy was employed to identify the vibrational modes of hydrogen-bonded water molecules that are altered by the substituting Sr^{2+} for Ca^{2+}. Our data show that the substitution substantially altered the vibrational modes of only a single water molecule: the water molecule whose D-O-D bending mode is eliminated during the catalytic step immediately prior to O-O bond formation. These data are most consistent with identifying the Ca^{2+}-bound W3 as the second substrate involved in O-O bond formation.

2.2 INTRODUCTION

The light-driven oxidation of water in photosystem II (PSII)[1] produces nearly all of the O_2 on Earth and powers the production of nearly all of Earth's biomass. Photosystem II is an integral membrane protein complex in the thylakoid membranes of cyanobacteria, algae, and plants (*1*-*5*). It is a 700 kDa homodimer *in vivo*. Each monomer contains 20 different subunits and nearly 60 organic and inorganic cofactors. The largest subunits include the membrane-spanning polypeptides CP47, CP43, D2, and D1. These have molecular weights of 56 kDa, 52 kDa, 39 kDa, and 38 kDa, respectively. The O_2-evolving catalytic center consists of an inorganic Mn_4CaO_5 cluster (Figure 2.1). Light-induced separations of charge within PSII drive the accumulation of oxidizing equivalents on this cluster. During each catalytic cycle, the cluster accumulates four oxidizing equivalents, cycling through five oxidation states termed S_n, where "n" denotes the number of oxidizing equivalents that are stored (n = 0 – 4). The S_1 state is predominant in dark-adapted samples. The S_4 state is a transient intermediate. Its formation initiates the utilization of the four stored oxidizing equivalents, the formation of the O-O bond, the release of O_2 and two protons, the re-binding of at least one substrate water molecule, and the regeneration of the S_0 state. An additional proton is released during each of the $S_0 \rightarrow S_1$ and $S_2 \rightarrow S_3$ transitions. The Mn_4CaO_5 cluster thus serves as the interface between one-electron photochemistry and the four-electron/four-proton process of water oxidation/O_2 formation (*6*-*9*).

Recent 1.85 Å (*5*), 1.9 Å, (*1*), and 1.95 Å (*2*) structural models of PSII show that the Mn_4CaO_5 cluster consists of a distorted Mn_3CaO_4 cube and a fourth Mn ion (labeled

Mn4) that is connected to the cube by one of the latter's corner oxo bridges (denoted O5) and by another oxygen bridging ligand (labeled O4). The ligands of the Mn and Ca ions include six carboxylate side chains (five from D1 and one from CP43) and one histidine side chain (from D1). In addition, two water molecules (W1 and W2) coordinate to Mn4 and two others (W3 and W4) coordinate to the Ca^{2+} ion. Networks of hydrogen bonds in the Mn_4CaO_5 cluster's environment efficiently transport protons away from the cluster and permit the access of water. These networks contain many water molecules and form at least three pathways connecting the thylakoid lumen with the cluster, with one including Mn4 and D1-D61, a second including the Ca^{2+} ion and Y_Z, the redox-active tyrosine residue whose radical form, $Y_Z^{\bullet}$, is the immediate oxidant of the Mn_4CaO_5 cluster in each S state, and a third including the Cl^- ion that is located near D2-K317 (*1, 8, 11-13*).

Our understanding of the O_2 formation reaction has improved rapidly over the past five years because of developments in crystallography (e.g., the development of femtosecond crystallography conducted with X-ray free electron lasers) and the interplay between new structural information, computational studies, and advanced biophysical methods including pulsed EPR spectroscopy, X-ray absorbance spectroscopy, and membrane inlet mass spectrometry [for recent reviews, see (*11-19*)]. This interplay has revealed that the Mn_4CaO_5 cluster is conformationally flexible, adopting "open cubane" and "closed cubane" conformations during the S state cycle, and that this conformational flexibility is central to the cluster's function (*20-38*). In the "open cubane" conformation, O5 coordinates to Mn4, forming an oxo bridge linking Mn4 with Mn3. In the "closed cubane" conformation, O5 coordinates to Mn1, forming an oxo bridge linking Mn1 with

Mn3 and forming one vertex of a distorted Mn_3CaO_4 cube. In the S_0 and S_1 states, the "open" conformation is favored, with Mn1 being a Mn(III) ion that has an open coordination position. In the S_2 state, the "open" and closed" conformations are nearly isoenergetic and readily interconvert so that either Mn1 or Mn4 is a five-coordinate Mn(III) ion depending on whether O5 is coordinated to Mn4 or Mn1, respectively. The "closed" conformation of the S_2 state, with Mn4 being five-coordinate, is an obligatory intermediate between the S_2 and S_3 states. During the $S_2 \rightarrow S_3$ transition, the one Mn(III) ion present in the S_2 state undergoes oxidation to Mn(IV) and a water-derived ligand moves from elsewhere on the cluster to join O5 between Mn1 and Mn4, thereby filling the empty Mn coordination position. Powerful evidence supporting the insertion of a water-derived ligand near O5 during the $S_2 \rightarrow S_3$ transition has been provided by a recent pulse EPR/electron-electron double resonance-detected NMR study (*27*) and by a very recent 2.35Å structural model of the S_3 state obtained with femtosecond XFEL crystallography (*39*). Consequently, the S_3 state consists of four six-coordinate Mn(IV) ions. The "open" conformation is favored in the S_3 state.

The two substrate waters are coordinated to the Mn_4CaO_5 cluster by at least the S_2 state (*16, 40, 41*). One of these becomes positioned for the formation of the O-O bond during the regeneration of the S_0 state, whereas the second becomes the water-derived ligand that joins O5 between Mn4 and Mn1 during the $S_2 \rightarrow S_3$ transition. The repositioning of this ligand ensures that the two oxygen atoms that will form the O-O bond are held in close proximity only after the S_3 state is fully formed, thereby preventing deleterious catalase-like activity in the lower S states (*15, 27-35, 42, 43*). The subsequent

formation of the $Y_Z^{\bullet}S_3$ state locks the two oxygen atoms in position for O-O bond formation (*44*). Considerable evidence supports identifying the first substrate molecule (or substrate-derived ligand) with the O5 oxo bridge (*45-47*). The identity of the second substrate water molecule is less clear. In one set of models (*29, 32, 35, 48-50*) [e.g., the "carousel" (*35, 48*) or "pivot" (*32, 49*) models], the second substrate is the Mn4-bound W2. In these models, W2 moves to a position between Mn4 and M1 during the $S_2 \rightarrow S_3$ transition and is replaced by a water molecule (labeled W_x or W_{new} in these models) that had previously formed a hydrogen bond with the O4 oxo bridge. In these models, W_x (or W_{new}) entered the environment of the Mn_4CaO_5 cluster during a previous S state cycle via the chain of water molecules and hydrogen bonds involving D1-D61. In a competing set of models (*23, 33, 51-53*), the second substrate is the Ca^{2+}-bound W3. In these models, W3 deprotonates and moves to a position between Mn4 and Mn1 during the $S_2 \rightarrow S_3$ transition. It is replaced by a nearby water molecule such as W5 (the water molecule that bridges W3 and W2) or the Ca^{2+}-bound W4. In these models, W5 (or W4) entered the environment of the Mn_4CaO_5 cluster during a previous S state cycle via the chain of water molecules and hydrogen bonds involving the Ca^{2+} ion and Y_Z.

Identifying the second substrate water molecule is essential for understanding the molecular mechanism of O_2 formation. In this study, FTIR difference spectroscopy was employed to determine if the second substrate water is the Mn4-bound W2 or the Ca^{2+}-bound W3. FTIR difference spectroscopy is an extremely sensitive probe of structural changes that occur during an enzyme's catalytic cycle (*54-57*). In PSII, the vibrational modes of many functional groups change frequency as the Mn_4CaO_5 cluster advances

through the S state cycle. These include many that have been assigned to carboxylate side chains or hydrogen-bonded water molecules (*58-64*). FTIR difference spectroscopy is particularly suitable for studying hydrogen-bonded water molecules. In PSII, the O–H stretching modes of water molecules that are weakly hydrogen-bonded have been monitored between 3700 and 3500 cm^{-1} (*62, 65-72*), highly polarizable networks of water molecules that are strongly hydrogen-bonded have been monitored between 3200 and 2500 cm^{-1} (*62, 66, 71-73*), and D-O-D bending modes have been monitored near 1210 cm^{-1} (*71, 74*).

Sr^{2+} is the only cation that can competitively replace Ca^{2+} in PSII and support O_2 formation (*75-77*). The substitution of Sr^{2+} for Ca^{2+} produces little change in the structural (*78, 79*) or electronic (*47, 80-82*) properties of the Mn_4CaO_5 cluster, but alters a feature at 606 cm^{-1} in the S_2–S_1 FTIR difference spectrum that corresponds to a Mn–O–Mn cluster mode (*83, 84*). Substituting Sr^{2+} for Ca^{2+} also slows the S state transitions (*76, 85-87*), especially the S_3 to S_0 transition. The substitution also alters the positions of water molecules in the immediate vicinity of the Ca^{2+} ion, especially those of W3, W4, and W5 (*10, 79, 88, 89*). The slowing of the S state transitions by Sr^{2+} has been attributed to the resulting alteration of the hydrogen bond network that links the Ca^{2+} ion and Y_Z with the Cl^- ion and D1-D61 (*10, 62, 79, 81, 90, 91*).

In this study, we examined the FTIR difference spectra of PSII core complexes for water vibrational modes altered by the substitution of Sr^{2+} for Ca^{2+}. Our data are most consistent with identifying W3 as the second substrate that becomes part of the O-O bond.

2.3 MATERIALS AND METHODS

Propagation of Cultures. Large volume cultures of *Synechocystis* sp. PCC 6803 having a hexahistidine tag on CP47 (*92*) were propagated in glass carboys as described earlier (*93*). To prepare Sr-containing PSII core complexes, $CaCl_2$ was replaced by an equivalent concentration of $SrCl_2$ in the growth media (*87, 94*).

Purification of PSII core complexes. Intact, O_2-producing PSII core complexes were purified as described earlier (*71*). For the purification of Sr-containing PSII, all buffers contained $SrCl_2$ instead of $CaCl_2$. The PSII core complexes were isolated in a buffer consisting of 1.2 M betaine, 10% (v/v) glycerol, 50 mM MES-NaOH (pH 6.0), 20 mM $CaCl_2$ or 20 mM $SrCl_2$, 5 mM $MgCl_2$, 50 mM histidine, 1 mM EDTA, and 0.03% (w/v) *n*-dodecyl *β*-D-maltoside. They were concentrated to approx. 1 mg of Chl/mL, flash-frozen in liquid N_2, and stored at −196 °C (vapor phase nitrogen).

Preparation of FTIR samples. Purified PSII core complexes were transferred into a buffer consisting of 40 mM sucrose, 10 mM MES-NaOH (pH 6.0), 5 mM $CaCl_2$ or 5 mM $SrCl_2$, 5 mM NaCl, 0.06% (w/v) *n*-dodecyl β-D-maltoside. They were then concentrated, mixed with 1/10 volume of fresh 100 mM potassium ferricyanide, spread in the center 13 mm of a 25 mm diameter BaF_2 window, and then dried lightly with a stream of dry N_2 gas (*71*). The lightly dried samples were rehydrated and maintained at a relative humidity of 99% by spotting six 1 μL droplets of 20% (v/v) glycerol in water around the window's periphery before a second window was placed on the first with a thin o-ring spacer in between. For samples having natural abundance $H_2{}^{16}O$ exchanged for $D_2{}^{16}O$ or $D_2{}^{18}O$, the lightly dried samples were rehydrated with 20% (v/v) glycerol$(OD)_3$ (98% D, Cambridge

Isotope Laboratories, Inc., Andover, MA) in $D_2{}^{16}O$ (99.9% D, Cambridge Isotope Laboratories, Inc., Andover, MA) or $D_2{}^{18}O$ (98% D, 97% 18O, Cambridge Isotope Laboratories, Inc., Andover, MA), respectively (*71, 74*). Sealed samples were equilibrated in the FTIR sample compartment at 0°C in darkness for 1.5 h, illuminated with 6 pre-flashes, then dark-adapted for 30 min (*71*). For each sample, the absorbance at 1657 cm^{-1} (amide I band) was 0.6 – 1.1.

FTIR Spectroscopy. Spectra were obtained with a Bruker Vertex 70 spectrometer (Bruker Optics, Billerica, MA) containing a pre-amplified, midrange D317 photovoltaic MCT detector (Kolmar Technologies, Inc., Newburyport, MA), as described previously (*71*). After dark adaptation, samples were illuminated at 0°C with six flashes at 13 s intervals. Two transmission spectra were recorded before the first flash and one transmission spectrum was recorded starting 0.33 s after the first and subsequent flashes (each transmission spectrum consisted of 100 scans). The 0.33 s delay allowed for the oxidation of $Q_A{}^{\bullet-}$ by the ferricyanide. The difference spectra of the successive S-state transitions (e.g., S_{n+1}–*minus*–S_n difference spectra, henceforth written $S_{n+1}-S_n$), were obtained by dividing the transmission spectrum obtained after the n^{th} flash by the transmission spectrum obtained immediately before the n^{th} flash, then converting the ratio to units of absorption. The background noise level and the stability of the baseline were obtained by dividing the second pre-flash transmission spectrum by the first and converting the ratio to units of absorption (these spectra are labeled dark−dark in each figure – note that these are control difference spectra obtained *without* a flash being given). The sample was then dark-adapted for 30 min and the cycle was repeated. For each sample, the

illumination cycle was repeated 15 times. The spectra of 30-62 samples were averaged (see figure legends).

Other Procedures. The concentrations of chlorophyll were measured as described earlier (*95*).

2.4 RESULTS

Mid-frequency Region. The mid-frequency difference spectra that were produced by four flash illuminations applied to Ca^{2+}-containing and Sr^{2+}-containing PSII from *Synechocystis* sp. 6803 are compared in Figure 2.2. The spectra produced by the first, second, third, and fourth flashes applied to the Ca^{2+}-containing PSII core complexes (black traces) closely resemble spectra presented previously for PSII purified from *Synechocystis* sp. PCC 6803, *Thermosynechococcus elongatus*, and spinach. These correspond predominantly to the S_2-S_1, S_3-S_2, S_0-S_3, and S_1-S_0 difference spectra, respectively [e.g., refs. (*58, 60, 61, 96-101*)]. The S_2-S_1 spectrum of Sr^{2+}-substituted PSII (upper red trace in Figure 2.2) exhibited significant changes in the symmetric carboxylate stretching [$\nu_{sym}(COO^-)$] region: the positive shoulder near 1434 cm^{-1} was diminished, the 1415(−) cm^{-1} feature was eliminated, the 1400(−) cm^{-1} peak was shifted to 1403 cm^{-1}, a positive feature appeared near 1390 cm^{-1}, and the 1364(+) cm^{-1} feature was diminished substantially. Changes were also observed in the asymmetric carboxylate stretching [$\nu_{asym}(COO^-)$]/amide II region: the 1586(+) cm^{-1} feature and the 1531(+)/1523(–) cm^{-1} derivative feature were diminished substantially. No significant changes were observed in the amide I or carbonyl stretching [ν(C=O)] regions (near 1650cm^{-1} and 1747 cm^{-1}, respectively). Similar changes in the S_2-S_1 spectrum produced by the biosynthetic

substitution of Sr^{2+} for Ca^{2+} have been reported in *Synechocystis* sp. PCC 6803 (*94*) and *Thermosynechococcus elongatus* (*102*) PSII core complexes and in Ca^{2+}-depleted spinach PSII membranes that had been reconstituted with Sr^{2+} (*62, 84, 102-105*).

The substitution of Sr^{2+} for Ca^{2+} induced fewer changes in the S_3-S_2, S_0-S_3, and S_1-S_0 spectra (Figure 2.2, bottom three pairs of spectra). In the S_3-S_2 spectrum, the 1507(+) cm^{-1} feature was enhanced and shifted to 1505 cm^{-1} and the 1495(−) and 1422(−) cm^{-1} features were eliminated. In the S_0-S_3 spectrum, the 1587(−) and 1365(−) cm^{-1} features were eliminated, reversing changes that were observed in the S_2-S_1 spectrum (Figure 2.2, top pair of traces). In the S_1-S_0 spectrum, the 1551(−) cm^{-1} feature was diminished, a positive feature appeared near 1431 cm^{-1}, and the 1411(–) /1395(+) cm^{-1} features were diminished and shifted slightly to higher frequencies. These changes also appear to reverse changes observed in the S_2-S_1 spectrum (Figure 2.2, top pair of spectra). Similar Sr^{2+}-induced changes have been reported in the corresponding spectra of *Thermosynechococcus elongatus* PSII core complexes (*102*) and spinach PSII membranes (*102*). Importantly, the features in the carbonyl stretching [ν(C=O)] regions appeared largely unchanged aside from a slight decrease in the amplitudes of the 1745(+) and 1746 (+) cm^{-1} features in the S_3-S_2 and S_0-S_3 spectra, respectively.

Strongly H-bonded O–H stretching region. The O–H stretching modes of O-H groups that are strongly hydrogen-bonded appear as very broad (positive) features between 3200 and 2500 cm^{-1} (*62, 66, 71-73*). These features, observed in *Synechocystis* sp. PCC 6803 and *Thermosynechococcus elongatus* PSII core complexes and spinach PSII membranes, are diminished or eliminated in the presence of D_2O (*66, 71*). These regions

of the difference spectra of Ca^{2+}-containing and Sr^{2+}-containing PSII from *Synechocystis* are compared in Figure 2.3. In the S_2-S_1 spectrum (Figure 2.3, upper traces), the broad feature is overlain with numerous positive features that correspond to a mixture of C–H stretching from aliphatic groups and N–H stretching from the imidazole group(s) of at least one histidine residues and to its(their) Fermi resonance overtones (*65, 66, 106*). Our data show that substituting Sr^{2+} for Ca^{2+} has no apparent effect on any of the features in this region. In contrast, in the S_2-S_1 spectrum, the broad feature was eliminated in the presence of D_2O (Figure 2.3, blue trace), showing that it corresponds to the O–H stretching modes of strongly hydrogen-bonded O-H groups. Previously, the broad feature in the S_2-S_1 spectrum was shown to be unaltered by the substitution of Sr^{2+} for Ca^{2+} in *Thermosynechococcus elongatus* PSII core complexes [see Figure S5 in ref. (*107*)] and in spinach PSII membranes (*62*).

Weakly Hydrogen-bonded O–H and O–D stretching regions. The O–H stretching modes of O-H groups that are weakly hydrogen-bonded appear between 3700 and 3500 cm^{-1} (*62, 65-69, 71, 72, 74, 108-113*). These features downshift 930-960 cm^{-1} in $D_2{}^{16}O$ and approximately 10 cm^{-1} in $H_2{}^{18}O$ (*65, 66, 71, 109*). These features have been studied in PSII from *Thermosynechococcus elongatus* (*65-67, 74*), *Synechocystis* sp. PCC 6803 (*68, 70-72*), and spinach (*62, 69*). In our Ca^{2+}-containing PSII core complexes, the S_2-S_1 spectrum exhibited a weak 3663(−) cm^{-1} feature, a weak 3619(+) cm^{-1} feature, and a strong 3584(−) cm^{-1} (Figure 2.4, upper black trace). Corresponding features in the O–D region were observed at 2711(–), 2681(+), and 2651(–) cm^{-1} (Figure 2.5, upper black trace). The substitution of Sr^{2+} for Ca^{2+} diminished the 3663(−) cm^{-1} feature, eliminated the 3619(+)

cm^{-1} feature, and slightly upshifted the 3584(−) cm^{-1} feature to 3586 cm^{-1} (upper red trace). Corresponding Sr^{2+}-induced changes were observed in the O–D region of the S_2-S_1 spectrum (Figure 2.5, upper red trace). Slight alterations in the weakly hydrogen-bonded O–H region have been reported in Sr^{2+}-substituted spinach PSII membranes (*62*).

The weakly hydrogen bonded O–H regions of the S_3-S_2, S_0-S_3, and S_1-S_0 spectra in our Ca^{2+}-containing *Synechocystis* PSII core complexes showed broad negative features with minima at approximately 3606, 3620, and 3617 cm^{-1}, respectively (Figure 4, lower black traces). The corresponding negative features in the O–D regions showed minima at approximately 2647, 2676, and 2663 cm^{-1}, respectively (Figure 2.5, lower black traces). The apparent Sr^{2+}-induced decrease in the intensity of the 3606 cm^{-1} feature in the O–H region of the S_3-S_2 spectrum (Figure 2.4, second red trace) may be caused by a baseline shift because a similar Sr^{2+}-induced decrease was not observed in the O–D region (Figure 2.5, second red trace). The substitution of Sr^{2+} for Ca^{2+} produced no significant alterations to the O–H or O–D regions of the S_0-S_3 spectrum (Figures 4 and 5, third set of traces), but may have caused a slight downshift and intensity increase of the 3617 cm^{-1} feature in both the O–H region and in the corresponding O–D region of the S_1-S_0 spectrum (Figures 4 and 5, fourth set of traces).

D-O-D Bending Region. D-O-D bending modes have very weak intensities and are best observed in $D_2{}^{16}O-D_2{}^{18}O$ double-difference spectra (*71, 74*). The mid-frequency difference spectra of Ca-containing PSII hydrated with $D_2{}^{16}O$ or $D_2{}^{18}O$ are compared in Figure 2.7 and the difference spectra of Sr-containing PSII hydrated with $D_2{}^{16}O$ or $D_2{}^{18}O$ are compared in Figure 2.8. In Figure 2.8, the difference spectra of the Sr-containing

samples were multiplied vertically by factors of 1.6 to 2.3 to maximize overlap with the corresponding spectra of the Ca-containing samples (as in Figure 2). To calculate the $D_2{}^{16}O-D_2{}^{18}O$ double-difference spectra, the difference spectra shown in Figures S1 and S2 were subtracted directly. The resulting $S_{n+1}-S_n$ $D_2{}^{16}O-D_2{}^{18}O$ double-difference spectra of Ca^{2+}-containing and Sr^{2+}-substituted *Synechocystis* PSII in the D-O-D bending [δ(DOD)] region are compared in Figure 2.6 (black and red traces, respectively). The double-difference spectra for Ca^{2+}-containing PSII resembled those reported previously for *Thermosynechococcus elongatus* (*74*) and *Synechocystis* sp. PCC 6803 (*71*). In the S_2-S_1 $D_2{}^{16}O-D_2{}^{18}O$ double-difference spectrum, the substitution of Sr^{2+} for Ca^{2+} decreased the amplitudes of the 1211(+) and 1180(+) cm^{-1} features and eliminated the 1149(+) cm^{-1} feature (Figure 2.6, upper pair of traces). In the S_3-S_2 $D_2{}^{16}O-D_2{}^{18}O$ double-difference spectrum, the substitution of Sr^{2+} for Ca^{2+} eliminated the 1239(−) cm^{-1} and the 1224(+) cm^{-1} feature (2nd pair of traces). In the S_0-S_3 $D_2{}^{16}O-D_2{}^{18}O$ double-difference spectrum, the substitution of Sr^{2+} for Ca^{2+} decreased the amplitude of the 1224(+) cm^{-1} feature and appeared to shift the 1242(−) cm^{-1} feature to 1237 cm^{-1} (3rd pair of traces). In the S_1-S_0 $D_2{}^{16}O-D_2{}^{18}O$ double-difference spectrum, the substitution of Sr^{2+} for Ca^{2+} appeared to eliminate the 1213(+) cm^{-1} feature and to increase the amplitudes of the 1199(–) and 1186(+) cm^{-1} features (4th pair of traces).

2.5 DISCUSSION

Carboxylate Residues. Isotopic labeling studies have shown that the features observed in the $S_{n+1}-S_n$ FTIR difference spectra of intact, Ca^{2+}-containing PSII preparations between 1450 and 1300 cm^{-1} correspond to changes in the symmetric COO^-

stretching modes of carboxylate groups and that the features observed between 1600 and 1450 cm^{-1} correspond to changes in the asymmetric COO^- stretching modes of carboxylate groups and amide II (NH bend and CN stretch) modes from the polypeptide backbone (*97, 98, 114*). In addition, changes to histidyl modes have been observed between 1120 and 1090 cm^{-1} (*106, 115*) and changes in the CN and NH_2 vibrations of a protonated Arg group (attributed to CP43-Arg357) have been observed between 1700 and 1550 cm^{-1} (*116*). The Sr^{2+}-induced changes to the mid-frequency difference spectra reported in this study (Figure 2.2) resemble those reported previously in Sr^{2+}-substituted PSII from *Synechocystis* sp. PCC 6803, *Thermosynechococcus elongatus*, and spinach (*62, 84, 94, 102-105*). These Sr^{2+}-induced perturbations have been interpreted as changes to the $\nu_{sym}(COO^-)$ modes of multiple carboxylate groups that ligate the Mn_4CaO_5 cluster (*94, 102*). These altered carboxylate ligands do not include the C-terminus of the D1 subunit (at D1-A344) because experiments performed with L-[1-^{13}C]alanine demonstrated that the $\nu_{sym}(COO^-)$ mode of D1-A344 does not change when Sr^{2+} substitutes for Ca^{2+} (*94*). The histidyl modes between 1120 and 1090 cm^{-1} also do not change when Sr^{2+} substitutes for Ca^{2+} (*102*).

Recently, the $\nu_{sym}(COO^-)$ region of the S_2-S_1 spectrum was simulated on the basis of QM/MM methodology (*63*). The QM region used in the analysis included the Mn_4CaO_5 cluster, Y_Z, the cluster's six carboxylate and single histidine protein ligands, additional residues that interact with these ligands or Y_Z (i.e., D1-D61, D1-H190, D1-H337, CP43-R357), and fifteen water molecules including W1, W2, W3, W4 and others that participate in a hydrogen-bond network located between D1-D61, the Ca^{2+} ion, and Y_Z. It was concluded that the $\nu_{sym}(COO^-)$ modes of the carboxylate groups that were included in the

QM region (including D1-D61) are strongly coupled. Consequently, it was concluded that multiple carboxylate groups contribute to most of the features in the $\nu_{sym}(COO^-)$ region of the S_2-S_1 spectrum (*63*)[2]. For example, in the simulated spectrum, the 1364(+) cm^{-1} feature that is diminished by Sr^{2+} substitution is comprised primarily of contributions from D1-E189 and D1-E354, with minor contributions from D1-D61, D1-D170, and D1-E189 (*63*).

The only substantial Sr^{2+}-induced change in the amide I and $\nu_{asym}(COO^-)$/amide II regions of the mid-frequency difference spectra is the diminished 1586(+) cm^{-1} feature in the S_2-S_1 spectrum and the corresponding decreased amplitude of the 1587(−) cm^{-1} feature in the S_0-S_3 spectrum (Figure 2.2). This feature corresponds to a $\nu_{asym}(COO^-)$ mode because it shifts 30 – 35 cm^{-1} in samples that are globally labeled with ^{13}C (*97, 98, 114, 124*) and is largely insensitive to global labeling with ^{15}N (*97, 98, 114, 122, 125*). The absence of significant Sr^{2+}-induced changes to the amide I and amide II modes in the mid-frequency $S_{n+1}-S_n$ spectra implies that the substitution of Sr^{2+} for Ca^{2+} produced little or no change in the protein structure that surrounds the Mn_4CaO_5 cluster. This conclusion correlates with magnetic resonance studies showing that the substitution produces little change in the cluster's electronic properties (*47, 80-82*) and with X-ray crystallographic (*79*), X-ray absorption (*78*), and computational (*10, 88, 89*) studies showing that the substitution produces little change in the structure of the Mn_4CaO_5 cluster or its surroundings.

Networks of H-bonds. Features in the ν(C=O) region of COOH groups in the $S_{n+1}-S_n$ spectra are probes of extensive hydrogen bond networks in the Mn_4CaO_5 cluster's environment (*60, 121, 123*). The 1747(−) cm^{-1} feature in the S_2-S_1 spectrum has been

identified with a carboxylate residue whose pK_a value decreases because of the charge that forms on the Mn_4CaO_5 cluster during the $S_1 \rightarrow S_2$ transition. This feature is diminished or eliminated by the D1-D61A, D1-E65A, D1-E329Q, D1-R334A, and D2-E312A mutations, and by overly dehydrating samples, providing evidence for an extensive hydrogen bond network extending over at least 20 Å (*71, 121, 123*). The small 1745(+) cm^{-1} feature in the S_3-S_2 spectrum has been identified with a carboxylate residue whose pK_a value increases because of structural changes that occur during the $S_2 \rightarrow S_3$ transition. This feature is altered by the D1-D61A mutation and eliminated by D1-Q165E and D1-E329Q mutations, providing evidence for another hydrogen bond network extending over at least 13 Å (*71, 123*). Elements of these networks may exist only transiently. The 1747(–) cm^{-1} and small 1745(+) cm^{-1} features appear to be reversed during the S_3 to S_0 transition, resulting in a 1746(+) cm^{-1} feature in the S_0-S_3 spectrum (*123*). Substituting Sr^{2+} for Ca^{2+} only slightly diminished the amplitudes of the 1747(–) cm^{-1} and 1745(+) cm^{-1} features in the S_2-S_1 and S_3-S_2 spectra, respectively, implying that the networks of hydrogen bonds probed by these features were largely unaffected by the substitution.

Hydrogen-bonded Water Molecules. Recently, the hydrogen-bonded O-H stretching regions of the S_2-S_1 spectrum were simulated with QM/MM methods (*62*). On the basis of these simulations, the broad positive feature observed between 3200 and 2500 cm^{-1} was assigned to the coupled O-H stretching modes of strongly hydrogen-bonded water molecules in the network of hydrogen bonds that links D1-D61 with the Ca^{2+} ion and Y_Z (*62*). This feature is dominated by the O-H stretching modes of W1 and W2 (*62*). The feature is positive because the hydrogen bonds of W1, W2, and the other water molecules

are strengthened by the charge that forms on the Mn_4CaO_5 cluster during the $S_1 \rightarrow S_2$ transition (*62*). This strengthening shifts the O-H stretching modes to lower frequencies. The positive features in the other $S_{n+1}-S_n$ spectra were assigned previously to the O-H stretching modes of strongly hydrogen-bonded waters in networks of hydrogen bonds that are highly polarizable (*66, 73*). The absence of Sr^{2+}-changes in these regions of the $S_{n+1}-S_n$ difference spectra implies that the substituting Sr^{2+} for Ca^{2+} has limited influence on networks of hydrogen bonds near W1 and W2. In contrast, the mutation D1-D61A eliminated the broad feature from the S_2-S_1 spectrum (*71*), consistent with the hydrogen bond that exits between this residue and W1 in the recent crystallographic structural models (*1, 2, 5*).

The QM/MM-based simulations mentioned in the previous paragraph assigned the features between 3700 and 3500 cm^{-1} in the S_2-S_1 spectrum to the coupled O-H stretching vibrations of *weakly* hydrogen-bonded water molecules in the network of hydrogen bonds that links D1-D61 with the Ca^{2+} ion and Y_Z (*62*). The features observed in the other $S_{n+1}-S_n$ spectra in this region are presumed to have the same origin (*66, 67*). Consequently, these features contain contributions from multiple water molecules. The D1-N181A mutation diminished and the D1-D61A and D1-E333Q mutations eliminated the 3663(−) cm^{-1} feature from the S_2-S_1 spectrum (*70-72*). The D1-D61A mutation also altered the broad 3606(−) cm^{-1} feature in the S_3-S_2 spectrum (*71*). Consequently, the D1-D61, D1-N181, and D1-E333 mutations influence the hydrogen bond network that connects D1-D61 with the Ca^{2+} ion and Y_Z. In the S_2-S_1 spectrum of Sr^{2+}-substituted PSII core complexes, the 3663(−) cm^{-1} feature was sharply diminished and the 3619(+) cm^{-1} feature was eliminated.

These alterations are consistent with Sr^{2+}-substitution causing slight perturbations in this network. These alterations are consistent with the crystallographic (*79*) and computational (*10, 88, 89*) studies showing that the substitution of Sr^{2+} for Ca^{2+} alters primarily the positions of W3, W4, and W5.

The D-O-D bending region. In a $D_2{}^{16}O-D_2{}^{18}O$ double-difference spectrum, the alteration of a single δ(DOD) mode is manifested by the appearance of four peaks, two from $D_2{}^{16}O$ and two from $D_2{}^{18}O$, although the number of peaks observed may be fewer because some features may overlap, thereby canceling their respective intensities. The number of features present in the $D_2{}^{16}O-D_2{}^{18}O$ double-difference spectrum corresponding to the $S_1 \rightarrow S_2$ transition (Figure 2.6, upper pair of traces) imply that the δ(DOD) modes of at least two D_2O molecules are altered during this transition (*71, 74*). For most of these features, the amplitude oscillates during the S state cycle. For example, the large 1211(+) cm^{-1} feature in the S_2-S_1 double-difference spectrum is negative (at 1211-1214 cm^{-1}) in the S_3-S_2 and S_0-S_3 double-difference spectra, and positive again (at 1213 cm^{-1}) in the S_1-S_0 double-difference spectrum. As another example, the large 1223(−) cm^{-1} feature in the S_2-S_1 double-difference spectrum is positive (at 1224 cm^{-1}) in the S_3-S_2 and S_0-S_3 double-difference spectra. These oscillations imply that the δ(DOD) modes that are altered during the S_1 to S_2 transition are altered reversibly during the S state cycle (*71, 74*). The D1-D61A mutation eliminates the 1223(–), 1211(+), and 1180(+) features from the $D_2{}^{16}O-D_2{}^{18}O$ double-difference spectrum of the $S_1 \rightarrow S_2$ transition (*71*). Consequently, one of the water molecules whose δ(DOD) mode changes reversibly during the S state cycle must interact with D1-D61 (*71*). The substitution of Sr^{2+} for Ca^{2+} produced little change in the

frequencies of the δ(DOD) modes observed in the $D_2{}^{16}O-D_2{}^{18}O$ double-difference spectrum of the $S_1 \rightarrow S_2$ transition (Figure 2.6, top traces), implying that the D_2O molecules whose δ(DOD) modes change reversibly during the S state cycle do not interact with the Ca^{2+} ion.

The most substantial Sr^{2+}-induced changes in the $D_2{}^{16}O-D_2{}^{18}O$ double-difference spectrum of the $S_2 \rightarrow S_3$ transition (Figure 2.6, second pair of traces) were the elimination of the 1239(−) and 1224(+) cm^{-1} features. The latter feature appears to correspond to the 1223(–) and 1224(+) cm^{-1} features in the S_2-S_1 and S_0-S_3 double-difference spectra, respectively. Consequently, the elimination of the 1239(–) and 1224(+) cm^{-1} features from the S_3-S_2 double-difference spectrum likely results from a Sr^{2+}-induced downshift of the 1239(–) cm^{-1} feature to 1224 cm^{-1}. In the S_0-S_3 double-difference spectrum (Figure 2.6, middle pair of traces), the substitution of Sr^{2+} for Ca^{2+} appears to downshift the 1242(−) cm^{-1} feature to 1237 cm^{-1}.

In Ca^{2+}-containing PSII core complexes, the 1239(−) and 1242(−) cm^{-1} features in the S_3-S_2 and S_0-S_3 double-difference spectra have no positive counterparts in the other double-difference spectra. This has been observed previously (*71, 74*). The absence of positive counterparts implies that the δ(DOD) mode of one water molecule is eliminated during each of the $S_2 \rightarrow S_3$ and $S_3 \rightarrow S_0$ transitions (*74*). The 1239(–) and 1242(–) cm^{-1} features may correspond to water molecules that undergo deprotonation during these transitions. However, during one or both of these transitions, the feature may correspond to the δ(DOD) mode of a water molecule that physically replaces the water molecule that underwent deprotonation.

In the 2.1 Å crystallographic structural model of Sr^{2+}-substituted PSII, W3 is the only water molecule whose position is altered substantially compared to its position in Ca^{2+}-containing PSII (*79*): the Sr^{2+}-W3 distance is 0.2-0.3 Å longer than the corresponding Ca^{2+}-W3 distance. Recent DFT (*88*) and QM/MM (*10, 89*) studies confirm the substantial Sr^{2+}-shift of W3, but also predict a substantial Sr^{2+}-induced shift in the positions of W4 (*10, 88, 89*) and W5 (*10*). The frequencies of δ(HOH) and δ(DOD) modes depend on the metal coordination (*126*) and hydrogen bonding environment (*127, 128*) of the water molecule. Consequently, those water molecules whose positions shift substantially in response to Sr^{2+}-substitution are likely to exhibit substantially altered δ(DOD) modes. In our data, the only water molecule whose δ(DOD) mode is altered substantially by substituting Sr^{2+} for Ca^{2+} is the water molecule whose δ(DOD) mode is eliminated during the $S_2 \rightarrow S_3$ transition. Consequently, we conclude that this water molecule corresponds to W3, W4, or W5. This conclusion is far more consistent with models identifying the second substrate water molecule as the Ca^{2+}-bound W3 (*23, 33, 51-53*) than with models identifying the second substrate water molecule as the Mn4-bound W2 (*29, 32, 35, 48-50*): the position of the Mn4-bound W2 is not altered substantially by the substitution of Sr^{2+} by Ca^{2+} in either the crystallographic or computational analyses. Consequently, our data support identifying W3 as the substrate molecule that deprotonates and moves to a position next to O5 between Mn4 and Mn1 during the $S_2 \rightarrow S_3$ transition as a prelude to O-O bond formation during the $S_3 \rightarrow S_4 \rightarrow S_0$ transition. The coordination position on Ca^{2+} vacated by W3 is unlikely to remain vacant. We suggest that W5 replaces W3 as a ligand to Ca^{2+} during the $S_2 \rightarrow S_3$ transition, as proposed in a recent DFT study (*33*). If this suggestion is

correct, the δ(DOD) mode of W5 would be eliminated during the $S_2 \rightarrow S_3$ transition and correspond to the 1239(−) cm^{-1} feature in the S_3-S_2 double-difference spectrum.

Movement of W3 and its replacement by W5 correlates with the conclusion of a recent time-resolved FTIR study of the $S_2 \rightarrow S_3$ transition that appeared while the current study was under review (*129*). Both this time-resolved FTIR study (*129*) and a recent time-resolved X-ray absorption study (*130*) showed that the $S_2 \rightarrow S_3$ transition involves rearrangements in a hydrogen bond network that includes the Mn_4CaO_4 cluster and its ligation environment. Changes in the positions of water molecules near the Mn_4CaO_5 cluster were also observed in the recent femtosecond XFEL crystallography study of the S_3 state (*39*). The time-resolved FTIR study showed that the $S_2 \rightarrow S_3$ transition includes a ~ 100 μsec phase that takes place before electron transfer and that represents changes to the C-O stretching mode of $Y_Z^{\bullet}$ (evidence for of strengthened hydrogen bond interaction with $Y_Z^{\bullet}$) in addition to changes in $\nu_{sym}(COO^-)$ modes of carboxylate groups and the O-H stretching modes of hydrogen bonded waters. The authors concluded that the ~ 100 μsec phase involves the rearrangement/reorientation of water molecules in a hydrogen bond network that includes both Y_Z and the Mn_4CaO_5 cluster, consistent with the movement of W3 to a position near O5 and the replacement of W3 by another water molecule in the network (*129*).

The 1242(−) cm^{-1} feature in the S_0-S_3 double-difference spectra may correspond to the water molecule that replaces O5 during the regeneration of the S_0 state, deprotonating in the process to form a hydroxo bridge between Mn4 and Mn1 (*30, 131*). However, if this water molecule is W5 (now bound to Ca^{2+} as a new "W3") as suggested in a recent DFT

study (*33*), it would likely be replaced on Ca^{2+} in turn by another water molecule that remains unidentified but is only slightly perturbed by the substitution of Sr^{2+} for Ca^{2+} because the 1242(−) cm^{-1} feature in the S_0−S_3 double-difference spectrum was shifted only 5 cm^{-1} by the substitution of Sr^{2+} for Ca^{2+}.

An outstanding question is why the negative features observed at 1242 cm^{-1} have no corresponding positive features in the other S state spectra. The $S_3 \rightarrow S_4 \rightarrow S_0$ transition is a multistep process that involves the rearrangement of networks of hydrogen bonds as O_2 is formed and released and at least one substrate water re-binds (*130, 132*). The many reorientations of water molecules during this transition may obscure the positive counterparts of the negative 1242 cm^{-1} features.

2.6 SUMMARY AND CONCLUSIONS

The substitution of Sr^{2+} for Ca^{2+} produced little or no perturbation to the polypeptide backbone and caused only slight perturbations to the carboxylate groups and hydrogen bond networks that surround the Mn_4CaO_5 cluster. The substitution of Sr^{2+} for Ca^{2+} substantially altered the δ(DOD) mode of only the water molecule whose δ(DOD) mode is eliminated during the $S_2 \rightarrow S_3$ transition. Because W3, W4, and W5 are the only water molecules whose positions are altered substantially in the crystallographic and computational studies of Sr^{2+}-substituted PSII, we conclude that W3 is the substrate water molecule that moves in deprotonated form to a position next to O5 between Mn4 and Mn1 during the S_2 to S_3 transition. Finally, we suggest that W5 moves to the coordination position on Ca^{2+} vacated by W3, in agreement with one of the conclusions of a recent DFT study.

2.7 ACKNOWLEDGEMENTS

The authors thank Anh P. Nguyen for growing the *Synechocystis* cells and helping with the purification of the PSII core complexes and thank V. S. Batista and coworkers for providing the QM/MM-optimized coordinates for the Mn_4CaO_5 and Mn_4SrO_5 clusters and their environments.

2.8 ADDITIONAL NOTES

[1]*Abbreviations:* Chl, chlorophyll; DCMU, 3-(3,4-dichlorophenyl)-1,1-dimethylurea; EDTA, ethylenediaminetetraacetic acid; EPR, electron paramagnetic resonance; EXAFS, extended X-ray absorption fine structure; FTIR, Fourier transform infrared; MES, 2-(N-morpholino)-ethanesulfonic acid; P_{680}, chlorophyll multimer that serves as the light-induced electron donor in PSII; PSII, photosystem II; Q_A, primary plastoquinone electron acceptor; XFEL, X-ray free electron laser; Y_Z, tyrosine residue that mediates electron transfer between the Mn_4O_5Ca cluster and $P_{680}^{+\bullet}$.

[2]The simulated $S_2{-}S_1$ FTIR difference spectra in ref. (*63*) disagree with earlier studies showing that the D1-D170H (*117, 118*), D1-E189Q (*119, 120*), D1-E189R (*120*), D1-E333Q (*70*), and D1-D342N (*93*) mutations produce little or no changes to the mid-frequency difference spectra of any of the S state transitions. The absence of mutation-induced changes in these studies was not the result of mutants losing their mutation: the integrity of each 21-liter culture propagated for the purification of mutation-bearing PSII was verified by extracting genomic DNA from an aliquot of the 21-liter culture, then amplifying and sequencing the target gene. Furthermore, features in the $S_2{-}S_1$ spectrum between 650 and 550 cm^{-1}, particularly a 606(+) cm^{-1} feature assigned to a Mn–O–Mn

cluster mode (*83, 84*), were altered by the D1-D170H (*117*) and D1-E189Q (*119*) mutations. Finally, mutations constructed at residues 5 – 11 Å from the closest Mn ion and outside the QM region examined in ref. (*63*) (e.g., D1-E65A, D1-Q165E, D1-N181A, D1-R334A, D2-E312A, and D2-K317A), cause numerous changes in the $\nu_{sym}(COO^{-})$ region of the $S_2{-}S_1$ spectrum (*72, 121-123*). Additional work will be required to understand the discrepancy between the spectral simulations in ref. (*63*) and the earlier mutagenesis studies.

2.9 REFERENCES

(1) Umena, Y., Kawakami, K., Shen, J.-R., and Kamiya, N. (2011) Crystal Structure of Oxygen-Evolving Photosystem II at a Resolution of 1.9 Å, *Nature 473*, 55-60.

(2) Suga, M., Akita, F., Hirata, K., Ueno, G., Murakami, H., Nakajima, Y., Shimizu, T., Yamashita, K., Yamamoto, M., Ago, H., and Shen, J.-R. (2015) Native structure of photosystem II at 1.95 Å resolution viewed by femtosecond X-ray pulses, *Nature 517*, 99-103.

(3) Ago, H., Adachi, H., Umena, Y., Tashiro, T., Kawakami, K., Kamiya, N., Tian, L., Han, G., Kuang, T., Liu, Z., Wang, F., Zou, H., Enami, I., Miyano, M., and Shen, J.-R. (2016) Novel Features of Eukaryotic Photosystem II Revealed by Its Crystal Structure Analysis from a Red Alga, *J. Biol. Chem. 291*, 5676-5687.

(4) Wei, X., Su, X., Cao, P., Liu, X., Chang, W., Li, M., Zhang, X., and Liu, Z. (2016) Structure of spinach photosystem II-LHII supercomplex at 3.2 Å resolution, *Nature 534*, 69-74.

(5) Tanaka, A., Fukushi, Y., and Kamiya, N. (2017) Two Different Structures of the Oxygen-Evolving Complex in the Same Polypeptide Frameworks of Photosystem II, *J. Am. Chem. Soc. 139*, 1718-1721.

(6) Messinger, J., Noguchi, T., and Yano, J. (2012) Photosynthetic O_2 Evolution, in *Molecular Solar Fuels* (Wydrzynski, T. and Hillier, W., Eds.) pp 163-207, Royal Society of Chemistry, Cambridge, UK.

(7) Vinyard, D. J., Ananyev, G. M., and Dismukes, G. C. (2013) Photosystem II: The Reaction Center of Oxygenic Photosynthesis, *Annu. Rev. Biochem. 82*, 577-606.

(8) Shen, J.-R. (2015) The Structure of Photosystem II and the Mechanism of Water Oxidation in Photosynthesis, *Annu. Rev. Plant Biol. 66*, 23-48.

(9) Krewald, V., Retegan, M., and Pantazis, D. A. (2016) Principles of Natural Photosynthesis, *Top. Curr. Chem. 371*, 23-48.

(10) Vogt, L., Ertem, M. Z., Pal, R., Brudvig, G. W., and Batista, V. S. (2015) Computational insights on crystal structures of the oxygen-evolving complex of photosystem II with either Ca^{2+} or Ca^{2+} substituted by Sr^{2+}, *Biochemistry 54*, 820-825.

(11) Vogt, L., Vinyard, D. J., Khan, S., and Brudvig, G. W. (2015) Oxygen-evolving complex of Photosystem II: an analysis of second-shell residues and hydrogen-bonding networks, *Curr. Opin. Chem. Biol. 25*, 152-158.

(12) Pérez-Navarro, M., Neese, F., Lubitz, W., Pantazis, D. A., and Cox, N. (2016) Recent developments in biological water oxidation, *Curr. Opin. Chem. Biol. 31*, 113-119.

(13) Askerka, M., Brudvig, G. W., and Batista, V. S. (2017) The O_2-Evolving Complex of Photosystem II: Recent Insights from Quantum Mechanics/Molecular Mechanics (QM/MM), Extended X-ray Absorption Fine Structure (EXAFS), and Femtosecond X-ray Crystallography Data, *Acc. Chem. Res. 50*, 41-48.

(14) Cox, N., Pantazis, D. A., Neese, F., and Lubitz, W. (2013) Biological Water Oxidation, *Acc. Chem. Res. 46*, 1588-1596.

(15) Siegbahn, P. E. M. (2013) Water oxidation mechanism in photosystem II, including oxidations, proton release pathways, O-O bond formation and O_2 release, *Biochim. Biophys. Acta 1827*, 1003-1019.

(16) Cox, N. and Messinger, J. (2013) Reflections on substrate water and dioxygen formation, *Biochim. Biophys. Acta 1827*, 1020-1030.

(17) Yano, J. and Yachandra, V. K. (2014) Mn_4Ca Cluster in Photosynthesis: Where and How Water is Oxidized to Dioxygen, *Chem. Rev. 114*, 4175-4250.

(18) Cox, N., Pantazis, D. A., Neese, F., and Lubitz, W. (2015) Artificial photosynthesis: understanding water splitting in nature, *Interface Focus 5*, -20150009.

(19) Krewald, V., Neese, F., and Pantazis, D. A. (2015) Resolving the Manganese Oxidation States in the Oxygen-evolving Catalyst of Natural Photosynthesis, *Isr. J. Chem. 55*, 1219-1232.

(20) Pantazis, D. A., Ames, W., Cox, N., Lubitz, W., and Neese, F. (2012) Two Interconvertable Structures that Explain the Spectroscopic Properties of the Oxygen-Evolving Complex of Photosystem II in the S_2 State, *Angew. Chem. Int. Ed. 51*, 9935-9940.

(21) Isobe, H., Shoji, M., Yamanaka, S., Umena, Y., Kawakami, K., Kamiya, N., Shen, J.-R., and Yamaguchi, K. (2012) Theoretical illumination of water-inserted structures of the $CaMn_4O_5$ cluster in the S_2 and S_3 states of oxygen-

evolving complex of photosystem II: full geometry optimizations by B3LYP hybrid density functional, *Dalton Trans. 41*, 13727-13740.

(22) Glöckner, C., Kern, J., Broser, M., Zouni, A., Yachandra, V. K., and Yano, J. (2013) Structural Changes of the Oxygen-evolving Complex in Photosystem II during the Catalytic Cycle, *J. Biol. Chem. 288*, 22607-22620.

(23) Bovi, D., Narzi, D., and Guidoni, L. (2013) The S_2 State of the Oxygen-Evolving Complex of Photosystem II Explored by QM/MM Dynamics: Spin Surfaces and Metastable States Suggest a Reaction Path Towards the S_3 State, *Angew. Chem. Int. Ed. 52*, 11744-11749.

(24) Saito, K. and Ishikita, H. (2014) Influence of the Ca^{2+} ion on the Mn_4Ca conformation and the H-bond network arrangement in Photosystem II, *Biochim. Biophys. Acta 1837*, 159-166.

(25) Retegan, M., Cox, N., Lubitz, W., Neese, F., and Pantazis, D. A. (2014) The first tyrosyl radical intermediate formed in the S_2-S_3 transition of photosystem II, *Phys. Chem. Chem. Phys. 16*, 11901-11910.

(26) Isobe, H., Shoji, M., Yamanaka, S., Mino, H., Umena, Y., Kawakami, K., Kamiya, N., Shen, J.-R., and Yamaguchi, K. (2014) Generalized approximate spin projection calculations of effective exchange integrals of the $CaMn_4O_5$ cluster in the S_1 and S_3 states of the oxygen evolving complex of photosystem II, *Phys. Chem. Chem. Phys. 16*, 11911-11923.

(27) Cox, N., Retegan, M., Neese, F., Pantazis, D. A., Boussac, A., and Lubitz, W. (2014) Electronic structure of the oxygen-evolving complex in photosystem II prior to O-O bond formation, *Science 345*, 804-808.

(28) Narzi, D., Bovi, D., and Guidoni, L. (2014) Pathway for Mn-cluster oxidation by tyrosine-Z in the S_2 state of photosystem II, *Proc. Natl. Acad. Sci. USA 111*, 8723-8728.

(29) Capone, M., Bovi, D., Narzi, D., and Guidoni, L. (2016) Reorganization of Substrate Waters between the Closed and Open Cubane Conformers during the S_2 to S_3 Transition in the Oxygen Evolving Complex, *Biochemistry 54*, 6439-6442.

(30) Krewald, V., Retegan, M., Cox, N., Messinger, J., Lubitz, W., DeBeer, S., Neese, F., and Pantazis, D. A. (2015) Metal oxidation states in biological water splitting, *Chem. Sci. 6*, 1676-1695.

(31) Isobe, H., Shoji, M., Shen, J.-R., and Yamaguchi, K. (2015) Chemical Equlibrium Models for the S_3 State of the Oxygen-Evolving Complex of Photosystem II, *Inorg. Chem. 55*, 502-511.

(32) Retegan, M., Krewald, V., Mamedov, F., Neese, F., Lubitz, W., Cox, N., and Pantazis, D. A. (2016) A five-coordinate Mn(IV) intermediate in biological water oxidation: spectroscopic signature and a pivot mechanism for water binding, *Chem. Sci. 7*, 72-84.

(33) Ugur, I., Rutherford, A. W., and Kaila, V. R. I. (2016) Redox-coupled substrate water reorganization in the active site of Photosystem II - The role of calcium in substrate water delivery, *Biochim. Biophys. Acta 1857*, 740-748.

(34) Krewald, V., Retegan, M., Neese, F., Lubitz, W., Pantazis, D. A., and Cox, N. (2016) Spin State as a Marker for the Structural Evolution of Nature's Water-Splitting Catalyst, *Inorg. Chem. 55*, 488-501.

(35) Askerka, M., Wang, J., Vinyard, D. J., Brudvig, G. W., and Batista, V. S. (2016) S_3 State of the O2-Evolving Complex of Photosystem II: Insights from QM/MM, EXAFS, and Femtosecond X-ray Diffraction, *Biochemistry 55*, 984.

(36) Chatterjee, R., Han, G., Kern, J., Gul, S., Fuller, F. D., Garachtchenko, A., Young, I. D., Weng, T.-C., Nordlund, D., Alonso-Mori, R., Bergmann, U., Sokaras, D., Hatekeyama, M., Yachandra, V. K., and Yano, J. (2016) Structural changes correlated with magnetic spin state isomorphism in the S_2 state of the Mn_4CaO_5 cluster in the oxygen-evolving complex of photosystem II, *Chem. Sci. 7*, 5236-5348.

(37) Shoji, M., Isobe, H., Nakajima, T., and Yamaguchi, K. (2016) Large-scale QM/MM calculations of the $CaMn_4O_5$ cluster in the oxygen-evolving complex of photosystem II: Comparisons with EXAFS structures, *Chem. Phys. Lett. 658*, 354-363.

(38) Zaharieva, I., Chernev, P., Berggren, G., Anderlund, M., Styring, S., Dau, H., and Haumann, M. (2016) Room-Temperature Energy-Sampling Kβ X-ray Emission Spectroscopy of the Mn_4Ca Complex of Photosystem II Reveals Three Manganese-Centered Oxidation Steps and Suggests Coordination Change Prior to O_2 Formation, *Biochemistry 55*, 4197-4211.

(39) Suga, M., Akita, F., Sugahara, M., Kubo, M., Nakajima, Y., Nakane, T., Yamashita, K., Umena, Y., Nakabayashi, M., Yamane, T., Nakano, T., Suzuki, M., Masuda, T., Inoue, S., Kimura, T., Nomura, T., Yonekura, S., Yu, L.-J., Sakamoto, T., Motomura, T., Chen, J.-H., Kato, Y., Noguchi, T., Tono, K., Joti, Y., Kameshima, T., Hatsui, T., Nango, E., Tanaka, R., Naitow, H., Matsuura,

Y., Yamashita, A., Yamamoto, M., Nureki, O., Yabashi, M., Ishikawa, T., Iwata, S., and Shen, J.-R. (2017) LIght-induced structural changes and the site of O=O bond formation in PSII caught by XFEL, *Nature 543*, 131-135.

(40) Hillier, W. and Wydrzynski, T. (2008) ^{18}O-Water Exchange in Photosystem II: Substrate Binding and Intermediates of the Water Splitting Cycle, *Coord. Chem. Rev. 252*, 306-317.

(41) Nilsson, H., Krupnik, T., Kargul, J., and Messinger, J. (2014) Substrate water exchange in photosystem II core complexes of the extremophilic red alga *Cyanidioschyzon merolae*, *Biochim. Biophys. Acta 1837*, 1257-1262.

(42) Siegbahn, P. E. M. (2013) Substrate Water Exchange of the Oxygen Evolving Complex in PSII in the S_1, S_2, and S_3 States, *J. Am. Chem. Soc. 135*, 9442-9449.

(43) Li, X. and Siegbahn, P. E. M. (2015) Alternative mechanisms for O_2 release and O-O bond formation in the oxygen evolving complex of photosystem II, *Phys. Chem. Chem. Phys. 17*, 12168-12174.

(44) Nilsson, H., Rappaport, F., Boussac, A., and Messinger, J. (2014) Substrate-water exchange in photosystem II is arrested before dioxygen formation, *Nature Commun. 5*, 4305-doi:10.1038/ncomms5305.

(45) Rapatskiy, L., Cox, N., Savitsky, A., Ames, W. M., Sander, J., Nowaczyk, M. M., Rögner, M., Boussac, A., Neese, F., Messinger, J., and Lubitz, W. (2012) Detection of Water-Binding Sites of the Oxygen-Evolving Complex of Photosystem II Using W-band ^{17}O Electron-Electron Double Resonance-Detected NMR Spectroscopy, *J. Am. Chem. Soc. 134*, 16619-16634.

(46) Pérez Navarro, M., Ames, W. M., Nilsson, H., Lohmiller, T., Pantazis, D. A., Rapatskiy, L., Nowaczyk, M. M., Neese, F., Boussac, A., Messinger, J., Lubitz, W., and Cox, N. (2013) Ammonia binding to the oxygen-evolving complex of photosystem II identified the solvent-exchangeable oxygen bridge (μ-oxo) of the manganese tetramer, *Proc. Natl. Acad. Sci. USA 110*, 15561-15566.

(47) Lohmiller, T., Krewald, V., Pérez Navarro, M., Retegan, M., Rapatskiy, L., Nowaczyk, M. M., Boussac, A., Neese, F., Lubitz, W., Pantazis, D. A., and Cox, N. (2014) Structure, ligands and substrate coordination of the oxygen-evolving complex of photosystem II in the S_2 state: a combined EPR and DFT study, *Phys. Chem. Chem. Phys. 16*, 11877-11892.

(48) Askerka, M., Vinyard, D. J., Brudvig, G. W., and Batista, V. S. (2015) NH_3 Binding to the S_2 State of the O_2-Evolving Complex of Photosystem II: Analogue to H_2O Binding during the S_2 to S_3 Transition, *Biochemistry 54*, 5783-5786.

(49) Retegan, M. and Pantazis, D. A. (2016) Interaction of methanol with the oxygen-evolving complex: atomistic models, channel identification, species dependence, and mechanistic implications, *Chem. Sci. 7*, 6463-6476.

(50) Capone, M., Narzi, D., Bovi, D., and Guidoni, L. (2016) Mechanism of Water Delivery to the Active Site of Photosystem II along the S_2 to S_3 Transition, *J. Phys. Chem. Lett. 7*, 592-596.

(51) Ames, W., Pantazis, D. A., Krewald, V., Cox, N., Messinger, J., Lubitz, W., and Neese, F. (2011) Theoretical Evaluation of Structural Models of the S_2 State in the Oxygen Evolving Complex of Photosystem II: Protonation States and Magnetic Interactions, *J. Am. Chem. Soc. 133*, 19743-19757.

(52) Shoji, M., Isobe, H., and Yamaguchi, K. (2015) QM/MM study of the S_2 to S_3 transition reaction in the oxygen-evolving complex of photosystem II, *Chem. Phys. Lett. 636*, 172-179.

(53) Isobe, H., Shoji, M., Shen, J.-R., and Yamaguchi, K. (2015) Strong Coupling between the Hydrogen Bonding Environment and Redox Chemistry during the S_2 to S_3 Transition in the Oxygen-Evolving Complex of Photosystem II, *J. Phys. Chem. B 119*, 13922-13933.

(54) Zscherp, C. and Barth, A. (2001) Reaction-Induced Infrared Difference Spectroscopy for the Study of Protein Reaction Mechanisms, *Biochemistry 40*, 1875-1883.

(55) Barth, A. and Zscherp, C. (2002) What Vibrations Tell Us About Proteins, *Q. Rev. Biophys. 35*, 369-430.

(56) Rich, P. R. and Iwaki, M. (2005) Infrared Protein Spectroscopy as a Tool to Study Protonation Reactions Within Proteins, in *Biophysical and Structural Aspects of Bioenergetics* (Wikström, M., Ed.) pp 314-333, Royal Society of Chemistry, Cambridge, U.K.

(57) Barth, A. (2007) Infrared Spectroscopy of Proteins, *Biochim. Biophys. Acta 1767*, 1073-1101.

(58) Noguchi, T. (2008) Fourier Transform Infrared Analysis of the Photosynthetic Oxygen-Evolving Center, *Coord. Chem. Rev. 251*, 336-346.

(59) Chu, H.-A. (2013) Fourier transform infrared difference spectroscopy for studying the molecular mechanism of photosynthetic water oxidation, *Frontiers Plant Sci. 4*, 146.

(60) Debus, R. J. (2015) FTIR Studies of Metal Ligands, Networks of Hydrogen Bonds, and Water Molecules near the Active Site Mn_4CaO_5 Cluster in Photosystem II, *Biochim. Biophys. Acta 1847*, 19-34.

(61) Noguchi, T. (2015) Fourier transform infrared difference and time-resolved infrared detection of the electron and proton transfer dynamics in photosynthetic water oxidation, *Biochim. Biophys. Acta 1847*, 35-45.

(62) Nakamura, S., Ota, K., Shibuya, Y., and Noguchi, T. (2016) Role of a Water Network around the Mn_4CaO_5 Cluster in Photosynthetic Water Oxidation: A Fourier Transform Infrared Spectroscopy and Quantum Mechanics/Molecular Mechanics Calculation Study, *Biochemistry 55*, 597-607.

(63) Nakamura, S. and Noguchi, T. (2016) Quantum mechanics/molecular mechanics simulation of the ligand vibrations of the water-oxidizing Mn_4CaO_5 cluster in photosystem II, *Proc. Natl. Acad. Sci. USA 113*, 12727-12732.

(64) Debus, R. J. (2016) Identifying carboxylate ligand vibrational modes in photosystem II with QM/MM methods, *Proc. Natl. Acad. Sci. USA 113*, 12613-12615.

(65) Noguchi, T. and Sugiura, M. (2000) Structure of an Active Water Molecule in the Water-Oxidizing Complex of Photosystem II as Studied by FTIR Spectroscopy, *Biochemistry 39*, 10943-10949.

(66) Noguchi, T. and Sugiura, M. (2002) FTIR Detection of Water Reactions During the Flash-Induced S-State Cycle of the Photosynthetic Water-Oxidizing Complex, *Biochemistry 41*, 15706-15712.

(67) Noguchi, T. (2007) FTIR Detection of Water Reactions in the Oxygen-Evolving Center of Photosystem II, *Phil. Trans. R. Soc. Lond. B 363*, 1189-1195.

(68) Shimada, Y., Suzuki, H., Tsuchiya, T., Tomo, T., Noguchi, T., and Mimuro, M. (2009) Effect of a Single-Amino Acid Substitution of the 43 kDa Chlorophyll Protein on the Oxygen-Evolving Reaction of the Cyanobacterium

Synechocystis sp. PCC 6803: Analysis of the Glu354Gln Mutation., *Biochemistry 48*, 6095-6103.

(69) Hou, L.-H., Wu, C.-M., Huang, H.-H., and Chu, H.-A. (2011) Effects of Ammonia on the Structure of the Oxygen-Evolving Complex in Photosystem II As Revealed by Light-Induced FTIR Difference Spectroscopy, *Biochemistry 50*, 9248-9254.

(70) Service, R. J., Yano, J., Dilbeck, D. L., Burnap, R. L., Hillier, W., and Debus, R. J. (2013) Participation of Glutamate-333 of the D1 Polypeptide in the Ligation of the Mn_4CaO_5 Cluster in Photosystem II, *Biochemistry 52*, 8452-8464.

(71) Debus, R. J. (2014) Evidence from FTIR Difference Spectroscopy That D1-Asp61 Influences the Water Reactions of the Oxygen-Evolving Mn_4CaO_5 Cluster of Photosystem II, *Biochemistry 53*, 2941-2955.

(72) Pokhrel, R., Debus, R. J., and Brudvig, G. W. (2015) Probing the Effect of Mutations of Asparagine 181 in the D1 Subunit of Photosystem II, *Biochemistry 54*, 1663-1672.

(73) Noguchi, T., Suzuki, H., Tsuno, M., Sugiura, M., and Kato, C. (2012) Time-Resolved Infrared Detection of the Proton and Protein Dynamics during Photosynthetic Oxygen Evolution, *Biochemistry 51*, 3205-3214.

(74) Suzuki, H., Sugiura, M., and Noguchi, T. (2008) Monitoring Water Reactions during the S-State Cycle of the Photosynthetic Water-Oxidizing Center: Detection of the DOD Bending Vibrations by Means of Fourier Transform Infrared Spectroscopy, *Biochemistry 47*, 11024-11030.

(75) Ghanotakis, D. F., Babcock, G. T., and Yocum, C. F. (1984) Calcium Reconstitutes High Rates of Oxygen Evolution in Polypeptide Depleted Photosystem II Preparations, *FEBS Lett. 167*, 127-130.

(76) Boussac, A. and Rutherford, A. W. (1988) Nature of the Inhibition of the Oxygen-Evolving Enzyme of Photosystem II by NaCl Washing and Reversed by the Addition of Ca^{2+} or Sr^{2+}, *Biochemistry 27*, 3476-3483.

(77) Vrettos, J. S., Stone, D. A., and Brudvig, G. W. (2001) Quantifying the Ion Selectivity of the Ca^{2+} Site in Photosystem II: Evidence for Direct Involvement of Ca^{2+} in O_2 Formation, *Biochemistry 40*, 7937-7945.

(78) Pushkar, Y., Yano, J., Sauer, K., Boussac, A., and Yachandra, V. K. (2008) Structural Changes in the Mn_4Ca Cluster and the Mechanism of Photosynthetic Water Splitting, *Proc. Natl. Acad. Sci. USA 105*, 1879-1884.

(79) Koua, F. H. M., Umena, Y., Kawakami, K., and Shen, J.-R. (2013) Structure of Sr-substituted photosystem II at 2.1 Å resolution and its implications in the mechanism of water oxidation, *Proc. Natl. Acad. Sci. USA 110*, 3889-3894.

(80) Cox, N., Rapatskiy, L., Su, J.-H., Pantazis, D. A., Sugiura, M., Kulik, L., Dorlet, P., Rutherford, A. W., Neese, F., Boussac, A., Lubitz, W., and Messinger, J. (2011) Effect of Ca^{2+}/Sr^{2+} Substitution on the Electronic Structure of the Oxygen-Evolving Complex of Photosystem II: A Combined Multifrequency EPR, ^{55}Mn-ENDOR, and DFT Study of the S_2 State, *J. Am. Chem. Soc. 133*, 3635-3648 (Correction pg. 14149).

(81) Chatterjee, R., Milikisiyants, S., Coates, C. S., Koua, F. H. M., Shen, J.-R., and Lakshmi, K. V. (2014) The structure and activation of substrate water molecules in Sr^{2+}-substituted photosystem II, *Phys. Chem. Chem. Phys. 16*, 20834-20843.

(82) Nagashima, H., Nakajima, Y., Shen, J.-R., and Mino, H. (2015) Proton Matrix ENDOR Studies on Ca^{2+}-depleted and Sr^{2+}-substituted Manganese Cluster in Photosystem II, *J. Biol. Chem. 290*, 28166-28174.

(83) Chu, H.-A., Sackett, H., and Babcock, G. T. (2000) Identification of a Mn-O-Mn Cluster Vibrational Mode of the Oxygen-Evolving Complex in Photosystem II by Low-Frequency FTIR Spectroscopy, *Biochemistry 39*, 14371-14376.

(84) Kimura, Y., Hasegawa, K., Yamanari, T., and Ono, T.-A. (2005) Studies on Photosynthetic Oxygen-Evolving Complex by Means of Fourier Transform Infrared Spectroscopy: Calcium and Chloride Cofactors, *Photosynth. Res. 84*, 245-250.

(85) Boussac, A., Sétif, P., and Rutherford, A. W. (1992) Inhibition of Tyrosine Z Photooxidation after Formation of the S_3-State in Ca^{2+}-Depleted and Cl^--Depleted Photosystem II, *Biochemistry 31*, 1224-1234.

(86) Westphal, K. L., Lydakis-Simantiris, N., Cukier, R. I., and Babcock, G. T. (2000) Effects of Sr^{2+}-Substitution on the Reduction Rates of Y_Z(dot) in PSII Membranes - Evidence for Concerted Hydrogen-Atom Transfer in Oxygen Evolution, *Biochemistry 39*, 16220-16229.

(87) Boussac, A., Rappaport, F., Carrier, P., Verbavatz, J.-M., Gobin, R., Kirilovsky, D., Rutherford, A. W., and Sugiura, M. (2004) Biosynthetic Ca^{2+}/Sr^{2+} Exchange in the Photosystem II Oxygen-Evolving Enzyme of *Thermosynechococcus elongatus*, *J. Biol. Chem. 279*, 22809-22819.

(88) Terrett, R., Petrie, S., Pace, R. J., and Stranger, R. (2014) What does the Sr-substituted 2.1 Å resolution crystal structure of photosystem II reveal about the water oxidation mechanism?, *Chem. Commun. 50*, 3187-3190.

(89) Pitari, F., Bovi, D., Narzi, D., and Guidoni, L. (2015) Characterization of the Sr^{2+}- and Cd^{2+}-Substituted Oxygen-Evolving Complex of Photosystem II by Quantum Mechanics/Molecular Mechanics Calculations, *Biochemistry 54*, 5959-5968.

(90) Rappaport, F., Ishida, N., Sugiura, M., and Boussac, A. (2011) Ca^{2+} determines the entropy changes associated with the formation of transition states during water oxidation by Photosystem II, *Energy Environ. Sci. 4*, 2520-2524.

(91) Boussac, A., Rutherford, A. W., and Sugiura, M. (2015) Electron Transfer Pathways from the S_2-States to the S_3-States either after a Ca^{2+}/Sr^{2+} or a Cl^-/I^- Exchange in Photosystem II from *Thermosynechococcus elongatus*, *Biochim. Biophys. Acta 1847*, 576-586.

(92) Debus, R. J., Campbell, K. A., Gregor, W., Li, Z.-L., Burnap, R. L., and Britt, R. D. (2001) Does Histidine 332 of the D1 Polypeptide Ligate the Manganese Cluster in Photosystem II? An Electron Spin Echo Envelope Modulation Study, *Biochemistry 40*, 3690-3699.

(93) Strickler, M. A., Walker, L. M., Hillier, W., Britt, R. D., and Debus, R. J. (2007) No Evidence from FTIR Difference Spectroscopy That Aspartate-342 of the D1 Polypeptide Ligates a Mn Ion That Undergoes Oxidation during the S_0 to S_1, S_1 to S_2, or S_2 to S_3 Transitions in Photosystem II, *Biochemistry 46*, 3151-3160.

(94) Strickler, M. A., Walker, L. M., Hillier, W., and Debus, R. J. (2005) Evidence from Biosynthetically Incorporated Strontium and FTIR Difference Spectroscopy that the C-Terminus of the D1 Polypeptide of Photosystem II Does Not Ligate Calcium, *Biochemistry 44*, 8571-8577.

(95) Hays, A.-M. A., Vassiliev, I. R., Golbeck, J. H., and Debus, R. J. (1998) Role of D1-His190 in Proton-Coupled Electron Transfer Reactions in Photosystem II: A Chemical Complementation Study, *Biochemistry 37*, 11352-11365.

(96) Noguchi, T. and Sugiura, M. (2002) Flash-Induced FTIR Difference Spectra of the Water Oxidizing Complex in Moderately Hydrated Photosystem II Core Films: Effect of Hydration Extent on S-State Transitions, *Biochemistry 41*, 2322-2330.

(97) Noguchi, T. and Sugiura, M. (2003) Analysis of Flash-Induced FTIR Difference Spectra of the S-State Cycle in the Photosynthetic Water-Oxidizing Complex by Uniform ^{15}N and ^{13}C Isotope Labeling, *Biochemistry 42*, 6035-6042.

(98) Yamanari, T., Kimura, Y., Mizusawa, N., Ishii, A., and Ono, T.-A. (2004) Mid- to Low-Frequency Fourier Transform Infrared Spectra of S-State Cycle for Photosynthetic Water Oxidation in *Synechocystis* sp. PCC 6803, *Biochemistry 43*, 7479-7490.

(99) Noguchi, T. (2007) Light-Induced FTIR Difference Spectroscopy as a Powerful Tool Toward Understanding the Molecular Mechanism of Photosynthetic Oxygen Evolution, *Photosyn. Res. 91*, 59-69.

(100) Debus, R. J. (2008) Protein Ligation of the Photosynthetic Oxygen-Evolving Center, *Coord. Chem. Rev. 252*, 244-258.

(101) Noguchi, T. (2013) Monitoring the reactions of photosynthetic water oxidation using infrared spectroscopy, *Biomedical Spectroscopy and Imaging 2*, 115-128.

(102) Suzuki, H., Taguchi, Y., Sugiura, M., Boussac, A., and Noguchi, T. (2006) Structural Perturbations of the Carboxylate Ligands to the Mn Cluster upon Ca^{2+}/Sr^{2+} Exchange in the S-state Cycle of Photosynthetic Oxygen Evolution as Studied by Flash-Induced FTIR Difference Spectroscopy, *Biochemistry 45*, 13454-13464.

(103) Kimura, Y., Hasegawa, K., and Ono, T.-A. (2002) Characteristic changes of the S_2/S_1 difference FTIR spectrum induced by Ca^{2+} depletion and metal cation substitution in the photosynthetic oxygen-evolving complex, *Biochemistry 41*, 5844-5853.

(104) De Riso, A., Jenson, D. L., and Barry, B. A. (2010) Calcium Exchange and Structural Changes during the Photosynthetic Oxygen Evolving Cycle, *Biophys. J. 91*, 1999-2008.

(105) Polander, B. C. and Barry, B. A. (2013) Calcium, Strontium, and Protein Dynamics during the S_2 to S_3 Transition in the Photosynthetic Oxygen-Evolving Cycle, *J. Phys. Chem. Lett. 4*, 3356-3362.

(106) Noguchi, T., Inoue, Y., and Tang, X.-S. (1999) Structure of a Histidine Ligand in the Photosynthetic Oxygen-Evolving Complex as Studied by Light-Induced Fourier Transform Infrared Spectroscopy, *Biochemistry 38*, 10187-10195.

(107) Nakamura, S., Nagao, R., Takahashi, R., and Noguchi, T. (2014) Fourier Transform Infrared Detection of a Polarizable Proton Trapped between Photooxidized Tyrosine Y_Z and a Coupled Histidine in Photosystem II: Relevance to the Proton Transfer Mechanism of Water Oxidation, *Biochemistry 53*, 3131-3144.

(108) Kandori, H. (2000) Role of internal water molecules in bacteriorhodopsin, *Biochim. Biophys. Acta 1460*, 177-191.

(109) Kandori, H. and Shichida, Y. (2000) Direct Observation of the Bridged Water Stretching Vibrations Inside a Protein, *J. Am. Chem. Soc. 122*, 11745-11746.

(110) Garczarek, F. and Gerwert, K. (2006) Functional waters in intraprotein proton transfer monitored by FTIR difference spectroscopy, *Nature 439*, 109-112.

(111) Iwata, T., Paddock, M. L., Okamura, M. Y., and Kandori, H. (2009) Identification of FTIR Bands Due to Internal Water Molecules around the Quinone Binding Sites in the Reaction Center from *Rhodobacter sphaeroides*, *Biochemistry 48*, 1220-1229.

(112) Freier, E., Wolf, S., and Gerwert, K. (2011) Proton transfer via a transient linear water-molecule chain in a membrane protein, *Proc. Natl. Acad. Sci. USA 108*, 11435-11439.

(113) Maréchal, A. and Rich, P. R. (2011) Water molecule reorganization in cytochrome *c* oxidase revealed by FTIR spectroscopy, *Proc. Natl. Acad. Sci. USA 108*, 8634-8638.

(114) Kimura, Y., Mizusawa, N., Ishii, A., Yamanari, T., and Ono, T.-A. (2003) Changes of Low-Frequency Vibrational Modes Induced by Universal ^{15}N- and ^{13}C-Isotope Labeling in S_2/S_1 FTIR Difference Spectrum of Oxygen-Evolving Complex, *Biochemistry 42*, 13170-13177.

(115) Kimura, Y., Mizusawa, N., Ishii, A., and Ono, T.-A. (2005) FTIR Detection of Structural Changes in a Histidine Ligand during S-State Cycling of Photosynthetic Oxygen-Evolving Complex, *Biochemistry 44*, 16072-16078.

(116) Shimada, Y., Suzuki, H., Tsuchiya, T., Mimuro, M., and Noguchi, T. (2011) Structural Coupling of an Arginine Side Chain with the Oxygen-Evolving Mn_4Ca Cluster in Photosystem II As Revealed by Isotope-Edited Fourier Transform Infrared Spectroscopy, *J. Am. Chem. Soc. 133*, 3808-3811.

(117) Chu, H.-A., Debus, R. J., and Babcock, G. T. (2001) D1-Asp170 is Structurally Coupled to the Oxygen Evolving Complex in Photosystem II as Revealed by Light-Induced Fourier Transform Infrared Difference Spectroscopy, *Biochemistry 40*, 2312-2316.

(118) Debus, R. J., Strickler, M. A., Walker, L. M., and Hillier, W. (2005) No Evidence from FTIR Difference Spectroscopy That Aspartate-170 of the D1 Polypeptide Ligates a Manganese Ion That Undergoes Oxidation during the S_0 to S_1, S_1 to S_2, or S_2 to S_3 Transitions in Photosystem II, *Biochemistry 44*, 1367-1374.

(119) Kimura, Y., Mizusawa, N., Ishii, A., Nakazawa, S., and Ono, T.-A. (2005) Changes in Structural and Functional Properties of Oxygen-Evolving Complex Induced by Replacement of D1-Glutamate 189 with Glutamine in Photosystem II: Ligation of Glutamate 189 Carboxylate to the Manganese Cluster, *J. Biol. Chem. 280*, 37895-37900.

(120) Strickler, M. A., Hillier, W., and Debus, R. J. (2006) No Evidence from FTIR Difference Spectroscopy that Glutamate-189 of the D1 Polypeptide Ligates a Mn Ion that Undergoes Oxidation During the S_0 to S_1, S_1 to S_2, or S_2 to S_3 Transitions in Photosystem II, *Biochemistry 45*, 8801-8811.

(121) Service, R. J., Hillier, W., and Debus, R. J. (2010) Evidence from FTIR Difference Spectroscopy of an Extensive Network of Hydrogen Bonds near the Oxygen-Evolving Mn_4Ca Cluster of Photosystem II Involving D1-Glu65, D2-Glu312, and D1-Glu329, *Biochemistry 49*, 6655-6669.

(122) Pokhrel, R., Service, R. J., Debus, R. J., and Brudvig, G. W. (2013) Mutation of Lysine 317 in the D2 Subunit of Photosystem II Alters Chloride Binding and Proton Transport, *Biochemistry 52*, 4758-4773.

(123) Service, R. J., Hillier, W., and Debus, R. J. (2014) A Network of Hydrogen Bonds near the Oxygen-Evolving Mn_4CaO_5 Cluster of Photosystem II Probed with FTIR Difference Spectroscopy, *Biochemistry 53*, 1001-1017.

(124) Noguchi, T., Sugiura, M., and Inoue, Y. (1999) FTIR Studies on the Amino-Acid Ligands of the Photosynthetic Oxygen-Evolving Mn-Cluster, in *Fourier Transform Spectroscopy: Twelfth International Conference* (Itoh, K. and Tasumi, M., Eds.) pp 459-460, Waseda University Press, Tokyo, Japan.

(125) Service, R. J., Yano, J., McConnell, I., Hwang, H. J., Niks, D., Hille, R., Wydrzynski, T., Burnap, R. L., Hillier, W., and Debus, R. J. (2011) Participation of Glutamate-354 of the CP43 Polypeptide in the Ligation of Manganese and the Binding of Substrate Water in Photosystem II, *Biochemistry 50*, 63-81.

(126) Suzer, S. and Andrews, L. (1987) IR Spectra of Complexes of Na, K, and Cs with H_2O in Solid Argon, *Chem. Phys. Lett. 140*, 300-305.

(127) Xantheas, S. S. and Dunning, T. H. (1993) *Ab Initio* studies of cyclic water clusters $(H_2O)_n$, n=1-6. 1. Optimal structurea and vibrational spectra, *J. Chem. Phys. 99*, 8774-8792.

(128) Devlin, J. P., Sadlej, J., and Buch, V. (1999) Infrared Spectra of Large H_2O Clusters: New Understanding of the Elusive Bending Mode of Ice, *J. Phys. Chem. A 105*, 974-983.

(129) Sakamoto, H., Shimizu, T., Nagao, R., and Noguchi, T. (2017) Monitoring the Reaction Process During the S_2 to S_3 Transition in Photosynthetic Water Oxidation Using Time-Resolved Infrared Spectroscopy, *J. Am. Chem. Soc. 139*, 2022-2029.

(130) Zaharieva, I., Dau, H., and Haumann, M. (2017) Sequential and Coupled Proton and Electron Transfer Events in the S_2 to S_3 Transition of Photosynthetic Water Oxidation Revealed by Time-Resolved X-ray Absorption Spectroscopy, *Biochemistry 55*, 6996-7004.

(131) Pal, R., Negre, C. F. A., Vogt, L., Pokhrel, R., Ertem, M. Z., Brudvig, G. W., and Batista, V. S. (2013) S_0-State Model of the Oxygen-Evolving Complex of Photosystem II, *Biochemistry 52*, 7703-7706.

(132) Klauss, A., Haumann, M., and Dau, H. (2015) Seven Steps of Alternating Electron and Proton Transfer in Photosystem II Water Oxidation Traced by Time-Resolved Photothermal Beam Deflection at Improved Sensitivity, *J. Phys. Chem. B 119*, 2677-2689.

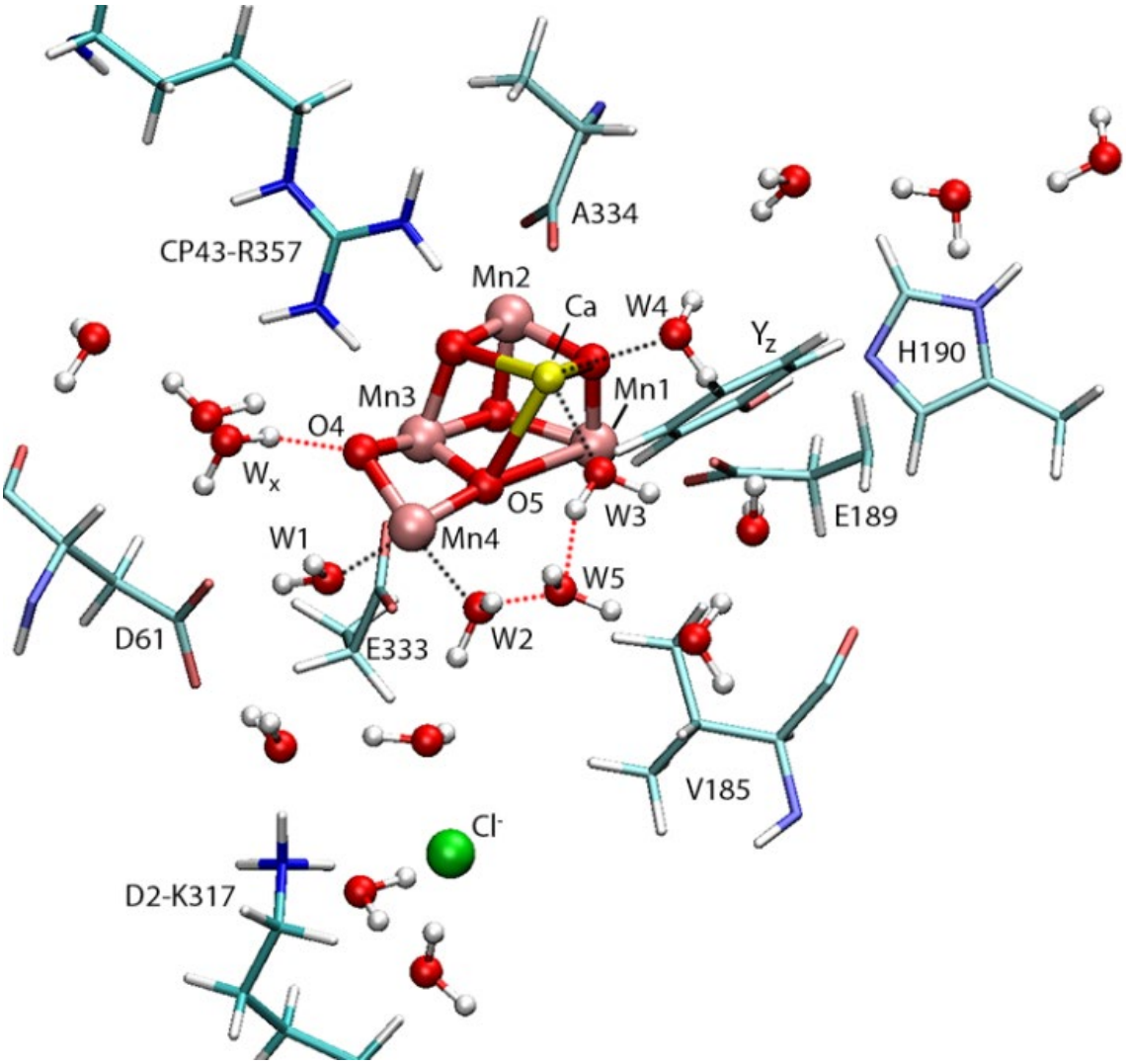

FIGURE 2.1 The Mn_4CaO_5 cluster and its environment showing three proposed water access/proton egress pathways each containing water molecules. Only selected residues are illustrated. Except as noted, the amino acid residues are from the D1 subunit. Salmon-colored spheres, manganese; yellow sphere, calcium; green sphere, chloride; red spheres, oxygen atoms of μ-oxo bridges and water molecules, including the water molecules coordinated to Mn4 (W1 and W2) and Ca^{2+} (W3 and W4) and other water molecules mentioned in the text (i.e., W_x and W5). The coordinates for this figure were constructed with QM/MM methods (*10*) starting from the coordinates in the 1.9 Å X-ray crystallographic model (*1*) and were kindly provided by V. S. Batista and coworkers.

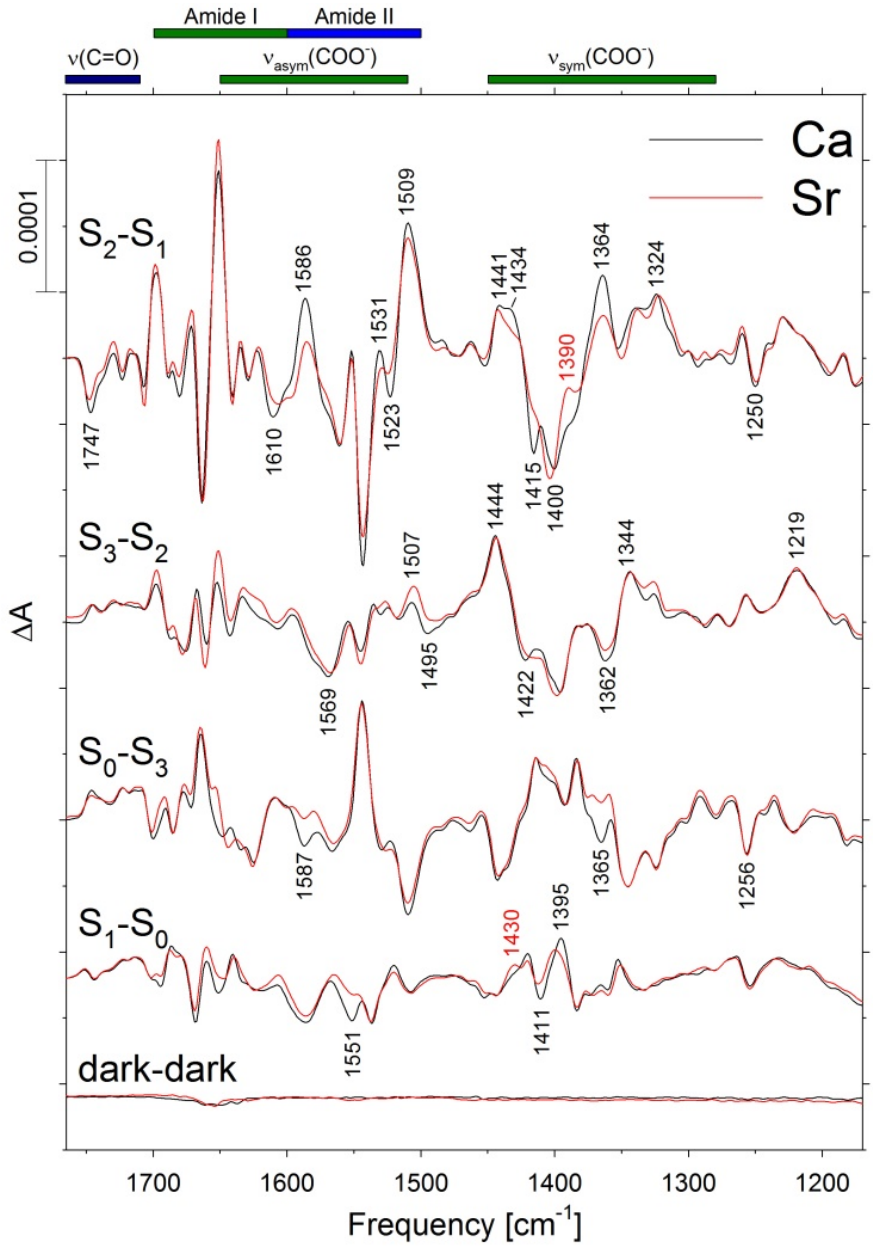

FIGURE 2.2 Mid-frequency FTIR difference spectra of Ca^{2+}-containing (black) and Sr^{2+}-containing (red) PSII core complexes produced by four flash illuminations. The spectra of 30 Ca^{2+}-containing and 36 Sr^{2+}-containing samples were averaged (44,100 and 54,000 scans, respectively). To facilitate comparisons, the spectra of the Sr^{2+}-containing samples were multiplied vertically by factors of 1.6 to 1.8 (approximately normalizing the spectra to the peak-to-peak amplitudes of the positive ferrocyanide band at 2038 cm^{-1} and the negative ferricyanide band at 2115 cm^{-1}). The dark−dark traces show the noise level and the stability of the baseline.

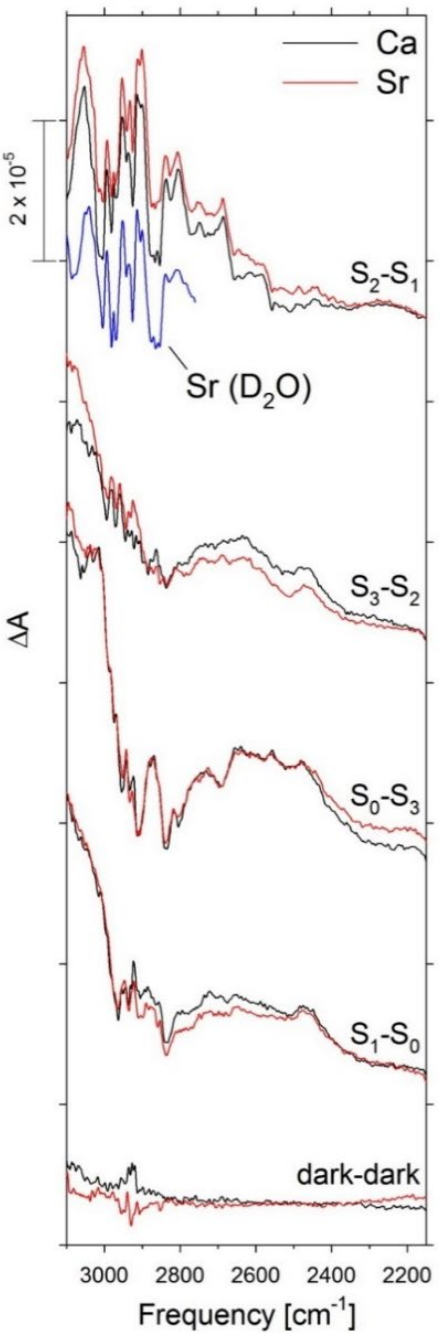

FIGURE 2.3 FTIR difference spectra of PSII core complexes containing Ca^{2+} (black) and Sr^{2+} (red) between 3100 and 2150 cm^{-1} in response to four flash illuminations. The data were collected simultaneously with the spectra in Figure 2.2. The spectra of the Sr^{2+}-containing samples were multiplied vertically as in Figure 2.2, and were shifted vertically to coincide approximately at 3700 cm^{-1}. Dark-dark traces show the noise level and the stability of the baseline. The upper set of traces includes the S_2-S_1 spectrum of Sr-PSII hydrated with $D_2{}^{16}O$ (blue).

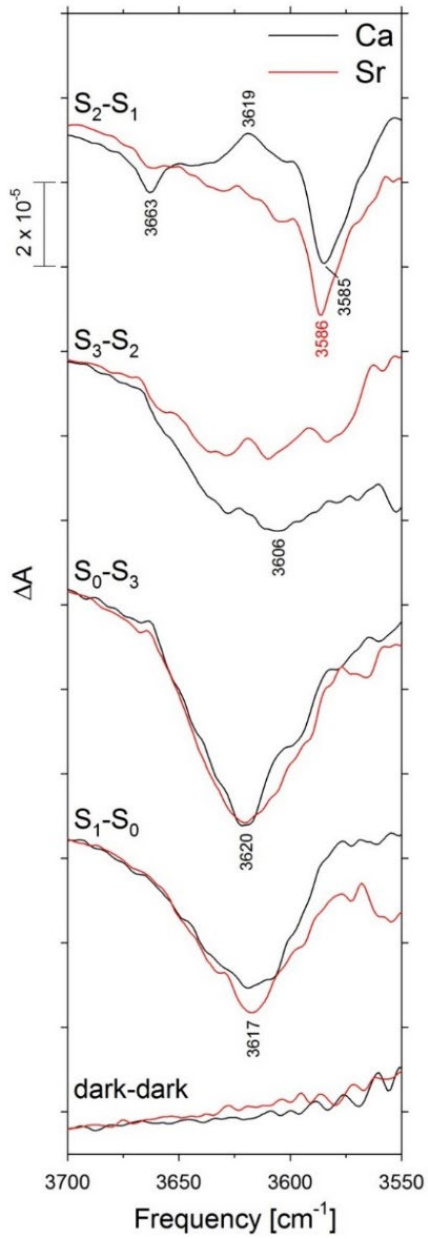

FIGURE 2.4 The FTIR difference spectra of PSII core complexes containing Ca^{2+} (black) or Sr^{2+} (red) in the weakly hydrogen-bonded O–H stretching region in response to four flash illuminations. The data were collected simultaneously with the spectra shown in Figure 2.2, were multiplied vertically as in Figure 2.2, and were shifted vertically to coincide at approximately 3700 cm^{-1}. Dark-dark traces show the noise level and the stability of the baseline.

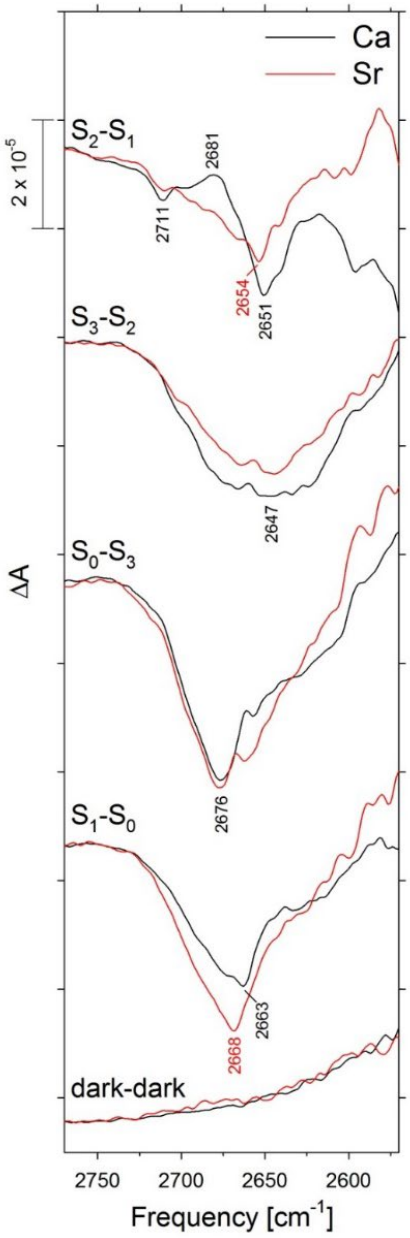

FIGURE 2.5 The FTIR difference spectra of PSII core complexes containing Ca^{2+} (black) or Sr^{2+} (red) in the weakly deuteron-bonded O–D stretching region in response to four successive flash illuminations. The spectra of 30 Ca^{2+}-containing and 61 Sr^{2+}-containing samples hydrated with $D_2{}^{16}O$ were averaged (48,000 and 91,500 scans, respectively). The data were recorded simultaneously with the $D_2{}^{16}O$ data shown in Figures S1 and S2, respectively. The spectra of the Sr^{2+}-containing samples were multiplied vertically by factors of 1.6 to 2.3 as in Figure 2.8, and were shifted vertically to coincide approximately at 2800 cm^{-1}. Dark-dark traces show the noise level and the stability of the baseline.

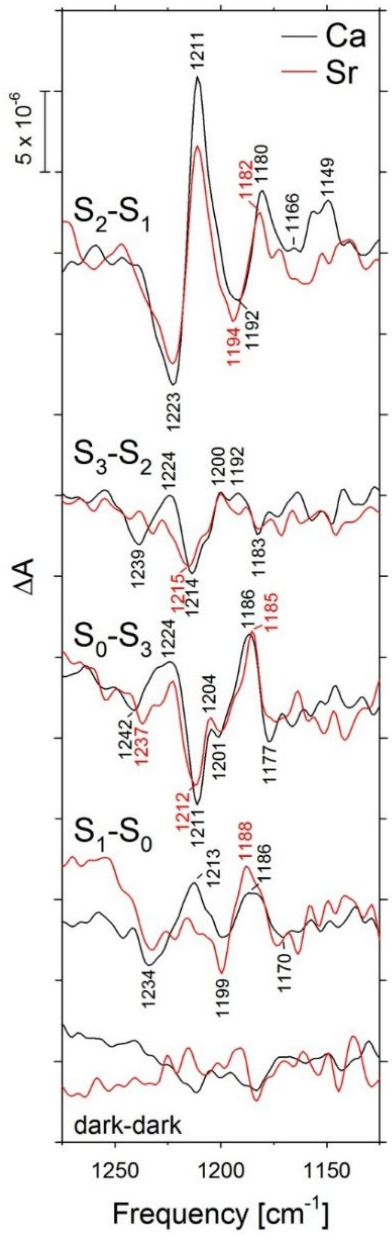

FIGURE 2.6 The $S_{n+1}-S_n$ $D_2{}^{16}O-D_2{}^{18}O$ double-difference spectra of PSII core complexes containing Ca^{2+} (black) or Sr^{2+} (red) in the D-O-D bending region. The data of Figures S1 and S2 were subtracted directly but were offset vertically to maximize overlap. The lower traces show the noise levels and were obtained by calculating the $D_2{}^{16}O-D_2{}^{18}O$ difference spectra of the dark−dark traces shown in Figures S1 and S2.

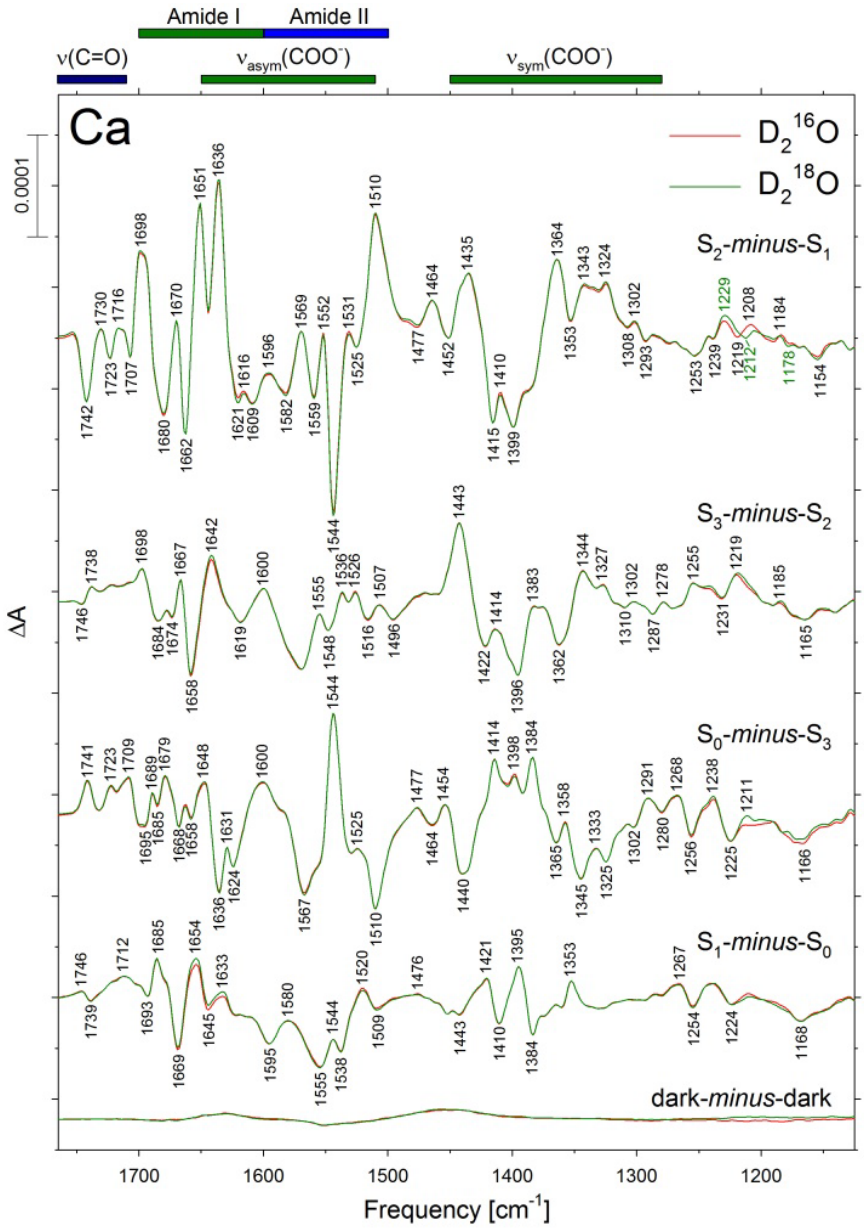

FIGURE 2.7 Comparison of the mid-frequency FTIR difference spectra of Ca^{2+}-containing PSII core complexes in response to four successive flash illuminations applied at 0°C after hydration with $D_2{}^{16}O$ (red) or $D_2{}^{18}O$ (green). The data represent the averages of 32 samples (48,000 scans for each trace). The data were normalized to maximize overlap. Dark-minus-dark control traces are included to show the noise level and the stability of the baseline (lower traces).

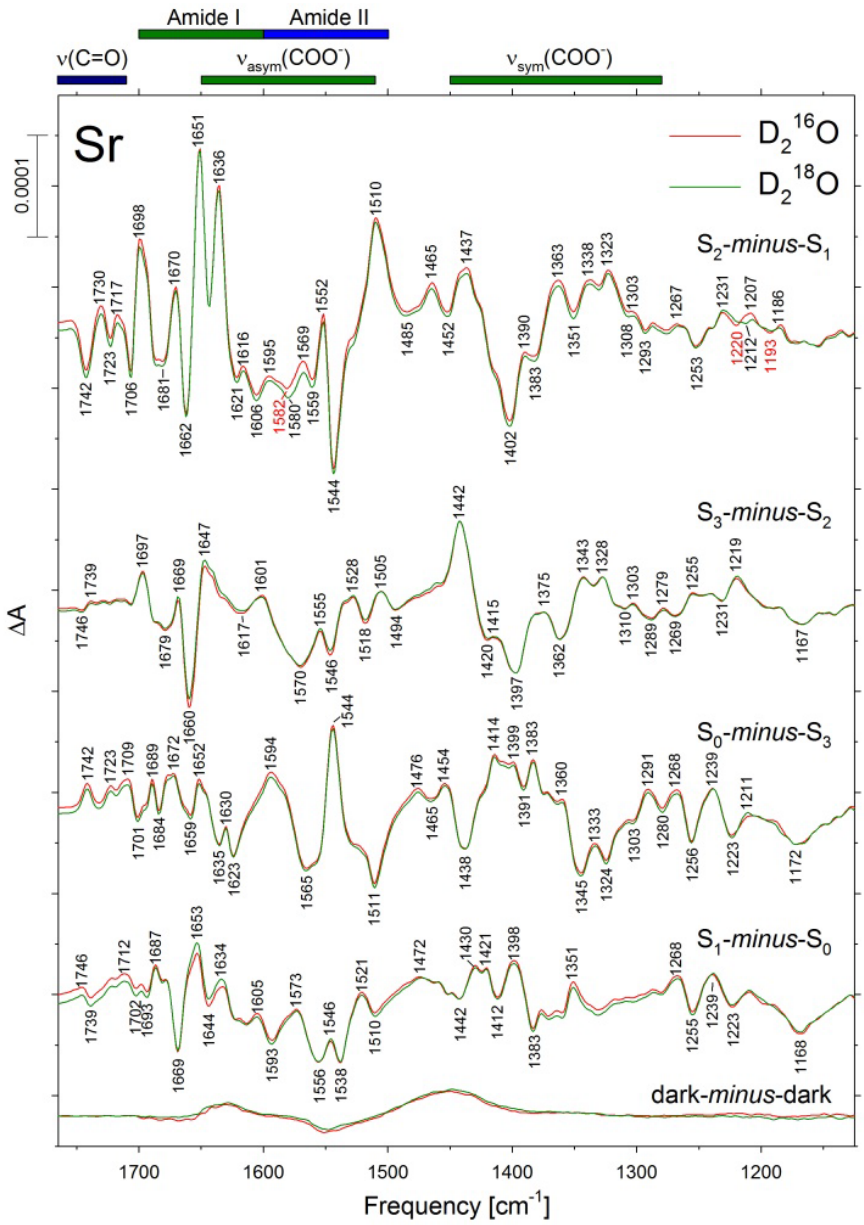

FIGURE 2.8 Comparison of the mid-frequency FTIR difference spectra of Sr^{2+}-containing PSII core complexes in response to four successive flash illuminations applied at 0°C after hydration with $D_2{}^{16}O$ (red) or $D_2{}^{18}O$ (green). The $D_2{}^{16}O$ and $D_2{}^{18}O$ data represent the averages of 61 samples (91,500 scans for each trace) and 62 samples (91,900 scans for each trace), respectively. The spectra have been multiplied vertically by factors of 1.6 to 2.3 to maximize overlap with the data of Ca-containing PSII (Figure 2.7) and are shown with the same vertical scale used in Figure 2.7. Dark-minus-dark control traces are included to show the noise level and the stability of the baseline (lower traces).

Chapter 3

Impact of D1-V185 on the Water Molecules that facilitate O_2 Formation by the Catalytic Mn_4CaO_5 Cluster in Photosystem II

3.1 ABSTRACT

The oxidations of the O_2-evolving Mn_4CaO_5 cluster in Photosystem II are coupled to the release of protons to the thylakoid lumen via one or more proton egress pathways. These pathways are comprised of extensive networks of hydrogen-bonded water molecules and amino acid side chains. The hydrophobic residue, D1-V185, is adjacent to numerous water molecules in one of these pathways. The D1-V185N mutation dramatically slows O-O bond formation. This impairment has been attributed to a disruption of water molecules that facilitate proton egress or whose rearrangement is required for catalysis. In this study, FTIR spectroscopy was employed to characterize the impact of the D1-V185N mutation. By analyzing carboxylate stretching modes, carbonyl stretching modes of carboxylic acids, O–H stretching modes of hydrogen-bonded water molecules, and D−O−D bending modes, we obtain evidence that the D1-V185N mutation perturbs the network of hydrogen bonds that extends from Y_Z to D1-D61 to a greater extent than any mutation yet examined, but does not alter the water molecules that interact directly with D1-D61. The mutation also alters the environments of the carboxylate groups whose pK_a values change in response to the S_1 to S_2 and S_2 to S_3 transitions. Finally, the mutation alters the environment of the water molecule whose bending mode vanishes during the S_2 to S_3 transition, consistent with assigning the Ca^{2+}-bound W3 as the water molecule that deprotonates and joins oxo

bridge O5 during the S_2 to S_3 transition, possibly as the second substrate water molecule for O_2 formation.

3.2 INTRODUCTION

Nearly all the molecular oxygen in the biosphere is produced by the catalytic Mn_4CaO_5 cluster in Photosystem II (PSII). Molecular oxygen is released as the by-product of oxidizing water to provide the electrons and protons needed by plants, algae, and cyanobacteria to drive ATP formation and CO_2 fixation. Our understanding of water oxidation by the Mn_4CaO_5 cluster has advanced rapidly in the last five years because of new developments in X-ray crystallography and the synergism between recent structural, computational, and advanced biophysical studies (for review, see refs *1-7*). PSII is a large protein complex that is integral to the thylakoid membrane. The structure of PII has been determined to 1.85 – 1.95 Å in cyanobacteria (*8-10*), 2.78 Å in a red alga (*11*), 2.7Å in pea (*12, 13*), 3.2 Å in spinach (*14*), and 5.2 Å in *Arabidopsis thaliana* (*15*). PSII is dimeric *in vivo*, with each monomer containing 20 – 22 subunits and having a molecular weight of approximately 350 kDa. At the core of each monomer is a heterodimer of two subunits known as D1 and D2. Light-induced separations of charge within the D1/D2 heterodimer drive the oxidation of the Mn_4CaO_5 cluster, with tyrosine Y_Z serving to transfer electrons from the Mn_4CaO_5 cluster to $P_{680}^{\bullet+}$. Four electrons are removed from the Mn_4CaO_5 cluster during each catalytic cycle, advancing the cluster through five oxidation states. These states are termed S_n, where "n" denotes the number of oxidizing equivalents stored (n = 0 – 4). The S_1 state predominates in dark-adapted samples. The S_4 state is a transient intermediate

whose formation triggers the utilization of the four stored oxidizing equivalents to form O_2 from two substrate-water-derived metal ligands, the regeneration of the S_0 state, and the binding of at least one of two new substrate water molecules. The cluster's metal ions are ligated by six carboxylate groups, one histidine side chain, and four water molecules. All but one of the amino acid ligands are provided by the D1 subunit.

In the highest resolution structures, the Mn_4CaO_5 cluster consists of a distorted Mn_3CaO_4 cube that is linked to a fourth Mn ion (denoted Mn4) by two oxo bridges (denoted O4 and O5, see Figure 3.1). Considerable evidence supports identifying O5 as the deprotonated form of one of the two substrate water molecules (*16-19*). It is present as a μ-hydroxo bridge in the S_0 state (*19*) and as a fully deprotonated μ-oxo bridge in the S_2 state (*16*). The Mn_4CaO_5 cluster is structurally flexible. In the S_2 state it interconverts between two nearly isoenergetic conformations (*20-24*). In one conformation, O5 coordinates to Mn4, leaving Mn1 five-coordinate. In the second conformation, O5 coordinates to Mn1, leaving Mn4 five-coordinate. During the S_2 to S_3 transition, an additional oxygen joins O5 between Mn4 and Mn1 (*25-29*). This additional oxygen [denoted O6 (*29*)] has been proposed to correspond to a water molecule that deprotonates and relocates from the Mn4-bound W2 position (*30-37*) or the Ca^{2+}-bound W3 position (*24, 38-42*). It is thought to correspond to a deprotonated form of the second substrate water molecule (*24, 26, 27, 29, 31, 33-35, 37-41, 43-46*). Its relocation to a position between Mn4 and Mn1 and adjacent to O5 during the S_2 to S_3 transition would ensure that the two substrate oxygen atoms have opposite spins as the O-O bond is formed in the S_4 state, substantially decreasing the activation energy for bond formation (*26, 27, 43, 47*). The relocation also would ensure

that the two oxygen atoms that will form the O-O bond are held in close proximity only after the S_3 state is fully formed, thereby preventing deleterious catalase-like activity in the lower S states (*27, 45*). The subsequent formation of the $Y_Z^{\bullet}S_3$ state locks the two oxygen atoms in position for O-O bond formation in the S_4 state (*48*).

The oxidations of the Mn_4CaO_5 cluster are coupled to the release of protons, with electrons and protons being removed alternatively as the S state cycle proceeds (*50-52*). The alternating deprotonations and oxidations prevent the redox potential of the Mn_4CaO_5 cluster from rising to levels that prevent its subsequent oxidation by the $Y_Z^{\bullet}$ radical anion. Deprotonation of the Mn_4CaO_5 cluster takes place via one or more proton egress pathways that link the Mn_4CaO_5 with the thylakoid lumen. These pathways are comprised of networks of hydrogen-bonded water molecules and protonatable amino acid side chains [e.g., refs (*53-61*)]. Elements of these networks are undoubtedly dynamic in nature (*55, 62*). One such network includes a series of hydrogen-bonded water molecules that stretches from Y_Z to D1-D61 (see Figure 3.1). D1-D61 is the initial residue of a proton egress pathway that facilitates the S_3 to S_4 transition (*63-69*). Adjacent to numerous water molecules in this network is the hydrophobic residue, D1-V185. The side-chain of this residue lies 3.7 Å from O5 and 3-5 Å from waters W2, W3, W5, W6, and W7. The D1-V185N mutation has been shown to dramatically slow the rate of O_2 release and extend the kinetic lag phase of the S_3 to S_4 transition (*70*). This lag phase occurs prior to Mn reduction/O_2 formation has been attributed to proton movement (*50-52, 71, 72*) and/or a structural rearrangement (*73*). The alterations caused by the D1-V185N mutation have been attributed to a disruption of the hydrogen bonded water molecules in the proton egress

pathway that facilitates the S_3 to S_4 transition (*70*). Indeed, the D1-V185N mutation was constructed to disrupt the orientation and dynamics of these water molecules (*70*).

FTIR difference spectroscopy is an ideal method for characterizing structural changes (*74-77*) and has been employed extensively to study the S state cycle in PSII (*78-84*). FTIR is especially suited for probing changes in hydrogen bonding. In PSII, the C=O stretching modes of hydrogen-bonded carboxylic acids have been monitored in the 1760 – 1730 cm^{-1} region (*67, 69, 85-89, 108*), the N-H stretching mode of the protonated histidyl group of D1-H337 that forms a strong hydrogen bond with the O3 oxo bridge has been monitored in the 3000 – 2400 cm^{-1} region (*90*), the O–H stretching modes of weakly hydrogen-bonded water molecules have been monitored in the 3700 – 3500 cm^{-1} region (*69, 88, 89, 91-98, 108*), the O–H stretching modes of strongly hydrogen-bonded water molecules have been monitored in the 3200 – 2500 cm^{-1} region (*69, 88, 89, 92, 97-99, 108*), and D−O−D bending modes have been monitored in the 1250 – 1150 cm^{-1} region (*69, 98, 100*). In this study, we employed FTIR spectroscopy to characterize the impact of the D1-V185N mutation on the carboxylate groups and water molecules that form part of a putative proton egress pathway leading from the Mn_4CaO_5 cluster to the thylakoid lumen. We find that the D1-V185N mutation perturbs this network to a greater extent than any other mutation yet examined, alters the environments of the carboxylate groups whose pK_a values change in response to the S_1 to S_2 and S_2 to S_3 transitions, and alters the environment of the water molecule whose D-O-D bending mode disappears during the S_2 to S_3 transition. The latter observation is consistent with identifying W3 as the water molecule that deprotonates and joins O5 during the S_2 to S_3 transition.

3.3 MATERIALS AND METHODS

Construction of Mutant and Propagation of Cultures. Cells and thylakoid membranes of the D1-V185N mutation-bearing strain of *Synechocystis* sp. PCC 6803 have been characterized previously (*70*). The mutation was constructed in the *psbA-2* gene of *Synechocystis* sp. PCC 6803 and transformed into a strain of *Synechocystis* that lacks all three *psbA* genes and contains a hexahistidine-tag (His-tag) fused to the C-terminus of CP47 (*101*). The wild-type strain described in this manuscript was constructed in an identical manner as the D1-V185N strain but with a transforming plasmid that carried no mutation. Large-scale cultures were propagated as described previously (*102*).

Purification of PSII core complexes. Oxygen-evolving PSII core complexes were purified as described previously in buffer containing 1.2 M betaine, 10% (v/v) glycerol, 50 mM MES-NaOH (pH 6.0), 20 mM $CaCl_2$, 5 mM $MgCl_2$, 50 mM histidine, 1 mM EDTA, and 0.03% (w/v) *n*-dodecyl *β*-D-maltoside (*69*). These were concentrated to approx. 1 mg of Chl/mL, flash-frozen, and stored at −80 °C.

Preparation of FTIR samples. PSII core complexes were transferred into 40 mM sucrose, 10 mM MES-NaOH (pH 6.0), 5 mM $CaCl_2$, 5 mM NaCl, 0.06% (w/v) *n*-dodecyl β-D-maltoside, concentrated, mixed with 1/10 volume of fresh 100 mM potassium ferricyanide, then dried lightly with dry N_2 gas (*98*). Samples were then rehydrated and maintained at a relative humidity of 95% by spotting six 1 μL droplets of 40% (v/v) glycerol in water around the window's periphery before a second window was placed on the first with a thin o-ring spacer in between. For samples having natural abundance $H_2{}^{16}O$ exchanged for $D_2{}^{16}O$ or $D_2{}^{18}O$, the lightly dried samples were rehydrated with 40% (v/v)

glycerol$(OD)_3$ (98% D, Cambridge Isotope Laboratories, Inc., Andover, MA) in $D_2{}^{16}O$ (99.9% D, Cambridge Isotope Laboratories, Inc., Andover, MA) or $D_2{}^{18}O$ (98% D, 97% 18O, Cambridge Isotope Laboratories, Inc., Andover, MA), respectively (*69, 98, 100*). Sealed samples were equilibrated in the FTIR sample compartment at 0°C in darkness for 1.5 h, illuminated with 6 pre-flashes, then dark-adapted for 30 min (*69, 98*). For each sample, the absorbance at 1657 cm^{-1} (amide I band) was 0.6 – 1.1.

FTIR Spectroscopy. Spectra were recorded with a Bruker Vertex 70 spectrometer (Bruker Optics, Billerica, MA) outfitted with a pre-amplified, midrange D317 photovoltaic MCT detector (Kolmar Technologies, Inc., Newburyport, MA), as described in ref. *98*. After dark adaptation, samples were given six flashes at 13 s intervals. Two transmission spectra were recorded before the first flash and one transmission spectrum was recorded starting 0.33 s after the first and subsequent flashes (each transmission spectrum consisted of 100 scans). The 0.33 s delay was included to allow the oxidation of $Q_A^{\bullet-}$ by the ferricyanide. Difference spectra of the successive S-state transitions (e.g., S_{n+1}–*minus*–S_n difference spectra, henceforth written $S_{n+1}-S_n$), were obtained by dividing the transmission spectrum obtained after the n^{th} flash by the transmission spectrum obtained before the n^{th} flash, then converting the ratio to units of absorption. The background noise level and the stability of the baseline were obtained by dividing the second pre-flash transmission spectrum by the first and converting the ratio to units of absorption (these spectra are labeled dark−dark in each figure – these are control difference spectra obtained *without* a flash being given). The sample was then dark-adapted for 30 min and the cycle was repeated. For each sample, the illumination cycle was repeated 15 times. The spectra of

20-61 samples were averaged (see figure legends). The amplitudes of the D1-V185N difference spectra were multiplied by factors of 1.2 to 1.4 to normalize the peaks corresponding to the reduction of ferricyanide to ferrocyanide by $Q_A^{\bullet -}$ (at 2115 and 2037 cm^{-1}, respectively) to those in the corresponding wild-type spectra (this procedure normalizes the spectra to the extent of flash-induced charge-separation).

Other Procedures. Chlorophyll concentrations were determined as described in ref. (*103*).

3.4 RESULTS

Midfrequency Region. The mid-frequency difference spectra produced by four flashes given to wild-type and D1-V185N PSII core complexes are compared in Figure 3.2 (black and red traces, respectively). The spectra produced by the first, second, third, and fourth flashes of the wild-type samples closely resemble spectra presented previously for PSII preparations from *Synechocystis* sp. PCC 6803, *Thermosynechococcus elongatus*, and spinach, and correspond predominantly to S_2-S_1, S_3-S_2, S_0-S_3, and S_1-S_0 difference spectra, respectively [e.g., refs. (*78-80, 82-84, 104-106*)]. The S_2-S_1 spectrum of D1-V185N PSII core complexes (upper red trace in Figure 3.2) showed substantial changes in throughout the mid-frequency region. In the amide I region, the 1707(-) cm^{-1} feature was enhanced and a positive feature appeared at 1677 cm^{-1} in place of the 1681(-) cm^{-1} and 1672(+) cm^{-1} features of the wild-type. In the asymmetric carboxylate stretching [$\nu_{asym}(COO^-)$] and amide II region, the 1629(-) cm^{-1} feature was enhanced, a positive feature appeared at 1603 cm^{-1}, the 1587(+) cm^{-1}, 1560(-) cm^{-1}, and 1544(-) cm^{-1} features were diminished substantially, a negative feature appeared at 1573 cm^{-1}, and the 1531(+)/1523(-) cm^{-1}

derivative feature was eliminated. The features in the symmetric carboxylate stretching [$\nu_{sym}(COO^-)$] region were diminished: the 1416(-)/1410 (+) cm^{-1} derivative feature shifted to 1423(-)/1416(+) cm^{-1}, the 1400 (-) cm^{-1} feature shifted to 1388(-) cm^{-1}, the 1364(+) cm^{-1} and 1354(-) cm^{-1} features shifted to 1368(+) cm^{-1} and 1360(-) cm^{-1}, respectively, and a small positive feature appeared at 1288 cm^{-1}. Also, the 1260(+)/1250(-) cm^{-1} feature was diminished. In the carbonyl stretching [ν(C=O)] region, the 1746(-) cm^{-1} feature was diminished and replaced by a negative feature at 1737 cm^{-1}. An expanded view of this region is shown in Figure 3.3 (top left panel).

The S_3-S_2 spectrum of D1-V185N also showed changes throughout the mid-frequency region (second set of traces in Figure 3.2). In the amide I region, a negative feature appeared at 1704 cm^{-1}, the 1697(+) cm^{-1} feature was enhanced, the 1687(-) cm^{-1} and 1675(-) cm^{-1} features were diminished, and the 1675(-)/1666(+)/1659(-) cm^{-1} feature was replaced with a negative feature at 1661 cm^{-1}. In the $\nu_{asym}(COO^-)$/amide II region, a negative feature appeared at 1622 cm^{-1}, and the 1537(+) cm^{-1} and 1524(+) cm^{-1} features were replaced with a 1549(+)/1541(-)/1531(+)/1521(-)/1509(+) cm^{-1} feature. In the $\nu_{sym}(COO^-)$ region, the 1423(-)/1414(+) cm^{-1} derivative feature was eliminated, the 1383(+) cm^{-1} feature shifted to 1376 cm^{-1}, and the 1344(+) cm^{-1} feature shifted to 1348 cm^{-1}. In the ν(C=O) region, the 1746(+) cm^{-1} feature was diminished and shifted to 1750 cm^{-1}. An expanded view of this region is shown in Figure 3.3 (top right panel).

The S_0-S_3 spectrum of D1-V185N was diminished substantially in amplitude and showed substantial changes throughout the mid-frequency region (Figure 3.2, 3rd set of traces). In the amide I region, the 1700(-) cm^{-1} and 1679(+) cm^{-1} features were nearly

eliminated. In the $\nu_{asym}(COO^-)$/amide II region, the 1650(-) cm^{-1} feature shifted to 1646 cm^{-1}, the 1642(+) cm^{-1} and 1625(-) cm^{-1} features were eliminated, the 1587(-) cm^{-1} feature was replaced with a 1583(+) cm^{-1} feature, the 1544(+) cm^{-1} and 1509(-) cm^{-1} features were sharply diminished, and the 1529(-)/1522(+) cm^{-1} feature was eliminated. In the $\nu_{sym}(COO^-)$ region, the 1443(-) cm^{-1} feature was sharply diminished, and the 1414(+)/1392(-)/1384(+)/1365(-)/1358(+) cm^{-1} feature was replaced with a 1424(+)/1416(-)/1402(+)/1376(-)/1365(+) cm^{-1} feature, the 1345(-) cm^{-1} feature shifted to 1349(-) cm^{-1}, and the 1324(-) and 1280(-) cm^{-1} features were diminished. In the ν(C=O) region, the 1746(+) cm^{-1} feature was eliminated (see expanded view in Figure 3.3, lower left panel).

The S_1-S_0 spectrum of D1-V185N also was diminished substantially in amplitude and showed substantial changes throughout the mid-frequency region (Figure 3.2, 4th set of traces). In the $\nu_{sym}(COO^-)$ region, the 1421(+) cm^{-1} and 1395(+) cm^{-1} features shifted to 1424(+) cm^{-1} and 1387(-) cm^{-1}, respectively. Most other features throughout in the mid-frequency region were sharply diminished or eliminated. In the ν(C=O) region, the 1753(+)/1745 cm^{-1} derivative feature was eliminated (see expanded view in Figure 3.3, lower right panel).

Strongly H-bonded O–H stretching region. The O–H stretching vibrations of strongly H-bonded OH groups are observed as very broad positive features between 3200 and 2500 cm^{-1} (*69, 88, 89, 92, 97-99,* ***108***). These features have been observed in PSII core complexes from *Synechocystis* sp. PCC 6803 and *Thermosynechococcus elongatus* and in PSII membranes from spinach and are diminished or eliminated (presumably downshifted) in the presence of D_2O (*69, 92*). These regions of wild-type and D1-V185N

PSII core complexes are compared in Figure 3.4. In the S_2-S_1 spectrum (Figure 3.4, upper traces), the broad feature is overlain with numerous positive features that correspond to the N–H stretching vibrations and their Fermi resonance overtones from the imidazole group of a histidine residue (*91, 92, 107*) recently identified as D1-H337 (*90*). Our data show that the D1-V185N mutation causes only slight perturbations in this region of any of the difference spectra.

Weakly H-bonded O–H stretching region. The O–H stretching vibrations of weakly hydrogen bonded OH groups of water molecules appear between 3700 and 3500 cm^{-1}. These features are shifted 930-960 cm^{-1} to lower frequencies in $D_2{}^{16}O$ and approximately 10 cm^{-1} to lower frequencies in $H_2{}^{18}O$ (*69, 91, 92*). These features have been examined in PSII from *Thermosynechococcus elongatus* (*91-93, 100*), *Synechocystis* sp. PCC 6803 (*69, 88, 89, 94, 96, 98* ***,108***), and spinach (*95, 97*). In our wild-type samples, this region of the S_2-S_1 spectrum exhibited a weak negative feature at 3663 cm^{-1}, a weak positive feature at 3617 cm^{-1}, and a large negative feature at 3584 cm^{-1} (Figure 3.5, upper black trace). Corresponding features in the O–D region were observed at 2710(–) cm^{-1}, 2682(+) cm^{-1}, and 2650(–) cm^{-1} (Figure 3.6, upper black trace). The D1-V185N mutation diminished the 3663(-) cm^{-1} feature and replaced the broad positive feature centered at 3617 cm^{-1} with a broad negative feature centered at 3619 cm^{-1} (Figure 3.5, upper black trace). Corresponding D1-V185N-induced changes were observed in the O–D region of the S_2-S_1 spectrum (Figure 3.6, upper red trace): the negative feature at 2710 cm^{-1} was diminished and the broad positive feature centered at 2682 cm^{-1} was replaced with a broad negative feature centered at 2683 cm^{-1}.

The weakly hydrogen bonded O–H regions of the S_3-S_2, S_0-S_3, and S_1-S_0 spectra in our wild-type samples showed broad negative features centered at approximately 3600, 3618, and 3611 cm^{-1}, respectively (Figure 3.5, lower black traces). The corresponding negative features in the O–D regions showed minima at 2634, 2675, and 2663 cm^{-1}, respectively (Figure 3.6, lower black traces). The apparent D1-V185N-induced decrease in the intensity of the 3600 cm^{-1} feature in the S_3-S_2 spectrum (Figure 3.5, second red trace) may be the result of a shift in the baseline because similar mutation-induced decrease was not observed in the O–D region (Figure 3.6, second red trace). The D1-V185N mutation produced little significant change in the O–H or O–D regions of the S_0-S_3 or S_1-S_0 spectra (Figures 5 and 6, third and fourth sets of traces).

D-O-D Bending Region. D-O-D vibrational modes appear near 1210 cm^{-1} (*100, 109*) and are inherently weak. However, they can be observed in $D_2{}^{16}O$-$D_2{}^{18}O$ double difference spectra (*69, 98, 100*). The mid-frequency FTIR difference spectra of wild-type PSII hydrated with $D_2{}^{16}O$ or $D_2{}^{18}O$ are shown in Figure 3.7. The corresponding spectra of D1-V185N are shown in Figure 3.8. In Figure 3.8, the difference spectra of the mutant samples were multiplied vertically by factors of 1.2 to normalize the spectra to the amplitudes of the negative peak of ferricyanide at 2115 cm^{-1} and the positive peak of ferrocyanide at 2037 cm^{-1} in the corresponding wild-type spectra shown in Figure 3.7. To calculate the $D_2{}^{16}O$-$D_2{}^{18}O$ double difference spectra, the difference spectra shown in Figures 7 and 8 were subtracted directly. The resulting S_{n+1}-S_n $D_2{}^{16}O$-$D_2{}^{18}O$ double difference spectra of wild-type and D1-V185N in the D-O-D bending [δ(DOD)] region are compared in Figure 3.9 (black and red traces, respectively). The double difference spectra

for the wild-type PSII core complexes resembled those reported previously for *Thermosynechococcus elongatus* (*100*) and *Synechocystis* sp. PCC 6803 (*69, 98*). The negative feature at 1263 cm^{-1} in the S_2-S_1 double difference spectrum was reported previously in spectra from *Thermosynechococcus elongatus* and was not assigned to a δ(DOD) mode (*100*). It has not been reported previously in spectra from *Synechocystis* sp. PCC 6803 (*69, 98*). It may be relevant that samples exhibiting this feature were equilibrated at a relative humidity of 95% (ref. *100* and this study), whereas samples not exhibiting this feature were equilibrated at a relative humidity of 99% (*69, 98*).

In the S_2-S_1 $D_2{}^{16}O$-*minus*-$D_2{}^{18}O$ double difference spectrum, the D1-V185N mutation shifted the intense 1221(-) and 1210(+) cm^{-1} to 1224(-) and 1212(+) cm^{-1}, respectively, shifted the less intense 1188(-) and 1174(+) cm^{-1} features to 1196(-) and 1184(+) cm^{-1}, respectively, and eliminated the negative feature at 1263 cm^{-1} (Figure 3.9, upper pair of traces). In the S_3-S_2 $D_2{}^{16}O$-$D_2{}^{18}O$ double difference spectrum, the D1-V185N mutation shifted the weak 1200(+) and 1192(-) cm^{-1} features to 1194(+) and 1184(-) cm^{-1}, respectively, diminished the 1238(-) cm^{-1} feature and shifted it to 1232 cm^{-1}, and eliminated the 1265(-) and 1171(+) cm^{-1} features. There were few recognizable features in the S_0-S_3 and S_1-S_0 $D_2{}^{16}O$-$D_2{}^{18}O$ double difference spectra (Figure 3.9, lower two pairs of traces), possibly because of the lower amplitudes of the S_0-S_3 and S_1-S_0 difference spectra, as was observed in spectra equilibrated with H_2O (Figure 3.2).

3.5 DISCUSSION

Carboxylate Residues. The oxidations of the Mn_4CaO_5 cluster during the S state cycle alter $\nu_{sym}(COO^-)$ and $\nu_{asym}(COO^-)$ modes of carboxylate groups and amide I and

amide II modes in the polypeptide backbone (*105, 106, 110*). On the basis of a recent QM/MM study, it was concluded that multiple carboxylate ligands of the Mn_4CaO_5 cluster contribute to most of the features in the $\nu_{sym}(COO^-)$ region of the S_2-S_1 spectrum (*111*). However, the individual mutation of four of the Mn_4CaO_5 clusters carboxylate ligands, D1-D170H (*112, 113*), D1-E189Q (*114, 115*), D1-E189R (*115*), D1-E333Q (*96*), and D1-D342N (*102*) produced little or no changes to any of the mid-frequency S_{n+1}-S_n FTIR difference spectra (also see ref. *116*). Experimentally, mutations constructed at residues involved in the network of hydrogen bonds that extend from at least D1-N298 and Y_Z to D1-D61 and the D1-E65/D1-R334/D2-E312 triad and located 5 – 11 Å from the nearest Mn ion (e.g., D1-D61A, D1-E65A, D1-N87A, D1-Q165E, D1-N181A, D1-R334A, D1-N298A, D2-E312A, and D2-K317A), cause numerous changes throughout the mid-frequency FTIR difference spectra, including in the $\nu_{sym}(COO^-)$ region of the S_2-S_1 spectrum (*67, 69, 85, 87-89, 108*).

Because D1-V185 is located adjacent to numerous water molecules in the network of hydrogen bonds that links Y_Z with D1-D61, the D1-V185N mutation would be expected to substantially perturb this network. Indeed, the D1-V185N mutation alters features in the $\nu_{sym}(COO^-)$ and $\nu_{asym}(COO^-)$/amide II regions of the S_2-S_1 spectrum to a greater extent than any mutation yet examined. In the $\nu_{sym}(COO^-)$ region, the substantial decrease of the 1400(-) cm^{-1} feature is also produced by the D1-Q165E and D1-R334Q mutations (*87*). The substantial decrease of the 1364(+) cm^{-1} feature is also produced by the D1-D61A (*69*), D1-Q165E (*87*), D1-R334A (*87*), D1-N298A (*108*), and D2-E312A (*67*) mutations, by the substitution of Sr^{2+} for Ca^{2+} (*97, 98, 117-120*), and to lesser extents by the D1-N181A (*88*)

and D2-K317A (*85*) mutations. Finally, alteration of the 1416(-)/1410(+) cm^{-1} feature is also produced by D1-D61A (*69*), D1-N87A (*89*), D1-N181A (*88*), D1-R334A (*87*), D1-N298A (*108*), and D2-K317A (*85*) mutations. In the $\nu_{asym}(COO^-)$/amide II region, the substantial decrease of the 1587(+) cm^{-1} feature is also produced by the D1-D61A (*67, 69*), D1-N181 (*88*), D1-Q165E (*87*), D1-R334A (*87*), D1-N298A (*108*), and D2-K317A (*85*) mutations. This feature corresponds to a $\nu_{asym}(COO^-)$ mode because it shifts in globally ^{13}C-labeled samples (*105, 106, 110, 121*) but not in globally ^{15}N-labeled samples (*85, 105, 106, 110, 122*). The substantial decrease of the 1544(-) cm^{-1} feature is also produced by the D1-D61A (*67, 69*), D1-E65A (*67*), D1-R334A (*87*), D1-N298A (*108*), and D2-E312A (*67*) mutations, and to a lesser extent by the D1-E329Q mutation (*67*). The elimination of the 1531(+)/1523(-) cm^{-1} feature is also produced by the D1-D61A (*67, 69*), D1-R334A (*87*), D1-N298A (*108*), D2-E312 (*67*), and D2-K317A (*85*) mutations and to a lesser extent in some preparations having Sr^{2+} substituted for Ca^{2+} (*98, 117, 119*). The 1544(-) and 1531(+)/1523(-) cm^{-1} features correspond to amide II modes because they shift in both ^{13}C labeled (*105, 106, 110, 121*) and ^{15}N labeled (*85, 105, 106, 110, 122*) samples.

These similarities of the D1-V185N-induced changes in the S_2-S_1 spectrum to those produced by the other mutations imply that the D1-V185N mutation perturbs the same extensive network of hydrogen bonds that is perturbed by the other mutations, as expected from the recent X-ray crystallographic structures (*8-10*). However, the overall extents of the changes to the $\nu_{sym}(COO^-)$ and $\nu_{asym}(COO^-)$/amide II regions are greater than those that are caused by the other mutations, implying that the D1-V185N mutation perturbs the

networks of hydrogen bonds located between Y_Z, D1-D61, and the D1-E65/D1-R334/D2-E312 triad to a greater extent than the other mutations.

In addition to altering features throughout the $\nu_{sym}(COO^-)$ and $\nu_{asym}(COO^-)$/amide II regions of the S_2-S_1 spectrum, the D1-V185N mutation also alters features throughout the S_3-S_2 spectrum. In wild-type PSII, the features in the S_0-S_3 and S_1-S_0 spectra reverse those in the S_2-S_1 and S_3-S_2 spectra (*78-80, 82-84*). Because of the alterations produced by the D1-V185N mutation to the S_2-S_1 and S_3-S_2 spectra, it is not surprising that the mutation produces substantial changes in these regions of the S_0-S_3 and S_1-S_0 spectra. The lower amplitudes of these spectra and the relative absence of features in the S_1-S_0 spectrum may reflect the lower efficiency of the S state transitions in the D1-V185N mutant (*70*).

Networks of H-bonds. The extensive networks of hydrogen bonds in the vicinity of the Mn_4CaO_5 cluster have been studied on the basis of changes to the ν(C=O) modes of protonated carboxylic acid groups (*67, 69, 85-89 ,108*). In the S_2-S_1 spectrum of wild-type, the 1746(-) cm^{-1} feature has been assigned to a carboxylate group whose pK_a value decreases in response to the charge that develops on the Mn_4CaO_5 cluster during the S_1 to S_2 transition. This feature is diminished or eliminated by the D1-D61A, D1-E65A, D1-E329Q, D1-R334A, D1-N298A, and D2-E312A mutations, and by overly dehydrating samples (*67, 69, 87, 108*). That the same ν(C=O) mode is altered by all of these mutations and treatments implies the existence of an extensive network of hydrogen bonds that extends more than 20 Å across the Mn_4CaO_5 cluster (*67, 69, 83, 87*). In the S_3-S_2 spectrum of wild-type, the small 1745(+) cm^{-1} feature has been assigned to a carboxylate group whose pK_a value increases in response to the structural changes that occur during the S_2 to

S_3 transition. This feature is altered by the D1-D61A mutation and eliminated by the D1-Q165E, D1-N298A, and D1-E329Q mutations (*67, 69, 87, 108*). That the same ν(C=O) mode is altered by all three mutations implies the existence of an additional network of hydrogen bonds that extends more than 13 Å across the Mn_4CaO_5 cluster (*69, 83, 87*). Elements of these networks of hydrogen bonds may exist only transiently (*55, 62*). During the S_3 to S_0 transition, the 1746(-) cm^{-1} and 1745(+) cm^{-1} features appear to be reversed, resulting in a positive feature at 1746 cm^{-1} in the S_0-S_3 spectrum (*83, 87*). The D1-V185N mutation alters the 1746(-) cm^{-1} feature in the S_2-S_1 spectrum, resulting in a feature with a maximum at 1737 cm^{-1} and a lower frequency shoulder. The mutation also alters the 1745(+) cm^{-1} feature in the S_3-S_2 spectrum, diminishing its intensity and shifting it to 1750 cm^{-1}. These alterations, in particular the 5-9 cm^{-1} shifts, have been observed in no other mutant. The shifts imply that the D1-V185N mutation alters the environments of the carboxylate groups whose pK_a values change in response to the S_1 to S_2 and S_2 to S_3 transitions.

Hydrogen-bonded Water Molecules. The broad positive feature observed between 3200 and 2500 cm^{-1} in the S_2-S_1 spectrum has been studied with QM/MM methods and attributed to the coupled O-H stretching vibrations of strongly hydrogen-bonded water molecules in the network that links D1-D61 with the Ca^{2+} ion and Y_Z (*97*). In the QM/MM analyses, the broad feature is dominated by the O-H stretching vibrations of W1 and W2 (*97*). This feature is eliminated by the D1-D61A mutation (*69*), consistent with the hydrogen bond that exists between this residue and W1 in the recent X-ray crystallographic structural models (*8-10*). The broad positive features in the other S_{n+1}-S_n spectra have been

assigned to the strongly hydrogen bonded O-H stretching vibrations of water molecules in networks of hydrogen bonds that are highly polarizable (*92, 99*). That the D1-V185N mutation only slightly perturbed these regions of the S_{n+1}-S_n spectra implies that D1-V185 has limited influence on the networks of hydrogen bonds in the vicinity of W1 and W2.

The features observed between 3700 and 3500 cm^{-1} in the S_2-S_1 spectrum also have been studied with QM/MM methods. They have been attributed to the coupled O-H stretching vibrations of weakly hydrogen-bonded water molecules in the extended network of hydrogen bonds that links D1-D61 with the Ca^{2+} ion and Y_Z (*97*). The broad negative features observed in the other S_{n+1}-S_n spectra in this region are presumed to have the same origin (*92, 93*). Consequently, these features contain contributions from multiple water molecules. The 3663(-) cm^{-1} and 3617(+) cm^{-1} features in the S_2-S_1 spectrum are diminished by the D1-N181A mutation and eliminated by the D1-D61A, D1-N298A, and D1-E333Q mutations (*69, 88, 96*, *108*). The 3617(+) cm^{-1} feature is also eliminated by the D1-N87A and D1-N87D mutations (*89, 108*). These features are also diminished sharply by the substitution of Sr^{2+} for Ca^{2+} (*98*). The broad negative feature centered at 3603 cm^{-1} in the S_3-S_2 spectrum is also altered by the D1-D61A mutation. Consequently, the Ca^{2+} ion and the D1-D61, D1-N87, D1-N181, D1-N298, and D1-E333 residues all influence the network of hydrogen bonds that links D1-D61 with the Ca^{2+} ion, Y_Z, and beyond. In the S_2-S_1 spectrum of D1-V185N PSII core complexes, the decrease of the 3663(-) cm^{-1} feature and the replacement of the broad positive 3617 cm^{-1} feature with a broad negative feature centered at 3619 cm^{-1} implies that D1-V185 participates in the same network of hydrogen bonds. The replacement of the 3617(+) cm^{-1} feature with a negative 3619(-) cm^{-1} feature

further implies that the perturbation of this extended network by the D1-V185N mutation is at least as substantial as the perturbations introduced by the D1-D61A mutation.

The D-O-D bending region. The H−O−H bending mode [δ(HOH)] is sensitive to hydrogen bond interactions and disappears when a water molecule deprotonates (*100*). Unfortunately, δ(HOH) modes appear near 1640 cm^{-1}, a congested region of the spectrum. In contrast, δ(DOD) modes appear near 1210 cm^{-1}, a region nearly devoid of overlapping protein modes (*100, 109*). Because these modes are very weak, they are detected in $D_2{}^{16}O$-$D_2{}^{18}O$ double difference spectra (*69, 98, 100*). In such a double difference spectrum, a shift of a single δ(DOD) mode would show as up to four peaks, two from $D_2{}^{16}O$ and two from $D_2{}^{18}O$. Fewer peaks may be observed because of spectral overlap. In wild-type samples, the number of features in the $D_2{}^{16}O$-$D_2{}^{18}O$ double difference spectrum of the S_1 to S_2 transition (Figure 3.9, upper pair of traces) implies that at least two δ(DOD) modes are shifted during this transition (*69, 98, 100*). In wild-type samples, the amplitudes of most of the features oscillate during the S state cycle. For example, the 1210(+) cm^{-1} feature in the S_2-S_1 double difference spectrum becomes negative (at 1211-1213 cm^{-1}) in the S_3-S_2 and S_0-S_3 double difference spectra and positive again (at 1213 cm^{-1}) in the S_1-S_0 double difference spectrum. Also, the 1221(-) cm^{-1} feature in the S_2-S_1 double difference spectrum becomes positive (at 1225 cm^{-1}) in the S_3-S_2 double difference spectrum and positive (at 1221 cm^{-1}) in the S_0-S_3 double difference spectrum. The oscillations imply that the δ(DOD) modes that are altered during the S_1 to S_2 transition are altered reversibly during the S state cycle (*69, 98, 100*). One of these DOD molecules must form a hydrogen bond with D1-D61 because the D1-D61A mutation eliminates the intense 1221(–) cm^{-1} and 1210(+)

cm^{-1} features from the S_2-S_1 $D_2{}^{16}O$-*minus*-$D_2{}^{18}O$ double difference spectrum (*69*). Because the D1-V185N mutation shifted the 1221(-) and 1210(+) cm^{-1} features in this spectrum (and the corresponding 1225(+) and 1213(-) features in the S_3-S_2 double difference spectrum) by only 2-3 cm^{-1} [no more than is observed between different wild-type sample preparations (*69, 98, 100*)], we conclude that the mutation has limited influence on the water molecules that interact with D1-D61. The same conclusion was reached on the basis of the limited perturbations caused by the D1-V185N mutation in the 3200 – 2500 cm^{-1} region of the S_2-S_1 spectrum (see above).

The larger 8-10 cm^{-1} mutation-induced shifts of the 1188(-) and 1174(+) cm^{-1} features in the S_2-S_1 double difference spectrum, in addition to other changes observed between 1200 and 1140 cm^{-1} in the S_2-S_1 and S_3-S_2 double difference spectra, shows that the D1-V185N mutation perturbs at least one water molecule whose bending mode changes reversibly during the S state cycle. This conclusion is consistent with the changes observed between 3700 and 3500 cm^{-1} in the S_2-S_1 spectrum that were attributed to D1-V185N-induced alterations in the extended network of hydrogen bonds that links D1-D61 with the Ca^{2+} ion and Y_Z (see above).

Another D1-V185N-induced alteration to the S_3-S_2 double difference spectrum (Figure 3.9, second pair of traces) is the decreased intensity of the 1238(-) cm^{-1} feature and its 6 cm^{-1} shift to 1232 cm^{-1}. In wild-type PSII, the 1238(–) cm^{-1} feature in the S_3-S_2 double difference spectra has no positive counterpart in any of the other double difference spectra, implying that the bending mode of one water molecule is eliminated during the S_2 to S_3 transition (*69, 98, 100*). Therefore, the 1238(–) cm^{-1} feature must correspond to a water

molecule that deprotonates during the S_2 to S_3 transition (or to a water molecule that physically replaces the water molecule that deprotonates, see below). The 1238(–) cm^{-1} feature in the S_3-S_2 double difference spectrum is eliminated or shifted substantially by the substitution of Sr^{2+} for Ca^{2+} (*98*). Because crystallographic (*123*) and computational (*49, 124, 125*) studies show that the substitution of Sr^{2+} for Ca^{2+} perturbs only W3, W4, and W5, it has been proposed that (1) W3 is the water molecule that deprotonates and joins O5 between Mn4 and Mn1 during the S_2 to S_3 transition and (2) W5 moves to the coordination position on Ca^{2+} vacated by W3 (*98*). Equating W5 with the 1238(–) cm^{-1} feature (*98*) would be consistent with this feature's alteration by the D1-V185N mutation: W5 is within 4.7 Å of D1-V185 in the recent X-ray crystallographic structures of PSII (*8-10*). Consequently, the D1-V185N-induced shift of the 1238(–) cm^{-1} feature in the S_3-S_2 double difference spectrum would be consistent with identifying W3 as the water molecule that deprotonates and joins O5 during the S_2 to S_3 transition.

3.6 SUMMARY AND CONCLUSIONS

The D1-V185N mutation perturbs the extensive network of hydrogen bonds that extends from Y_Z to D1-D61 to a greater extent than any other mutation yet examined, yet does not alter water molecules that interact directly with D1-D61. These perturbations are likely the reason that the mutation dramatically slows the structural rearrangement or proton release event that is the rate-limiting step for the S_3 to S_4 transition. The mutation also alters the environments of the carboxylate groups whose pK_a values change in response to the S_1 to S_2 and S_2 to S_3 transitions. Finally, the mutation alters the environment of the water molecule whose bending mode disappears during the S_2 to S_3 transition,

consistent with assigning the Ca^{2+}-bound W3 as the water molecule that deprotonates and joins O5 during the S_2 to S_3 transition, possibly as the second substrate water molecule for O_2 formation.

3.7 ACKNOWLEDGEMENTS

The authors are grateful to Anh P. Nguyen for maintaining the mutant and wild-type cultures of *Synechocystis* sp. PCC 6803 and for purifying the thylakoid membranes that were used for the isolation of PSII core complexes and to V. S. Batista and coworkers for providing the QM/MM-optimized coordinates for the Mn_4CaO_5 cluster and its environments.

Work supported by the Department of Energy, Office of Basic Energy Sciences, Division of Chemical Sciences (grant DE-SC0005291 to R. J. D. for FTIR studies) and by the National Science Foundation (MCB-1716408 to R. L. B. for mutant construction).

3.8 ADDITIONAL NOTES

Abbreviations: Chl, chlorophyll; EDTA, ethylenediaminetetraacetic acid; FTIR, Fourier transform infrared; MES, 2-(N-morpholino)-ethanesulfonic acid; P_{680}, chlorophyll multimer that serves as the light-induced electron donor in PSII; PSII, photosystem II; Q_A, primary plastoquinone electron acceptor; XFEL, X-ray free electron laser; Y_Z, tyrosine residue that mediates electron transfer between the Mn_4O_5Ca cluster and $P_{680}^{+\bullet}$.

3.9 REFERENCES

(1) Cox, N. and Messinger, J. (2013) Reflections on substrate water and dioxygen formation, *Biochim. Biophys. Acta 1827*, 1020-1030.

(2) Yano, J. and Yachandra, V. K. (2014) Mn_4Ca Cluster in Photosynthesis: Where and How Water is Oxidized to Dioxygen, *Chem. Rev. 114*, 4175-4250.

(3) Shen, J.-R. (2015) The Structure of Photosystem II and the Mechanism of Water Oxidation in Photosynthesis, *Annu. Rev. Plant Biol. 66*, 23-48.

(4) Krewald, V., Retegan, M., and Pantazis, D. A. (2016) Principles of Natural Photosynthesis, *Top. Curr. Chem. 371*, 23-48.

(5) Pérez-Navarro, M., Neese, F., Lubitz, W., Pantazis, D. A., and Cox, N. (2016) Recent developments in biological water oxidation, *Curr. Opin. Chem. Biol. 31*, 113-119.

(6) Askerka, M., Brudvig, G. W., and Batista, V. S. (2017) The O_2-Evolving Complex of Photosystem II: Recent Insights from Quantum Mechanics/Molecular Mechanics (QM/MM), Extended X-ray Absorption Fine Structure (EXAFS), and Femtosecond X-ray Crystallography Data, *Acc. Chem. Res. 50*, 41-48.

(7) Vinyard, D. J. and Brudvig, G. W. (2017) Progress Toward a Molecular Mechanism of Water Oxidation in Photosystem II, *Annu. Rev. Phys. Chem. 68*, 101-116.

(8) Umena, Y., Kawakami, K., Shen, J.-R., and Kamiya, N. (2011) Crystal Structure of Oxygen-Evolving Photosystem II at a Resolution of 1.9 Å, *Nature 473*, 55-60.

(9) Suga, M., Akita, F., Hirata, K., Ueno, G., Murakami, H., Nakajima, Y., Shimizu, T., Yamashita, K., Yamamoto, M., Ago, H., and Shen, J.-R. (2015) Native structure of photosystem II at 1.95 Å resolution viewed by femtosecond X-ray pulses, *Nature 517*, 99-103.

(10) Tanaka, A., Fukushi, Y., and Kamiya, N. (2017) Two Different Structures of the Oxygen-Evolving Complex in the Same Polypeptide Frameworks of Photosystem II, *J. Am. Chem. Soc. 139*, 1718-1721.

(11) Ago, H., Adachi, H., Umena, Y., Tashiro, T., Kawakami, K., Kamiya, N., Tian, L., Han, G., Kuang, T., Liu, Z., Wang, F., Zou, H., Enami, I., Miyano, M., and

Shen, J.-R. (2016) Novel Features of Eukaryotic Photosystem II Revealed by Its Crystal Structure Analysis from a Red Alga, *J. Biol. Chem. 291*, 5676-5687.

(12) Su, X., Ma, J., Wei, X., Cao, P., Zhu, D., Chang, W., Liu, Z., and Li, M. (2017) Structure and assembly mechanism of plant $C_2S_3M_2$-type PSII-LHCII supercomplex, *Science 357*, 815-820.

(13) Cao, P., Su, X., Pan, X., Liu, Z., Chang, W., and Li, M. (2018) Structure, assembly and energy transfer of plant photosystem II supercomplex, *Biochim. Biophys. Acta* (in press).

(14) Wei, X., Su, X., Cao, P., Liu, X., Chang, W., Li, M., Zhang, X., and Liu, Z. (2016) Structure of spinach photosystem II-LHII supercomplex at 3.2 Å resolution, *Nature 534*, 69-74.

(15) van Bezouwen, L. S., Caffarri, S., Kale, R. S., Kouril, R., Thunnissen, A.-M. W. H., Oostergetal, G. T., and Boekem, E. J. (2017) Subunit and chlorophyll organization of the plant photosystem II supercomplex, *Nature Plants 3*, 17080.

(16) Rapatskiy, L., Cox, N., Savitsky, A., Ames, W. M., Sander, J., Nowaczyk, M. M., Rögner, M., Boussac, A., Neese, F., Messinger, J., and Lubitz, W. (2012) Detection of Water-Binding Sites of the Oxygen-Evolving Complex of Photosystem II Using W-band ^{17}O Electron-Electron Double Resonance-Detected NMR Spectroscopy, *J. Am. Chem. Soc. 134*, 16619-16634.

(17) Pérez Navarro, M., Ames, W. M., Nilsson, H., Lohmiller, T., Pantazis, D. A., Rapatskiy, L., Nowaczyk, M. M., Neese, F., Boussac, A., Messinger, J., Lubitz, W., and Cox, N. (2013) Ammonia binding to the oxygen-evolving complex of photosystem II identified the solvent-exchangeable oxygen bridge (μ-oxo) of the manganese tetramer, *Proc. Natl. Acad. Sci. USA 110*, 15561-15566.

(18) Lohmiller, T., Krewald, V., Pérez Navarro, M., Retegan, M., Rapatskiy, L., Nowaczyk, M. M., Boussac, A., Neese, F., Lubitz, W., Pantazis, D. A., and Cox, N. (2014) Structure, ligands and substrate coordination of the oxygen-evolving complex of photosystem II in the S_2 state: a combined EPR and DFT study, *Phys. Chem. Chem. Phys. 16*, 11877-11892.

(19) Lohmiller, T., Krewald, V., Sedoud, A., Rutherford, A. W., Neese, F., Lubitz, W., Pantazis, D. A., and Cox, N. (2017) The First State in the Catalytic Cycle of the Water-Oxidizing Enzyme: Identification of a Water-Derived μ-Hydroxo Bridge, *J. Am. Chem. Soc. 139*, 14412-14424.

(20) Pantazis, D. A., Ames, W., Cox, N., Lubitz, W., and Neese, F. (2012) Two Interconvertable Structures that Explain the Spectroscopic Properties of the Oxygen-Evolving Complex of Photosystem II in the S_2 State, *Angew. Chem. Int. Ed. 51*, 9935-9940.

(21) Isobe, H., Shoji, M., Yamanaka, S., Umena, Y., Kawakami, K., Kamiya, N., Shen, J.-R., and Yamaguchi, K. (2012) Theoretical illumination of water-inserted structures of the $CaMn_4O_5$ cluster in the S_2 and S_3 states of oxygen-evolving complex of photosystem II: full geometry optimizations by B3LYP hybrid density functional, *Dalton Trans. 41*, 13727-13740.

(22) Glöckner, C., Kern, J., Broser, M., Zouni, A., Yachandra, V. K., and Yano, J. (2013) Structural Changes of the Oxygen-evolving Complex in Photosystem II during the Catalytic Cycle, *J. Biol. Chem. 288*, 22607-22620.

(23) Saito, K. and Ishikita, H. (2014) Influence of the Ca^{2+} ion on the Mn_4Ca conformation and the H-bond network arrangement in Photosystem II, *Biochim. Biophys. Acta 1837*, 159-166.

(24) Bovi, D., Narzi, D., and Guidoni, L. (2013) The S_2 State of the Oxygen-Evolving Complex of Photosystem II Explored by QM/MM Dynamics: Spin Surfaces and Metastable States Suggest a Reaction Path Towards the S_3 State, *Angew. Chem. Int. Ed. 52*, 11744-11749.

(25) Siegbahn, P. E. M. (2008) A Structure-Consistent Mechanism for Dioxygen Formation in Photosystem II, *Chem. Eur. J. 14*, 8290-8302.

(26) Siegbahn, P. E. M. (2013) Water oxidation mechanism in photosystem II, including oxidations, proton release pathways, O-O bond formation and O_2 release, *Biochim. Biophys. Acta 1827*, 1003-1019.

(27) Cox, N., Retegan, M., Neese, F., Pantazis, D. A., Boussac, A., and Lubitz, W. (2014) Electronic structure of the oxygen-evolving complex in photosystem II prior to O-O bond formation, *Science 345*, 804-808.

(28) Zaharieva, I., Chernev, P., Berggren, G., Anderlund, M., Styring, S., Dau, H., and Haumann, M. (2016) Room-Temperature Energy-Sampling Kβ X-ray Emission Spectroscopy of the Mn_4Ca Complex of Photosystem II Reveals Three Manganese-Centered Oxidation Steps and Suggests Coordination Change Prior to O_2 Formation, *Biochemistry 55*, 4197-4211.

(29) Suga, M., Akita, F., Sugahara, M., Kubo, M., Nakajima, Y., Nakane, T., Yamashita, K., Umena, Y., Nakabayashi, M., Yamane, T., Nakano, T., Suzuki,

M., Masuda, T., Inoue, S., Kimura, T., Nomura, T., Yonekura, S., Yu, L.-J., Sakamoto, T., Motomura, T., Chen, J.-H., Kato, Y., Noguchi, T., Tono, K., Joti, Y., Kameshima, T., Hatsui, T., Nango, E., Tanaka, R., Naitow, H., Matsuura, Y., Yamashita, A., Yamamoto, M., Nureki, O., Yabashi, M., Ishikawa, T., Iwata, S., and Shen, J.-R. (2017) Light-induced structural changes and the site of O=O bond formation in PSII caught by XFEL, *Nature 543*, 131-135.

(30) Askerka, M., Vinyard, D. J., Brudvig, G. W., and Batista, V. S. (2015) NH_3 Binding to the S_2 State of the O_2-Evolving Complex of Photosystem II: Analogue to H_2O Binding during the S_2 to S_3 Transition, *Biochemistry 54*, 5783-5786.

(31) Capone, M., Bovi, D., Narzi, D., and Guidoni, L. (2016) Reorganization of Substrate Waters between the Closed and Open Cubane Conformers during the S_2 to S_3 Transition in the Oxygen Evolving Complex, *Biochemistry 54*, 6439-6442.

(32) Askerka, M., Wang, J., Vinyard, D. J., Brudvig, G. W., and Batista, V. S. (2016) S_3 State of the O2-Evolving Complex of Photosystem II: Insights from QM/MM, EXAFS, and Femtosecond X-ray Diffraction, *Biochemistry 55*, 984.

(33) Retegan, M., Krewald, V., Mamedov, F., Neese, F., Lubitz, W., Cox, N., and Pantazis, D. A. (2016) A five-coordinate Mn(IV) intermediate in biological water oxidation: spectroscopic signature and a pivot mechanism for water binding, *Chem. Sci. 7*, 72-84.

(34) Capone, M., Narzi, D., Bovi, D., and Guidoni, L. (2016) Mechanism of Water Delivery to the Active Site of Photosystem II along the S_2 to S_3 Transition, *J. Phys. Chem. Lett. 7*, 592-596.

(35) Retegan, M. and Pantazis, D. A. (2016) Interaction of methanol with the oxygen-evolving complex: atomistic models, channel identification, species dependence, and mechanistic implications, *Chem. Sci. 7*, 6463-6476.

(36) Wang, J., Askerka, M., Brudvig, G. W., and Batista, V. S. (2017) Crystallographic Data Support the Carousel Mechanism of Water Supply to the Oxygen-Evolving Complex of Photosystem II, *ACS Energy Lett. 2*, 2299-2306.

(37) Guo, Y., Li, H., He, L.-L., Zhao, D.-X., Gong, L.-D., and Yang, Z.-Z. (2017) The open-cubane oxo-oxyl coupling mechanism dominates photosythetic oxygen evolution: a comprehensive DFT investigation on O-O bond formation in the S_4 state, *Phys. Chem. Chem. Phys. 19*, 13909-13923.

(38) Ames, W., Pantazis, D. A., Krewald, V., Cox, N., Messinger, J., Lubitz, W., and Neese, F. (2011) Theoretical Evaluation of Structural Models of the S_2 State in the Oxygen Evolving Complex of Photosystem II: Protonation States and Magnetic Interactions, *J. Am. Chem. Soc. 133*, 19743-19757.

(39) Shoji, M., Isobe, H., and Yamaguchi, K. (2015) QM/MM study of the S_2 to S_3 transition reaction in the oxygen-evolving complex of photosystem II, *Chem. Phys. Lett. 636*, 172-179.

(40) Isobe, H., Shoji, M., Shen, J.-R., and Yamaguchi, K. (2015) Strong Coupling between the Hydrogen Bonding Environment and Redox Chemistry during the S_2 to S_3 Transition in the Oxygen-Evolving Complex of Photosystem II, *J. Phys. Chem. B 119*, 13922-13933.

(41) Ugur, I., Rutherford, A. W., and Kaila, V. R. I. (2016) Redox-coupled substrate water reorganization in the active site of Photosystem II - The role of calcium in substrate water delivery, *Biochim. Biophys. Acta 1857*, 740-748.

(42) Beal, N. J., Corry, T. A., and O'Malley, P. J. (2018) A Comparison of Experimental and Broken Symmetry Density Functional (BS-DFT) Calculated Electron Paramagnectic Resonance (EPR) Parameters for Intermediates Involved in the S_2 to S_3 State Transition of Nature's Oxygen Evolving Complex, *J. Phys. Chem. B 122*, 1394-1407.

(43) Siegbahn, P. E. M. (2009) Structures and Energetics for O_2 Formation in Photosystem II, *Acc. Chem. Res. 42*, 1871-1880.

(44) Li, X. and Siegbahn, P. E. M. (2015) Alternative mechanisms for O_2 release and O-O bond formation in the oxygen evolving complex of photosystem II, *Phys. Chem. Chem. Phys. 17*, 12168-12174.

(45) Krewald, V., Retegan, M., Neese, F., Lubitz, W., Pantazis, D. A., and Cox, N. (2016) Spin State as a Marker for the Structural Evolution of Nature's Water-Splitting Catalyst, *Inorg. Chem. 55*, 488-501.

(46) Siegbahn, P. E. M. (2018) Water Oxidation by PSII: A Quantum Chemical Approach, in *Mechanisms of Primary Energy Transduction in Biology* (Wikström, M., Ed.) pp 273-295, Royal Society of Chemistry, London.

(47) Siegbahn, P. E. M. (2006) O-O Bond Formation in the S_4 State of the Oxygen-Evolving Complex in Photosystem II, *Chem. Eur. J. 12*, 9217-9227.

(48) Nilsson, H., Rappaport, F., Boussac, A., and Messinger, J. (2014) Substrate-water exchange in photosystem II is arrested before dioxygen formation, *Nature Commun. 5*, 4305.

(49) Vogt, L., Ertem, M. Z., Pal, R., Brudvig, G. W., and Batista, V. S. (2015) Computational Insights on Crystal Structures of the Oxygen-Evolving Complex of Photosystem II with Either Ca^{2+} or Ca^{2+} Substituted by Sr^{2+}, *Biochemistry 54*, 820-825.

(50) Klauss, A., Haumann, M., and Dau, H. (2012) Alternating electron and proton transfer steps in photosynthetic water oxidation, *Proc. Natl. Acad. Sci. USA 109*, 16035-16040.

(51) Klauss, A., Haumann, M., and Dau, H. (2015) Seven Steps of Alternating Electron and Proton Transfer in Photosystem II Water Oxidation Traced by Time-Resolved Photothermal Beam Deflection at Improved Sensitivity, *J. Phys. Chem. B 119*, 2677-2689.

(52) Zaharieva, I., Dau, H., and Haumann, M. (2017) Sequential and Coupled Proton and Electron Transfer Events in the S_2 to S_3 Transition of Photosynthetic Water Oxidation Revealed by Time-Resolved X-ray Absorption Spectroscopy, *Biochemistry 55*, 6996-7004.

(53) Murray, J. W. and Barber, J. (2007) Structural Characteristics of Channels and Pathways in Photosystem II Including the Identification of an Oxygen Channel, *J. Struct. Biol. 159*, 228-237.

(54) Gabdulkhakov, A., Guskov, A., Broser, M., Kern, J., Müh, F., Saenger, W., and Zouni, A. (2009) Probing the Accessibility of the Mn_4Ca Cluster in Photosystem II: Channels Calculation, Noble Gas Derivatization, and Cocrystallization with DMSO, *Structure 17*, 1223-1234.

(55) Bondar, A.-N. and Dau, H. (2012) Extended protein/water H-bond networks in photosynthetic water oxidation, *Biochim. Biophys. Acta 1817*, 1177-1190.

(56) Vassiliev, S., Zaraiskaya, T., and Bruce, D. (2012) Exploring the energetics of water permeation in photosystem II by multiple steered molecular dynamics simulations, *Biochim. Biophys. Acta 1817*, 1671-1678.

(57) Ogata, K., Yuki, T., Hatakeyama, M., Uchida, W., and Nakamura, S. (2013) All-Atom Molecular Dynamics Simulation of Photosystem II Embedded in Thylakoid Membranes, *J. Am. Chem. Soc. 135*, 15670-15673.

(58) Bao, H., Dilbeck, D. L., and Burnap, R. L. (2013) Proton transport facilitating water-oxidation: the role of second sphere ligands surrounding the catalytic metal cluster, *Photosynth. Res. 116*, 215-219.

(59) Linke, K. and Ho, F. M. (2014) Water in Photosystem II: Structural, functional, and mechanistic considerations, *Biochim. Biophys. Acta 1837*, 14-32.

(60) Vogt, L., Vinyard, D. J., Khan, S., and Brudvig, G. W. (2015) Oxygen-evolving complex of Photosystem II: an analysis of second-shell residues and hydrogen-bonding networks, *Curr. Opin. Chem. Biol. 25*, 152-158.

(61) Takoaka, T., Sakashita, N., Saito, K., and Ishikita, H. (2016) pK_a of a Proton-Conducting Water Chain in Photosystem II, *J. Phys. Chem. Lett. 7*, 1925-1932.

(62) Guerra, F., Siemers, M., Mielack, C., and Bondar, A.-N. (2018) Dynamics of Long-Distance Hydrogen-Bond Networks in Photosystem II, *J. Phys. Chem. B* 4625-4641.

(63) Hundelt, M., Hays, A.-M. A., Debus, R. J., and Junge, W. (1998) Oxygenic Photosystem II: The Mutation D1-D61N in *Synechocystis* sp. PCC 6803 Retards S-State Transitions without Affecting Electron Transfer from Y_Z to P_{680}^+, *Biochemistry 37*, 14450-14456.

(64) Clausen, J., Debus, R. J., and Junge, W. (2004) Time-Resolved Oxygen Production by PSII: Chasing Chemical Intermediates, *Biochim. Biophys. Acta 1655*, 184-194.

(65) Ferreira, K. N., Iverson, T. M., Maghlaoui, K., Barber, J., and Iwata, S. (2004) Architecture of the Photosynthetic Oxygen-Evolving Center, *Science 303*, 1831-1838.

(66) Ishikita, H., Saenger, W., Loll, B., Biesiadka, J., and Knapp, E.-W. (2006) Energetics of a Possible Proton Exit Pathway for Water Oxidation in Photosystem II, *Biochemistry 45*, 2063-2071.

(67) Service, R. J., Hillier, W., and Debus, R. J. (2010) Evidence from FTIR Difference Spectroscopy of an Extensive Network of Hydrogen Bonds near the Oxygen-Evolving Mn_4Ca Cluster of Photosystem II Involving D1-Glu65, D2-Glu312, and D1-Glu329, *Biochemistry 49*, 6655-6669.

(68) Dilbeck, D. L., Hwang, H. J., Zaharieva, I., Gerencser, L., Dau, H., and Burnap, R. L. (2012) The D1-D61N Mutation in *Synechocystis* sp. PCC 6803 Allows

the Observation of pH-Sensitive Intermediates in the Formation and Release of O_2 from Photosystem II, *Biochemistry 51*, 1079-1091.

(69) Debus, R. J. (2014) Evidence from FTIR Difference Spectroscopy That D1-Asp61 Influences the Water Reactions of the Oxygen-Evolving Mn_4CaO_5 Cluster of Photosystem II, *Biochemistry 53*, 2941-2955.

(70) Dilbeck, D. L., Bao, H., Neveu, C. L., and Burnap, R. L. (2013) Perturbing the Water Cavity Surrounding the Manganese Cluster by Mutating the Residue D1-Valine Has a Strong Effect on the Water Oxidation Mechanism of Photosystem II, *Biochemistry 52*, 6824-6833.

(71) Haumann, M., Liebisch, P., Müller, C., Barra, M., Grabolle, M., and Dau, H. (2005) Photosynthetic O_2 Formation Tracked by Time-Resolved X-ray Experiments, *Science 310*, 1019-1021.

(72) Gerencsér, L. and Dau, H. (2010) Water Oxidation by Photosystem II: H_2O-D_2O Exchange and the Influence of pH Support Formation of an Intermediate by Removal of a Proton before Dioxygen Creation, *Biochemistry 49*, 10098-10106.

(73) Bao, H. and Burnap, R. L. (2015) Structural rearrangements preceding dioxygen formation by the water oxidation complex of photosystem II, *Proc. Natl. Acad. Sci. USA 112*, E6139-E6147.

(74) Zscherp, C. and Barth, A. (2001) Reaction-Induced Infrared Difference Spectroscopy for the Study of Protein Reaction Mechanisms, *Biochemistry 40*, 1875-1883.

(75) Barth, A. and Zscherp, C. (2002) What Vibrations Tell Us About Proteins, *Q. Rev. Biophys. 35*, 369-430.

(76) Rich, P. R. and Iwaki, M. (2005) Infrared Protein Spectroscopy as a Tool to Study Protonation Reactions Within Proteins, in *Biophysical and Structural Aspects of Bioenergetics* (Wikström, M., Ed.) pp 314-333, Royal Society of Chemistry, Cambridge, U.K.

(77) Barth, A. (2007) Infrared Spectroscopy of Proteins, *Biochim. Biophys. Acta 1767*, 1073-1101.

(78) Noguchi, T. (2007) Light-Induced FTIR Difference Spectroscopy as a Powerful Tool Toward Understanding the Molecular Mechanism of Photosynthetic Oxygen Evolution, *Photosyn. Res. 91*, 59-69.

(79) Noguchi, T. (2008) Fourier Transform Infrared Analysis of the Photosynthetic Oxygen-Evolving Center, *Coord. Chem. Rev. 251*, 336-346.

(80) Debus, R. J. (2008) Protein Ligation of the Photosynthetic Oxygen-Evolving Center, *Coord. Chem. Rev. 252*, 244-258.

(81) Chu, H.-A. (2013) Fourier transform infrared difference spectroscopy for studying the molecular mechanism of photosynthetic water oxidation, *Frontiers Plant Sci. 4*, 146.

(82) Noguchi, T. (2013) Monitoring the reactions of photosynthetic water oxidation using infrared spectroscopy, *Biomedical Spectroscopy and Imaging 2*, 115-128.

(83) Debus, R. J. (2015) FTIR Studies of Metal Ligands, Networks of Hydrogen Bonds, and Water Molecules near the Active Site Mn_4CaO_5 Cluster in Photosystem II, *Biochim. Biophys. Acta 1847*, 19-34.

(84) Noguchi, T. (2015) Fourier transform infrared difference and time-resolved infrared detection of the electron and proton transfer dynamics in photosynthetic water oxidation, *Biochim. Biophys. Acta 1847*, 35-45.

(85) Pokhrel, R., Service, R. J., Debus, R. J., and Brudvig, G. W. (2013) Mutation of Lysine 317 in the D2 Subunit of Photosystem II Alters Chloride Binding and Proton Transport, *Biochemistry 52*, 4758-4773.

(86) Suzuki, H., Yu, J., Kobayashi, T., Nakanishi, H., Nixon, P. J., and Noguchi, T. (2013) Functional Roles of D2-Lys317 and the Interacting Chloride Ion in the Water Oxidation Reaction of Photosystem II As Revealed by Fourier Transform Infrared Analysis, *Biochemistry 52*, 4748-4757.

(87) Service, R. J., Hillier, W., and Debus, R. J. (2014) A Network of Hydrogen Bonds near the Oxygen-Evolving Mn_4CaO_5 Cluster of Photosystem II Probed with FTIR Difference Spectroscopy, *Biochemistry 53*, 1001-1017.

(88) Pokhrel, R., Debus, R. J., and Brudvig, G. W. (2015) Probing the Effect of Mutations of Asparagine 181 in the D1 Subunit of Photosystem II, *Biochemistry 54*, 1663-1672.

(89) Banerjee, G., Ghosh, I., Kim, C. J., Debus, R. J., and Brudvig, G. W. (2017) Substitution of the D1-N87 site in photosystem II of cyanobacteria mimics the chloride-binding characteristics of spinach photosystem II, *J. Biol. Chem. 293*, 2487-2497.

(90) Nakamura, S. and Noguchi, T. (2017) Infrared Determination of the Protonation State of a Key Histidine Residue in the Photosynthetic Water Oxidizing Center, *J. Am. Chem. Soc. 139*, 9364-9375.

(91) Noguchi, T. and Sugiura, M. (2000) Structure of an Active Water Molecule in the Water-Oxidizing Complex of Photosystem II as Studied by FTIR Spectroscopy, *Biochemistry 39*, 10943-10949.

(92) Noguchi, T. and Sugiura, M. (2002) FTIR Detection of Water Reactions During the Flash-Induced S-State Cycle of the Photosynthetic Water-Oxidizing Complex, *Biochemistry 41*, 15706-15712.

(93) Noguchi, T. (2007) FTIR Detection of Water Reactions in the Oxygen-Evolving Center of Photosystem II, *Phil. Trans. R. Soc. Lond. B 363*, 1189-1195.

(94) Shimada, Y., Suzuki, H., Tsuchiya, T., Tomo, T., Noguchi, T., and Mimuro, M. (2009) Effect of a Single-Amino Acid Substitution of the 43 kDa Chlorophyll Protein on the Oxygen-Evolving Reaction of the Cyanobacterium *Synechocystis* sp. PCC 6803: Analysis of the Glu354Gln Mutation., *Biochemistry 48*, 6095-6103.

(95) Hou, L.-H., Wu, C.-M., Huang, H.-H., and Chu, H.-A. (2011) Effects of Ammonia on the Structure of the Oxygen-Evolving Complex in Photosystem II As Revealed by Light-Induced FTIR Difference Spectroscopy, *Biochemistry 50*, 9248-9254.

(96) Service, R. J., Yano, J., Dilbeck, D. L., Burnap, R. L., Hillier, W., and Debus, R. J. (2013) Participation of Glutamate-333 of the D1 Polypeptide in the Ligation of the Mn_4CaO_5 Cluster in Photosystem II, *Biochemistry 52*, 8452-8464.

(97) Nakamura, S., Ota, K., Shibuya, Y., and Noguchi, T. (2016) Role of a Water Network around the Mn_4CaO_5 Cluster in Photosynthetic Water Oxidation: A Fourier Transform Infrared Spectroscopy and Quantum Mechanics/Molecular Mechanics Calculation Study, *Biochemistry 55*, 597-607.

(98) Kim, C. J. and Debus, R. J. (2017) Evidence from FTIR Difference Spectroscopy That a Substrate H_2O Molecule for O_2 Formation in Photosystem II is Provided by the Ca Ion of the Catalytic Mn_4CaO_5 Cluster, *Biochemistry 56*, 2558-2570.

(99) Noguchi, T., Suzuki, H., Tsuno, M., Sugiura, M., and Kato, C. (2012) Time-Resolved Infrared Detection of the Proton and Protein Dynamics during Photosynthetic Oxygen Evolution, *Biochemistry 51*, 3205-3214.

(100) Suzuki, H., Sugiura, M., and Noguchi, T. (2008) Monitoring Water Reactions during the S-State Cycle of the Photosynthetic Water-Oxidizing Center: Detection of the DOD Bending Vibrations by Means of Fourier Transform Infrared Spectroscopy, *Biochemistry 47*, 11024-11030.

(101) Debus, R. J., Campbell, K. A., Gregor, W., Li, Z.-L., Burnap, R. L., and Britt, R. D. (2001) Does Histidine 332 of the D1 Polypeptide Ligate the Manganese Cluster in Photosystem II? An Electron Spin Echo Envelope Modulation Study, *Biochemistry 40*, 3690-3699.

(102) Strickler, M. A., Walker, L. M., Hillier, W., Britt, R. D., and Debus, R. J. (2007) No Evidence from FTIR Difference Spectroscopy That Aspartate-342 of the D1 Polypeptide Ligates a Mn Ion That Undergoes Oxidation during the S_0 to S_1, S_1 to S_2, or S_2 to S_3 Transitions in Photosystem II, *Biochemistry 46*, 3151-3160.

(103) Hays, A.-M. A., Vassiliev, I. R., Golbeck, J. H., and Debus, R. J. (1998) Role of D1-His190 in Proton-Coupled Electron Transfer Reactions in Photosystem II: A Chemical Complementation Study, *Biochemistry 37*, 11352-11365.

(104) Noguchi, T. and Sugiura, M. (2002) Flash-Induced FTIR Difference Spectra of the Water Oxidizing Complex in Moderately Hydrated Photosystem II Core Films: Effect of Hydration Extent on S-State Transitions, *Biochemistry 41*, 2322-2330.

(105) Noguchi, T. and Sugiura, M. (2003) Analysis of Flash-Induced FTIR Difference Spectra of the S-State Cycle in the Photosynthetic Water-Oxidizing Complex by Uniform ^{15}N and ^{13}C Isotope Labeling, *Biochemistry 42*, 6035-6042.

(106) Yamanari, T., Kimura, Y., Mizusawa, N., Ishii, A., and Ono, T.-A. (2004) Mid- to Low-Frequency Fourier Transform Infrared Spectra of S-State Cycle for Photosynthetic Water Oxidation in *Synechocystis* sp. PCC 6803, *Biochemistry 43*, 7479-7490.

(107) Noguchi, T., Inoue, Y., and Tang, X.-S. (1999) Structure of a Histidine Ligand in the Photosynthetic Oxygen-Evolving Complex as Studied by Light-Induced Fourier Transform Infrared Spectroscopy, *Biochemistry 38*, 10187-10195.

(108) Nagao, R., Ueoka-Nakanishi, and Noguchi, T. (2017) D1-Asn-298 in photosystem II is involved in a hydrogen-bond network near the redox-active tyrosine Y_Z for proton exit during water oxidation, *J. Biol. Chem. 292*, 20046-20057.

(109) Venyaminov, S. Yu. and Prendergast, F. G. (1997) Water (H_2O and D_2O) Molar Aborptivity in the 1000-4000 cm^{-1} Range and Quantitative Infrared Spectroscpy of Aqueous Solutions, *Anal. Biochem. 248*, 234-245.

(110) Kimura, Y., Mizusawa, N., Ishii, A., Yamanari, T., and Ono, T.-A. (2003) Changes of Low-Frequency Vibrational Modes Induced by Universal ^{15}N- and ^{13}C-Isotope Labeling in S_2/S_1 FTIR Difference Spectrum of Oxygen-Evolving Complex, *Biochemistry 42*, 13170-13177.

(111) Nakamura, S. and Noguchi, T. (2016) Quantum mechanics/molecular mechanics simulation of the ligand vibrations of the water-oxidizing Mn_4CaO_5 cluster in photosystem II, *Proc. Natl. Acad. Sci. USA 113*, 12727-12732.

(112) Chu, H.-A., Debus, R. J., and Babcock, G. T. (2001) D1-Asp170 is Structurally Coupled to the Oxygen Evolving Complex in Photosystem II as Revealed by Light-Induced Fourier Transform Infrared Difference Spectroscopy, *Biochemistry 40*, 2312-2316.

(113) Debus, R. J., Strickler, M. A., Walker, L. M., and Hillier, W. (2005) No Evidence from FTIR Difference Spectroscopy That Aspartate-170 of the D1 Polypeptide Ligates a Manganese Ion That Undergoes Oxidation during the S_0 to S_1, S_1 to S_2, or S_2 to S_3 Transitions in Photosystem II, *Biochemistry 44*, 1367-1374.

(114) Kimura, Y., Mizusawa, N., Ishii, A., Nakazawa, S., and Ono, T.-A. (2005) Changes in Structural and Functional Properties of Oxygen-Evolving Complex Induced by Replacement of D1-Glutamate 189 with Glutamine in Photosystem II: Ligation of Glutamate 189 Carboxylate to the Manganese Cluster, *J. Biol. Chem. 280*, 37895-37900.

(115) Strickler, M. A., Hillier, W., and Debus, R. J. (2006) No Evidence from FTIR Difference Spectroscopy that Glutamate-189 of the D1 Polypeptide Ligates a Mn Ion that Undergoes Oxidation During the S_0 to S_1, S_1 to S_2, or S_2 to S_3 Transitions in Photosystem II, *Biochemistry 45*, 8801-8811.

(116) Debus, R. J. (2016) Identifying carboxylate ligand vibrational modes in photosystem II with QM/MM methods, *Proc. Natl. Acad. Sci. USA 113*, 12613-12615.

(117) Strickler, M. A., Walker, L. M., Hillier, W., and Debus, R. J. (2005) Evidence from Biosynthetically Incorporated Strontium and FTIR Difference Spectroscopy that the C-Terminus of the D1 Polypeptide of Photosystem II Does Not Ligate Calcium, *Biochemistry 44*, 8571-8577.

(118) De Riso, A., Jenson, D. L., and Barry, B. A. (2010) Calcium Exchange and Structural Changes during the Photosynthetic Oxygen Evolving Cycle, *Biophys. J. 91*, 1999-2008.

(119) Suzuki, H., Taguchi, Y., Sugiura, M., Boussac, A., and Noguchi, T. (2006) Structural Perturbations of the Carboxylate Ligands to the Mn Cluster upon Ca^{2+}/Sr^{2+} Exchange in the S-state Cycle of Photosynthetic Oxygen Evolution as Studied by Flash-Induced FTIR Difference Spectroscopy, *Biochemistry 45*, 13454-13464.

(120) Polander, B. C. and Barry, B. A. (2013) Calcium, Strontium, and Protein Dynamics during the S_2 to S_3 Transition in the Photosynthetic Oxygen-Evolving Cycle, *J. Phys. Chem. Lett. 4*, 3356-3362.

(121) Noguchi, T., Sugiura, M., and Inoue, Y. (1999) FTIR Studies on the Amino-Acid Ligands of the Photosynthetic Oxygen-Evolving Mn-Cluster, in *Fourier Transform Spectroscopy: Twelfth International Conference* (Itoh, K. and Tasumi, M., Eds.) pp 459-460, Waseda University Press, Tokyo, Japan.

(122) Service, R. J., Yano, J., McConnell, I., Hwang, H. J., Niks, D., Hille, R., Wydrzynski, T., Burnap, R. L., Hillier, W., and Debus, R. J. (2011) Participation of Glutamate-354 of the CP43 Polypeptide in the Ligation of Manganese and the Binding of Substrate Water in Photosystem II, *Biochemistry 50*, 63-81.

(123) Koua, F. H. M., Umena, Y., Kawakami, K., and Shen, J.-R. (2013) Structure of Sr-substituted photosystem II at 2.1 Å resolution and its implications in the mechanism of water oxidation, *Proc. Natl. Acad. Sci. USA 110*, 3889-3894.

(124) Terrett, R., Petrie, S., Pace, R. J., and Stranger, R. (2014) What does the Sr-substituted 2.1 Å resolution crystal structure of photosystem II reveal about the water oxidation mechanism?, *Chem. Commun. 50*, 3187-3190.

(125) Pitari, F., Bovi, D., Narzi, D., and Guidoni, L. (2015) Characterization of the Sr^{2+}- and Cd^{2+}-Substituted Oxygen-Evolving Complex of Photosystem II by Quantum Mechanics/Molecular Mechanics Calculations, *Biochemistry 54*, 5959-5968.

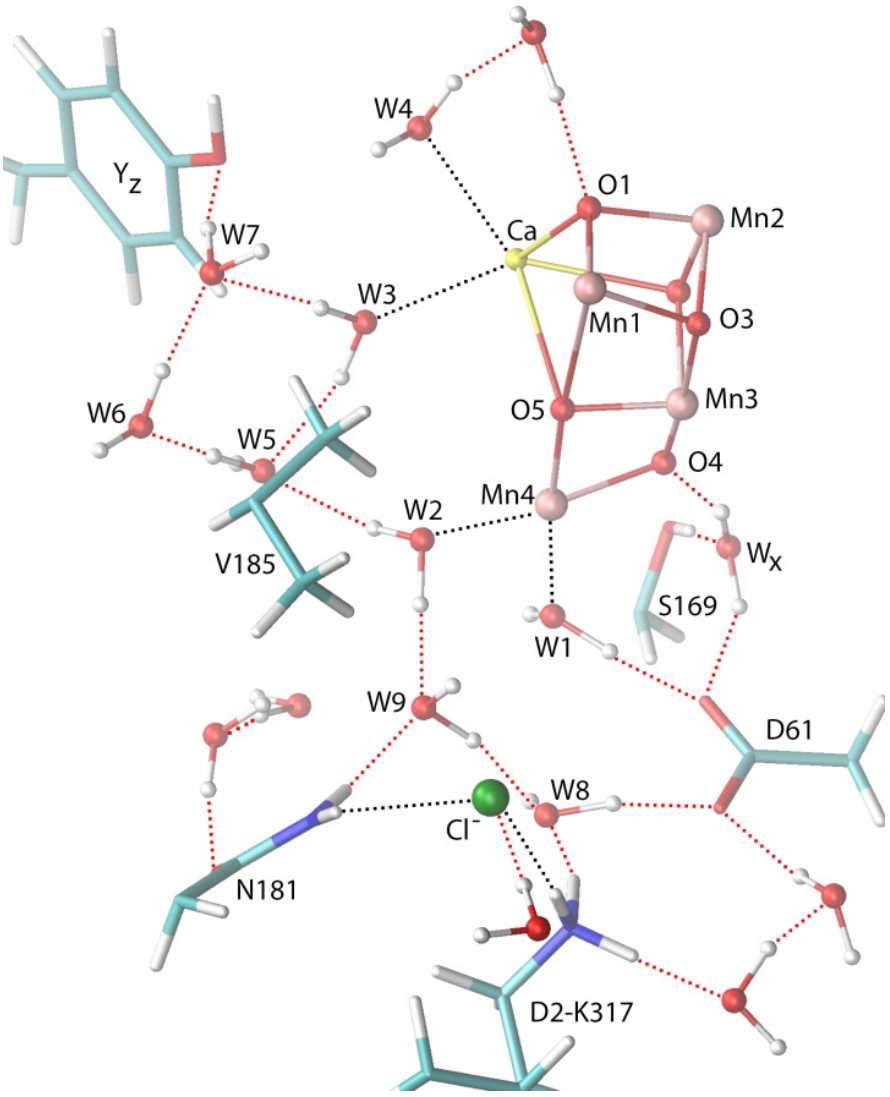

FIGURE 3.1 Water molecules and selected residues in the vicinity of the Mn_4CaO_5 cluster. Residues are from the D1 subunit unless noted otherwise. Salmon-colored spheres, manganese ions; yellow sphere, calcium; green sphere, chloride; red spheres, oxygen atoms of μ-oxo bridges and water molecules. The coordinates for this figure were constructed with QM/MM methods (*49*) based on the coordinates in the 1.9 Å X-ray crystallographic model (*8*) and were kindly provided by V. S. Batista and coworkers.

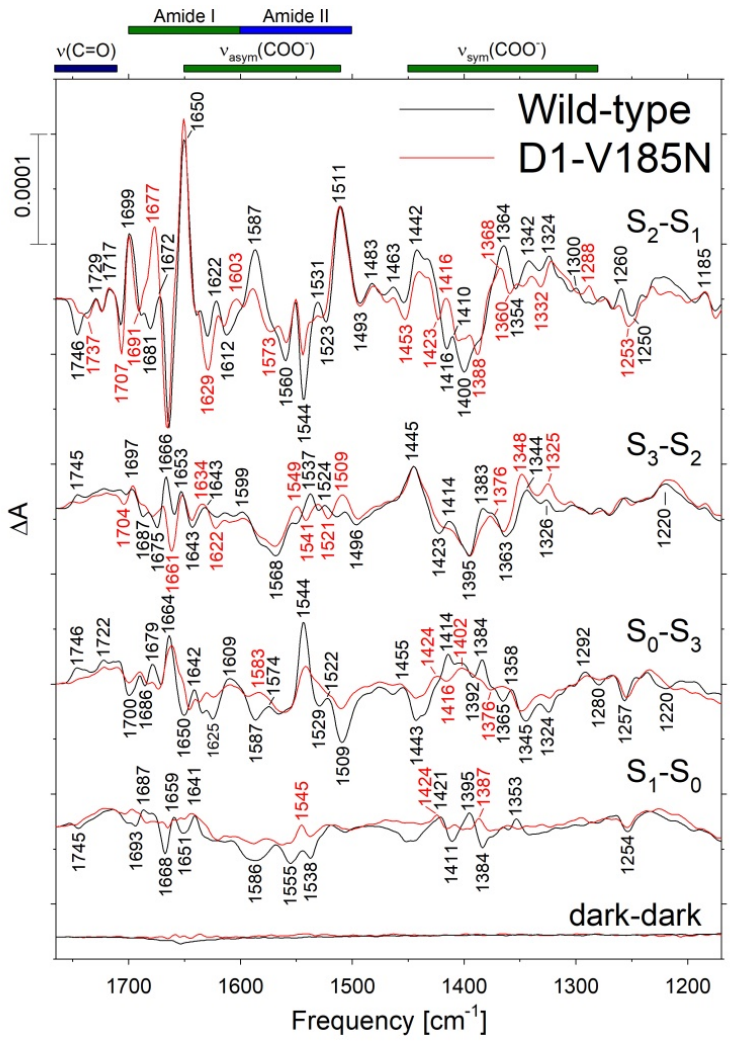

FIGURE 3.2 Mid-frequency FTIR difference spectra of wild-type (black) and D1-V185N (red) PSII core complexes in response to four successive flash illuminations applied at 0ºC. The data (plotted from 1770 cm^{-1} to 1170 cm^{-1}) represent the averages of 22 wild-type and 20 D1-V185N samples (33,000 and 30,000 scans, respectively). The D1-V185N spectra were multiplied vertically by factors of 1.2 to 1.4 to approximately normalize the wild-type and mutant spectra to the extent of flash-induced charge separation. The dark-dark control trace of the mutant (lower red trace) also multiplied by a factor of 1.4. The dark-dark control traces show the noise level and the stability of the baseline.

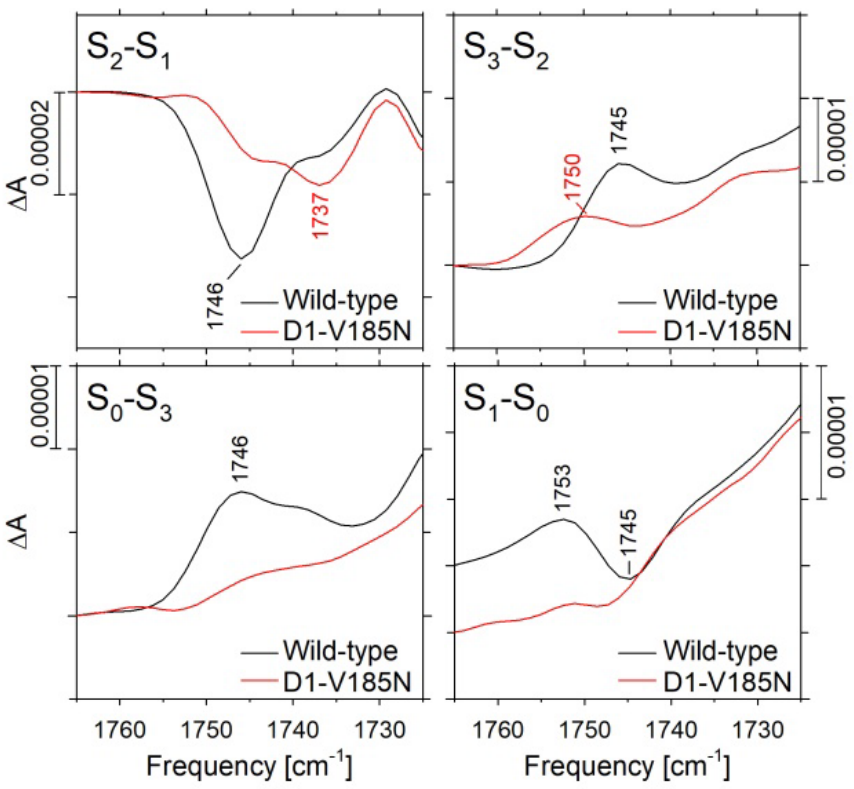

FIGURE 3.3 FTIR difference spectra of wild-type (black) and D1-V185N (red) PSII core complexes in the ν(C=O) region. The data are expanded from those shown in Figure 3.2.

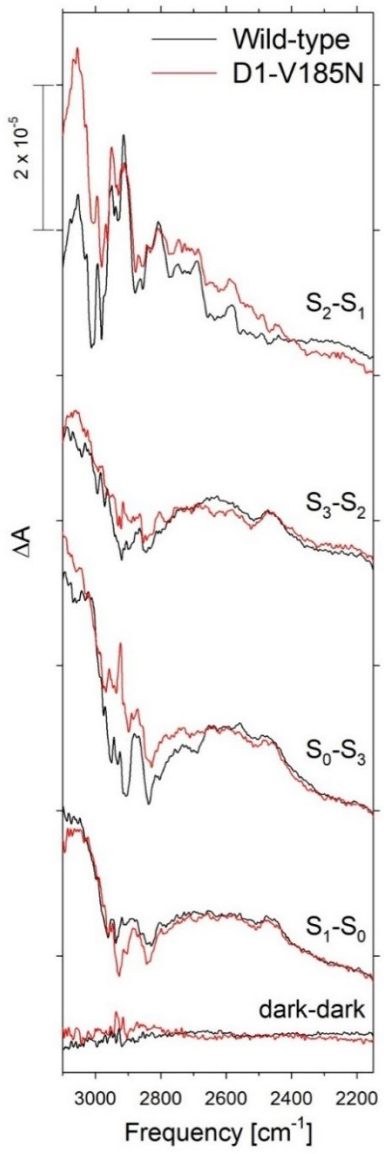

FIGURE 3.4 FTIR difference spectra of wild-type (black) and D1-V185N (red) PSII core complexes between 3100 and 2150 cm^{-1} in response to four successive flash illuminations applied at 0°C. The data were collected simultaneously with that shown in Figure 3.2. The spectra of the D1-V185N samples were multiplied vertically as in Figure 3.2, and were shifted vertically to coincide approximately at 3700 cm^{-1}. Dark-dark control traces show the noise level and the stability of the baseline (lower traces).

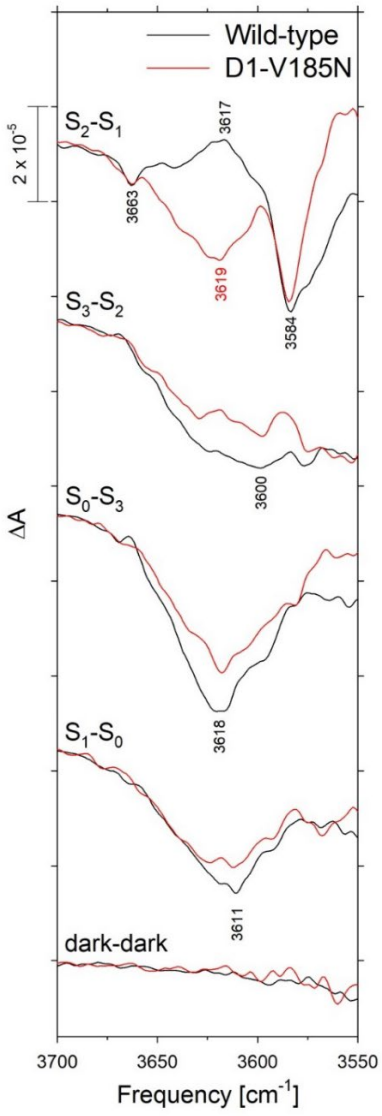

FIGURE 3.5 FTIR difference spectra of wild-type (black) and D1-V185N (red) PSII core complexes in the weakly hydrogen bonded O–H stretching region in response to four successive flash illuminations applied at 0°C. The data were collected simultaneously with that shown in Figure 3.2, were multiplied vertically as in Figure 3.2, and were shifted vertically to coincide approximately at 3700 cm^{-1}. Dark-dark control traces show the noise level and the stability of the baseline (lower traces).

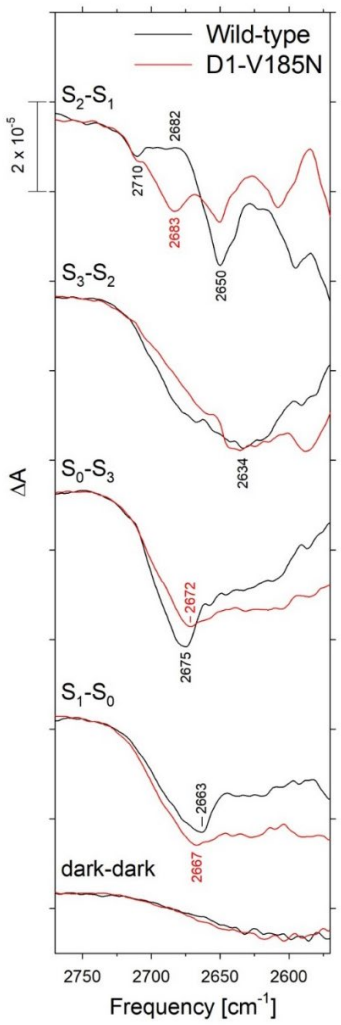

FIGURE 3.6 FTIR difference spectra of wild-type (black) and D1-V185N (red) PSII core complexes in the O–D stretching region in response to four successive flash illuminations applied at 0°C. The data represent the averages of 32 wild-type and 61 D1-V185N samples (48,000 and 90,300 scans, respectively) after hydration with $D_2{}^{16}O$ and were recorded simultaneously with the $D_2{}^{16}O$ data shown in Figures 3.7 and 3.8, respectively. The D1-V185N spectra were multiplied vertically by factors of 1.2 as in Figure 3.8 and were shifted vertically to coincide approximately at 2750 cm^{-1}. Dark-dark control traces show the noise level and the stability of the baseline (lower traces).

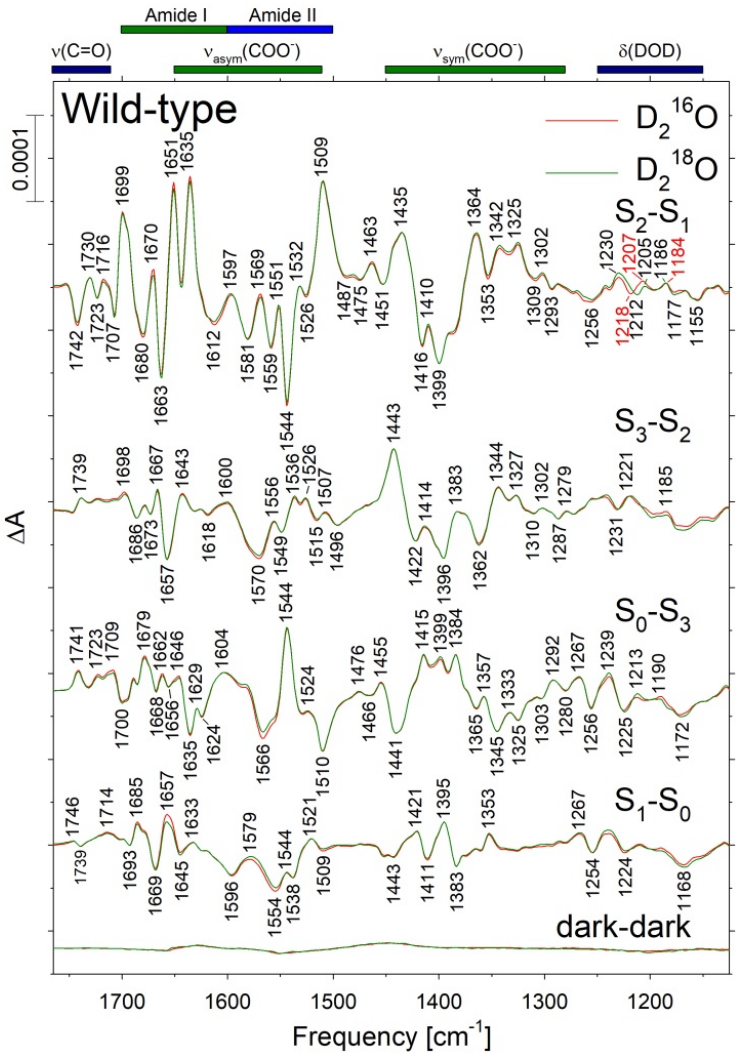

FIGURE 3.7 Mid-frequency FTIR difference spectra of wild-type PSII core complexes in response to four successive flash illuminations applied at 0°C after hydration with $D_2{}^{16}O$ (red) or $D_2{}^{18}O$ (green). The $D_2{}^{16}O$ and $D_2{}^{18}O$ data represent the averages of 32 samples (48,000 scans for each trace) and 30 samples (44,400 scans for each trace), respectively. The dark-dark control traces show the noise level and the stability of the baseline (lower traces).

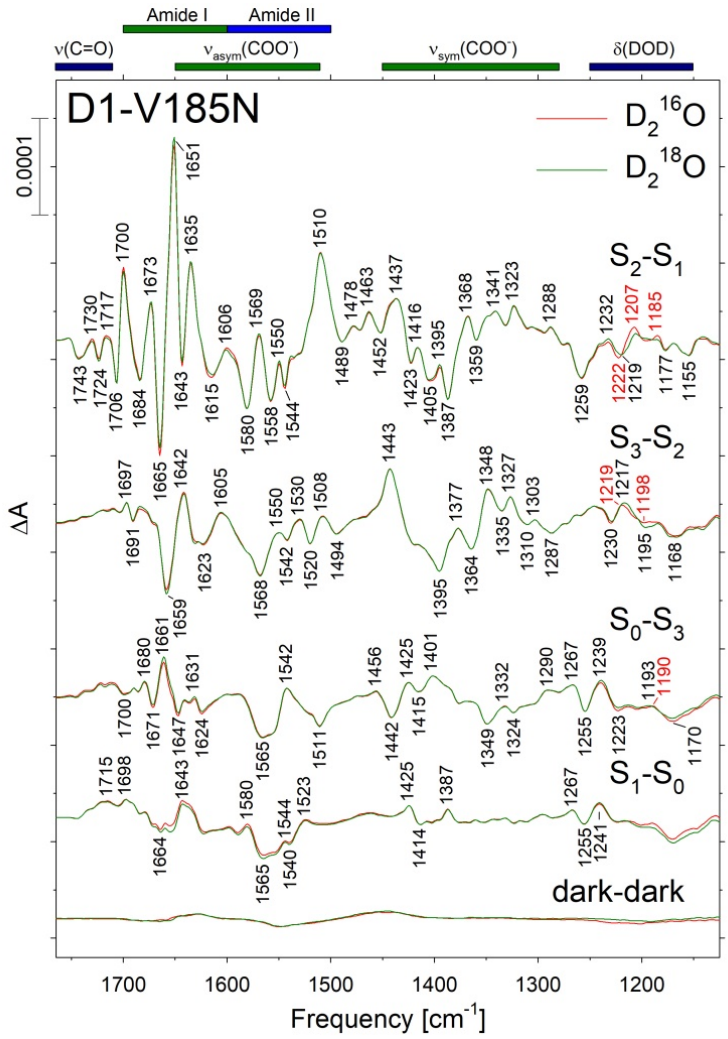

FIGURE 3.8 Mid-frequency FTIR difference spectra of D1-V185N PSII core complexes in response to four successive flash illuminations applied at 0°C after hydration with $D_2{}^{16}O$ (red) or $D_2{}^{18}O$ (green). The $D_2{}^{16}O$ and $D_2{}^{18}O$ data represent the averages of 61 samples (90,300 scans for each trace) and 60 samples (89,900 scans for each trace), respectively. The D1-V185N spectra have been multiplied vertically by factors of 1.2 to approximately normalize the spectra to the extent of flash-induced charge separation in the corresponding wild-type spectra of Figure 3.7. The dark-dark control traces were also multiplied by factors of 1.2 and show the noise level and the stability of the baseline (lower traces).

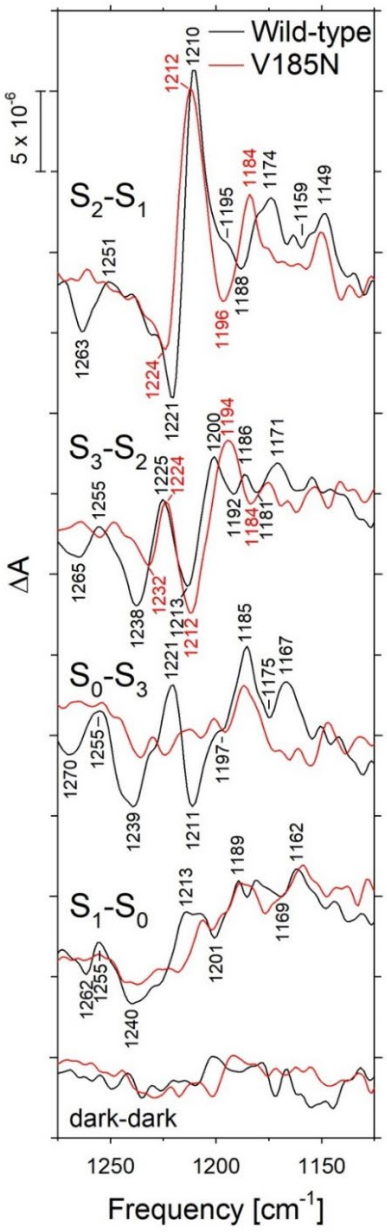

FIGURE 3.9 The S_{n+1}-S_n $D_2{}^{16}O$-$D_2{}^{18}O$ double difference spectra of wild-type (black) and D1-V185N (red) PSII core complexes in the D-O-D bending region. The data of Figures 3.7 and 3.8 were subtracted directly but were offset vertically to maximize overlap. The lower traces show the noise levels and were obtained by calculating the $D_2{}^{16}O$-$D_2{}^{18}O$ difference spectra of the dark-dark traces shown in Figures 3.7 and 3.8.

Chapter 4

One of the substrate waters for O_2 formation in Photosystem II is provided by the water-splitting Mn_4CaO_5 cluster's Ca^{2+} ion

4.1 ABSTRACT

During the catalytic step immediately prior to O-O bond formation in Photosystem II, a water molecule deprotonates and moves next to the water-splitting Mn_4CaO_5 cluster's O5 oxo bridge. Considerable evidence identifies O5 as one of the two substrate waters that ultimately form O_2. The relocated oxygen, known as O6 or O*x*, may be the second. It is currently debated whether O6/O*x* originates as the Mn-bound water denoted W2 or as the Ca^{2+}-bound water denoted W3. To distinguish between these two possibilities, we analyzed the D-O-D bending mode of the water molecule that deprotonates/relocates to become O6/O_x. We show that this D-O-D bending mode is not altered by the D1-S169A mutation. Previously, we showed that this D-O-D bending mode is altered substantially when Sr^{2+} is substituted for Ca^{2+}. Because Sr^{2+}/Ca^{2+} substitution alters this D-O-D bending mode but the D1-S169A mutation does not, we conclude that the water-derived oxygen that relocates and becomes O6/O*x* derives from the Ca^{2+}-bound W3. This conclusion provides an important constraint for proposed mechanisms of O-O bond formation in Photosystem II.

4.2 INTRODUCTION

The Mn_4CaO_5 cluster in Photosystem II (PSII) produces nearly all the molecular oxygen on Earth. The oxygen is released as the by-product of oxidizing water to provide the electrons and protons that ultimately drive the production of all of Earth's biomass. Our understanding of water oxidation by the Mn_4CaO_5 cluster has advanced rapidly in recent

years because of new developments in X-ray crystallography and the synergism between structural, computational, and advanced biophysical studies (for recent reviews, see refs *1-4*). PSII is a large protein complex that is integral to the thylakoid membrane and is dimeric *in vivo*. Each monomer contains approximately 20 subunits and has a molecular weight of approximately 350 kDa. Its structure has been determined to 1.85 – 1.95 Å in cyanobacteria with crystallography (*5-7*) and to 2.7 – 5.2 Å in various plant species with cryo-EM (*8-11*). Structures of reaction intermediates have been determined to 2.35 Å (*12*) and recently to 2.04 – 2.08 Å (*13*) in cyanobacteria with serial femtosecond crystallography. At the core of each PSII monomer is a heterodimer of two subunits known as D1 and D2. Light-induced electron transfer within the D1/D2 heterodimer drives the oxidation of the Mn_4CaO_5 cluster, with tyrosine Y_Z serving to transfer electrons from the Mn_4CaO_5 cluster to $P_{680}^{\bullet+}$. The Mn_4CaO_5 cluster is arranged as a distorted Mn_3CaO_4 cube that is linked to a fourth Mn ion (denoted Mn4) by two oxo bridges (see Figure 4.1). One of these bridges is denoted O5. Considerable evidence supports identifying O5 as the deprotonated form of one of the two substrate water molecules that ultimately form the O-O bond (*14-17*). Four electrons are removed from the Mn_4CaO_5 cluster during each catalytic cycle, advancing the cluster through five reaction intermediates termed S_n, where "n" denotes the number of oxidizing equivalents stored (n = 0 – 4). The S_1 state predominates in dark-adapted samples. Both substrate water molecules are bound to the Mn_4CaO_5 cluster by at least the S_2 state (*18-20*). The S_4 state is a transient intermediate whose formation triggers the utilization of the four stored oxidizing equivalents to form O_2 from two substrate-water-derived metal ligands. This process regenerates the S_0 state. Because of its transient nature,

the S_4 state remains uncharacterized. Recent efforts have concentrated on characterizing the S_3 state, the transition between the S_2 and S_3 states, and the identity of the second water-derived oxygen that combines with O5 to form the O-O bond.

The S_2 state consists of three six-coordinate Mn(IV) ions and one five-coordinate Mn(III) ion. The Mn(III) ion becomes a six-coordinate Mn(IV) ion during the S_2 to S_3 transition (*22*). The S_2 state can adopt two nearly isoenergetic forms that differ in the location of O5 (*23, 24*). Both forms are observable at cryogenic temperatures, but in the recent 2.08 Å room-temperature structure of the S_2 state, only one of these is evident: O5 coordinates to Mn4 and the five-coordinate Mn(III) is Mn1 (*13, 25*). During the S_2 to S_3 transition, a water molecule or water-derived metal ligand deprotonates and moves to a position on Mn1 in close proximity to O5, completing this Mn ion's coordination shell (*12, 13, 22*). This water-derived oxygen has been identified in the recent 2.35 Å (*12*) and 2.07 Å (*13*) structures of the S_3 state. It has been denoted O6 (*12*) or O*x* (*13*). This oxygen is frequently identified as a deprotonated form of the second substrate water molecule (*22, 26-37*) although, rather than being the second substrate itself, it may be positioned to replace O5 during the S_4 to S_0 transition, becoming a substrate during the next cycle of O_2 formation (*13*).

The origin of O_6/O*x* is under debate. In one set of models (*31-33, 35, 38-41*) [e.g., the "carousel" (*38, 39*) and "pivot" (*33, 35*) models], O_6/O*x* originates from the Mn4-bound W2. In these models, during the S_2 to S_3 transition, W2 deprotonates and relocates to the O5 position, O5 relocates to the O_6/O*x* position, and W2 is replaced on Mn4 by a water molecule (labeled W_x) that had previously formed a hydrogen bond with the O4 oxo bridge.

Consequently, in the S_3 state, W2 has become O5, O5 has become O_6/O*x*, and Wx occupies the same position on Mn4 that had been occupied by W2 in the S_2 state. In a competing set of models (*29, 30, 34, 37, 42-44*), O_6/O*x* originates from the Ca^{2+}-bound W3. In most of these models (*29, 30, 34, 37, 44*), during the S_2 to S_3 transition, the relocation of W3 is coupled to its deprotonation[1] and it is replaced on Ca^{2+} by a nearby water molecule such as W5 (the water molecule that bridges W3 and W2). Consequently, in the S_3 state, W3 has become O_6/O*x* and W5 (or another water molecule) occupies the same position on Ca^{2+} that had been occupied by W3 in the S_2 state[2].

Whether O6/O*x* is the second substrate and combines with O5 to form O_2 in the S_4 state (*22, 26-37*) or is simply positioned in the S_3 state to replace O5 during the S_4 to S_0 transition (*13*), determining its origin during the S_2 to S_3 transition is essential for understanding the molecular mechanism of O_2 formation. In this study, D-O-D vibrational modes were analyzed to determine if O6/O*x* originates from the Mn4-bound W2 or the Ca^{2+}-bound W3 (D-O-D modes were analyzed instead of H-O-H modes because the latter appear in a congested spectral region). During the S_2 to S_3 transition, one D-O-D bending mode is eliminated (*45-48*), meaning that the water molecule corresponding to this mode either deprotonates or relocates to a different environment. If O6/O*x* originates from the Mn4-bound W2, this mode must correspond to Wx (or to a nearby water molecule that replaces Wx during this transition). If O6/O*x* originates from the Ca^{2+}-bound W3, this mode must correspond to W5 or another nearby water molecule that replaces W3 during this transition.

The side chain of D1-S169 forms a hydrogen bond with Wx and its backbone carbonyl forms a hydrogen bond with W1 (D1-D61 also forms a hydrogen bond with W1). A recent computational study has shown that the D1-S169A mutation causes structural perturbations that are localized near this residue and Wx (*49*). Therefore, if O6/O*x* originates from the Mn4-bound W2, the D1-S169A mutation should alter the D-O-D bending mode of Wx (or the water that replaces Wx). Similarly, crystallographic (*50*) and computational (*21, 51, 52*) studies have shown that substituting Sr^{2+} for Ca^{2+} causes structural perturbations that are localized primarily near the Ca^{2+} ion and that include W3 and W5. Therefore, if O6/O*x* originates from the Ca^{2+}-bound W3, then substituting Sr^{2+} for Ca^{2+} should alter the D-O-D bending mode of the water molecule that replaces W3 (e.g., W5).

In this study, we show that the D-O-D bending mode that is eliminated during the S_2 to S_3 transition is not altered by the D1-S169A mutation. Previously, we showed that this mode is altered substantially when Sr^{2+} is substituted for Ca^{2+} (*47*). Because Sr^{2+}/Ca^{2+} substitution alters this D-O-D bending mode substantially but the D1-S169A mutation does not, we conclude that the water-derived oxygen that relocates to Mn1 during the S_2 to S_3 transition derives from the Ca^{2+}-bound W3. This conclusion provides an important constraint for proposed mechanisms of O-O bond formation in Photosystem II.

4.3 MATERIALS AND METHODS

Construction of Mutants and Purification of PSII Core Complexes. The D1-S169A mutation was constructed in the *psbA-2* gene of *Synechocystis* sp. PCC 6803 as described previously (*49*). Large-scale cultures of mutation-bearing *Synechocystis* cells were

propagated as described previously (*46*). The wild-type strain described in this manuscript was constructed in an identical manner as the mutant strain but with a transforming plasmid that carried no mutation. Oxygen-evolving PSII core complexes were purified under dim green light at 4 °C with a Ni-NTA superflow affinity resin (Qiagen, Valencia, CA) as described previously (*46*). The purified PSII core complexes were suspended in 1.2 M betaine, 10% (v/v) glycerol, 50 mM MES-NaOH (pH 6.0), 20 mM $CaCl_2$, 5 mM $MgCl_2$, 50 mM histidine, 1 mM EDTA, and 0.03 % (w/v) n-dodecyl β-D-maltoside, concentrated to approx. 1 mg of Chl per mL, flash-frozen in liquid N_2, and stored at −80 °C. To verify the integrity of the large-scale cultures that were harvested for the purification of D1-S169A PSII core complexes, an aliquot of each large-scale culture was set aside and the sequence of the relevant portion of the *psbA-2* gene was obtained after PCR amplification of genomic DNA (*53*). No trace of the wild-type codon was detected in any of the mutant cultures.

Preparation of FTIR samples. PSII core complexes were transferred into 40 mM sucrose, 10 mM MES-NaOH (pH 6.0), 5 mM $CaCl_2$, 5 mM NaCl, 0.06% (w/v) *n*-dodecyl β-D-maltoside, concentrated, mixed with 1/10 volume of fresh 100 mM potassium ferricyanide, spread in the center 13 mm of a 25 mm BaF_2 window, then dried lightly with N_2 gas (*47*). The lightly dried samples were rehydrated with six 1 μL drops of a solution of 20% (v/v) glycerol$(OD)_3$ (98% D, Cambridge Isotope Laboratories, Inc., Andover, MA) in $D_2{}^{16}O$ (99.9% D, Cambridge Isotope Laboratories, Inc., Andover, MA) or $D_2{}^{18}O$ (98% D, 97% ^{18}O, Cambridge Isotope Laboratories, Inc., Andover, MA), respectively (*45-48*). A second window was placed over the first with a thin O-ring spacer in between (*46-48*).

Sealed samples were equilibrated in the FTIR sample compartment at 0°C in darkness for 1.5 h, illuminated with 6 pre-flashes, then dark-adapted for 30 min (*46-48*). For each sample, the absorbance at 1657 cm^{-1} (amide I band) was 0.6 – 1.1.

FTIR Spectroscopy. Spectra were recorded with a Bruker Vertex 70 spectrometer (Bruker Optics, Billerica, MA) outfitted with a pre-amplified, midrange D317 photovoltaic MCT detector (Kolmar Technologies, Inc., Newburyport, MA), as described previously (*47*). After dark adaptation (see previous paragraph), samples were given six flashes at 13 s intervals. Two transmission spectra were recorded before the first flash and one transmission spectrum was recorded starting 0.33 s after the first and subsequent flashes (each transmission spectrum consisted of 100 scans). The 0.33 s delay was included to allow the oxidation of $Q_A^{\bullet-}$ by the ferricyanide. Difference spectra of the successive S-state transitions (e.g., S_{n+1}–*minus*–S_n difference spectra, written as $S_{n+1}-S_n$ in this study), were obtained by dividing the transmission spectrum obtained after the n^{th} flash by the transmission spectrum obtained before the n^{th} flash, then converting the ratio to units of absorption. The background noise level and the stability of the baseline were obtained by dividing the second pre-flash transmission spectrum by the first and converting the ratio to units of absorption (these spectra are labeled dark−dark in each figure – these are control difference spectra obtained *without* a flash being given). The sample was then dark-adapted for 30 min and the cycle was repeated. For each sample, the illumination cycle was repeated 19 times. The spectra of 30-60 samples were averaged (see figure legends). The amplitudes of the D1-S169A difference spectra were multiplied by factors of 1.14 to 1.25 to normalize the amplitudes of the peaks corresponding to the reduction of ferricyanide to ferrocyanide

by $Q_A^{\bullet-}$ (at 2115 and 2037 cm^{-1}, respectively) to those in the corresponding wild-type spectra (this procedure normalizes the spectra to the extent of flash-induced charge-separation).

4.4 RESULTS

The mid-frequency FTIR difference spectra produced by the first, second, third, and fourth flashes applied to wild-type PSII core complexes hydrated with $D_2{}^{16}O$ or $D_2{}^{18}O$ are compared in Figure 4.2. These closely resemble the difference spectra reported previously for wild-type samples rehydrated in $D_2{}^{16}O$ or $D_2{}^{18}O$ (*45-48*) and correspond predominantly to S_2-S_1, S_3-S_2, S_0-S_3, and S_1-S_0 FTIR difference spectra, respectively. Corresponding spectra from D1-S169A PSII core complexes rehydrated in $D_2{}^{16}O$ or $D_2{}^{18}O$ are compared in Figure 4.3. The spectra produced by the third and fourth flashes applied to the D1-S169A PSII (labeled S_0-S_3 and S_1-S_0 in Figure 4.3) are more distinct than in our previous study (*49*) because many more spectra were averaged for this study owing to the weak intensities of D-O-D bending modes. The amplitudes of the D1-S169A difference spectra are lower than those of wild-type despite being normalized to the extent of flash-induced charge-separation in the wild-type. Despite the lower amplitudes, the spectra produced by the first three flashes are recognizable as corresponding predominantly to S_2-S_1, S_3-S_2, and S_0-S_3 difference spectra. The lower amplitudes of the D1-S169A difference spectra and the relatively indistinct nature of the difference spectrum produced by the 4^{th} flash probably arise because (i) some D1-S169A PSII reaction centers lack functional Mn_4CaO_5 clusters both *in vivo* and *in vitro* (*49*), and (ii) the efficiency of the S state cycle is diminished in D1-S169A compared to wild-type (i.e., the "miss parameter" in D1-S169A

is twice that in wild-type) (*49*). The larger "miss parameter" means that a significant fraction of D1-S169A PSII fails to advance to the next S state following each saturating flash. In wild-type PSII, the features in the mid-frequency FTIR difference spectra oscillate during the S state transitions, so that features that appear during the S_1 to S_2 and S_2 to S_3 transitions are reversed during the S_3 to S_0 and S_0 to S_1 transitions (*54-62*). Therefore, if significant fractions of mutant PSII reaction centers fail to advance between S states in response to saturating flashes, PSII centers that undergo the S_3 to S_0 or S_0 to S_1 transitions after the third or fourth flashes will have the spectral features corresponding to these transitions partly canceled by PSII centers undergoing the S_1 to S_2 or S_2 to S_3 transitions, giving rise to difference spectra having low amplitudes. This situation undoubtedly applies to the D1-S169A difference spectra produced by the third flash and especially the fourth flash in Figure 4.3. Because the D1-D169A "S_1-S_0" spectrum obtained after the fourth flash undoubtedly corresponds to a substantial mixture of S state transitions, these fourth-flash double difference spectra will not be considered further here.

The alterations to the FTIR difference spectra caused by the D1-S169A mutation, e.g., the diminished features at 1679(-), 1544(-), 1532(+), 1525(-), 1415(-), and 1409(+) cm^{-1} in the S_2-S_1 spectrum and the absence of features at 1667(+), 1516(-), 1422(-), and 1413(+) cm^{-1} in the S_3-S_2 spectrum were noted in our previous study of the D1-S169A mutant and were attributed to mutation-induced alterations to the network of hydrogen bonds that extends from D1-D61 to the Ca^{2+} ion and Y_Z (*49*).

Because D-O-D vibrational modes have very weak intensities, they are best observed in $D_2{}^{16}O$ – $D_2{}^{18}O$ double difference spectra (*45-48*). To calculate $D_2{}^{16}O$ – $D_2{}^{18}O$

double difference spectra, the difference spectra shown in Figure 4.2 and Figure 4.3 were subtracted directly. The resulting S_{n+1}-S_n $D_2{}^{16}O$-$D_2{}^{18}O$ double difference spectra of wild-type and D1-S169A in the D-O-D bending [δ(DOD)] region are compared in Figure 4.4 (black and red traces, respectively). The double difference spectra for wild-type resemble those reported previously for *Thermosynechococcus elongatus* (*45*) and *Synechocystis* sp. PCC 6803 (*46-48*). The features between 1270 and 1250 cm^{-1} do not appear in all published wild-type double difference spectra (*45-48*). Subtle differences in sample humidity have been speculated to be the cause of this lack of reproducibility (*48*). These features will not be considered further here. In contrast, the features at 1241 cm^{-1} in the wild-type S_3-S_2 and S_0-S_3 double difference spectra vary only 1-3 cm^{-1} between studies, the features between 1225 and 1200 cm^{-1} in the S_2-S_1, S_3-S_2, S_0-S_3 , and S_1-S_0 wild-type double difference spectra vary only 1-3 cm^{-1}, and the weaker features between 1195 and 1170 vary 1-6 cm^{-1} (*45-48*). In this study, the features between 1240 and 1170 cm^{-1} in the $D_2{}^{16}O - D_2{}^{18}O$ double difference spectra of D1-S169A aligned well with those in wild-type, with shifts of only 1-2 cm^{-1} (e.g., their frequencies were effectively unchanged from wild-type).

However, in the mutant S_2-S_1 double difference spectrum (top red trace in Figure 4.4), the features at 1220(-) and 1213(+) cm^{-1} showed substantially lower intensities than the corresponding features of wild-type. In addition, a new positive feature appeared at 1228 cm^{-1}. In the mutant S_3-S_2 double difference spectrum (second red trace in Figure 4.4), all of the main features between 1275 and 1200 cm^{-1} aligned closely with those in wild-type but the positive features near 1173 cm^{-1} were replaced with negative features near 1179 cm^{-1}. In the mutant S_0-S_3 double difference spectrum (third red trace in Figure 4.4),

all of the main features aligned closely with those in wild-type, but the amplitudes were substantially lower than in wild-type.

4.5 DISCUSSION

The alteration of a single D-O-D bending mode in a S_{n+1}-S_n difference spectrum could produce up to four peaks in a $D_2{}^{16}O$-$D_2{}^{18}O$ double difference spectrum, two corresponding to $D_2{}^{16}O$ and two corresponding to $D_2{}^{18}O$. However, spectral overlap will cause fewer peaks to be evident. In wild-type samples, the number of features in the $D_2{}^{16}O$-$D_2{}^{18}O$ double difference spectrum of the S_1 to S_2 transition (e.g., Figure 4.4, upper pair of traces) implies that at least two δ(DOD) modes are altered during this transition (*45-48*). In wild-type samples, the amplitudes of most of these features oscillate during the S state cycle. For example, the 1211(+) cm^{-1} feature in the S_2-S_1 double difference spectrum becomes negative (at 1212-1216 cm^{-1}) in the S_3-S_2 and S_0-S_3 double difference spectra and positive again (at 1215 cm^{-1}) in the S_1-S_0 double difference spectrum. Also, the 1222(-) cm^{-1} feature in the S_2-S_1 double difference spectrum becomes positive (at 1226 cm^{-1}) in the S_3-S_2 double difference spectrum and positive (at 1221 cm^{-1}) in the S_0-S_3 double difference spectrum. The oscillations imply that most of the δ(DOD) modes that are altered during the S_1 to S_2 transition are altered reversibly during the S state cycle (*45-48*). Some of these modes must correspond to the water molecules that were identified as moving during the S state transitions in the recent X-ray crystallographic structures of the S_2 (*13*), S_3 (*12, 13*), and S_0 (*13*) states, including the water labeled W20 in ref. *13* and W195 in ref. *49*. Some must correspond to water molecules that interact with D1-D61 because the 1222(-), 1211(+), and 1179(+) cm^{-1} features in the S_2-S_1 $D_2{}^{16}O$-$D_2{}^{18}O$ double difference spectrum

are eliminated by the D1-D61A mutation (*46*). The frequencies of the modes that are eliminated by the D1-D61A mutation appear to be largely unaltered by the D1-S169A mutation, but the substantially lower amplitudes of the 1220(-) and 1213(+) cm^{-1} features in the D1-D169A S_2-S_1 double difference spectrum and of the corresponding 1223(+) and 1212(-) cm^{-1} features in the D1-S169A S_0-S_3 double difference spectrum imply that a second δ(DOD) mode may contribute to these features in wild-type. Therefore, at least one D-O-D molecule whose δ(DOD) mode changes reversibly during the S state cycle may be altered by the D1-S169A mutation. The δ(DOD) mode of this D-O-D molecule may correspond to the 1228(+) cm^{-1} feature in the mutant S_2-S_1 double difference spectrum. This D-O-D molecule may correspond to Wx or to another water molecule nearby. According to a recent QM/MM analysis, the D1-S169A mutation alters the positions of Wx and W20/W195 (*49*).

The 1241(–) cm^{-1} features in the wild-type S_3-S_2 and S_0-S_3 double difference spectra have no positive counterparts in any other double difference spectrum (*45-48*). The lack of any positive counterparts implies that the bending mode of a single water molecule is eliminated during each of the S_2 to S_3 and S_3 to S_0 transitions (*45-48*). Therefore, the 1241(–) cm^{-1} features correspond to one water molecule that either deprotonates or relocates to a different environment during the S_2 to S_3 transition and to another that deprotonates or relocates to a different environment during the S_3 to S_0 transition. The data of Figure 4.4 (second and third set of traces) show that the D1-S169A mutation does not alter either of these modes significantly.

S_2 to S_3 transition. The side chain of D1-S169 forms a hydrogen bond with Wx. The recent QM/MM study of the D1-S169A mutation shows that the structural perturbations caused by this mutation are localized near this residue, with Wx shifting 0.5 Å, W20/W195 shifting 0.3 Å, and D1-D61 and CP43-R357 shifting 0.18 and 0.12 Å, respectively (*49*). Because the D1-S169A mutation shifts the position of Wx and eliminates a hydrogen bond involving Wx, the mutation should alter the δ(DOD) mode of Wx and other water molecules in its vicinity. Therefore, if O6/O*x* originates from the Mn4-bound W2, the D1-S169A mutation should alter the δ(DOD) mode that vanishes during the S_2 to S_3 transition. However, our data show that the D1-S169A mutation does *not* alter this mode. Both crystallographic (*50*) and computational (*21, 51, 52*) studies have shown that substituting Sr^{2+} with Ca^{2+} causes structural perturbations that are localized near the Ca^{2+} ion and that include W3 and W5. Consequently, if O6/O*x* originates from the Ca^{2+}-bound W3, then Sr^{2+}/Ca^{2+} substitution should alter the δ(DOD) mode of the water molecule that replaces W3 (e.g., W5). We showed previously that Sr^{2+}/Ca^{2+} substitution eliminates or (more likely) downshifts the 1241(-) cm^{-1} feature in the S_3-S_2 double difference spectrum by 15 cm^{-1}, moving it underneath the 1226(+) cm^{-1} feature (*47*). We also showed that the 1241(-) cm^{-1} feature is shifted approximately 6 cm^{-1} by the D1-V185N mutation (*48*). Identifying this feature with W5 would be consistent with its alteration by the D1-V185N mutation because W5 is only 4.7 Å from D1-V185 (*5-7*). The replacement of W3 by W5 during the S_2 to S_3 transition was proposed originally on the basis of DFT calculations (*34*). On the basis of additional recent DFT calculations, it has been proposed that the alterations produced by substituting Sr^{2+} for Ca^{2+} are less localized that thought previously and that

Sr^{2+}/Ca^{2+} substitution causes the p*K*a values of W1, W2, D1-D61, D1-His332, and D1-His337 to increase (*63*). Nevertheless, Sr^{2+}/Ca^{2+} substitution substantially alters the δ(DOD) mode of only a *single* water molecule, the water whose δ(DOD) mode vanishes during the S_2 to S_3 transition (*47*).

The deprotonation/relocation of W3 to the O6/O*x* position and its replacement by W5 or another nearby water molecule would be consistent with recent a time-resolved FTIR study (*64*). The results of this study show that the S_2 to S_3 transition includes a ~ 100 μsec phase that precedes electron transfer and that represents changes to the C-O stretching mode of $Y_Z^{\bullet}$ (evidence of a strengthened hydrogen bond interaction with $Y_Z^{\bullet}$) in addition to changes in $\nu_{sym}(COO^-)$ modes of carboxylate groups and the O-H stretching modes of hydrogen bonded water molecules. This phase was attributed to the rearrangement/reorientation of water molecules in a network of hydrogen bonds that includes both Y_Z and the Mn_4CaO_5 cluster, consistent with the relocation of W3 and its replacement by another water molecule in the network (*64*). A W3 origin for O6/O*x* also would be consistent with the recent serial femtosecond crystallography study of the S_1, S_2, S_3, and S_0 states at 2.04 – 2.07 Å and, indeed, was proposed by the study's authors (*13*). Several water molecules near oxo bridge O1 (which bridges Mn1 and the Ca^{2+} ion) were observed to move during the individual S state transitions and O6/O*x* is coordinated to both Mn1 and the Ca^{2+} ion in the 2.07 Å structure of the S_3 state, (*13*).

The S_3 to S_0 transition. The S_3 to S_0 transition is a multistep process involving the movements of water molecules and the rearrangement of networks of hydrogen bonds as O_2 is formed and released and at least one substrate water molecule is re-bound (*13, 65,*

66). The 1241(-) cm^{-1} feature in the wild-type S_0-S_3 double difference spectra may correspond to the water molecule that is expected to replace O5 during the regeneration of the S_0 state. This water would deprotonate during the process of forming a hydroxo bridge between Mn4 and Mn1 during the S_4 to S_0 transition (*17, 67, 68*) and would further deprotonate to form an oxo bridge during the S_0 to S_1 transition (*17*). The origin of this water molecule remains unknown, but because the 1241 cm^{-1} feature is shifted no more than 2 cm^{-1} by the D1-S169A mutation (Figure 4.4) and is shifted only 5 cm^{-1} when Sr^{2+} is substituted for Ca^{2+} (*47*), it must not interact strongly with either D1-S169 or with the Ca^{2+} ion. It should be noted, however, that the same computational study that proposed that W5 replaces W3 on Ca^{2+} during the S_2 to S_3 transition also proposed that this water molecule relocates again during the S_4 to S_0 transition, moving to the O5 position for the next cycle of O_2 formation (*34*).

4.6 SUMMARY AND CONCLUSIONS

In this study, we show that the D-O-D bending mode that is eliminated during the S_2 to S_3 transition is not altered by the D1-S169A mutation. Because the substitution of Sr^{2+} for Ca^{2+} alters this D-O-D bending mode substantially (*47*) but the D1-S169A mutation does not, we conclude that the water-derived oxygen that relocates to Mn1 during the S_2 to S_3 transition derives from the Ca^{2+}-bound W3. We also conclude that the water molecule that is expected to replace O5 during the S_4 to S_0 transition does not interact strongly with either the Ca^{2+} ion or D1-S169. These conclusions provide important constraints for proposals for the molecular mechanism of O-O bond formation in Photosystem II.

4.7 ACKNOWLEDGEMENTS

We thank Anh P. Nguyen for maintaining the mutant and wild-type cultures of *Synechocystis* sp. PCC 6803 and for purifying the thylakoid membranes that were used for the isolation of PSII core complexes and V. S. Batista and coworkers for providing the QM/MM-optimized coordinates for the Mn_4CaO_5 cluster and its environments. This work was supported by the Department of Energy, Office of Basic Energy Sciences, Division of Chemical Sciences, grant DE-SC0005291.

4.8 ADDITIONAL NOTES

Abbreviations: Chl, chlorophyll; EDTA, ethylenediaminetetraacetic acid; FTIR, Fourier transform infrared; MES, 2-(N-morpholino)-ethanesulfonic acid; P_{680}, chlorophyll multimer that serves as the light-induced electron donor in PSII; PSII, photosystem II; Q_A, primary plastoquinone electron acceptor; Y_Z, tyrosine residue that mediates electron transfer between the Mn_4O_5Ca cluster and $P_{680}^{+\bullet}$.

[1] Whether deprotonation precedes (34, 44) or follows (30, 37) relocation depends on the specific model.

[2] In some variations (29, 30), W3 relocates to Mn4, with O5 first moving to Mn1, so that W3 becomes O5 and O5 becomes O6/Ox.

4.9 REFERENCES

(1) Pérez-Navarro, M., Neese, F., Lubitz, W., Pantazis, D. A., and Cox, N. (2016) Recent developments in biological water oxidation, *Curr. Opin. Chem. Biol. 31*, 113-119.

(2) Askerka, M., Brudvig, G. W., and Batista, V. S. (2017) The O_2-Evolving Complex of Photosystem II: Recent Insights from Quantum Mechanics/Molecular Mechanics (QM/MM), Extended X-ray Absorption Fine Structure (EXAFS), and Femtosecond X-ray Crystallography Data, *Acc. Chem. Res. 50*, 41-48.

(3) Pantazis, D. A. (2018) Missing Pieces in the Puzzle of Biological Water Oxidation, *ACS Catalysis 8*, 9477-9507.

(4) Lubitz, W., Chrysina, M., and Cox, N. (2019) Water oxidation in photosystem II, *Photosynth. Res. 142*, 105–125.

(5) Umena, Y., Kawakami, K., Shen, J.-R., and Kamiya, N. (2011) Crystal Structure of Oxygen-Evolving Photosystem II at a Resolution of 1.9 Å, *Nature 473*, 55-60.

(6) Suga, M., Akita, F., Hirata, K., Ueno, G., Murakami, H., Nakajima, Y., Shimizu, T., Yamashita, K., Yamamoto, M., Ago, H., and Shen, J.-R. (2015) Native structure of photosystem II at 1.95 Å resolution viewed by femtosecond X-ray pulses, *Nature 517*, 99-103.

(7) Tanaka, A., Fukushi, Y., and Kamiya, N. (2017) Two Different Structures of the Oxygen-Evolving Complex in the Same Polypeptide Frameworks of Photosystem II, *J. Am. Chem. Soc. 139*, 1718-1721.

(8) Wei, X., Su, X., Cao, P., Liu, X., Chang, W., Li, M., Zhang, X., and Liu, Z. (2016) Structure of spinach photosystem II-LHII supercomplex at 3.2 A resolution, *Nature 534*, 69-74.

(9) van Bezouwen, L. S., Caffarri, S., Kale, R. S., Kouril, R., Thunnissen, A.-M. W. H., Oostergetal, G. T., and Boekem, E. J. (2017) Subunit and chlorophyll organization of the plant photosystem II supercomplex, *Nature Plants 3*, Article No. 17080.

(10) Su, X., Ma, J., Wei, X., Cao, P., Zhu, D., Chang, W., Liu, Z., and Li, M. (2017) Structure and assembly mechanism of plant $C_2S_3M_2$-type PSII-LHCII supercomplex, *Science 357*, 815-820.

(11) Cao, P., Su, X., Pan, X., Liu, Z., Chang, W., and Li, M. (2018) Structure, assembly and energy transfer of plant photosystem II supercomplex, *Biochim. Biophys. Acta 1859*, 633-644.

(12) Suga, M., Akita, F., Sugahara, M., Kubo, M., Nakajima, Y., Nakane, T., Yamashita, K., Umena, Y., Nakabayashi, M., Yamane, T., Nakano, T., Suzuki, M., Masuda, T., Inoue, S., Kimura, T., Nomura, T., Yonekura, S., Yu, L.-J., Sakamoto, T., Motomura, T., Chen, J.-H., Kato, Y., Noguchi, T., Tono, K., Joti, Y., Kameshima, T., Hatsui, T., Nango, E., Tanaka, R., Naitow, H., Matsuura, Y., Yamashita, A., Yamamoto, M., Nureki, O., Yabashi, M., Ishikawa, T., Iwata, S., and Shen, J.-R. (2017) Light-induced structural changes and the site of O=O bond formation in PSII caught by XFEL, *Nature 543*, 131-135.

(13) Kern, J., Chatterjee, R., Young, I. D., Fuller, F. D., Lassalle, L., Ibrahim, M., Gul, S., Fransson, T., Brewster, A. S., Alpert, B., Hussein, R., Zhang, M., Douthit, L., de Lichtenberg, C., Cheah, M. H., Shevela, D., Wersig, J., Seuffert, I., Sokaras, D., Pastor, E., Weninger, C., Kroll, T., Sierra, R. G., Aller, P., Butryn, A., Orville, A. M., Liang, M., Batyuk, A., Koglin, J. E., Carbajo, S., Boutet, S., Moriarty, N. W., Holton, J. M., Dobbek, H., Adams, P. D., Bergmann, U., Sauter, N. K., Zouni, A., Messinger, J., Yano, J., and Yachandra, V. K. (2018) Structures of the intermediates of Kok's photosynthetic water oxidation clock, *Nature 563*, 421-425.

(14) Rapatskiy, L., Cox, N., Savitsky, A., Ames, W. M., Sander, J., Nowaczyk, M. M., Rögner, M., Boussac, A., Neese, F., Messinger, J., and Lubitz, W. (2012) Detection of Water-Binding Sites of the Oxygen-Evolving Complex of Photosystem II Using W-band ^{17}O Electron-Electron Double Resonance-Detected NMR Spectroscopy, *J. Am. Chem. Soc. 134*, 16619-16634.

(15) Pérez Navarro, M., Ames, W. M., Nilsson, H., Lohmiller, T., Pantazis, D. A., Rapatskiy, L., Nowaczyk, M. M., Neese, F., Boussac, A., Messinger, J., Lubitz, W., and Cox, N. (2013) Ammonia binding to the oxygen-evolving complex of photosystem II identified the solvent-exchangeable oxygen bridge (μ-oxo) of the manganese tetramer, *Proc. Natl. Acad. Sci. USA 110*, 15561-15566.

(16) Lohmiller, T., Krewald, V., Pérez Navarro, M., Retegan, M., Rapatskiy, L., Nowaczyk, M. M., Boussac, A., Neese, F., Lubitz, W., Pantazis, D. A., and Cox, N. (2014) Structure, ligands and substrate coordination of the oxygen-

evolving complex of photosystem II in the S_2 state: a combined EPR and DFT study, *Phys. Chem. Chem. Phys. 16*, 11877-11892.

(17) Lohmiller, T., Krewald, V., Sedoud, A., Rutherford, A. W., Neese, F., Lubitz, W., Pantazis, D. A., and Cox, N. (2017) The First State in the Catalytic Cycle of the Water-Oxidizing Enzyme: Identification of a Water-Derived μ-Hydroxo Bridge, *J. Am. Chem. Soc. 139*, 14412-14424.

(18) Hillier, W. and Wydrzynski, T. (2008) ^{18}O-Water Exchange in Photosystem II: Substrate Binding and Intermediates of the Water Splitting Cycle, *Coord. Chem. Rev. 252*, 306-317.

(19) Cox, N. and Messinger, J. (2013) Reflections on substrate water and dioxygen formation, *Biochim. Biophys. Acta 1827*, 1020-1030.

(20) Nilsson, H., Krupnik, T., Kargul, J., and Messinger, J. (2014) Substrate water exchange in photosystem II core complexes of the extremophilic red alga *Cyanidioschyzon merolae*, *Biochim. Biophys. Acta 1837*, 1257-1262.

(21) Vogt, L., Ertem, M. Z., Pal, R., Brudvig, G. W., and Batista, V. S. (2015) Computational Insights on Crystal Structures of the Oxygen-Evolving Complex of Photosystem II with Either Ca^{2+} or Ca^{2+} Substituted by Sr^{2+}, *Biochemistry 54*, 820-825.

(22) Cox, N., Retegan, M., Neese, F., Pantazis, D. A., Boussac, A., and Lubitz, W. (2014) Electronic structure of the oxygen-evolving complex in photosystem II prior to O-O bond formation, *Science 345*, 804-808.

(23) Pantazis, D. A., Ames, W., Cox, N., Lubitz, W., and Neese, F. (2012) Two Interconvertable Structures that Explain the Spectroscopic Properties of the Oxygen-Evolving Complex of Photosystem II in the S_2 State, *Angew. Chem. Int. Ed. 51*, 9935-9940.

(24) Isobe, H., Shoji, M., Yamanaka, S., Umena, Y., Kawakami, K., Kamiya, N., Shen, J.-R., and Yamaguchi, K. (2012) Theoretical illumination of water-inserted structures of the $CaMn_4O_5$ cluster in the S_2 and S_3 states of oxygen-evolving complex of photosystem II: full geometry optimizations by B3LYP hybrid density functional, *Dalton Trans. 41*, 13727-13740.

(25) Chatterjee, R., Lassalle, L., Gul, S., Fuller, F. D., Young, I. D., Ibrahim, M., de Lichtenberg, C., Cheah, M. H., Zouni, A., Messinger, J., Yachandra, V. K.,

Kern, J., and Yano, J. (2019) Structural isomers of the S_2 state in photosystem II: do they exist at room temperature and are they important for function?, *Physiol. Plant. 166*, 60-72.

(26) Siegbahn, P. E. M. (2009) Structures and Energetics for O_2 Formation in Photosystem II, *Acc. Chem. Res. 42*, 1871-1880.

(27) Siegbahn, P. E. M. (2013) Water oxidation mechanism in photosystem II, including oxidations, proton release pathways, O-O bond formation and O_2 release, *Biochim. Biophys. Acta 1827*, 1003-1019.

(28) Li, X. and Siegbahn, P. E. M. (2015) Alternative mechanisms for O_2 release and O-O bond formation in the oxygen evolving complex of photosystem II, *Phys. Chem. Chem. Phys. 17*, 12168-12174.

(29) Isobe, H., Shoji, M., Shen, J.-R., and Yamaguchi, K. (2015) Strong Coupling between the Hydrogen Bonding Environment and Redox Chemistry during the S_2 to S_3 Transition in the Oxygen-Evolving Complex of Photosystem II, *J. Phys. Chem. B 119*, 13922-13933.

(30) Shoji, M., Isobe, H., and Yamaguchi, K. (2015) QM/MM study of the S_2 to S_3 transition reaction in the oxygen-evolving complex of photosystem II, *Chem. Phys. Lett. 636*, 172-179.

(31) Capone, M., Narzi, D., Bovi, D., and Guidoni, L. (2016) Mechanism of Water Delivery to the Active Site of Photosystem II along the S_2 to S_3 Transition, *J. Phys. Chem. Lett. 7*, 592-596.

(32) Capone, M., Bovi, D., Narzi, D., and Guidoni, L. (2016) Reorganization of Substrate Waters between the Closed and Open Cubane Conformers during the S_2 to S_3 Transition in the Oxygen Evolving Complex, *Biochemistry 54*, 6439-6442.

(33) Retegan, M., Krewald, V., Mamedov, F., Neese, F., Lubitz, W., Cox, N., and Pantazis, D. A. (2016) A five-coordinate Mn(IV) intermediate in biological water oxidation: spectroscopic signature and a pivot mechanism for water binding, *Chem. Sci. 7*, 72-84.

(34) Ugur, I., Rutherford, A. W., and Kaila, V. R. I. (2016) Redox-coupled substrate water reorganization in the active site of Photosystem II - The role of calcium in substrate water delivery, *Biochim. Biophys. Acta 1857*, 740-748.

(35) Retegan, M. and Pantazis, D. A. (2016) Interaction of methanol with the oxygen-evolving complex: atomistic models, channel identification, species dependence, and mechanistic implications, *Chem. Sci. 7*, 6463-6476.

(36) Siegbahn, P. E. M. (2018) Water Oxidation by PSII: A Quantum Chemical Approach, in *Mechanisms of Primary Energy Transduction in Biology* (Wikström, M., Ed.) pp 273-295, Royal Society of Chemistry, London.

(37) Siegbahn, P. E. M. (2018) The S_2 to S_3 transition for water oxidation in PSII (photosystem II), revisited, *Phys. Chem. Chem. Phys. 20*, 22926-22931.

(38) Askerka, M., Vinyard, D. J., Brudvig, G. W., and Batista, V. S. (2015) NH_3 Binding to the S_2 State of the O_2-Evolving Complex of Photosystem II: Analogue to H_2O Binding during the S_2 to S_3 Transition, *Biochemistry 54*, 5783-5786.

(39) Askerka, M., Wang, J., Vinyard, D. J., Brudvig, G. W., and Batista, V. S. (2016) S_3 State of the O2-Evolving Complex of Photosystem II: Insights from QM/MM, EXAFS, and Femtosecond X-ray Diffraction, *Biochemistry 55*, 981-984.

(40) Wang, J., Askerka, M., Brudvig, G. W., and Batista, V. S. (2017) Crystallographic Data Support the Carousel Mechanism of Water Supply to the Oxygen-Evolving Complex of Photosystem II, *ACS Energy Lett. 2*, 2299-2306.

(41) Guo, Y., Li, H., He, L.-L., Zhao, D.-X., Gong, L.-D., and Yang, Z.-Z. (2017) The open-cubane oxo-oxyl coupling mechanism dominates photosythetic oxygen evolution: a comprehensive DFT investigation on O-O bond formation in the S_4 state, *Phys. Chem. Chem. Phys. 19*, 13909-13923.

(42) Ames, W., Pantazis, D. A., Krewald, V., Cox, N., Messinger, J., Lubitz, W., and Neese, F. (2011) Theoretical Evaluation of Structural Models of the S_2 State in the Oxygen Evolving Complex of Photosystem II: Protonation States and Magnetic Interactions, *J. Am. Chem. Soc. 133*, 19743-19757.

(43) Bovi, D., Narzi, D., and Guidoni, L. (2013) The S_2 State of the Oxygen-Evolving Complex of Photosystem II Explored by QM/MM Dynamics: Spin Surfaces and Metastable States Suggest a Reaction Path Towards the S_3 State, *Angew. Chem. Int. Ed. 52*, 11744-11749.

(44) Beal, N. J., Corry, T. A., and O'Malley, P. J. (2018) A Comparison of Experimental and Broken Symmetry Density Functional (BS-DFT) Calculated Electron Paramagnectic Resonance (EPR) Parameters for Intermediates Involved in the S_2 to S_3 State Transition of Nature's Oxygen Evolving Complex, *J. Phys. Chem. B 122*, 1394-1407.

(45) Suzuki, H., Sugiura, M., and Noguchi, T. (2008) Monitoring Water Reactions during the S-State Cycle of the Photosynthetic Water-Oxidizing Center: Detection of the DOD Bending Vibrations by Means of Fourier Transform Infrared Spectroscopy, *Biochemistry 47*, 11024-11030.

(46) Debus, R. J. (2014) Evidence from FTIR Difference Spectroscopy That D1-Asp61 Influences the Water Reactions of the Oxygen-Evolving Mn_4CaO_5 Cluster of Photosystem II, *Biochemistry 53*, 2941-2955.

(47) Kim, C. J. and Debus, R. J. (2017) Evidence from FTIR Difference Spectroscopy That a Substrate H_2O Molecule for O_2 Formation in Photosystem II is Provided by the Ca Ion of the Catalytic Mn_4CaO_5 Cluster, *Biochemistry 56*, 2558-2570.

(48) Kim, C. J., Bao, H., Burnap, R. L., and Debus, R. J. (2018) Impact of D1-V185 on the Water Molecules that faciliate O_2 Formation by the Catalytic Mn_4CaO_5 Cluster in Photosystem II, *Biochemistry 57*, 4299-4311.

(49) Ghosh, I., Banerjee, G., Kim, C. J., Reiss, K., Batista, V. S., Debus, R. J., and Brudvig, G. W. (2019) D1-S169A Substitution of Photosystem II Perturbs Water Oxidation, *Biochemistry 58*, 1379-1387.

(50) Koua, F. H. M., Umena, Y., Kawakami, K., and Shen, J.-R. (2013) Structure of Sr-substituted photosystem II at 2.1 Å resolution and its implications in the mechanism of water oxidation, *Proc. Natl. Acad. Sci. USA 110*, 3889-3894.

(51) Pitari, F., Bovi, D., Narzi, D., and Guidoni, L. (2015) Characterization of the Sr^{2+}- and Cd^{2+}-Substituted Oxygen-Evolving Complex of Photosystem II by Quantum Mechanics/Molecular Mechanics Calculations, *Biochemistry 54*, 5959-5968.

(52) Terrett, R., Petrie, S., Pace, R. J., and Stranger, R. (2014) What does the Sr-substituted 2.1 Å resolution crystal structure of photosystem II reveal about the water oxidation mechanism?, *Chem. Commun. 50*, 3187-3190.

(53) Chu, H.-A., Nguyen, A. P., and Debus, R. J. (1994) Site-Directed Photosystem II Mutants with Perturbed Oxygen Evolving Properties: 1. Instability or Inefficient Assembly of the Manganese Cluster *In Vivo*, *Biochemistry 33*, 6137-6149.

(54) Noguchi, T. and Sugiura, M. (2002) Flash-Induced FTIR Difference Spectra of the Water Oxidizing Complex in Moderately Hydrated Photosystem II Core Films: Effect of Hydration Extent on S-State Transitions, *Biochemistry 41*, 2322-2330.

(55) Noguchi, T. and Sugiura, M. (2003) Analysis of Flash-Induced FTIR Difference Spectra of the S-State Cycle in the Photosynthetic Water-Oxidizing Complex by Uniform ^{15}N and ^{13}C Isotope Labeling, *Biochemistry 42*, 6035-6042.

(56) Yamanari, T., Kimura, Y., Mizusawa, N., Ishii, A., and Ono, T.-A. (2004) Mid- to Low-Frequency Fourier Transform Infrared Spectra of S-State Cycle for Photosynthetic Water Oxidation in *Synechocystis* sp. PCC 6803, *Biochemistry 43*, 7479-7490.

(57) Noguchi, T. (2007) Light-Induced FTIR Difference Spectroscopy as a Powerful Tool Toward Understanding the Molecular Mechanism of Photosynthetic Oxygen Evolution, *Photosyn. Res. 91*, 59-69.

(58) Noguchi, T. (2008) Fourier Transform Infrared Analysis of the Photosynthetic Oxygen-Evolving Center, *Coord. Chem. Rev. 251*, 336-346.

(59) Debus, R. J. (2008) Protein Ligation of the Photosynthetic Oxygen-Evolving Center, *Coord. Chem. Rev. 252*, 244-258.

(60) Noguchi, T. (2013) Monitoring the reactions of photosynthetic water oxidation using infrared spectroscopy, *Biomedical Spectroscopy and Imaging 2*, 115-128.

(61) Debus, R. J. (2015) FTIR Studies of Metal Ligands, Networks of Hydrogen Bonds, and Water Molecules near the Active Site Mn_4CaO_5 Cluster in Photosystem II, *Biochim. Biophys. Acta 1847*, 19-34.

(62) Noguchi, T. (2015) Fourier transform infrared difference and time-resolved infrared detection of the electron and proton transfer dynamics in photosynthetic water oxidation, *Biochim. Biophys. Acta 1847*, 35-45.

(63) Boussac, A., Ugur, I., Marion, A., Sugiura, M., Kaila, V. R. I., and Rutherford, A. W. (2018) The low spin - high spin equilibrium in the S_2-state of the water oxidizing enzyme, *Biochim. Biophys. Acta 1859*, 342-356.

(64) Sakamoto, H., Shimizu, T., Nagao, R., and Noguchi, T. (2017) Monitoring the Reaction Process During the S_2 to S_3 Transition in Photosynthetic Water Oxidation Using Time-Resolved Infrared Spectroscopy, *J. Am. Chem. Soc. 139*, 2022-2029.

(65) Klauss, A., Haumann, M., and Dau, H. (2015) Seven Steps of Alternating Electron and Proton Transfer in Photosystem II Water Oxidation Traced by Time-Resolved Photothermal Beam Deflection at Improved Sensitivity, *J. Phys. Chem. B 119*, 2677-2689.

(66) Zaharieva, I., Dau, H., and Haumann, M. (2017) Sequential and Coupled Proton and Electron Transfer Events in the S_2 to S_3 Transition of Photosynthetic Water Oxidation Revealed by Time-Resolved X-ray Absorption Spectroscopy, *Biochemistry 55*, 6996-7004.

(67) Pal, R., Negre, C. F. A., Vogt, L., Pokhrel, R., Ertem, M. Z., Brudvig, G. W., and Batista, V. S. (2013) S_0-State Model of the Oxygen-Evolving Complex of Photosystem II, *Biochemistry 52*, 7703-7706.

(68) Krewald, V., Retegan, M., Cox, N., Messinger, J., Lubitz, W., DeBeer, S., Neese, F., and Pantazis, D. A. (2015) Metal oxidation states in biological water splitting, *Chem. Sci. 6*, 1676-1695.

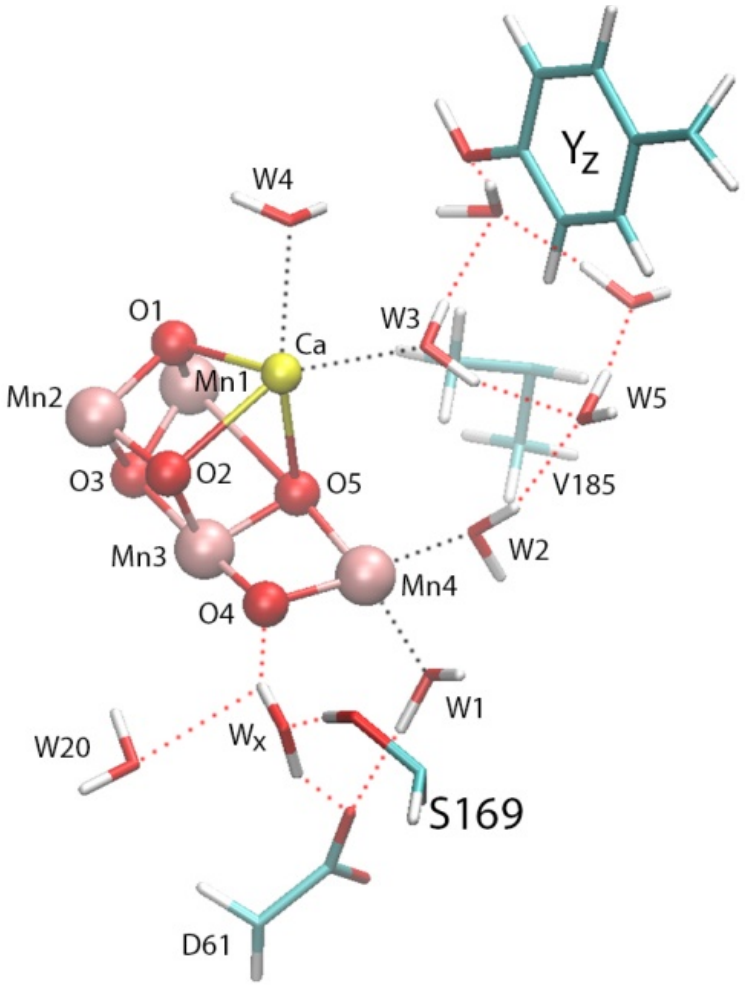

FIGURE 4.1 Water molecules and selected residues in the vicinity of the Mn_4CaO_5 cluster. All residues shown are from the D1 subunit. The salmon-colored spheres are manganese ions. The yellow sphere is the Ca^{2+} ion. The red spheres are the oxygen atoms of μ-oxo bridges. The coordinates for this figure were constructed with QM/MM methods (*21*) based on the coordinates in the 1.9 Å X-ray crystallographic model (*5*) and were kindly provided by V. S. Batista and coworkers.

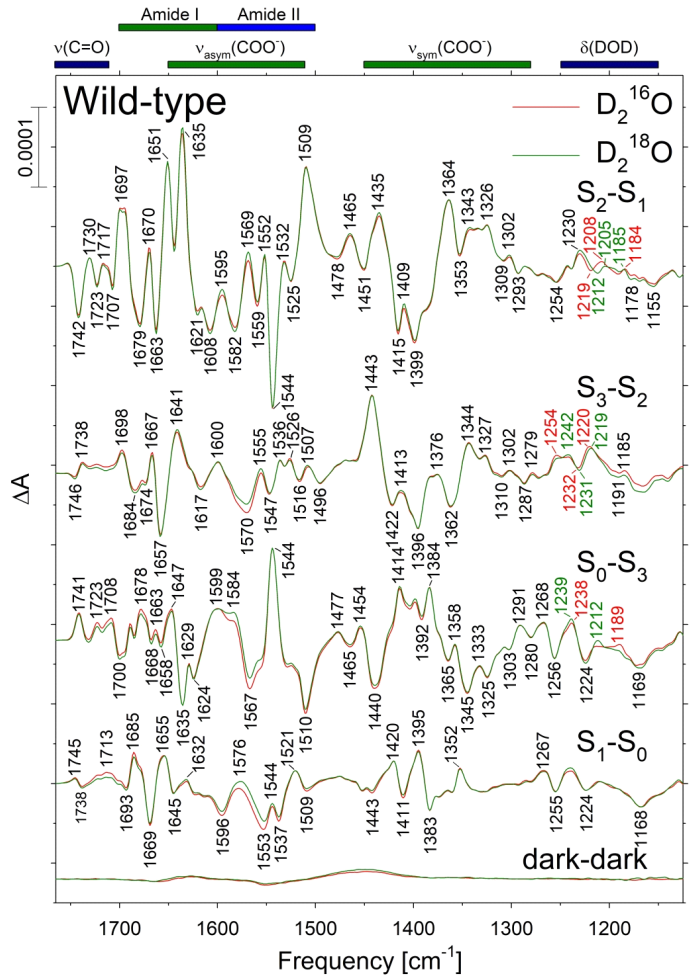

FIGURE 4.2 Mid-frequency FTIR difference spectra of wild-type PSII core complexes in response to four successive flash illuminations applied at 0°C after hydration with $D_2{}^{16}O$ (red) or $D_2{}^{18}O$ (green). The $D_2{}^{16}O$ data represent the averages of 30 samples (56,800 scans for each trace) and the $D_2{}^{18}O$ data represent the averages of 30 samples (57,000 scans for each trace). The dark-dark control traces show the noise level and the stability of the baseline (lower traces).

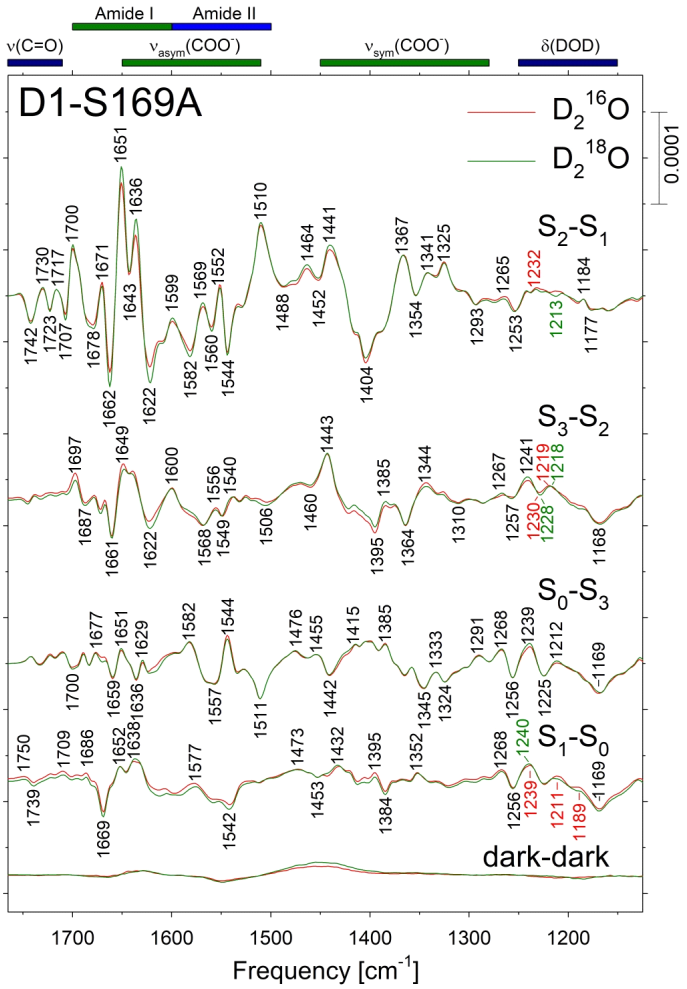

FIGURE 4.3 Mid-frequency FTIR difference spectra of D1-S169A PSII core complexes in response to four successive flash illuminations applied at 0°C after hydration with $D_2{}^{16}O$ (red) or $D_2{}^{18}O$ (green). The $D_2{}^{16}O$ data represent the averages of 60 samples (112,500 scans for each trace) and the $D_2{}^{18}O$ data represent the averages of 60 samples (114,000 scans for each trace). The spectra have been multiplied vertically by factors of 1.14 to 1.25 to normalize the spectra to the extent of flash-induced charge separation in the corresponding wild-type spectra (Figure 4.2). The dark-dark control traces show the noise level and the stability of the baseline (lower traces). The dark-dark control traces were multiplied by factors of 1.15.

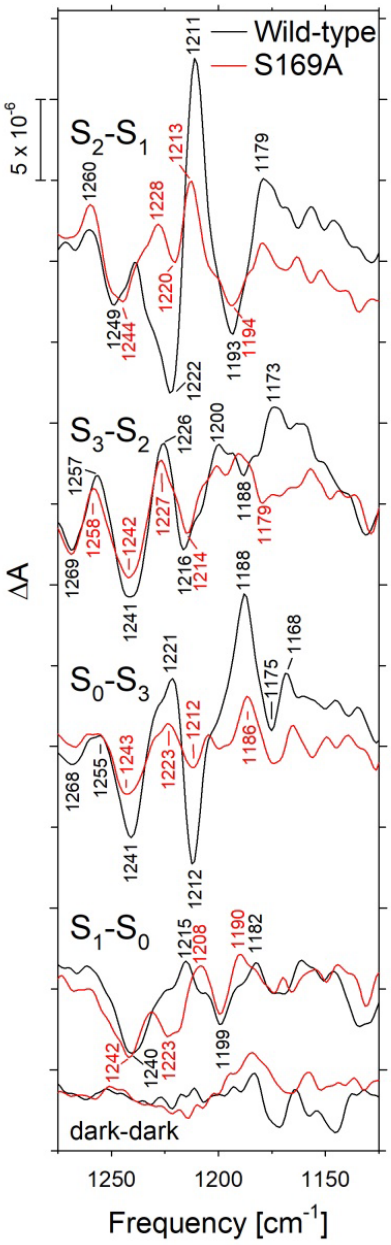

FIGURE 4.4 The S_{n+1}-S_n $D_2{}^{16}O$-$D_2{}^{18}O$ double difference spectra of wild-type (black) and D1-S169A (red) PSII core complexes in the D-O-D bending region. The data of Figure 4.2 were subtracted directly but were offset vertically to maximize overlap. The lower traces show the noise levels and were obtained by calculating the $D_2{}^{16}O$-$D_2{}^{18}O$ difference spectra of the dark-dark traces shown in Figure 4.2.

Chapter 5

Roles of D1-Glu189 and D1-Glu329 in O_2 formation by the water-splitting Mn_4Ca cluster in Photosystem II

5.1 ABSTRACT

During the catalytic step that precedes O-O bond formation in Photosystem II, a water molecule deprotonates and moves next to the water-splitting Mn_4CaO_5 cluster's O5 oxo bridge. The relocated oxygen, known as O6 or O*x*, may serve as a substrate, combining with O5 to form O_2 during the final step in the catalytic cycle, or may be positioned to become a substrate during the next catalytic cycle. Recent serial femtosecond X-ray crystallographic studies show that the flexibility of D1-E189 plays a critical role in facilitating the relocation of O_6/O*x*. In this study, the D1-E189G and D1-E189S mutations were characterized with FTIR difference spectroscopy. The data show that both mutations support Mn_4Ca cluster assembly, substantially inhibit advancement beyond the S_2 state, and substantially alter the network of H bonds that surrounds the Mn_4Ca cluster. Previously, the D1-E189Q, D1-E189K, and D1-E189R mutations were shown to have little impact on the activity, electron transfer rates, or spectral properties of Photosystem II. A rationale for this behavior is presented. The residue D1-E329 interacts with water molecules in the O1 water network that has been suggested recently to supply substrate during the catalytic cycle. Characterization of the D1-E329A mutant with FTIR difference spectroscopy shows that this mutation does not substantially perturb the structure of PSII or the water molecules whose O-H stretching modes change during the catalytic cycle. This result provides additional evidence that the water molecules whose vibrational properties

change during the S_1 to S_2 transition are confined approximately to the region bounded by D1-N87, D1-N298, and D2-K317.

5.2 INTRODUCTION

Plants, algae, and cyanobacteria use sunlight as an inexhaustible source of energy and water as an inexhaustible source of electrons and protons to supply nearly all of Earth's molecular oxygen and drive the production of Earth's biomass. The oxygen is released as the by-product of water oxidation by the Mn_4Ca cluster in Photosystem II. Our understanding of water oxidation by the Mn_4Ca cluster has advanced rapidly in recent years because of the advent of XFEL-based serial femtosecond X-ray crystallography and the growing synergism between structural, computational, and advanced biophysical studies (for recent reviews, see refs (*1-5*)). PSII is a large protein complex that is integral to the thylakoid membrane. Its core is dimeric *in vivo*. Peripheral to the core is the light-harvesting apparatus. Each monomer of the PSII core contains approximately 20 subunits and has a molecular weight of approximately 350 kDa. The structure of PSII has been determined to 1.85 – 1.95 Å in cyanobacteria (*6-12*) and to between 2.7 and 5.3 Å in a number of algae and plants (*13-20*). Structures of intermediates of water oxidation by the Mn_4Ca cluster have been determined to 2.35 Å (*21*), 2.04 – 2.08 Å (*11*), 2.15 – 2.50 Å (*22*), and recently to 2.01 – 2.27 (*12*) in cyanobacteria with serial femtosecond X-ray crystallography.

At the core of each PSII monomer is a heterodimer of two subunits known as D1 and D2. Light-induced charge separation between P_{680} and a pheophytin molecule in the D1/D2 heterodimer drives the oxidation of the Mn_4Ca cluster, with the redox-active

tyrosine Y_Z serving to transfer electrons from the Mn_4Ca cluster to $P_{680}^{\bullet+}$. Four electrons are removed from the Mn_4Ca cluster during each catalytic cycle, advancing the cluster through five reaction intermediates termed S_n, where "n" denotes the number of oxidizing equivalents stored (n = 0 – 4). The S_1 state predominates in dark-adapted samples. Both substrate water molecules are bound to the Mn_4Ca cluster by at least the S_2 state (*23-25*). The S_4 state is a transient intermediate whose formation triggers the utilization of the four stored oxidizing equivalents to form O_2 from two substrate-water-derived metal ligands. This process regenerates the S_0 state and involves the binding of at least one of the two new substrate water molecules. Because of its transient nature, the S_4 state remains uncharacterized. The Mn_4Ca cluster's five metal ions are connected by oxo bridges and are ligated by six bridging carboxylate groups and one histidine side chain. All but one of these protein ligands are provided by the D1 polypeptide (see Figure 5.1). Numerous immobilized water molecules are located on or near the Mn_4Ca cluster, including two that are bound to Mn4 (these are denoted W1 and W2) and two that are bound to the Ca ion (these are denoted W3 and W4).

The Mn_4Ca cluster is arranged as a distorted Mn_3CaO_4 cube that is linked to a fourth Mn ion (denoted Mn4) by two oxo bridges, although in the dark-stable S_1 state, the distance between Mn1 and O5 is too long to be a bond (*7-9, 11, 12*). One of the oxo bridges is denoted O5. While not yet definitive, a growing body of evidence supports identifying O5 as the deprotonated form of one of the two substrate water molecules that ultimately form the O-O bond (*26-30*). The S_2 state consists of three six-coordinate Mn(IV) ions and one five-coordinate Mn(III) ion (*31-36*). The S_3 state consists of four octahedrally-coordinated

Mn(IV) ions (*37-40*). Multiple conformers of the Mn_4Ca cluster in the S_2 (*41-46*) and S_3 (*40, 42, 44-48*) states are observed at cryogenic temperatures. These conformers differ in spin state. In the S_2 state, the low spin conformer gives rise to the multiline EPR signal, whereas high-spin conformers give rise to broad, featureless signals at $g = 4.1$ to $g = 4.7$ (*41-46*). The different conformers are in equilibrium. There is increasing evidence that a high-spin conformer of the S_2 state is a required intermediate between the S_2 and S_3 states (*2, 40, 44-46, 48-52*). In terms of structure, the prevailing view of the S_2 state conformers is that O5 toggles between Mn4 and Mn1, with the low-spin conformer having O5 bound to Mn4 (the "open" conformation) and a high spin conformer having O5 bound to Mn1 (giving rise to a cubane-like "closed" conformation) (*53-55*). In this view, the toggling of O5 is linked to a redox isomerization, with the five-coordinate Mn(III) ion being located at the Mn1 position in the "open" conformer and at the Mn4 position in the "closed" conformer. However, it has been argued that the "closed" conformer is too high in energy (*56*), is inconsistent with recent EXAFS data of the high spin conformer (*57, 58*), and cannot account for chemical treatments that alter the equilibrium between high spin and low spin conformers (*59*). Furthermore, only the open conformer has been observed in serial room temperature femtosecond X-ray crystallographic studies of intermediates between the S_2 and S_3 states (*11, 12*). Consequently, several models for high-spin conformers of the S_2 state having "open" configurations have been proposed recently (*30, 45, 46, 56, 59-61*).

During the S_2 to S_3 transition, a water molecule, or water-derived metal ligand, deprotonates and moves to a position on Mn1 in close proximity to O5, completing this

Mn ion's coordination shell (*11, 12, 21, 22, 37-39, 62-65*). This oxygen has been denoted O6 (*21, 22*) or O*x* (*11, 12*) and forms an oxo or hydroxo bridge connecting Mn1 with the Ca ion. It also forms an H bond with D1-Glu189. The origin of O_6/O*x* has been the subject of debate. In one set of models (e.g., the "carousel" (*51, 66*) and "pivot" (*50, 67*) models), O_6/O*x* originates from the Mn4-bound W2. In a competing set of models (*56, 68-73*), O_6/O*x* originates from the Ca^{2+}-bound W3. The recent serial femtosecond X-ray crystallographic data are more compatible with O_6/O*x* originating from W3 (*11, 12, 22*). In these data, W3 appears to be replenished via W4 from a network of H bonded water molecules (labeled O1 in refs. (*11, 12, 22*)) that connects W4 with the lumenal surface and includes residues from CP43 and PsbV. Several water molecules in the O1 network appear to be slightly mobile during the S_2 to S_3 transition and the density of W27 decreases concomitant with the appearance of O_6/O*x* (*12*). If O_6/O*x* originates from W3, then this oxygen could be a deprotonated form of the second substrate water molecule that combines with O5 in a radical-coupling mechanism to form the O-O bond (*37, 50, 56, 62, 63, 65, 67-69, 74-78*). On the other hand, recent time-resolved membrane inlet mass spectrometry (TR-MIMS) data are more compatible with the second substrate being a deprotonated form of W2 (*30*). If O_6/O*x* originates from W3 (*11, 12, 22, 56, 68-73*) and W2 is the second substrate water molecule (*30*), then O_6/O*x* may simply be positioned on Mn1 during the S_2 to S_3 transition to replace O5 during the S_4 to S_0 transition, thereby becoming a substrate during the next cycle of O_2 formation (*11, 30*).

The recent serial femtosecond X-ray crystallographic studies show that the flexibility of D1-E189 plays a critical role in facilitating the relocation/insertion of O_6/O*x*

during the S_2 to S_3 transition (*11, 12, 22*). In the S_1 and S_2 states, the carboxylate group of this residue coordinates to Mn1 and interacts weakly with the Ca ion and a nearby water molecule (labeled W25 in ref. (*12*), see Figure 5.1). W25 forms an H bond with tyrosine Y_Z and bridges W3 and W4, the two water ligands of the Ca ion. During the initial stages of the S_2 to S_3 transition (during the first 50 μs after the light-induced excitation of P_{680}), D1-E189 moves ~ 0.4 Å away from the Ca ion to accommodate the subsequent insertion of O_6/O*x* (this take place mostly from 150 – 250 μs and is complete by ~ 400 μs) while still coordinating to Mn1 (*11, 12*). By 150 μs, D1-E189 has also moved ~ 0.3 Å away from W25 to form an H bond with O_6/O*x* (*12*). The D1-E189 residue has been examined extensively with site-directed mutagenesis. Of the 17 mutations constructed at this position, only the Q, K, R, I, and L mutations support photoautotrophic growth (*79-81*). The light-saturated steady-state rates of O_2 formation by cells containing the Q, K, and R mutations are 70-80% compared to the rate of wild-type cells. The corresponding rates in cells containing the I and L mutations are 60% and 40%, respectively. The PSII reaction centers in all 17 mutants contain photo-oxidable Mn ions, with the percentage ranging from a high of 87-89% in the Q, K, R, I, D, and N mutants to a low of 30-40% in the A, T, and M mutants (*79, 80*). In analyses of mutation-bearing PSII core complexes, the Q mutation caused no apparent changes to the S_1 and S_2 multiline EPR signals (*80, 81*), the Q, K, and R mutations caused no apparent changes to the rates of electron transfer from Y_Z to $P_{680}^{\bullet+}$ or from the Mn_4Ca cluster to $Y_Z^{\bullet}$ during the S_1 to S_2, S_2 to S_3 or S_3 to S_0 transitions (*82*), and the Q and R mutations caused no significant changes to the mid-frequency FTIR difference spectra of the individual S state transitions (*81, 83*). In contrast, all mutations

having smaller side chains were non-photoautotrophic and supported no significant rates of O_2 formation (*79, 80*). In response to continuous illumination at 273 K, PSII core complexes bearing the D, N, H, G, and S mutations seemed unable to advance beyond an apparent $S_2Y_Z^{\bullet}$ state (*80*). Interestingly, PSII core complexes bearing the D, N, H, G, and S mutations exhibited neither the S_1 nor the S_2 multiline EPR signals (*80*), raising the possibility that the Mn clusters in these mutants were not fully assembled. On the basis of the observations described in this paragraph, it was proposed that D1-E189, rather than coordinate to the Mn_4Ca cluster, instead participates in a network of H bonds near the Mn_4Ca cluster that is vital for S state turnover and that can be maintained by the side chains of Q, K, and R (*79, 80, 82, 83*). Because D1-Glu189 is now known to ligate both Mn1 and Ca, and because of the importance of this residue's flexibility for the relocation/insertion of O_6/O*x* during the S_2 to S_3 transition (*11, 12, 22*), in this study we have reexamined the D1-E189G and D1-E189S mutants with FTIR difference spectroscopy. Our data show that a modified form of the S_2 state is formed in a fraction of both mutants, demonstrating that neither mutation completely inhibits cluster assembly. Our data also confirm that advancement of the S state cycle beyond the S_2 state is largely inhibited by both mutations and show that both mutations substantially alter the network of H bonds that surrounds the Mn_4Ca cluster.

The oxidations of the Mn_4Ca cluster are coupled to the release of protons, with electrons and protons being removed alternatively as the S state cycle proceeds (*64, 84, 85*). This alternation prevents the redox potential of the Mn_4Ca cluster from rising to levels that prevent its subsequent oxidation by $Y_Z^{\bullet}$. Deprotonations take place via the extensive

network of H bonds that surrounds the Mn_4Ca cluster. Multiple pathways leading to the thylakoid membrane are visible in this network. This network is comprised of protonatable amino acid side chains and water molecules. The O-H stretching modes of some of these water molecules are strongly coupled (*86*) and change as the Mn_4Ca cluster advances through the S state cycle (*87-90*). The changes that occur during the S_1 to S_2 transition to the O-H stretching modes of *weakly* H bonded water molecules are modified by the individual mutation of numerous residues (e.g., D1-D61 (*91*), D1-N87 (*92*), D1-S169 (*93*), D1-N181 (*94*), D1-N298 (*95*), D1-E333 (*96*), CP43-E354Q (*97*)) and when Sr^{2+} is substituted for Ca^{2+} (*70*). The changes that occur during the S_1 to S_2 transition to the O-H stretching modes of *strongly* H bonded water molecules are modified by the individual mutation of only a few residues (D1-D61 (*91*), D1-S169 (*93*), D1-N181 (*94*), and D1-N298 (*95*)). These mutation- and treatment-induced modifications confirm the strongly-coupled nature of these modes and help localize the water molecules involved. However, the mutations and treatments that alter water O-H stretching modes during the S_1 to S_2 transition do not alter the changes to these modes during any of the other S state transitions, with the exception of D1-D61A for the S_2 to S_3 transition (*91*). One possibility is that the water O-H stretching modes that change during the S_2 to S_3, S_3 to S_0, and S_0 to S_1 transitions correspond primarily to water molecules in the O1 network that has been proposed on the basis of recent serial femtosecond X-ray crystallographic studies (*11, 12, 22*) to be a substrate entry pathway. The positions of several water molecules in this network change slightly during the S_2 to S_3 transition (*12*). It should be possible to test this possibility by

constructing mutations of the residues that interact with these water molecules. One such reside is D1-E329.

The carbonyl oxygen of D1-E329 forms an H bond with the π-nitrogen of D1-H332, a ligand of Mn1. The side chain of D1-E329 interacts with water molecules W31 and W34 in the O1 network, and also with W80. It is also in close proximity to W32, one of the water molecules in the O1 network whose position changes slightly during the S_2 to S_3 transition. The side chain of D1-E329 also interacts with the side chain of CP43-T412, which in turn interacts with W31 in the O1 network and with W80 (see Figure 5.1). Previously, on the basis of the elimination of the ν(C=O) modes of protonated carboxylate residues by the D1-E329Q mutation, we demonstrated that D1-E329 participates in those parts of the H bond network that govern the carboxylate pK_a changes that accompany the individual S state transitions (*98, 99*). To determine if this residue influences water molecules in the O1 network, in this study we analyzed the FTIR difference spectra of PSII core complexes from the D1-E329A mutant. Our data show that this mutation has no apparent influence on any of the water molecules whose O-H stretching modes change during the individual S state transitions. This result provides additional evidence that the water molecules whose vibrational properties change during the S_1 to S_2 transition are confined approximately to the region bounded by D1-N87, D1-N298, and D2-K317. Analysis of additional mutations will be required to determine if the O-H stretching modes of H bonded water molecules that change during the S_2 to S_3, S_3 to S_0, and S_0 to S_1 transitions correspond primarily to water molecules in the O1 channel.

5.3 MATERIALS AND METHODS

Construction of Mutants and Purification of PSII Core Complexes. The D1-E189G, D1-E189S, and D1-E329A mutations were constructed in the *psbA-2* gene of *Synechocystis* sp. PCC 6803 as described previously (*79, 100*). Large-scale cultures of mutation-bearing *Synechocystis* cells were propagated as described previously (*91*). The wild-type strain described in this manuscript was constructed in an identical manner as the mutant strains but with a transforming plasmid that carried no mutation (*100*). Oxygen-evolving PSII core complexes were purified under dim green light at 4 °C with a Ni-NTA superflow affinity resin (Qiagen, Valencia, CA) as described previously (*91*). The purified PSII core complexes were suspended in 1.2 M betaine, 10% (v/v) glycerol, 50 mM MES-NaOH (pH 6.0), 20 mM $CaCl_2$, 5 mM $MgCl_2$, 50 mM histidine, 1 mM EDTA, and 0.03 % (w/v) n-dodecyl β-D-maltoside, concentrated to approx. 1 mg of Chl per mL, flash-frozen in liquid N_2, and stored at −80 °C. To verify the integrity of the large-scale cultures that were harvested for the purification of the PSII core complexes, an aliquot of each large-scale culture was set aside and the sequence of the relevant portion of the *psbA-2* gene was obtained after PCR amplification of genomic DNA (*100*). No trace of the wild-type codon was detected in any of the mutant cultures.

Preparation of FTIR samples. PSII core complexes were transferred into 40 mM sucrose, 10 mM MES-NaOH (pH 6.0), 5 mM $CaCl_2$, 5 mM NaCl, 0.06% (w/v) *n*-dodecyl β-D-maltoside, concentrated, mixed with 1/10 volume of fresh 100 mM potassium ferricyanide, spread in the center 13 mm of a 25 mm BaF_2 window, then dried lightly with N_2 gas (*70*). The lightly dried samples were rehydrated with six 1 μL drops of a solution

of 20% (v/v) glycerol to maintain the sample humidity at 99% RH (*101*). A second window was placed over the first with a thin O-ring spacer in between (*70, 72, 91, 102*). Sealed samples were equilibrated in the FTIR sample compartment at 0°C in darkness for 1.5 h, illuminated with 6 pre-flashes, then dark-adapted for 30 min (*70, 72, 91, 102*). For each sample, the absorbance at 1657 cm^{-1} (amide I band) was 0.6 – 1.1.

FTIR Spectroscopy. Spectra were recorded with a Bruker Vertex 70 spectrometer (Bruker Optics, Billerica, MA) outfitted with a pre-amplified, midrange D317 photovoltaic MCT detector (Kolmar Technologies, Inc., Newburyport, MA), as described in ref. (*70*). Actinic flashes (~20 mJ/flash, ~7 ns fwhm) were provided by a frequency-doubled Q-switched Nd:YAG laser (BRIO, Quantel USA, Bozeman, MT). After dark adaptation, samples were given six flashes at 13 s intervals. Two transmission spectra were recorded before the first flash and one transmission spectrum was recorded starting 0.33 s after the first and subsequent flashes (each transmission spectrum consisted of 100 scans). The 0.33 s delay was included to allow the oxidation of $Q_A^{\bullet-}$ by the ferricyanide. Difference spectra of the successive S-state transitions (e.g., S_{n+1}–*minus*–S_n difference spectra, written as $S_{n+1}-S_n$ in this study), were obtained by dividing the transmission spectrum obtained after the n^{th} flash by the transmission spectrum obtained before the n^{th} flash, then converting the ratio to units of absorption. The background noise level and the stability of the baseline were obtained by dividing the second pre-flash transmission spectrum by the first and converting the ratio to units of absorption (these spectra are labeled dark−dark in each figure – these are control difference spectra obtained *without* a flash being given). The sample was then dark-adapted for 30 min and the cycle was repeated. For each sample, the

illumination cycle was repeated 19 times. The spectra of 9-20 samples were averaged (see figure legends). The amplitudes of the D1-E189G and D1-E189S difference spectra were multiplied by factors of 4.0 to 5.2 to normalize the amplitudes of the peaks corresponding to the reduction of ferricyanide to ferrocyanide by $Q_A^{\bullet-}$ (at 2115 and 2037 cm^{-1}, respectively) to those in the corresponding wild-type spectra (this procedure normalizes the spectra to the extent of flash-induced charge-separation involving the formation of $Q_A^{\bullet-}$).

Other Procedures. Chlorophyll concentrations and initial light-saturated rates of O_2 evolution were measured as described previously (*103*).

5.4 RESULTS

D1-E189G and D1-E189S cells were characterized previously (*80*). They are non-photoautotrophic and evolve no O_2. D1-E329A cells are photoautotrophic and evolve oxygen at approximately 80% the rate of wild-type cells under light-saturated conditions. The PSII core-complexes isolated from D1-E329A cells for this study exhibited a maximal light-saturated oxygen-evolution rate of 5.7 ± 0.2 mmol of O_2 (mg of Chl•hr)$^{-1}$, similar to the rate typically measured for wild-type in this laboratory (5.3 ± 0.2 mmol of O_2 (mg of Chl•hr)$^{-1}$, e.g., ref. (*96*)).

FTIR characterization of D1-E189G and D1-E189S. The mid-frequency FTIR difference spectra produced by the first, second, third, and fourth flashes given to wild-type PSII core complexes correspond predominantly to the S_2-S_1, S_3-S_2, S_0-S_3, and S_1-S_0 FTIR difference spectra, respectively (*87-90*). The spectra of D1-E189G, D1-E189S, and wild-type PSII core complexes are compared in Figure 5.2. The amplitudes of the D1-

E189G and D1-E189S spectra produced by the first flash are considerably lower than that of the corresponding spectra of wild-type but are recognizable as corresponding predominantly to the S_2-S_1 spectrum. The lower amplitudes (25-30% compared to wild-type before normalization) were expected because some PSII reaction centers in these mutants lack photo-oxidizable Mn ions ((*80*) and see below) and because a previous study reported that significant fractions of Mn clusters in these mutants fail to reduce $Y_Z^{\bullet}$ after a flash, although they protect $Y_Z^{\bullet}$ from reduction by exogenous Mn^{2+} ions (*80*).

The amplitudes of the D1-E189G and D1-E189S spectra produced by the second, third, and fourth flashes were extremely low. In the second-flash spectra, the features in the ν_{sym}(C=O) region, e.g., those at 1446(+) cm^{-1}, 1425(-) cm^{-1}, 1415(+) cm^{-1}, and 1399(-) cm^{-1} in D1-E189G, could represent either a small fraction of centers that advanced to the S_2 state (having not done so in response to the first flash because of a non-zero miss parameter), a small fraction of centers that advanced to the S_3 state, or a combination of both. However, the partial reversal of features observed in this region of the third flash spectra of D1-E189G, e.g., those at 1443(-) cm^{-1}, 1424(+) cm^{-1}, and 1414(-) cm^{-1} suggest that a small fraction of mutant PSII centers advance to the S_3 and S_0 states. Many features in the mutant spectra produced by the second, third, and fourth flashes, e.g., those at 1703(-) cm^{-1}, 1696(+) cm^{-1}, 1553(+) cm^{-1}, 1541(-) cm^{-1}, 1517(-) cm^{-1}, 1502 (+) cm^{-1}, and 1253(-) cm^{-1} resemble those of $Y_D^{\bullet}$-Y_D (*104-107*). In Mn-depleted PSII core complexes from *Synechocystis* sp. PCC 6803, the $Y_D^{\bullet}$ radical decays in minutes in the presence of ferrocyanide (produced by the reduction of ferricyanide by $Q_A^{\bullet -}$) (*108*). Because 25-30% of PSII reaction centers in D1-E189G and D1-E189S cells have been estimated to lack Mn

ions (*80*), the oxidation of some Y_D in D1-E189G and D1-E189S PSII core complexes in response to flashes spaced 13 sec apart was expected and demonstrates the presence of some PSII core complexes lacking Mn ions. Some of the features of $Y_D^{\bullet}$-Y_D are also present in the first flash spectra (e.g., the features at 1704(-) cm^{-1}, 1696(+) cm^{-1}, and 1253(-) cm^{-1}). The other features of $Y_D^{\bullet}$-Y_D (e.g., those at 1553(+) cm^{-1}, 1541(-) cm^{-1}, 1517(-) cm^{-1}, 1502 (+) cm^{-1}) undoubtedly underlie the altered features of the S_2-S_1 spectra in the mutants. The features of $Y_D^{\bullet}$-Y_D appear to dominate the spectra of the mutants that are produced by the second, third, and fourth flashes.

The mid-frequency S_2-S_1 spectra of D1-E189G and D1-E189S PSII core complexes were altered substantially compared to wild-type. In the carbonyl stretching [ν(C=O)] region, the negative feature at 1747 cm^{-1} was eliminated. In the amide I region, the 1680 (-)/1671(+) cm^{-1} feature was diminished and upshifted 2-6 cm^{-1} and the 1663(-)/1651(+) cm^{-1} feature was diminished. In the overlapping asymmetric carboxylate stretching [$\nu_{asym}(COO^-)$] and amide II region, the 1610 (-) cm^{-1}, 1586(+) cm^{-1}, and 1561(-) cm^{-1} features were diminished and upshifted by 7-17 cm^{-1}, the 1543(-) cm^{-1} feature and the 1531(+)/1523(-) cm^{-1} derivative features were abolished, and the 1510(+) cm^{-1} feature was sharply diminished. In the symmetric carboxylate stretching [$\nu_{sym}(COO^-)$] region, the 1434(+) cm^{-1} feature was upshifted to 1443(+) cm^{-1}, the 1416(-)/1410 (+) cm^{-1} derivative feature was upshifted to 1424(-)/1417(+) cm^{-1}, the 1401 (-) cm^{-1} feature was downshifted by 7 cm^{-1} to 1394 cm^{-1}, and the 1364(+) cm^{-1} feature was eliminated, being replaced by a small negative feature at 1362 cm^{-1}. In addition, the positive feature at 1260 cm^{-1} was eliminated.

FTIR characterization of D1-E329A. The mid-frequency FTIR difference spectra of D1-E329A and wild-type PSII core complexes are compared in Figure 5.3. The amplitudes of the D1-E329A spectra were similar to those of wild-type and the individual spectra largely resembled those of wild-type. The main mutation-induced alterations were in the ν(C=O), amide I, and overlapping amide II/$\nu_{asym}(COO^-)$ regions. In the ν(C=O) region, the mutation eliminated the 1747(-) cm^{-1} feature from the S_2-S_1 spectrum, the 1745(+) cm^{-1} feature from the S_3-S_2 spectrum, the 1746(+) cm^{-1} feature from the S_0-S_3 spectrum, and the 1750(+)/1743(-) cm^{-1} derivative feature from the S_1-S_0 spectrum. In the amide I region of the S_2-S_1 spectrum, the 1697(+) cm^{-1} and 1671(+) cm^{-1} features were diminished, the 1664(-) cm^{-1} and 1651(+) cm^{-1} features were enhanced, a small positive feature appeared at 1687 cm^{-1}, and a large negative feature appeared at 1678 cm^{-1}. The 1687(+) cm^{-1} and 1678(-) cm^{-1} features were reversed in the S_0-S_3 spectrum. In the overlapping amide II/$\nu_{asym}(COO^-)$ region, the 1544(-) cm^{-1} amide II feature in the S_2-S_1 spectrum was diminished, as was the corresponding 1544(+) cm^{-1} feature in the S_0-S_3 spectrum.

Changes in the O–H stretching vibrations of *strongly* H bonded O-H groups of water molecules in PSII can be observed as very broad positive features between 3200 and 2300 cm^{-1} (*87-90*). This region of the FTIR difference spectra of D1-E329A PSII core complexes is compared with wild-type in Figure 5.4 (left panel). In each of the S_{n+1}-S_n spectra, the broad features in this region are largely unaltered by the D1-E329A mutation. However, the broad feature in the S_2-S_1 spectra is overlain with numerous sharp, positive peaks (left panel of Figure 5.4, upper traces). These sharp features correspond to Fermi

resonance peaks that arise from coupling between H bonded His N-H stretching modes and combinations/overtones of imidazole ring modes (*109, 110*). These features form during the S_1 to S_2 transition and are reversed during the S_3 to S_0 transition (*109, 110*). In our wild-type data, these features are present in the S_2-S_1 spectrum and appear to reverse during the S_3 to S_0 transition and, to a lesser extent, during the S_0 to S_1 transition (see S_0-S_3 and S_1-S_0 spectra in the left panel of Figure 5.4). However, the apparent reversal during the S_0 to S_1 transition may correspond to PSII centers advancing from S_3 to S_0 after the fourth flash because of a non-zero miss parameter. In D1-E329A, the sharp positive features near 2820 cm^{-1} in the S_2-S_1 spectrum and the corresponding sharp negative features near 2820 cm^{-1} in the S_0-S_3 and S_1-S_0 spectra are absent or are sharply decreased. These features are shown more clearly in wild-type-*minus*-D1-E329A double difference spectra that are presented in the right panel of Figure 5.4. These spectra show that the Fermi resonance peak centered near 2820 cm^{-1} that forms in wild-type during the S_1 to S_2 transition and that is largely reversed during the S_3 to S_0 transition is absent or sharply diminished in the mutant.

Changes in the O–H stretching vibrations of *weakly* H bonded O-H groups of water molecules in PSII can be observed as mostly negative features between 3700 and 3500 cm^{-1} (*87-90*). This region of the FTIR difference spectra of D1-E329A PSII core complexes is compared with wild-type in Figure 5.5. In the S_2-S_1 spectrum, the D1-E329A mutation slightly shifts the small 3663(-) cm^{-1} feature to 3661 cm^{-1}, the 3617(+) cm^{-1} feature to 3608 cm^{-1}, and the large 3585(-) cm^{-1} feature to 3584 cm^{-1}. Differences between D1-E329A and wild-type in the S_3-S_2, S_0-S_3, and S_1-S_0 spectra are minor.

The differences that are observed could reflect baseline shifts, especially in the S_3-S_2 spectrum.

5.5 DISCUSSION

D1-E189. In the dark-stable S_1 state, the side chain of D1-Glu189 coordinates to Mn1 with one oxygen and to the Ca ion (weakly) with the other (*6-12*). A long-standing mystery is that substituting the side chain of D1-E189 with the side chains of Q, K, and R has little impact on the spectral properties, electron transfer rates, and O_2 evolution activity of PSII (*79-83*). In contrast, substituting D1-E189 with smaller and less flexible side chains such as D, N, H, G, and S eliminates or substantially inhibits advancement beyond an apparent $S_2Y_Z^{\bullet}$ state (*80*). Because PSII core complexes bearing the D, N, H, G, and S mutations exhibited neither the S_1 nor the S_2 multiline EPR signals (*80*), the possibility existed that the PSII reaction centers in these mutants do not fully assemble the Mn_4Ca cluster. Our data confirm that Mn_4Ca clusters assemble in the D1-E189G and D1-E189S mutants in a fraction PSII centers: a single flash produces an altered, but recognizable S_2-S_1 FTIR difference spectrum in both mutants. The fractions of PSII centers assembling clusters are 25-30% on the basis of the normalization factors applied to the S_2-S_1 spectra, but may be higher because some Mn clusters in these mutants fail to reduce $Y_Z^{\bullet}$ after a flash (*80*). Our data also confirm that the D1-E189G and D1-E189S mutations substantially inhibit advancement beyond the S_2 state: the second, third, and fourth flashes applied to D1-E189G and D1-E189S PSII core complexes produced very weak spectral features, some of which demonstrate advancement to the S_3 and S_0 states in a very small fraction of PSII centers. However, the spectra produced by these flashes appear to be dominated by

features corresponding to Y_D oxidation (i.e., features of the FTIR difference spectrum of $Y_D^{\bullet}$-Y_D). These features also appear to be present in the spectra produced by the first flash and presumably arise from PSII centers lacking Mn clusters.

The alterations of the mid-frequency S_2-S_1 FTIR difference spectrum produced by the D1-E189G and D1-E189S mutations are more extensive than produced by any other mutation studied so far, with the possible exception of D1-V185N (a non-conservative mutation of a residue located adjacent to numerous water molecules in the extensive network of H bonds that links Y_Z with D1-D61) (*102*). In the ν(C=O) region, the negative feature at 1747 cm^{-1} is also eliminated by the D1-E65A (*98*), D1-N298A (*95*), and D2-E312A (*98*) mutations and by sample dehydration (*98*) and is diminished by the CP43-E354Q (*111*), D1-D61A (*91*), D1-R334A (*99*), D1-V185N (*102*), and D1-S169A (*73, 93*) mutations. This feature downshifts in D_2O and has been assigned to a protonated carboxylate group whose pK_a decreases in response to the charge the develops on the Mn_4Ca cluster during the S_1 to S_2 transition (*98, 99*). In the $\nu_{asym}(COO^-)$/amide II region, the substantial decrease of the 1586(+) cm^{-1} feature is also produced by the D2-K317A (*112*), D1-D61A (*91, 98*), D1-Q165E (*99*), D1-R334A (*99*), D1-N181 (*94*), D1-N298A (*95*), D1-V185N (*102*), and D1-S169A (*73, 93*) mutations. However, most of the mutations examined previously only diminished this feature's intensity. In contrast, the D1-E189G and D1-E189S mutations caused it to upshift by 8-13 cm^{-1}. Only the D1-D61A and D1-N298A mutations have been reported to cause shifts previously (4 cm^{-1} downshift in D1-D61A (*91, 98*) and 2-3 cm^{-1} upshift in D1-N298A (*95*)), although a recent characterization of the D1-S169A mutation reports an upshift of 6 cm^{-1} (*113*). This feature corresponds to

a $\nu_{asym}(COO^{-})$ mode because it shifts in globally ^{13}C-labeled samples (*114-117*) but not in globally ^{15}N-labeled samples (*111, 112, 115-117*). This mode's 8-13 cm^{-1} shift in D1-E189G and D1-E189S implies that these mutations alter this mode's environment to a greater extent than any mutation examined previously. A substantial decrease of the 1544(-) cm^{-1} feature is also produced by the D1-D61A (*91, 98*), D1-E65A (*98*), D2-E312A (*98*), D1-R334A (*99*), D1-N298A (*95*), and D1-S169A (*73, 93*) mutations, and to a lesser extent by the D1-E329Q (*98*) and D1-E329A (this study) mutations. However, this feature is decreased to a greater extent by D1-E189G and D1-E189S than by any other mutation yet examined, except possibly D1-N298A. The elimination of the 1531(+)/1523(-) cm^{-1} feature is also caused by the D1-D61A (*91, 98*), D2-E312 (*98*), D2-K317A (*112*), D1-R334A (*99*), D1-N181A (*91*), D1-N298A (*95*), D1-V185N (*102*), and D1-S169A (*93*) mutations and to a lesser extent in some preparations having Sr^{2+} substituted for Ca^{2+} (*70, 118, 119*). The 1544(-) and 1531(+)/1523(-) cm^{-1} features correspond to amide II modes because they shift in both ^{13}C labeled (*114-117*) and ^{15}N labeled (*111, 112, 115-117*) samples. The greater decrease of the 1544 cm^{-1} feature by D1-E189G and D1-E189S implies an even greater alteration to some parts of the protein backbone than by most mutations examined previously. The substantial decrease of the 1509(+) cm^{-1} feature is also produced by the D1-D61A (*102*) mutation, and to lesser extents by the CP43-E354Q (*97, 111*), D2-K317A (*112*), D1-E333Q (*96*), D1-R334A (*99*), D1-Q165E (*99*), D1-S169A (*73, 93, 113*), and D1-N298A (*95*) mutations. This feature corresponds to overlapping amide II and $\nu_{asym}(COO^{-})$ modes (*111*). In the $\nu_{sym}(COO^{-})$ region, alterations between 1434 cm^{-1} and 1400 cm^{-1}, particularly the upshift or elimination of the 1416(-)/1410(+) cm^{-1}

feature, are also produced by the CP43-E354Q (*111*), D1-K317A (*112*), D1-R334A (*99*), D1-D61A (*91*), D1-N181A (*94*), D1-N87D (*92*), D1-V185N (*102*), and D1-S169A (*73, 93*) mutations. A substantial decrease of the 1364(+) cm^{-1} feature is also produced by the D2-E312A (*98*), D1-Q165E (*99*), D1-R334A (*99*), D1-D61A (*91*), D1-N298A (*95*), and D1-V185N (*102*) mutations, by the substitution of Sr^{2+} for Ca^{2+} (*70, 86, 118-121*), and to lesser extents by the D1-N181A (*94*) and D2-K317A (*112*) mutations. However, the decrease of this feature produced by D1-E189G and D1-E189S mutations is more extreme: the feature is entirely eliminated, being replaced by a small negative feature at 1362 cm^{-1}.

As described in the previous paragraph, the alterations to the S_2-S_1 FTIR difference spectrum produced by the D1-E189G and D1-E189S mutations resemble those produced by many other mutations that perturb the extensive network of H bonds that surrounds the Mn_4Ca cluster, a region bounded approximately by D1-N87, D1-N298, and D2-K317. These similarities show that the D1-E189G and D1-E189S mutations perturb the same extensive network of H bonds. Because D1-E189 coordinates to Mn1, one might expect that these mutations would also perturb the structure of the Mn_4Ca cluster itself. Indeed, on the basis of a computational study that was based on a refinement of the original 1.9 Å structure of PSII, the orientation of D1-E189 was predicted to "tune" the Mn_4Ca cluster's electronic properties (*122*). The absence of S_1 and S_2 state multiline EPR signals in mutant PSII core complexes having D1-E189 replaced with D, N, H, G, or S (*80*) supports this prediction. Furthermore, the alterations to the S_2 state multiline EPR signal produced by Sr/Ca exchange, Ca depletion, and NH_3-binding/annealing have been attributed to subtle changes in the ligation environment of the S_2 state's single Mn(III) ion (*29, 33, 123-125*).

In the low-spin conformer of the S_2 state that gives rise to the multiline EPR signal, this Mn(III) ion is located at the Mn1 position and is coordinated to by D1-E189. Therefore, mutation of this residue would be expected to perturb the magnetic properties of the S_2 state. The absence of the S_1 and S_2 state multiline EPR signals in mutant PSII core complexes having D1-E189 replaced with D, N, H, G, or S (*80*) implies that replacing D1-E189 with a small, inflexible side chain at least subtly perturbs the Mn_4Ca cluster's structure in addition to perturbing the structural components of the network of H bonds that surrounds the Mn_4Ca cluster.

Why, then, does replacing the side chain of D1-E189 with Q *not* modify the S_1 and S_2 state multiline EPR signals (*80, 81*), why does replacing E with Q or R *not* significantly alter the appearance of the mid-frequency FTIR difference spectra (*81, 83*), and why does replacing E with the strikingly dissimilar side chains of Q, K, or R permit steady-state O_2 evolution rates that are 70-80% of wild-type (*80, 81*) and *not* significantly alter the rates of electron transfer from Mn_4Ca to $Y_Z^{\bullet}$ or from Y_Z to $P_{680}^{+\bullet}$ (*82*)? One explanation is that cells containing the Q, R, and K mutations have replaced the mutated amino acid residue with the native E side chain, despite there being no wild-type gene in the organism (all cultures harvested for the spectroscopic studies cited above had the relevant portion of their psbA-2 gene amplified by PCR and sequenced to verify the presence of the mutated codon and the absence of the wild-type codon). Such a replacement was recently reported for a newly constructed D1-D170H mutation (*113*), although no mechanism was provided to explain how cells would convert the mutated amino acid residue to wild-type in the absence of the wild-type gene[a]. However, it should be noted that D1-E189Q, D1-E189R, and D1-

E189K cells evolve O_2 at only 70-80% the rate of wild-type (*80, 81*), that the S_2/S_1 midpoint potential in D1-E189Q cells and PSII core complexes is decreased substantially compared to wild-type (*81*), and that the D1-E189Q mutation alters the low-frequency S_2-S_1 FTIR difference spectrum between 640 and 570 cm^{-1} (*81*), including the 625(-) cm^{-1} and 606(+) cm^{-1} features that have been assigned to Mn-O-Mn cluster modes (*116, 133, 134*) and a 577(-) cm^{-1} feature that has been assigned to a cluster skeletal vibration or a Mn-O stretching mode (*116*). Therefore, despite the Q, R, and K mutations having little impact on the spectral properties and electron transfer rates (*79-83*), the properties of D1-E189Q, D1-E189R, and D1-E189K cells and PSII core complexes are not completely those of wild-type. In addition, it would be curious that, if cells can convert Q, R, and K to the wild-type E, they don't appear to similarly convert any of the 12 mutations that eliminate photoautotrophic growth (*80*), i.e., D, N, H, A, T, M, C, F, Y, V, G, and S.

Another explanation is suggested by the flexibility and H bonding characteristics of the Q, R, and K side chains in comparison to the native E. Photothermal beam deflection (*84, 85*) and time-resolved X-ray absorption (*64*) measurements have shown that proton movements precede Mn oxidation during the S_2 to S_3 transition. Time-resolved IR studies have shown that the initial phase of the S_2 to S_3 transition (during the first 100 μs after the light-induced excitation of P_{680}) involves changes in the network of H bonds that link Y_Z with the Mn_4Ca cluster (*65, 136*). The recent serial femtosecond X-ray crystallographic studies show that the side chain of D1-E189 moves during the S_2 to S_3 transition to accommodate the relocation/insertion of O_6/O*x* (*11, 12, 22*). In the most recent study (*12*), within 50 μs of the excitation of $P_{680,}$ D1-Glu189 moves away from the Ca ion by ~ 0.4 Å

(*12*). By 150 μs, this residue also moves away from W25 by ~ 0.3 Å, thereby weakening the H bond between D1-Glu189 and this water molecule, which in turn forms an H bond with the phenoxyl group of Y_Z. The latter movement positions D1-Glu189 to form an H bond with O_6/O*x*, whose density begins to appear ~ 150 μs and becomes maximal at ~ 400 μs (*12*). The movement of D1-Glu189 away from the Ca ion and W25 occurs before electron transfer from Mn_4Ca to $Y_Z^{\bullet}$ has begun. These movements also bring W25 and W3 closer together and have been suggested to facilitate the subsequent deprotonation of W3 by W25 (with W25 relaying the proton to Y_Z) in preparation for W3's transfer to the O_6/O*x* position as a hydroxide ligand (*12*). *Central to these proton movements and the relocation of* O_6/O*x are the flexibility and H bonding characteristics of the side chain of D1-Glu189*. We suggest that the flexibility and H bonding characteristics of the Q, K, and R side chains explain why these disparate functional groups support the S_2 to S_3 transition in the D1-E189Q, D1-E189K, and D1-E189R mutants: the flexibility and H bonding characteristics of Q, K, and R could maintain a network of H bonded water molecules linking Y_Z and the Ca ion and facilitate the deprotonation/relocation of W3 during the S_2 to S_3 transition even if the exact make-up of the network differs from that present in wild-type PSII[*b*]. In addition, if the rate-limiting steps are not altered, electron transfer from Y_Z to $P_{680}^{\bullet+}$ and from the Mn_4Ca cluster to $Y_Z^{\bullet}$ may occur with the same rates as in wild-type. In contrast, smaller side chains such as those of D, N, H, G, or S presumably lack the H bonding characteristics and/or flexibility to support the proton movements that precede Mn oxidation during the S_2 to S_3 transition. Consequently, these mutations may prevent advancement beyond the $S_2Y_Z^{\bullet}$ state in the same manner as the removal of Ca^{2+} or Cl^- or the treatment with

inhibitors such as F^- or acetate (*42, 137, 138*). We also suggest that the ligation environment of Mn1 is sufficiently similar in D1-E189Q and wild-type to support the appearance of the normal S_1 and S_2 state multiline EPR signals in the mutant (the EPR properties of the K and R mutants have not yet been reported). The substantial alterations to the S_2-S_1 FTIR spectrum produced by the D1-E189G and D1-E189S mutations show that small, inflexible side chains substantially alter the network of H bonds extending from D1-D61 to Y_Z. We suggest that these alterations alter the magnetic properties of the Mn_4Ca cluster in the S_1 state and the ligation environment of Mn1 in the S_2 state sufficiently to prevent formation of the S_1 and S_2 multiline EPR signals.

D1-E329 – protein vibrational modes. One of the most striking D1-E329A-induced alterations to the mid-frequency FTIR difference spectra is the elimination of the main features in the ν(C=O) region from all the S_{n+1}-S_n spectra. These features were shown previously to be eliminated by the D1-E329Q mutation (*98*). The elimination of the 1747(-) cm^{-1} feature from the S_2-S_1 spectrum, the 1745(+) cm^{-1} feature from the S_3-S_2 spectrum, the 1746(+) cm^{-1} feature from the S_0-S_3 spectrum and the 1750(+)/1743(-) cm^{-1} derivative-shaped feature from the S_1-S_0 transition were interpreted previously as showing that D1-E329 participates in those parts of the H bond net network surrounding the Mn_4Ca cluster that govern the carboxylate pK_a changes that accompany the individual S state transitions (*98, 99*). The participation of D1-E329 in this H bond network is also suggested by the decreased amplitude of the 1544(-) cm^{-1} feature in the D1-E329A S_2-S_1 spectrum, as was discussed above in connection with the D1-E189 mutations. The D1-E329A-induced alterations to the amide I region are also noteworthy, particularly the appearance of a large

negative feature at 1678 cm^{-1} in the S_2-S_1 spectrum and its apparent reversal in the S_0-S_3 spectrum. The D1-E329Q mutation perturbs the amide I region to a much lesser extent and does not produce the 1678(-) cm^{-1} feature in the S_2-S_1 spectrum (*98*). Although the 1678(-) cm^{-1} feature is located in a region where one might expect features from the ν(C=O) vibrations of Asn or Gln or the $\nu_{asym}(CN_3)H_5^+$ vibration of Arg (*139*), this feature more likely reflects a rearrangement of the backbone carbonyl of D1-E329. The side chain of this residue forms a hydrogen bond with CP43-T412. Because E and Q are isosteric, this hydrogen bond may be maintained in the D1-E329Q mutation, but the absence of this interaction in D1-E329A may alter the backbone carbonyl of the residue at this position. This point will be discussed further below.

D1-E329 – strongly H bonded water molecules. The broad features observed between 3200 cm^{-1} and 2200 cm^{-1} in the individual FTIR difference spectra have been assigned to the vibrations of polarizable protons in the network of H bonds that surrounds the Mn_4Ca cluster (*86, 140*). On the basis of a QM/MM analysis (*86*), it was concluded that the broad feature in the S_2-S_1 spectrum is dominated by the O-H stretching modes of W1 and W2 (*86*). The D1-D61A mutation eliminates this feature (*91*), consistent with the H bond that exists between this residue and W1 (*6, 7, 9, 11, 12, 21, 22*). Other mutations that alter this feature to a substantial degree are D1-S169A (*93*), D1-N181A (*94*), and D1-N298A (*95*). This broad feature is largely unaltered by the D1-E329A mutation. Given the large distance between D1-E189 and the two water molecules, W1 and W2, the absence of a substantial alteration of the broad feature in the S_2-S_1 spectrum of D1-E329A is not surprising. The feature's positive amplitude implies that the increased charge that develops

on the Mn_4Ca cluster during the S_1 to S_2 transition strengthens the H bonds in which W1 and W2 participate (*86*). The positive features in this region of the other S_{n+1}-S_n FTIR difference spectra imply that the structural changes and water/proton relocations that take place during these transitions strengthen the H bonds of the water molecules that give rise to these features. The lack of any substantial D1-E329A-induced alteration to the broad features of the S_3-S_2, S_0-S_3, and S_1-S_0 spectra in this region show that the H bonded water molecules that give rise to the positive features in these spectra do not interact with D1-E329.

As noted earlier, the sharp features that overlie the broad features in this region correspond to Fermi resonance peaks that arise from coupling between His N-H stretching modes and combinations/overtones of imidazole ring modes (*109, 110*). That the Fermi resonance peaks centered at 2820 cm^{-1} are eliminated or substantially diminished by the D1-E329A mutation implies that the N-H stretching mode giving rise to these resonance peaks has been altered. Such an alteration could be caused by a change to the strength of the H bond of the N-H group. Recently, this group has been assigned as the Nτ-H moiety of D1-H337 (*110*). One possibility is that the alterations to the polypeptide backbone caused by the D1-E329A mutation alter the Nτ-H stretching mode of D1-H337 sufficiently to diminish/eliminate the Fermi resonance peaks near 2820 cm^{-1}. However, the other Fermi resonance peaks in the S_2-S_1 spectrum appear to be unaltered. Another possibility is that the sharp features in these spectra include Fermi resonance peaks involving D1-H332. The Nπ-H group of D1-H332 forms an H bond with the backbone carbonyl of D1-E329. The alterations to the polypeptide backbone produced by the D1-E329A mutation, manifested

in part by the appearance of the 1678(-) cm^{-1} feature in the S_2-S_1 spectrum, may alter the interaction between the Nπ-H group of D1-H332 and the backbone carbonyl sufficiently to diminish/eliminate the Fermi resonance peaks of D1-H332 without altering those of D1-H337[c].

D1-E329 – weakly H bonded water molecules. The features observed between 3700 cm^{-1} and 3500 cm^{-1} in the individual FTIR difference spectra have been assigned to weakly H bonded O-H stretching modes of water molecules that are coupled to the Mn_4Ca cluster. Negative features correspond to water molecules that either deprotonate or form stronger hydrogen bonds (i.e., weakly H bonded O-H groups become strongly H bonded). Unlike the features in the mid-frequency FTIR difference spectra, the features in the weakly H bonded O-H stretching region do not oscillate during the S state cycle. The lack of oscillations has been attributed, at least in part, to the consumption of the two substrate water molecules during the S state cycle (*86, 89, 90, 140*). On the basis of the same QM/MM analysis mentioned previously (*86*), the features in this region of the S_2-S_1 spectrum were concluded to arise from O-H stretching modes that are highly coupled (*86*). Only nine water molecules between D2-E317 and Y_Z were included in the QM/MM calculations. Nevertheless, the localization to this region and its vicinity of the water molecules whose weakly H bonded O-H stretching modes change during the S_1 to S_2 transition has been confirmed by the analyses of numerous mutations. For example, the 3663(-) cm^{-1} and 3617(+) cm^{-1} features in the S_2-S_1 spectrum are eliminated by the D1-D61A (*91*), D1-S169A (*93*), D1-N298A (*95*), D1-E333Q (*96*), and CP43-E354 (*97*) mutations and are diminished by the D1-N181A and D1-N181S mutations (*94*). The

3617(+) cm^{-1} feature is also eliminated by the D1-N87A (*92*), N87D (*92*), and D1-V185N (*102*) mutations and by the substitution of Sr^{2+} for Ca^{2+} (*70*). The minor alterations to the features in this region of in the S_2-S_1 spectrum that are produced by the D1-E329A mutation provides additional evidence that the water molecules whose vibrational properties change during the S_1 to S_2 transition are confined approximately to the region bounded by D1-N87, D1-N298, and D2-K317. None of the mutations mentioned in this paragraph (except D1-D61A during the S_2 to S_3 transition (*91*)) alter the features in this region of the S_3-S_2, S_0-S_3, or S_1-S_0 spectra. We find that the same appears to be true for the D1-E329A mutant.

Our analysis of the D1-E329A mutation was an initial attempt to test the possibility that the O-H stretching modes of H bonded water molecules that change during the S_2 to S_3, S_3 to S_0, and S_0 to S_1 transitions correspond primarily to water molecules in the O1 channel. That the D1-E329A mutation causes little substantial change to the features of either strongly H bonded or weakly H bonded water molecules in the S_3-S_2, S_0-S_3, or S_1-S_0 spectra shows that analysis of additional mutations will be required to test this possibility further.

5.6 SUMMARY AND CONCLUSION

In this study, we showed that the D1-E189G and D1-E189S mutations support Mn_4Ca cluster assembly, substantially inhibit advancement beyond the S_2 state, and substantially alter the network of H bonds that surrounds the Mn_4Ca cluster. We provided rational for the D1-E189Q, D1-E189K, and D1-E189R mutations' little impact on the activity, electron transfer rates, and spectral properties of Photosystem II. We also showed that the D1-E329A mutant does not substantially perturb the structure of PSII or the water

molecules whose O-H stretching modes change during the catalytic cycle, providing additional evidence that the water molecules whose vibrational properties change during the S_1 to S_2 transition are confined approximately to the region bounded by D1-N87, D1-N298, and D2-K317.

5.7 ACKNOWLEDGEMENTS

We thank Anh P. Nguyen for maintaining the mutant and wild-type cultures of *Synechocystis* sp. PCC 6803 and for purifying the thylakoid membranes that were used for the isolation of PSII core complexes. This work was supported by the Department of Energy, Office of Basic Energy Sciences, Division of Chemical Sciences, grant DE-SC0005291.

5.8 ADDITIONAL NOTES

Abbreviations: Chl, chlorophyll; EDTA, ethylenediaminetetraacetic acid; FTIR, Fourier transform infrared; MES, 2-(N-morpholino)-ethanesulfonic acid; P_{680}, chlorophyll multimer that serves as the light-induced electron donor in PSII; PSII, photosystem II; Q_A, primary plastoquinone electron acceptor; Y_Z, tyrosine residue that mediates electron transfer between the Mn_4O_5Ca cluster and $P_{680}^{+\bullet}$, Y_D, tyrosine residue that acts as an additional electron donor to $P_{680}^{+\bullet}$

[a]*The* original D1-D170H mutations were constructed independently in the psbA-2 (*100*) and psbA-3 (*126*) genes of *Synechocystis* sp. PCC 6803 and were transformed into independently constructed *Synechocystis* host strains that lacked all three psbA genes. The mutation was also constructed in *Chlamydomonas reinhardtii* (*127*). The resulting D1-

D170H cells were only weakly photoautotrophic, assembled Mn_4Ca clusters in only approx. 50% of their PSII centers, and evolved O_2 at only approx. 50% the rate of wild-type cells. Mn-depleted D1-D170H PSII core complexes showed an elevated K_m for binding Mn^{2+} to the high-affinity Mn binding site (*126*), illumination of Mn-depleted D1-D170H PSII core particles in the presence of Mn^{2+} ions produced a Mn^{3+} ion having altered parallel polarization EPR properties compared to wild-type (*128*), and photoactivation of Mn-depleted D1-D170H resulted in the accumulation of non-functional high-valent Mn ions in approx. 50% of the mutant PSII centers (*129*). Although the EPR/ESEEM properties (*123, 130*) and the mid-frequency FTIR difference spectra (*131, 132*) of intact D1-D170H PSII core complexes exhibited no significant perturbations, the low-frequency S_2-S_1 FTIR difference spectrum showed that the mutation shifts the 606 cm^{-1} Mn-O-Mn cluster mode (*116, 133, 134*) to 612 cm^{-1} (*131*). Therefore, the properties of the original D1-D170H mutations were not completely those of wild-type. In Ref. (*113*), no mechanism was provided to explain how cells can convert D1-H170 to the D1-D170 in the absence of the wild-type gene, although it was suggested that D1-D170H cells might be extremely sensitive to light. However, none of the other 19 mutations constructed at D1-D170 have been reported to be particularly light-sensitive (*79, 100, 126, 127*). In contrast, many mutations constructed in the *C*-terminal domain of the D1 polypeptide, e.g., at D1-H332, D1-E333, D1-H337, or D1-D342, are so light-sensitive that, for many mutations, cells had to be propagated in very dim light to permit analysis (*135*). Furthermore, none of the mutations constructed at these *C*-terminal residues exhibited wild-type properties (*135*). If cells can convert D1-H170 to D1-D170 in the absence of the wild-type gene, it is curious

that they don't appear to similarly convert any the 17 non-photoautotrophic mutations constructed at this position, many of which prevent assembly of the Mn_4Ca cluster (*79, 100, 126*). Also, it should be noted that the photoautotrophic mutant D1-D170E has properties that are perturbed compared to wild-type (*126, 128, 129*) and that the weakly photoautotrophic mutant D1-D170V was originally isolated as a weakly photoautotrophic pseudo-revertant of the non-photoautotrophic mutant, D1-D170A (*79*).

[b]To explain the photoautotrophic growth of the mutants D1-E189L and D1-E189I, it has been proposed (*80*) that the relative bulk and hydrophobicity of Leu and Ile cause structural perturbations that permit the missing D1-E189 carboxylate group to be replaced by another residue or by a water molecule or hydroxide ion. A similar explanation was advanced (*79*) to explain the ability of D1-D170V cells to grow photoautotrophically and the ability of D1-D170L and D1-D170I cells to evolve O_2 despite the role of D1-D170 as a bridging ligand between Mn4 and the Ca ion.

[c]This possibility was suggested to us by a reviewer.

5.9 REFERENCES

(1) Vinyard, D. J. and Brudvig, G. W. (2017) Progress Toward a Molecular Mechanism of Water Oxidation in Photosystem II. *Annu. Rev. Phys. Chem. 68*, 101-116.

(2) Pantazis, D. A. (2018) Missing Pieces in the Puzzle of Biological Water Oxidation. *ACS Catalysis 8*, 9477-9507.

(3) Lubitz, W., Chrysina, M., and Cox, N. (2019) Water oxidation in photosystem II. *Photosynth. Res.* 105-125.

(4) Huang, H.-L. and Brudvig, G. W. (2020) Oxygen Evolution of Photosystem II, in *Comprehensive Coordination Chemistry III, Vol. 8* pp 1-21.

(5) Cox, N., Pantazis, D. A., and Lubitz, W. (2020) Current Understanding of the Mechanism of Water Oxidation in Photosystem II and Its Relation to XFEL Data. *Annu. Rev. Biochem. 89*, 795-820.

(6) Umena, Y., Kawakami, K., Shen, J.-R., and Kamiya, N. (2011) Crystal Structure of Oxygen-Evolving Photosystem II at a Resolution of 1.9 Å. *Nature 473*, 55-60.

(7) Suga, M., Akita, F., Hirata, K., Ueno, G., Murakami, H., Nakajima, Y., Shimizu, T., Yamashita, K., Yamamoto, M., Ago, H., and Shen, J.-R. (2015) Native structure of photosystem II at 1.95 Å resolution viewed by femtosecond X-ray pulses. *Nature 517*, 99-103.

(8) Young, I. D., Ibrahim, M., Chatterjee, R., Gul, S., Fuller, F. D., Koroidov, S., Brewster, A. S., Tran, R., Alonso-Mori, R., Kroll, T., Michels-Clark, T., Laksmono, H., Sierra, R. G., Stan, C. A., Hussein, R., Zhang, M., Douthit, L., Kubin, M., de Lichtenberg, C., Pham, L. V., Nilsson, H., Cheah, M. H., Shevela, D., Saracini, C., Bean, M. A., Seuffert, I., Sokaras, D., Weng, T.-C., Pastor, E., Weninger, C., Fransson, T., Lassalle, L., Bräuer, P., Aller, P., Docker, P. T., Andi, B., Orville, A. M., Glownia, J. M., Nelson, S., Sikorski, M., Zhu, D., Hunter, M. S., Lane, T. J., Aquila, A., Koglin, J. E., Robinson, J., Liang, M., Boutet, S., Lyubimov, A. Y., Uervirojnangkoorn, M., Moriarty, N. W., Liebschner, D., Afonine, P. V., Waterman, D. G., Evans, G., Wernet, P., Dobbek, H., Weis, W. I., Brunger, A. T., Zwart, P. H., Adams, P. D., Zouni, A., Messinger, J., Bergmann, U., Kern, J., Yachandra, V. K., and Yano, J. (2016) Structure of photosystem II and substrate binding at room temperature. *Nature 540*, 453-457.

(9) Tanaka, A., Fukushi, Y., and Kamiya, N. (2017) Two Different Structures of the Oxygen-Evolving Complex in the Same Polypeptide Frameworks of Photosystem II. *J. Am. Chem. Soc. 139*, 1718-1721.

(10) Hellmich, J., Bommer, M., Burkhardt, A., Ibrahim, M., Kern, J., Meents, A., Müh, F., Dobbek, H., and Zouni, A. (2014) Native-like Photosystem II Superstructure at 2.44 Å Resolution thorugh Detergent Extraction from the Protein Crystal. *Structure 22*, 1607-1615.

(11) Kern, J., Chatterjee, R., Young, I. D., Fuller, F. D., Lassalle, L., Ibrahim, M., Gul, S., Fransson, T., Brewster, A. S., Alpert, B., Hussein, R., Zhang, M., Douthit, L., de Lichtenberg, C., Cheah, M. H., Shevela, D., Wersig, J., Seuffert, I., Sokaras, D., Pastor, E., Weninger, C., Kroll, T., Sierra, R. G., Aller, P., Butryn, A., Orville, A. M., Liang, M., Batyuk, A., Koglin, J. E., Carbajo, S., Boutet, S., Moriarty, N. W., Holton, J. M., Dobbek, H., Adams, P. D., Bergmann, U., Sauter, N. K., Zouni, A., Messinger, J., Yano, J., and Yachandra, V. K. (2018) Structures of the intermediates of Kok's photosynthetic water oxidation clock. *Nature 563*, 421-425.

(12) Ibrahim, M., Fransson, T., Chatterjee, R., Cheah, M. H., Hussein, R., Lassalle, L., Sutherlin, K. D., Young, I. D., Fuller, F. D., Gul, S., Kim, I.-S., Simon, P. S., de Lichtenberg, C., Chernev, P., Bogacz, I., Pham, C. C., Orville, A. M., Saichek, N., Northen, T., Batyuk, A., Carbajo, S., Alonso-Mori, R., Tono, K., Owada, S., Bhowmick, A., Bolotovsky, R., Mendez, D., Moriarty, N. W., Holton, J. M., Dobbek, H., Brewster, A. S., Adams, P. D., Sauter, N., Bergmann, U., Zouni, A., Messinger, J., Kern, J., Yachandra, V. K., and Yano, J. (2020) Untangling the sequence of events during the $S_2 \rightarrow S_3$ transition in photosystem II and implications for the water oxidation mechanism. *Proc. Natl. Acad. Sci. USA 117*, 12624-12635.

(13) Ago, H., Adachi, H., Umena, Y., Tashiro, T., Kawakami, K., Kamiya, N., Tian, L., Han, G., Kuang, T., Liu, Z., Wang, F., Zou, H., Enami, I., Miyano, M., and Shen, J.-R. (2016) Novel Features of Eukaryotic Photosystem II Revealed by Its Crystal Structure Analysis from a Red Alga. *J. Biol. Chem. 291*, 5676-5687.

(14) Wei, X., Su, X., Cao, P., Liu, X., Chang, W., Li, M., Zhang, X., and Liu, Z. (2016) Structure of spinach photosystem II-LHII supercomplex at 3.2 Å resolution. *Nature 534*, 69-74.

(15) Su, X., Ma, J., Wei, X., Cao, P., Zhu, D., Chang, W., Liu, Z., and Li, M. (2017) Structure and assembly mechanism of plant $C_2S_3M_2$-type PSII-LHCII supercomplex. *Science 357*, 815-820.

(16) van Bezouwen, L. S., Caffarri, S., Kale, R. S., Kouril, R., Thunnissen, A.-M. W. H., Oostergetal, G. T., and Boekema, E. J. (2017) Subunit and chlorophyll organization of the plant photosystem II supercomplex. *Nature Plants 3*, -Article No. 17080.

(17) Sheng, X., Watanabe, A., Li, A., Kim, E., Song, C., Murata, K., Song, D., Minagawa, J., and Liu, Z. (2019) Structural insight into light harvesting for photosystem II in green algae. *Nature Plants 5*, 1320-1330.

(18) Shen, L., Huang, Z., Chang, S., Wang, W., Wang, J., Kuang, T., Han, G., Shen, J.-R., and Zhang, X. (2019) Structure of a $C_2S_2M_2N_2$-type PSII-LHCII supercomplex from the green alga *Chlamydomonas reinhardtii*. *Proc. Natl. Acad. Sci. USA 116*, 21246-21255.

(19) Nagao, R., Kato, K., Suzuki, T., Ifuku, K., Uchiyama, I., Kashino, Y., Dohmae, N., Akimoto, S., Shen, J.-R., Miyazaki, N., and Akita, F. (2019) Structural basis for energy harvesting and dissipation in a diatom PSII-FCPII supercomplex. *Nature Plants 5*, 890-901.

(20) Pi, X., Zhao, S., Wang, W., Liu, D., Xu, C., Han, G., Kuang, T., Sui, S. F., and Shen, J.-R. (2019) The pigment-protein network of a diatom photosystem II-light-harvesting antenna supercomplex. *Science 365*, 463-and eaax4406.

(21) Suga, M., Akita, F., Sugahara, M., Kubo, M., Nakajima, Y., Nakane, T., Yamashita, K., Umena, Y., Nakabayashi, M., Yamane, T., Nakano, T., Suzuki, M., Masuda, T., Inoue, S., Kimura, T., Nomura, T., Yonekura, S., Yu, L.-J., Sakamoto, T., Motomura, T., Chen, J.-H., Kato, Y., Noguchi, T., Tono, K., Joti, Y., Kameshima, T., Hatsui, T., Nango, E., Tanaka, R., Naitow, H., Matsuura, Y., Yamashita, A., Yamamoto, M., Nureki, O., Yabashi, M., Ishikawa, T., Iwata, S., and Shen, J.-R. (2017) Light-induced structural changes and the site of O=O bond formation in PSII caught by XFEL. *Nature 543*, 131-135.

(22) Suga, M., Akita, F., Yamashita, K., Nakajima, Y., Ueno, G., Li, H., Yamane, T., Hirata, K., Umena, Y., Yonekura, S., Yu, L.-J., Murakami, H., Nomura, T., Kimura, T., Kubo, M., Baba, S., Kumasaka, T., Tono, K., Yabashi, M., Isobe, H., Yamaguchi, K., Yamamoto, M., Ago, H., and Shen, J.-R. (2019) An oxyl/oxo mechanism for oxygen-oxygen coupling in PSII revealed by an x-ray free-electron laser. *Science 366*, 334-338.

(23) Hillier, W. and Wydrzynski, T. (2008) ^{18}O-Water Exchange in Photosystem II: Substrate Binding and Intermediates of the Water Splitting Cycle. *Coord. Chem. Rev. 252*, 306-317.

(24) Cox, N. and Messinger, J. (2013) Reflections on substrate water and dioxygen formation. *Biochim. Biophys. Acta 1827*, 1020-1030.

(25) Nilsson, H., Krupnik, T., Kargul, J., and Messinger, J. (2014) Substrate water exchange in photosystem II core complexes of the extremophilic red alga *Cyanidioschyzon merolae*. *Biochim. Biophys. Acta 1837*, 1257-1262.

(26) Lohmiller, T., Krewald, V., Sedoud, A., Rutherford, A. W., Neese, F., Lubitz, W., Pantazis, D. A., and Cox, N. (2017) The First State in the Catalytic Cycle of the Water-Oxidizing Enzyme: Identification of a Water-Derived μ-Hydroxo Bridge. *J. Am. Chem. Soc. 139*, 14412-14424.

(27) Rapatskiy, L., Cox, N., Savitsky, A., Ames, W. M., Sander, J., Nowaczyk, M. M., Rögner, M., Boussac, A., Neese, F., Messinger, J., and Lubitz, W. (2012) Detection of Water-Binding Sites of the Oxygen-Evolving Complex of Photosystem II Using W-band ^{17}O Electron-Electron Double Resonance-Detected NMR Spectroscopy. *J. Am. Chem. Soc. 134*, 16619-16634.

(28) Pérez Navarro, M., Ames, W. M., Nilsson, H., Lohmiller, T., Pantazis, D. A., Rapatskiy, L., Nowaczyk, M. M., Neese, F., Boussac, A., Messinger, J., Lubitz, W., and Cox, N. (2013) Ammonia binding to the oxygen-evolving complex of photosystem II identified the solvent-exchangeable oxygen bridge (μ-oxo) of the manganese tetramer. *Proc. Natl. Acad. Sci. USA 110*, 15561-15566.

(29) Lohmiller, T., Krewald, V., Pérez Navarro, M., Retegan, M., Rapatskiy, L., Nowaczyk, M. M., Boussac, A., Neese, F., Lubitz, W., Pantazis, D. A., and Cox, N. (2014) Structure, ligands and substrate coordination of the oxygen-evolving complex of photosystem II in the S_2 state: a combined EPR and DFT study. *Phys. Chem. Chem. Phys. 16*, 11877-11892.

(30) de Lichtenberg, C. and Messinger, J. (2020) Substrate water exchange in the S_2 state of photosystem II is dependent on the conformation of the Mn_4Ca cluster. *Phys. Chem. Chem. Phys. 22*, 12894-12908.

(31) Peloquin, J. M., Campbell, K. A., Randall, D. W., Evanchik, M. A., Pecoraro, V. L., Armstrong, W. H., and Britt, R. D. (2000) ^{55}Mn ENDOR of the S_2-state Multiline EPR Signal of Photosystem II: Implications on the Structure of the Tetranuclear Mn Cluster. *J. Am. Chem. Soc. 122*, 10926-10942.

(32) Kulik, L., Epel, B., Lubitz, W., and Messinger, J. (2007) Electronic Structure of the Mn_4O_xCa Cluster in the S_0 and S_2 States of the Oxygen-Evolving

Complex of Photosystem II Based on Pulse ^{55}Mn-ENDOR and EPR Spectroscopy. *J. Am. Chem. Soc. 129*, 13421-13435.

(33) Cox, N., Rapatskiy, L., Su, J.-H., Pantazis, D. A., Sugiura, M., Kulik, L., Dorlet, P., Rutherford, A. W., Neese, F., Boussac, A., Lubitz, W., and Messinger, J. (2011) Effect of Ca^{2+}/Sr^{2+} Substitution on the Electronic Structure of the Oxygen-Evolving Complex of Photosystem II: A Combined Multifrequency EPR, ^{55}Mn-ENDOR, and DFT Study of the S_2 State. *J. Am. Chem. Soc. 133*, 3635-3648 (Correction pg. 14149).

(34) Krewald, V., Retegan, M., Cox, N., Messinger, J., Lubitz, W., DeBeer, S., Neese, F., and Pantazis, D. A. (2015) Metal oxidation states in biological water splitting. *Chem. Sci. 6*, 1676-1695.

(35) Cheah, M. H., Zhang, M., Shevela, D., Mamedov, F., Zouni, A., and Messinger, J. (2020) Assessment of the manganese cluster's oxidation state via photoactivation of photosystem II microcrystals. *Proc. Natl. Acad. Sci. USA 117*, 141-145.

(36) Pantazis, D. A. (2020) Evaluation of new low-valent computational models for the oxygen-evolving complex of photosystem II. *Chem. Phys. Lett. 753*, - Article 137629.

(37) Cox, N., Retegan, M., Neese, F., Pantazis, D. A., Boussac, A., and Lubitz, W. (2014) Electronic structure of the oxygen-evolving complex in photosystem II prior to O-O bond formation. *Science 345*, 804-808.

(38) Zaharieva, I., Chernev, P., Berggren, G., Anderlund, M., Styring, S., Dau, H., and Haumann, M. (2016) Room-Temperature Energy-Sampling Kβ X-ray Emission Spectroscopy of the Mn_4Ca Complex of Photosystem II Reveals Three Manganese-Centered Oxidation Steps and Suggests Coordination Change Prior to O_2 Formation. *Biochemistry 55*, 4197-4211.

(39) Schuth, N., Zaharieva, I., Chernev, P., Berggren, G., Anderlund, M., Styring, S., Dau, H., and Haumann, M. (2018) K□ X-ray Emission Spectroscopy on the Photosynthetic Oxygen-Evolving Complex Supports Manganese Oxidation and Water Binding in the S_3 State. *Inorg. Chem. 57*, 10424-10430.

(40) Pantazis, D. A. (2019) The S_3 State of the Oxygen-Evolving Complex: Overview of Spectroscopy and XFEL Crystallography with a Critical Evaluation of Early-Onset Models for O-O Bond Formation. *Inorganics 7*, 55.

(41) Boussac, A. and Rutherford, A. W. (2000) Comparative study of the *g*=4.1 EPR signals in the S_2 state of photosystem II. *Biochim. Biophys. Acta 1457*, 145-156.

(42) Haddy, A. (2007) EPR spectroscopy of the manganese cluster of photosystem II. *Photosynth. Res. 92*, 357-368.

(43) Pokhrel, R. and Brudvig, G. W. (2014) Oxygen-evolving complex of photosystem II: correlating structure with spectroscopy. *Phys. Chem. Chem. Phys. 16*, 11812-11821.

(44) Boussac, A., Rutherford, A. W., and Sugiura, M. (2015) Electron Transfer Pathways from the S_2-States to the S_3-States either after a Ca^{2+}/Sr^{2+} or a Cl^-/I^- Exchange in Photosystem II from *Thermosynechococcus elongatus*. *Biochim. Biophys. Acta 1847*, 576-586.

(45) Boussac, A., Ugur, I., Marion, A., Sugiura, M., Kaila, V. R. I., and Rutherford, A. W. (2018) The low spin - high spin equilibrium in the S_2-state of the water oxidizing enzyme. *Biochim. Biophys. Acta 1859*, 342-356.

(46) Boussac, A. (2019) Temperature dependence of the high-spin S_2 to S_3 transition in Photosystem II: Mechanistic consequences. *Biochim. Biophys. Acta 1860*, 508-518.

(47) Petrouleas, V., Koulougliotis, D., and Ioannidis, N. (2005) Trapping of Metalloradical Intermediates of the S-States at Liquid Helium Temperatures. Overview of the Phenomenologyand Mechanistic Implications. *Biochemistry 44*, 6723-6728.

(48) Krewald, V., Neese, F., and Pantazis, D. A. (2019) Implications of structural heterogeneity for the electronic structure of the final oxygen-evolving intermediate in photosystem II. *J. Inorg. Biochem. 199*, -110797.

(49) Narzi, D., Bovi, D., and Guidoni, L. (2014) Pathway for Mn-cluster oxidation by tyrosine-Z in the S_2 state of photosystem II. *Proc. Natl. Acad. Sci. USA 111*, 8723-8728.

(50) Retegan, M., Krewald, V., Mamedov, F., Neese, F., Lubitz, W., Cox, N., and Pantazis, D. A. (2016) A five-coordinate Mn(IV) intermediate in biological water oxidation: spectroscopic signature and a pivot mechanism for water binding. *Chem. Sci. 7*, 72-84.

(51) Askerka, M., Wang, J., Vinyard, D. J., Brudvig, G. W., and Batista, V. S. (2016) S_3 State of the O_2-Evolving Complex of Photosystem II: Insights from QM/MM, EXAFS, and Femtosecond X-ray Diffraction. *Biochemistry 55*, 981-984.

(52) Chrysina, M., Heyno, E., Kutin, Y., Reus, M., Nilsson, H., Nowaczyk, M. M., DeBeer, S., Neese, F., Messinger, J., Lubitz, W., and Cox, N. (2019) Five-coordinate Mn^{IV} intermediate in the activation of nature's water splitting cofactor. *Proc. Natl. Acad. Sci. USA 116*, 16841-16846.

(53) Pantazis, D. A., Ames, W., Cox, N., Lubitz, W., and Neese, F. (2012) Two Interconvertable Structures that Explain the Spectroscopic Properties of the Oxygen-Evolving Complex of Photosystem II in the S_2 State. *Angew. Chem. Int. Ed. 51*, 9935-9940.

(54) Isobe, H., Shoji, M., Yamanaka, S., Umena, Y., Kawakami, K., Kamiya, N., Shen, J.-R., and Yamaguchi, K. (2012) Theoretical illumination of water-inserted structures of the $CaMn_4O_5$ cluster in the S_2 and S_3 states of oxygen-evolving complex of photosystem II: full geometry optimizations by B3LYP hybrid density functional. *Dalton Trans. 41*, 13727-13740.

(55) Bovi, D., Narzi, D., and Guidoni, L. (2013) The S_2 State of the Oxygen-Evolving Complex of Photosystem II Explored by QM/MM Dynamics: Spin Surfaces and Metastable States Suggest a Reaction Path Towards the S_3 State. *Angew. Chem. Int. Ed. 52*, 11744-11749.

(56) Siegbahn, P. E. M. (2018) The S_2 to S_3 transition for water oxidation in PSII (photosystem II), revisited. *Phys. Chem. Chem. Phys. 20*, 22926-22931.

(57) Chatterjee, R., Han, G., Kern, J., Gul, S., Fuller, F. D., Garachtchenko, A., Young, I. D., Weng, T.-C., Nordlund, D., Alonso-Mori, R., Bergmann, U., Sokaras, D., Hatekeyama, M., Yachandra, V. K., and Yano, J. (2016) Structural changes correlated with magnetic spin state isomorphism in the S_2 state of the Mn_4CaO_5 cluster in the oxygen-evolving complex of photosystem II. *Chem. Sci. 7*, 5236-5348.

(58) Chatterjee, R., Lassalle, L., Gul, S., Fuller, F. D., Young, I. D., Ibrahim, M., de Lichtenberg, C., Cheah, M. H., Zouni, A., Messinger, J., Yachandra, V. K., Kern, J., and Yano, J. (2019) Structural isomers of the S_2 state in photosystem II: do they exist at room temperature and are they important for function? *Physiol. Plant. 166*, 60-72.

(59) Corry, T. A. and O'Malley, P. J. (2019) Proton Isomers Rationalize the High- and Low-Spin Forms of the S_2 State Intermediate in the Water-Oxidizing Reaction of Photosystem II. *J. Phys. Chem. Lett. 10*, 5226-5230.

(60) Pushkar, Y., Ravari, A. K., Jensen, S. C., and Palenik, M. (2019) Early Binding of Substrate Oxygen Is Responsible for a Spectroscopically Distinct S_2 State in Photosystem II. *J. Phys. Chem. Lett. 10*, 5284-5291.

(61) Corry, T. A. and O'Malley, P. J. (2020) Molecular identification of a high spin deprotonated intermediate during the S_2 to S_3 transition of Nature's water oxidising complex. *J. Am. Chem. Soc. 142*, 10240-10243.

(62) Siegbahn, P. E. M. (2009) Structures and Energetics for O_2 Formation in Photosystem II. *Acc. Chem. Res. 42*, 1871-1880.

(63) Siegbahn, P. E. M. (2013) Water oxidation mechanism in photosystem II, including oxidations, proton release pathways, O-O bond formation and O_2 release. *Biochim. Biophys. Acta 1827*, 1003-1019.

(64) Zaharieva, I., Dau, H., and Haumann, M. (2016) Sequential and Coupled Proton and Electron Transfer Events in the S_2 to S_3 Transition of Photosynthetic Water Oxidation Revealed by Time-Resolved X-ray Absorption Spectroscopy. *Biochemistry 55*, 6996-7004.

(65) Sakamoto, H., Shimizu, T., Nagao, R., and Noguchi, T. (2017) Monitoring the Reaction Process During the S_2 to S_3 Transition in Photosynthetic Water Oxidation Using Time-Resolved Infrared Spectroscopy. *J. Am. Chem. Soc. 139*, 2022-2029.

(66) Askerka, M., Vinyard, D. J., Brudvig, G. W., and Batista, V. S. (2015) NH_3 Binding to the S_2 State of the O_2-Evolving Complex of Photosystem II: Analogue to H_2O Binding during the S_2 to S_3 Transition. *Biochemistry 54*, 5783-5786.

(67) Retegan, M. and Pantazis, D. A. (2016) Interaction of methanol with the oxygen-evolving complex: atomistic models, channel identification, species dependence, and mechanistic implications. *Chem. Sci. 7*, 6463-6476.

(68) Isobe, H., Shoji, M., Shen, J.-R., and Yamaguchi, K. (2015) Strong Coupling between the Hydrogen Bonding Environment and Redox Chemistry during the

S_2 to S_3 Transition in the Oxygen-Evolving Complex of Photosystem II. *J. Phys. Chem. B 119*, 13922-13933.

(69) Ugur, I., Rutherford, A. W., and Kaila, V. R. I. (2016) Redox-coupled substrate water reorganization in the active site of Photosystem II - The role of calcium in substrate water delivery. *Biochim. Biophys. Acta 1857*, 740-748.

(70) Kim, C. J. and Debus, R. J. (2017) Evidence from FTIR Difference Spectroscopy That a Substrate H_2O Molecule for O_2 Formation in Photosystem II is Provided by the Ca Ion of the Catalytic Mn_4CaO_5 Cluster. *Biochemistry 56*, 2558-2570.

(71) Beal, N. J., Corry, T. A., and O'Malley, P. J. (2018) A Comparison of Experimental and Broken Symmetry Density Functional (BS-DFT) Calculated Electron Paramagnectic Resonance (EPR) Parameters for Intermediates Involved in the S_2 to S_3 State Transition of Nature's Oxygen Evolving Complex. *J. Phys. Chem. B 122*, 1394-1407.

(72) Kim, C. J. and Debus, R. J. (2019) One of the Subsrate Waters for O_2 Formation in Photosystem II is Provided by the Water-Splitting Mn_4CaO_5 Cluster's Ca^{2+} Ion. *Biochemistry 58*, 3185-3192.

(73) Shimada, Y., Kitajima-Ihara, T., Nagao, R., and Noguchi, T. (2020) Role of the O4 Channel in Photosynthetic Water Oxidation as Revealed by Fourier Transform Infrared Difference and Time-Resolved Infrared Analysis of the D1-S169A Mutant. *J. Phys. Chem. B 124*, 1470-1480.

(74) Li, X. and Siegbahn, P. E. M. (2015) Alternative mechanisms for O_2 release and O-O bond formation in the oxygen evolving complex of photosystem II. *Phys. Chem. Chem. Phys. 17*, 12168-12174.

(75) Shoji, M., Isobe, H., and Yamaguchi, K. (2015) QM/MM study of the S_2 to S_3 transition reaction in the oxygen-evolving complex of photosystem II. *Chem. Phys. Lett. 636*, 172-179.

(76) Capone, M., Narzi, D., Bovi, D., and Guidoni, L. (2016) Mechanism of Water Delivery to the Active Site of Photosystem II along the S_2 to S_3 Transition. *J. Phys. Chem. Lett. 7*, 592-596.

(77) Capone, M., Bovi, D., Narzi, D., and Guidoni, L. (2016) Reorganization of Substrate Waters between the Closed and Open Cubane Conformers during the

S_2 to S_3 Transition in the Oxygen Evolving Complex. *Biochemistry 54*, 6439-6442.

(78) Siegbahn, P. E. M. (2018) Water Oxidation by PSII: A Quantum Chemical Approach, in *Mechanisms of Primary Energy Transduction in Biology* (Wikström, M., Ed.) pp 273-295, Royal Society of Chemistry, London.

(79) Chu, H.-A., Nguyen, A. P., and Debus, R. J. (1995) Amino Acid Residues that Influence the Binding of Manganese or Calcium to Photosystem II. 1. The Lumenal Inter-Helical Domains of the D1 Polypeptide. *Biochemistry 34*, 5839-5858.

(80) Debus, R. J., Campbell, K. A., Pham, D. P., Hays, A.-M. A., and Britt, R. D. (2000) Glutamate 189 of the D1 Polypeptide Modulates the Magnetic and Redox Properties of the Manganese Cluster and Tyrosine Y_Z in Photosystem II. *Biochemistry 39*, 6275-6287.

(81) Kimura, Y., Mizusawa, N., Ishii, A., Nakazawa, S., and Ono, T.-A. (2005) Changes in Structural and Functional Properties of Oxygen-Evolving Complex Induced by Replacement of D1-Glutamate 189 with Glutamine in Photosystem II: Ligation of Glutamate 189 Carboxylate to the Manganese Cluster. *J. Biol. Chem. 280*, 37895-37900.

(82) Clausen, K., Winkler, S., Hays, A. M., Hundelt, M., Debus, R. J., and Junge, W. (2001) Photosynthetic Water Oxidation in *Synechocystis* sp PCC6803: Mutations D1-E189K, R and Q are Without Influence on Electron Transfer at the Donor Side of Photosystem II. *Biochim. Biophys. Acta 1506*, 224-235.

(83) Strickler, M. A., Hillier, W., and Debus, R. J. (2006) No Evidence from FTIR Difference Spectroscopy that Glutamate-189 of the D1 Polypeptide Ligates a Mn Ion that Undergoes Oxidation During the S_0 to S_1, S_1 to S_2, or S_2 to S_3 Transitions in Photosystem II. *Biochemistry 45*, 8801-8811.

(84) Klauss, A., Haumann, M., and Dau, H. (2012) Alternating electron and proton transfer steps in photosynthetic water oxidation. *Proc. Natl. Acad. Sci. USA 109*, 16035-16040.

(85) Klauss, A., Haumann, M., and Dau, H. (2015) Seven Steps of Alternating Electron and Proton Transfer in Photosystem II Water Oxidation Traced by Time-Resolved Photothermal Beam Deflection at Improved Sensitivity. *J. Phys. Chem. B 119*, 2677-2689.

(86) Nakamura, S., Ota, K., Shibuya, Y., and Noguchi, T. (2016) Role of a Water Network around the Mn_4CaO_5 Cluster in Photosynthetic Water Oxidation: A Fourier Transform Infrared Spectroscopy and Quantum Mechanics/Molecular Mechanics Calculation Study. *Biochemistry 55*, 597-607.

(87) Noguchi, T. (2008) Fourier Transform Infrared Analysis of the Photosynthetic Oxygen-Evolving Center. *Coord. Chem. Rev. 251*, 336-346.

(88) Noguchi, T. (2013) Monitoring the reactions of photosynthetic water oxidation using infrared spectroscopy. *Biomedical Spectroscopy and Imaging 2*, 115-128.

(89) Debus, R. J. (2015) FTIR Studies of Metal Ligands, Networks of Hydrogen Bonds, and Water Molecules near the Active Site Mn_4CaO_5 Cluster in Photosystem II. *Biochim. Biophys. Acta 1847*, 19-34.

(90) Noguchi, T. (2015) Fourier transform infrared difference and time-resolved infrared detection of the electron and proton transfer dynamics in photosynthetic water oxidation. *Biochim. Biophys. Acta 1847*, 35-45.

(91) Debus, R. J. (2014) Evidence from FTIR Difference Spectroscopy That D1-Asp61 Influences the Water Reactions of the Oxygen-Evolving Mn_4CaO_5 Cluster of Photosystem II. *Biochemistry 53*, 2941-2955.

(92) Banerjee, G., Ghosh, I., Kim, C. J., Debus, R. J., and Brudvig, G. W. (2017) Substitution of the D1-N87 site in photosystem II of cyanobacteria mimics the chloride-binding characteristics of spinach photosystem II. *J. Biol. Chem. 293*, 2487-2497.

(93) Ghosh, I., Banerjee, G., Kim, C. J., Reiss, K., Batista, V. S., Debus, R. J., and Brudvig, G. W. (2019) D1-S169A Substitution of Photosystem II Perturbs Water Oxidation. *Biochemistry 58*, 1379-1387.

(94) Pokhrel, R., Debus, R. J., and Brudvig, G. W. (2015) Probing the Effect of Mutations of Asparagine 181 in the D1 Subunit of Photosystem II. *Biochemistry 54*, 1663-1672.

(95) Nagao, R., Ueoka-Nakanishi, H., and Noguchi, T. (2017) D1-Asn-298 in photosystem II is invovled in a hydrogen-bond network near the redox-active tyrosine Y_Z for proton exit during water oxidation. *J. Biol. Chem. 292*, 20046-20057.

(96) Service, R. J., Yano, J., Dilbeck, D. L., Burnap, R. L., Hillier, W., and Debus, R. J. (2013) Participation of Glutamate-333 of the D1 Polypeptide in the Ligation of the Mn_4CaO_5 Cluster in Photosystem II. *Biochemistry 52*, 8452-8464.

(97) Shimada, Y., Suzuki, H., Tsuchiya, T., Tomo, T., Noguchi, T., and Mimuro, M. (2009) Effect of a Single-Amino Acid Substitution of the 43 kDa Chlorophyll Protein on the Oxygen-Evolving Reaction of the Cyanobacterium *Synechocystis* sp. PCC 6803: Analysis of the Glu354Gln Mutation. *Biochemistry 48*, 6095-6103.

(98) Service, R. J., Hillier, W., and Debus, R. J. (2010) Evidence from FTIR Difference Spectroscopy of an Extensive Network of Hydrogen Bonds near the Oxygen-Evolving Mn_4Ca Cluster of Photosystem II Involving D1-Glu65, D2-Glu312, and D1-Glu329. *Biochemistry 49*, 6655-6669.

(99) Service, R. J., Hillier, W., and Debus, R. J. (2014) A Network of Hydrogen Bonds near the Oxygen-Evolving Mn_4CaO_5 Cluster of Photosystem II Probed with FTIR Difference Spectroscopy. *Biochemistry 53*, 1001-1017.

(100) Chu, H.-A., Nguyen, A. P., and Debus, R. J. (1994) Site-Directed Photosystem II Mutants with Perturbed Oxygen Evolving Properties: 1. Instability or Inefficient Assembly of the Manganese Cluster *In Vivo*. *Biochemistry 33*, 6137-6149.

(101) Noguchi, T. and Sugiura, M. (2002) Flash-Induced FTIR Difference Spectra of the Water Oxidizing Complex in Moderately Hydrated Photosystem II Core Films: Effect of Hydration Extent on S-State Transitions. *Biochemistry 41*, 2322-2330.

(102) Kim, C. J., Bao, H., Burnap, R. L., and Debus, R. J. (2018) Impact of D1-V185 on the Water Molecules that faciliate O_2 Formation by the Catalytic Mn_4CaO_5 Cluster in Photosystem II. *Biochemistry 57*, 4299-4311.

(103) Hays, A.-M. A., Vassiliev, I. R., Golbeck, J. H., and Debus, R. J. (1998) Role of D1-His190 in Proton-Coupled Electron Transfer Reactions in Photosystem II: A Chemical Complementation Study. *Biochemistry 37*, 11352-11365.

(104) Noguchi, T., Inoue, Y., and Tang, X. S. (1997) Structural coupling between the oxygen-evolving Mn cluster and a tyrosine residue in photosystem II as

revealed by Fourier transform infrared spectroscopy. *Biochemistry 36*, 14705-14711.

(105) Hienerwadel, R., Boussac, A., Breton, J., Diner, B. A., and Berthomieu, C. (1997) Fourier Transform Infrared Difference Spectroscopy of Photosystem II Tyrosine D using Site-Directed Mutagenesis and Specific Isotope Labeling. *Biochemistry 36*, 14712-14723.

(106) Chu, H.-A., Hillier, W., and Debus, R. J. (2004) Evidence that the C-Terminus of the D1 Polypeptide is Ligated to the Manganese Ion that Undergoes Oxidation During the S_1 to S_2 Transition: An Isotope-Edited FTIR Study. *Biochemistry 43*, 3152-3166.

(107) Takahashi, R., Sugiura, M., and Noguchi, T. (2007) Water Molecules Coupled to the Redox-Active Tyrosine Y_D in Photosystem II as Detected by FTIR Spectroscopy. *Biochemistry 46*, 14245-14249.

(108) Metz, J. G., Nixon, P. J., Rögner, M., Brudvig, G. W., and Diner, B. A. (1989) Directed Alteration of the D1 Polypeptide of Photosystem II: Evidence that Tyrosine-161 is the Redox Component, Z, Connecting the Oxygen-Evolving Complex to the Primary Electron Donor, P680. *Biochemistry 28*, 6960-6969.

(109) Noguchi, T., Inoue, Y., and Tang, X.-S. (1999) Structure of a Histidine Ligand in the Photosynthetic Oxygen-Evolving Complex as Studied by Light-Induced Fourier Transform Infrared Spectroscopy. *Biochemistry 38*, 10187-10195.

(110) Nakamura, S. and Noguchi, T. (2017) Infrared Determination of the Protonation State of a Key Histidine Residue in the Photosynthetic Water Oxidizing Center. *J. Am. Chem. Soc. 139*, 9364-9375.

(111) Service, R. J., Yano, J., McConnell, I., Hwang, H. J., Niks, D., Hille, R., Wydrzynski, T., Burnap, R. L., Hillier, W., and Debus, R. J. (2011) Participation of Glutamate-354 of the CP43 Polypeptide in the Ligation of Manganese and the Binding of Substrate Water in Photosystem II. *Biochemistry 50*, 63-81.

(112) Pokhrel, R., Service, R. J., Debus, R. J., and Brudvig, G. W. (2013) Mutation of Lysine 317 in the D2 Subunit of Photosystem II Alters Chloride Binding and Proton Transport. *Biochemistry 52*, 4758-4773.

(113) Kitajima-Ihara, T., Suzuki, T., Nakamura, S., Shimada, Y., Nagao, R., Dohmae, N., and Noguchi, T. (2020) Fourier transform infrared and mass spectrometry

analyses of a site-directed mutant of D1-Asp170 as a ligand to the water-oxidizing Mn_4CaO_5 cluster in photosystem II. *Biochim. Biophys. Acta 1861*, -Article 148086.

(114) Noguchi, T., Sugiura, M., and Inoue, Y. (1999) FTIR Studies on the Amino-Acid Ligands of the Photosynthetic Oxygen-Evolving Mn-Cluster, in *Fourier Transform Spectroscopy: Twelfth International Conference* (Itoh, K. and Tasumi, M., Eds.) pp 459-460, Waseda University Press, Tokyo, Japan.

(115) Noguchi, T. and Sugiura, M. (2003) Analysis of Flash-Induced FTIR Difference Spectra of the S-State Cycle in the Photosynthetic Water-Oxidizing Complex by Uniform ^{15}N and ^{13}C Isotope Labeling. *Biochemistry 42*, 6035-6042.

(116) Kimura, Y., Mizusawa, N., Ishii, A., Yamanari, T., and Ono, T.-A. (2003) Changes of Low-Frequency Vibrational Modes Induced by Universal ^{15}N- and ^{13}C-Isotope Labeling in S_2/S_1 FTIR Difference Spectrum of Oxygen-Evolving Complex. *Biochemistry 42*, 13170-13177.

(117) Yamanari, T., Kimura, Y., Mizusawa, N., Ishii, A., and Ono, T.-A. (2004) Mid-to Low-Frequency Fourier Transform Infrared Spectra of S-State Cycle for Photosynthetic Water Oxidation in *Synechocystis* sp. PCC 6803. *Biochemistry 43*, 7479-7490.

(118) Strickler, M. A., Walker, L. M., Hillier, W., and Debus, R. J. (2005) Evidence from Biosynthetically Incorporated Strontium and FTIR Difference Spectroscopy that the C-Terminus of the D1 Polypeptide of Photosystem II Does Not Ligate Calcium. *Biochemistry 44*, 8571-8577.

(119) Suzuki, H., Taguchi, Y., Sugiura, M., Boussac, A., and Noguchi, T. (2006) Structural Perturbations of the Carboxylate Ligands to the Mn Cluster upon Ca^{2+}/Sr^{2+} Exchange in the S-state Cycle of Photosynthetic Oxygen Evolution as Studied by Flash-Induced FTIR Difference Spectroscopy. *Biochemistry 45*, 13454-13464.

(120) De Riso, A., Jenson, D. L., and Barry, B. A. (2010) Calcium Exchange and Structural Changes during the Photosynthetic Oxygen Evolving Cycle. *Biophys. J. 91*, 1999-2008.

(121) Polander, B. C. and Barry, B. A. (2013) Calcium, Strontium, and Protein Dynamics during the S_2 to S_3 Transition in the Photosynthetic Oxygen-Evolving Cycle. *J. Phys. Chem. Lett. 4*, 3356-3362.

(122) Ames, W., Pantazis, D. A., Krewald, V., Cox, N., Messinger, J., Lubitz, W., and Neese, F. (2011) Theoretical Evaluation of Structural Models of the S_2 State in the Oxygen Evolving Complex of Photosystem II: Protonation States and Magnetic Interactions. *J. Am. Chem. Soc. 133*, 19743-19757.

(123) Stich, T. A., Yeagle, G. J., Service, R. J., Debus, R. J., and Britt, R. D. (2011) Ligation of D1-His332 and D1-Asp170 to the Manganese Cluster of Photosystem II from *Synechocystis* Assessed by Multifrequency Pulse EPR Spectroscopy. *Biochemistry 50*, 7390-7404.

(124) Lohmiller, T., Cox, N., Su, J.-H., Messinger, J., and Lubitz, W. (2012) The Basic Properties of the Electronic Structure of the Oxygen-Evolving Complex of Photosystem II Are Not Perturbed by Ca^{2+} Removal. *J. Biol. Chem. 287*, 24721-24733.

(125) Marchiori, D. A., Oyala, P. H., Debus, R. J., Stich, T. A., and Britt, R. D. (2018) Structural Effects of Ammonia Binding to the Mn_4CaO_5 Cluster of Photosystem II. *J. Phys. Chem. B 122*, 1588-1599.

(126) Nixon, P. J. and Diner, B. A. (1992) Aspartate 170 of the Photosystem II Reaction Center Polypeptide D1 is Involved in the Assembly of the Oxygen-Evolving Manganese Cluster. *Biochemistry 31*, 942-948.

(127) Whitelegge, J. P., Koo, D., Diner, B. A., Domian, I., and Erickson, J. M. (1995) Assembly of the Photosystem II Oxygen-Evolving Complex is Inhibited in *psb*A Site-Directed Mutants of *Chlamydomonas reinhardtii*. *J. Biol. Chem. 270*, 225-235.

(128) Campbell, K. A., Force, D. A., Nixon, P. J., Dole, F., Diner, B. A., and Britt, R. D. (2000) Dual-Mode EPR Detects the Initial Intermediate in Photoassembly of the Photosystem II Mn Cluster: The Influence of Amino Acid Residue 170 of the D1 Polypeptide on Mn Coordination. *J. Am. Chem. Soc. 122*, 3754-3761.

(129) Hwang, H. J., McLain, A., Debus, R. J., and Burnap, R. L. (2007) Photoassembly of the Manganese Cluster in Mutants Perturbed in the High Affinity Mn-Binding Site of the H_2O-Oxidation Complex of Photosystem II. *Biochemistry 46*, 13648-13657.

(130) Debus, R. J., Aznar, C., Campbell, K. A., Gregor, W., Diner, B. A., and Britt, R. D. (2003) Does Aspartate 170 of the D1 Polypeptide Ligate the Manganese Cluster in Photosystem II? An EPR and ESEEM Study. *Biochemistry 42*, 10600-10608.

(131) Chu, H.-A., Debus, R. J., and Babcock, G. T. (2001) D1-Asp170 is Structurally Coupled to the Oxygen Evolving Complex in Photosystem II as Revealed by Light-Induced Fourier Transform Infrared Difference Spectroscopy. *Biochemistry 40*, 2312-2316.

(132) Debus, R. J., Strickler, M. A., Walker, L. M., and Hillier, W. (2005) No Evidence from FTIR Difference Spectroscopy That Aspartate-170 of the D1 Polypeptide Ligates a Manganese Ion That Undergoes Oxidation during the S_0 to S_1, S_1 to S_2, or S_2 to S_3 Transitions in Photosystem II. *Biochemistry 44*, 1367-1374.

(133) Chu, H.-A., Sackett, H., and Babcock, G. T. (2000) Identification of a Mn-O-Mn Cluster Vibrational Mode of the Oxygen-Evolving Complex in Photosystem II by Low-Frequency FTIR Spectroscopy. *Biochemistry 39*, 14371-14376.

(134) Kimura, Y., Ishii, A., Yamanari, T., and Ono, T.-A. (2005) Water-Sensitive Low-Frequency Vibrations of Reaction Intermediates during S-State Cycling in Photosynthetic Water Oxidation. *Biochemistry 44*, 7613-7622.

(135) Chu, H.-A., Nguyen, A. P., and Debus, R. J. (1995) Amino Acid Residues that Influence the Binding of Manganese or Calcium to Photosystem II. 2. The Carboxy-terminal Domain of the D1 Polypeptide. *Biochemistry 34*, 5859-5882.

(136) Takemoto, H., Sugiura, M., and Noguchi, T. (2019) Proton Release Process during the S_2-to-S_3 Transition of Photosynthetic Water Oxidation As Revealed by the pH Dependence of Kinetics Monitored by Time-Resolved Infrared Spectroscopy. *Biochemistry 58*, 4276-4283.

(137) Debus, R. J. (1992) The Manganese and Calcium Ions of Photosynthetic Oxygen Evolution. *Biochim. Biophys. Acta 1102*, 269-352.

(138) Britt, R. D., Peloquin, J. M., and Campbell, K. A. (2000) Pulsed and Parallel-Polarization EPR Characterization of the Photosystem II Oxygen-Evolving Complex. *Annu. Rev. Biophys. Biomol. Struct. 29*, 463-495.

(139) Barth, A. (2000) The Infrared Absorption of Amino Acid Side Chains. *Prog. Biophys. Molec. Biol. 74*, 141-173.

(140) Noguchi, T. and Sugiura, M. (2002) FTIR Detection of Water Reactions During the Flash-Induced S-State Cycle of the Photosynthetic Water-Oxidizing Complex. *Biochemistry 41*, 15706-15712.

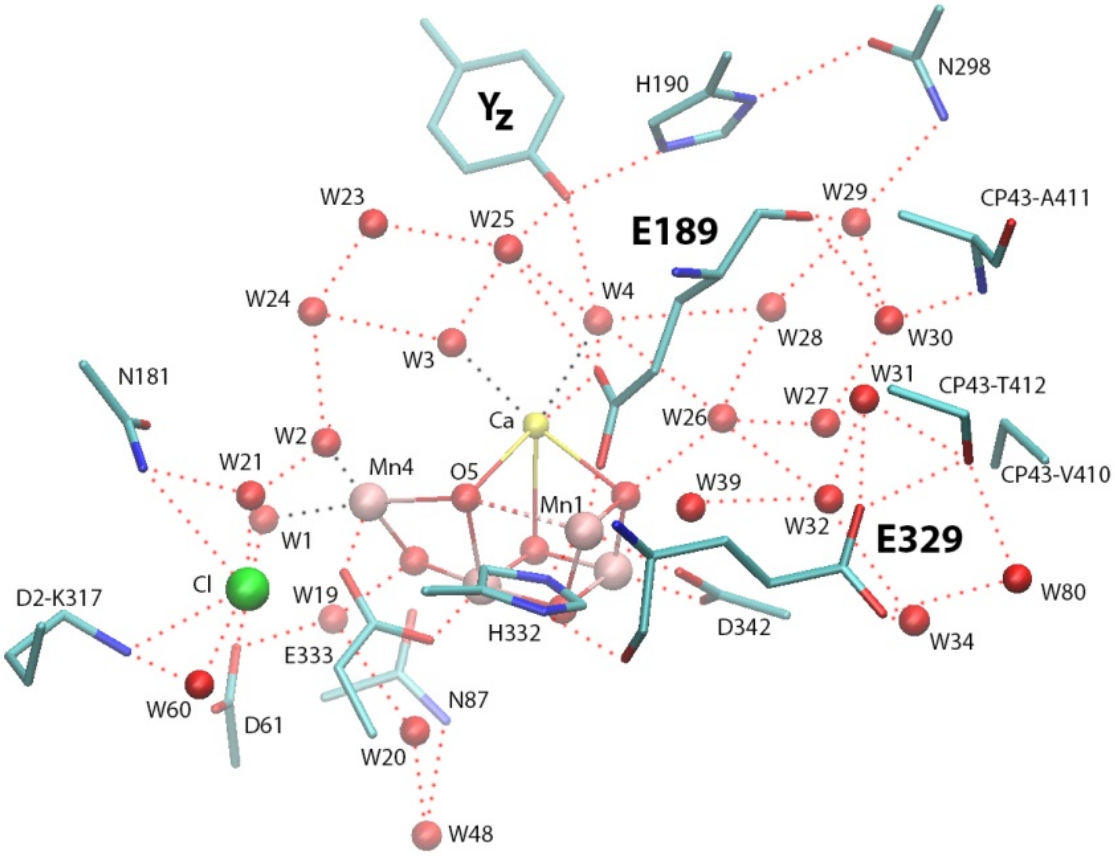

FIGURE 5.1 Water molecules and selected residues in the vicinity of the Mn_4CaO_5 cluster based on 4UB6 (*7*). All residues shown are from the D1 subunit unless indicated otherwise. The salmon-colored spheres are the manganese ions. The yellow sphere is the Ca^{2+} ion. The green sphere is the Cl^- ion. The red spheres are the oxygen atoms of water molecules and μ-oxo bridges. The unusually long "bond" between Mn1 and O5 is depicted with a dashed line. Water molecules are labeled as in ref. (*12*).

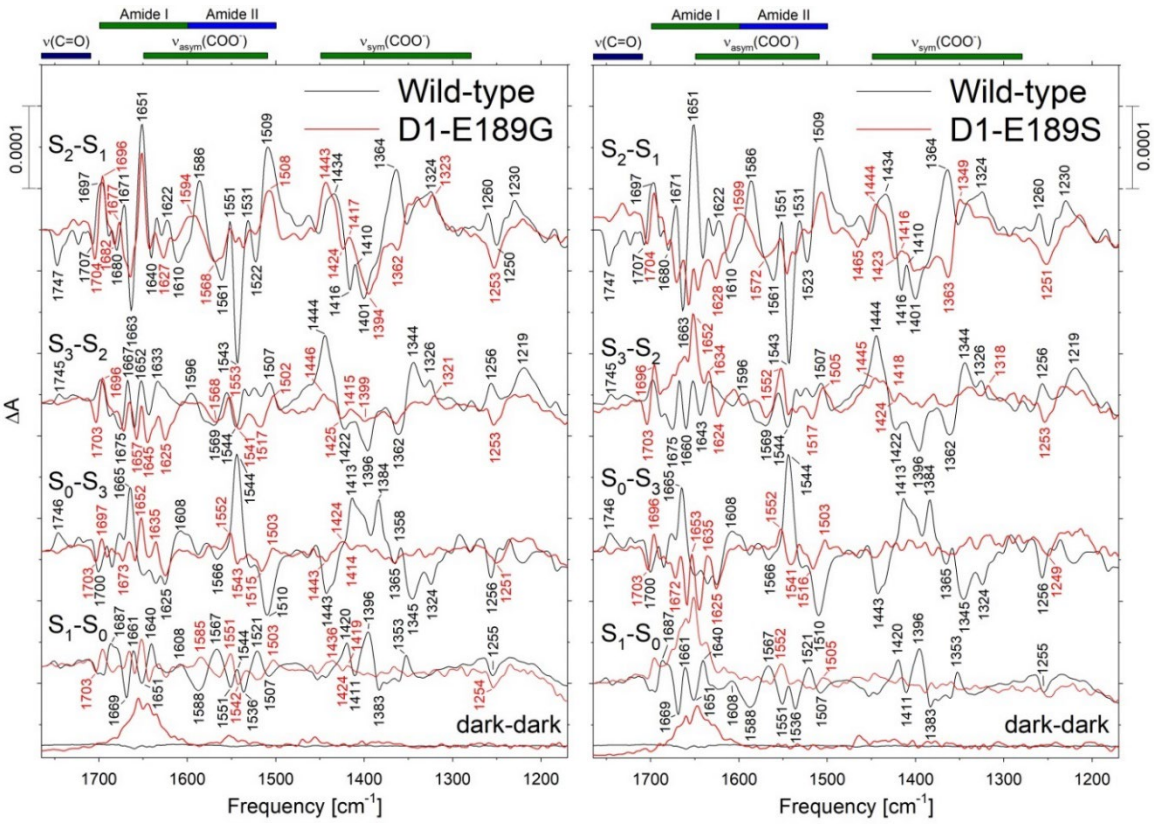

FIGURE 5.2 Mid-frequency FTIR difference spectra of wild-type (black), D1-E189G (left panel, red), and D1-E189S (right panel, red) PSII core complexes in response to four successive flash illuminations applied at 0°C. The wild-type data represent the averages of 16 samples (30,400 scans for each trace). The D1-E189G data represent the averages of 20 samples (35,000 scans for each trace). The D1-E189S data represent the averages of 8 samples (15,200 scans for each trace). The D1-E189G spectra were multiplied by factors of 4.0 to 5.7 and the D1-E189S spectra were multiplied by factors of 3.4 to 5.9 to normalize the wild-type and mutant spectra to the extent of the flash-induced formation of $Q_A^{\bullet-}$. The dark-dark control traces show the noise level and the stability of the baseline (lower traces). The dark-dark control traces of the mutants were multiplied by a factor of 4.0.

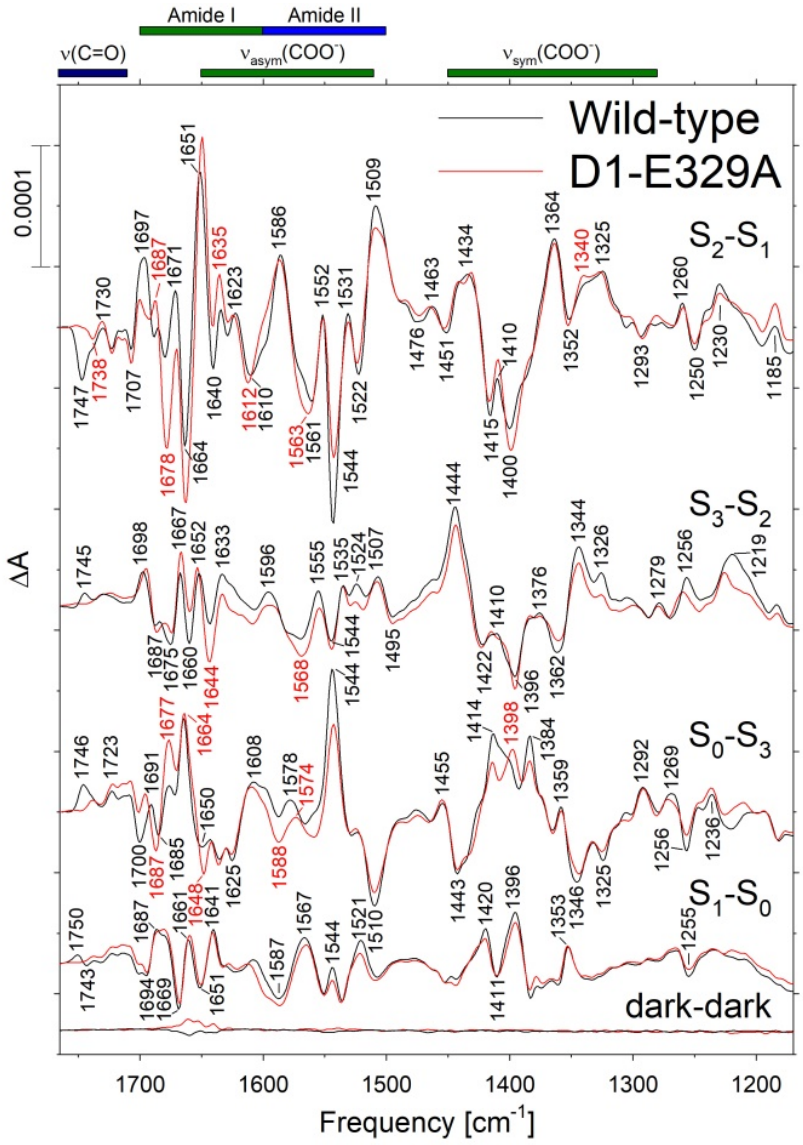

FIGURE 5.3 Mid-frequency FTIR difference spectra of wild-type (black) and D1-E329A (red) PSII core complexes in response to four successive flash illuminations applied at 0°C. The wild-type data are the same as depicted in Figure 5.2 and represent the averages of 16 samples (30,400 scans for each trace). The D1-E329A data represent the averages of 9 samples (15,400 scans for each trace). The dark-dark control traces show the noise level and the stability of the baseline (lower traces).

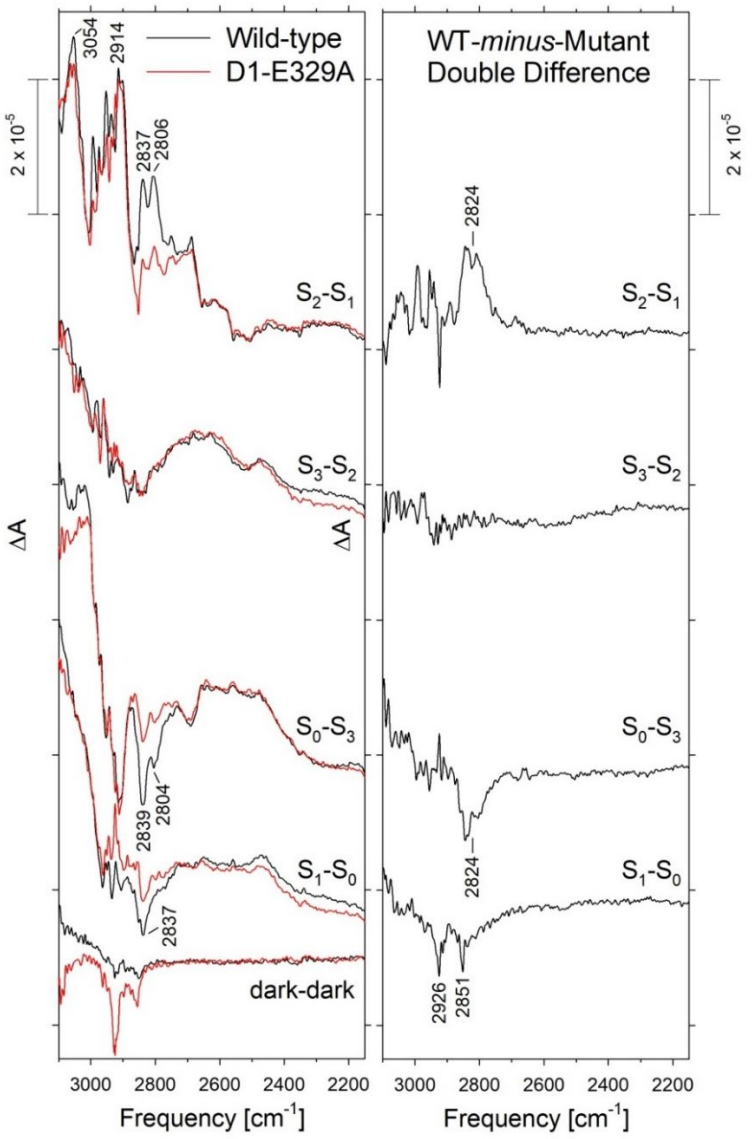

FIGURE 5.4 Left Panel: FTIR difference spectra of wild-type (black) and D1-E329A (red) PSII core complexes between 3100 and 2150 cm^{-1} in response to four successive flash illuminations applied at 0°C. The data were collected simultaneously with those that are shown in Figure 5.3. Dark-dark control traces show the noise level and the stability of the baseline (lower traces). Right Panel: Wild-type-*minus*-D1-E329A double difference spectra. The difference spectra shown in the left panel were subtracted directly.

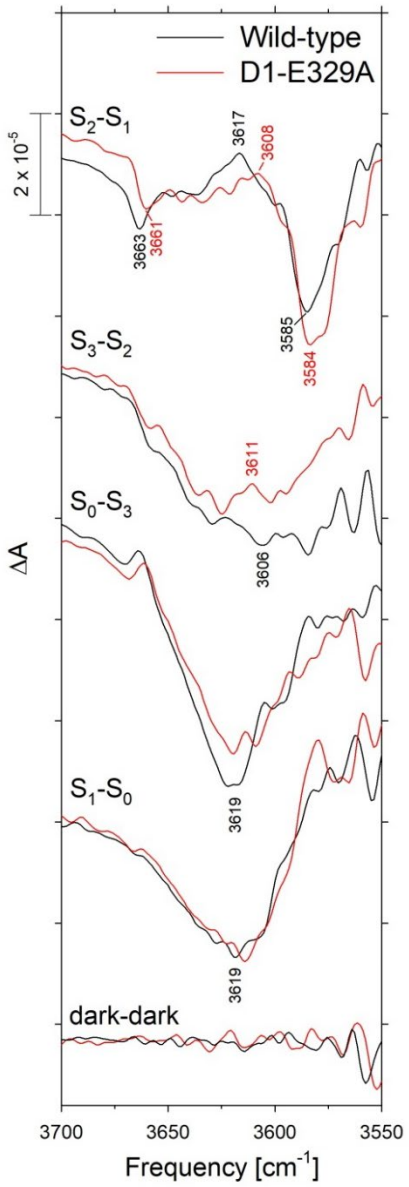

FIGURE 5.5 FTIR difference spectra of wild-type (black) and D1-E329A (red) PSII core complexes in the weakly hydrogen bonded O–H stretching region in response to four successive flash illuminations applied at 0°C. The data were collected simultaneously with those that are shown in Figure 5.3. Dark-dark control traces show the noise level and the stability of the baseline (lower traces).